Interrogating a range of biological targets using chemical biology

A thesis submitted to the University of Sheffield for the award of the degree

Doctor of Philosophy

By

Thomas Grieves (M. Chem.)

Department of Molecular Biology and Biotechnology

University of Sheffield

November 2012

Contents

Figures and Tables

Figures

Tables

Acknowledgements

I would like to thank the Medical Research Council and Unilever for funding this work.

Special thanks must go to my supervisor Professor David Hornby for providing direction and regular opportunities to work in exciting new areas. None of this work would have been possible without the input of Dr Qaiser Sheikh, who provided advice and suggestions on a daily basis.

Thanks must also go to Professor Anthony Ryan, Dr Patrick Fairclough and Dr Joshua Swann for their assistance and collaboration on the biodegradable packaging work.

I would also like to thank my parents for their constant support over the last four years and Jo for her regular encouragement and input.

Abstract

Chemical biology uses the tools of chemistry in order to study and better understand biological systems. Techniques such as synthetic chemistry have proved invaluable in the discovery of novel medicines to treat a host of conditions. Polymer chemistry has already provided large numbers of synthetic materials with wildly varying physical and mechanical properties which are useful in every facet of day-to-day life. However, the need for further innovation still remains. Fewer and fewer new medicines make it into clinical use every year as discovery of genuinely novel treatments becomes more difficult and regulatory approval becomes more and more difficult to obtain. The ubiquity of synthetic polymers inevitably results in large amounts waste products which were often useful in the first place because of their exceptional stability. This work describes the application of chemical biology techniques to the process of drug discovery and also to the development of biodegradable packaging materials.

High serum cholesterol levels are a major cause of atherosclerosis which in turn is a major cause of heart disease. Ischemic heart disease is the number one cause of death worldwide. Cholesterol lowering drugs, known as statins, are strongly associated in a reduction of mortality rates from heart disease. A library of novel statin compounds was screened for its ability to inhibit HMG-CoA reductase. Several of these compounds showed *in vitro* activity at least as good as the existing best in class drugs and may also display a novel mode of HMG-CoA reductase binding.

The rise of antibiotic resistance is a major concern and the need for novel antibacterial drugs has become critical. A number of novel fluoroquinolone compounds were screened for their antibacterial properties. None of these compounds showed activity *in vitro* although their structures may function as prodrugs *in vivo*.

The sachet market provides an opportunity for low earners in developing countries to afford detergents and toiletries. Poor waste disposal infrastructures mean that waste sachets have become a major environmental concern. The possibility of producing a biodegradable shampoo sachet using existing commercially available materials was investigated. A novel, ‘bilayer’ approach proved unsuccessful due to limitations in the cellulose and polyvinyl alcohol materials used. A simpler approach using a type of polyhydroxyalkanoate was also unsuccessful. While several biodegradable polymers are currently available, all have limitations to their use as packaging materials particularly when storing liquids.

Abbreviations

3HHx	-	3-Hydroxyhexanoate
3HV	-	3-Hydroxyvalerate
4HB	-	4-Hydroxybutyrate
ABC	-	ATP-binding Cassette
ABC	-	ATP-binding cassette
ADP	-	Adenosine Diphosphate
AMP	-	Adenosine Monophosphate
AMPK	-	AMP-activated Protein Kinase
Apo	-	Apolipoprotein
ATP	-	Adenosine Triphosphate
CAP	-	Catabolite Gene Activator Protein
CERP	-	Cholesterol Efflux Regulatory Protein
CETP	-	Cholesterol Ester Transfer Protein
CNS	-	Central Nervous System
CoA	-	Coenzyme A
DMSO	-	Dimethyl Sulfoxide
DNA	-	Deoxyribonucleic Acid
ER	-	Endoplasmic Reticulum
FH	-	Familial Hypercholesterolemia
GABA	-	Gamma-aminobutyric acid
GI	-	Gastrointestinal
HA	-	Hydroxyalkanoate
HDL	-	High Density Lipoprotein

HMG-CoA	-	3-hydroxy-3-methylglutaryl coenzyme A
IDL	-	Intermediate Density Lipoprotein
LCAT	-	Lecithin Cholesterol Acyltransferase
LDL	-	Low Density Lipoprotein
LRP	-	LDL-related Protein
MATE	-	Multi-drug and Toxic Compound Extrusion
MCL	-	Medium Chain Length
MF	-	Major Facilitator
MIC	-	Minimum Inhbitory Concentration
MPC	-	Mutant Prevention Concentration
mRNA	-	Messenger RNA
MVTR	-	Moisture Vapour Transmission Rate
NADH	-	Nicotinamide Adenine Dinucleotide
NADPH	-	Nicotinamide Adenine Dinucleotide Phosphate
NMR	-	Nuclear Magnetic Resonance
oxLDL	-	Oxidised LDL
P(3HB)	-	Poly(3-hydroxybutyrate)
PHA	-	Polyhydroxyalkanoate
PHB	-	Poly(3-hydroxybutyrate)
PLA	-	Poly(lactic acid)
PP2A	-	Protein Phosphatase 2A
PVOH	-	Polyvinyl Alcohol
RNA	-	Ribonucleic Acid
RND	-	Resistance-nodulation-division

S1P	-	Site-1 Protease
S2P	-	Site-2 Protease
SCL	-	Short Chain Length
SMR	-	Small Multidrug Resistance
SR-B1	-	Scavenger Receptor Class B Type 1
SRE	-	Sterol Regulatory Element
SREBP	-	Sterol Regulatory Element Binding Protein
TCA	-	Tricarboxylic Acid
tRNA	-	Transfer RNA
UTI	-	Urinary Tract Infection
VLDL	-	Very Low Density Liporotein

Chapter 1

1. Introduction

1.1 Synthetic Chemistry and Drug Development

One of the most influential approaches to drug discovery has been the search for and discovery of naturally occurring compounds which bring therapeutic benefits in the treatment of particular medical conditions. Isolation, purification and characterisation of such compounds may then give some insight into the mechanisms by which these natural products act. Indeed, it was the isolation of aspirin from willow bark which allowed Vane (1971) to prove that the compound inhibits cyclooxygenase enzymes. Many common drugs are either found in nature, or are derived from natural products. In 1990, 80 % of available drugs were natural products or related analogues (Li and Vederas, 2009). Advances in synthetic chemistry over time have allowed easier synthesis of many complex molecules including many naturally occurring compounds, such as the complex ring structure of taxol (Masters *et al.*, 1995). Coupled with advances in structural biology leading the elucidation of the structures of many drug targets this has allowed far more targeted development of drugs. So much so, in fact, that during the 1990s the proportion of new drugs derived from natural sources fell to only 50 % and between 2005 and 2007 only thirteen of the new drugs approved for use in the USA were natural-product derived (Harvey, 2008).

The rise of synthetic chemistry has coincided with a decrease in the number of drugs being approved for clinical use. Approval for new drugs is now much more difficult to obtain (Bennani, 2012). Where, in the past, many compounds were novel treatments for certain conditions, now new drugs must be proven to be significantly more effective than the existing best in class treatment. There is also an unhelpful emphasis on so called blockbuster drugs within the pharmaceutical industry which has led to only a limited range of drug targets being investigated in the hope of finding a compound which will generate large revenues to sustain the scale of the pharmaceutical sector. The expiring patents on a number of existing blockbuster drugs combined with the failure to successfully discover new drugs to replace them has led to a reduction in spending on research and development, amplified by the current economic downturn.

To overcome such problems, evermore innovative methods of designing, synthesising and testing new compounds are required. Also important is an increased understanding of pharmacokinetics and the effects of compounds not only on their intended target but on other systems in the body. The problem of drug resistance must also be addressed as many existing treatments are ineffective for some patients who posses variation in the gene encoding the drug target. Synthesis of increasingly varied libraries of drug analogues and investigation of their interactions with different targets will inevitably lead to better appreciation of the properties required for effective treatments. Potentially, should all of these factors be understood to a sufficient level, the design of compounds could take place almost entirely via modelling. This would allow large numbers of compounds to be “virtually” screened for their level of interaction with a drug target and their possible side-effects due to interactions with other proteins in the body.

Some of the greatest successes of natural product discovery have been in the field of antibiotics. Penicillin was famously isolated from *Penicillium* fungi and many other common antibacterial drugs were originally discovered in nature. Other common antibacterial drugs have completely synthetic origins although often their antibacterial properties were discovered by accident as was the case for nalidixic acid (Jacoby and Hooper, 2012). A major barrier to successful discovery of new antibacterial compounds is the development of resistant bacterial strains. Mutations in the genes encoding drug targets in humans develop resistance mutations very slowly. However, due to the rapid rate at which bacteria divide, antibiotic resistance mutations can accumulate very quickly. Bacterial strains resistant to multiple drugs are now a serious problem in hospitals and the discovery of novel antibacterial drugs is urgently needed in order to treat infections caused by these strains. New drugs must employ novel mechanisms of action which are able to circumvent mechanisms of antibacterial resistance (Drlica *et al.*, 2012).

1.2 Polymer Chemistry and Biodegradable Packaging Materials

The field of polymer chemistry has allowed the creation of a diverse range of materials with hugely varying mechanical properties. A significant focus of the field is in the development of plastics. These are most commonly derived from non-renewable fossil fuels such as oil and are in widespread use as packaging materials for a variety of products. Unfortunately, the majority of commercially used plastics are not biodegradable and so, when discarded, end up in landfill sites or simply as litter. Waste packaging is a significant problem on a global scale. In the European Union (EU) approximately 10 million tonnes of plastic packaging waste are produced every year (European Commission, 2012). The waste disposal infrastructure in developed countries such as those found in the EU is generally good and around 30 % of this waste is recycled. In developing countries, however, the infrastructure is poor with no avenues for recycling. In India, an estimated two million tonnes of plastics waste are produced every year, 42 % of which comes from packaging materials (Chandrappa and Das, 2012). The degradation times of many plastics in widespread use can be as long as centuries. This results in the constant accumulation of plastic waste which is unsustainable.

Development of novel, biodegradable packaging materials is highly desirable. If the volume of packaging waste can be reduced it will have an immediate impact on the associated pollution and health issues. Additionally, many existing biodegradable polymers are not derived from fossil fuels so an increase in their use would have the secondary benefit of decreasing the consumption of non-renewable energy sources. However, a range of different packaging materials are required for the packaging of different items. This requires the production of a number of different biodegradable materials with varying physical and mechanical properties in order to fulfil these needs. An understanding of the mechanisms by which materials are broken down in nature by microorganisms is essential for the development of successful biodegradable packaging. Different packaging materials will have different fates and encounter different populations of microorganisms. Design of novel biodegradable plastics must take

into account the mechanical properties of the material as well as whether or not it will be successfully broken down by the environment.

1.3 Chemical Biology Approaches

The work described here involves the use of chemical biology techniques in order to investigate a range of biological targets related to both drug discovery and polymer chemistry. Chapters two and three relate to testing the *in vitro* activities of novel drug molecules. Chapter two contains details of the testing of hypolipidaemic drugs. These are an important tool in treatment of heart disease, the number one cause of death in the UK (Murray *et al.*, 2013). Chapter three describes the testing of novel antibacterial compounds. Chapters four and five deal with the design of a biodegradable packaging solution intended for use in developing countries. In view of the diversity of biological targets addressed, each Chapter includes a more specific introduction to the background literature related to each topic.

Chapter 2

2. Small Molecule Inhibitors of HMG-CoA Reductase

2.1 Introduction

2.1.1 Cholesterol

Cholesterol is a membrane lipid found in eukaryotes. Its structure comprises a steroid with a hydrocarbon chain attached at the C17 position. It plays an essential role in regulating membrane fluidity and is found in virtually all animal membranes (Berg *et al.*, 2002). Cholesterol and its associated biochemistry is one of the most intensely studied areas of biology and no fewer than thirteen Nobel Prizes have been awarded to scientists for work in this field.

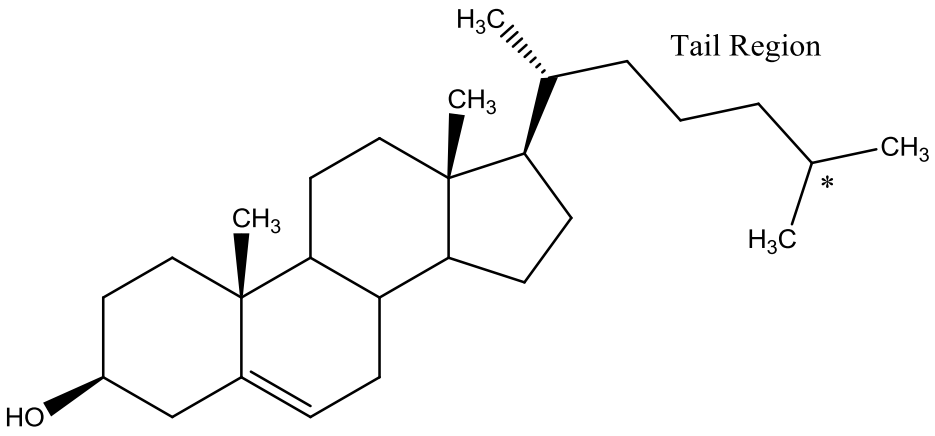

Figure 2.1. The structure of cholesterol.

The hydroxyl group forms hydrogen bonds with the hydrophilic head groups of membrane phospholipids. The linear tail region forms van der Waals interactions with hydrophobic fatty acid chains. The site of addition of the hydroxyl group of oxysterol is indicated (*).

The hydroxyl group of cholesterol is able to form a hydrogen bond with the hydrophilic head group of a membrane phospholipid (Berg *et al.*, 2002). This allows the cholesterol molecule to insert into the membrane, increasing the van der Waals interactions between neighbouring membrane lipids in the process. An increase in the amount of cholesterol in a membrane causes a reduction in membrane fluidity. This has an important effect in regulating the permeability of the membrane (Berg *et al.*, 2002). In humans, cholesterol is obtained from the diet but is also synthesised *de novo* via the mevalonate pathway (Bloch, 1965).

2.1.2 Dietary Cholesterol Uptake

In a typical Western diet, an individual will consume around 300-500 mg of cholesterol per day and a further 1100-1500 mg of cholesterol reaches the small intestinal lumen from bile and the turnover of intestinal mucosal epithelium (Wang, 2007). Due to its poor solubility in aqueous conditions, cholesterol must be solubilised by bile acids before it can be absorbed by the intestine. Hydrophobic bile acids form mixed micelles with fatty acids, monoacylglycerides, lysophospholipids and cholesterol (Wang *et al.*, 1999). These particles facilitate the uptake of cholesterol from the intestinal lumen into enterocytes via the cholesterol transporter NPC1L1 (Davis *et al.*, 2004).

Once cholesterol has been absorbed from the intestine it is transported in the blood and lymph, along with triacylglycerols, in the form of lipoprotein particles. These particles are made up of a core region consisting of hydrophobic lipids surrounded by a hydrophilic shell made up of polar lipids and proteins. Different forms of lipoprotein are classified based upon their densities and these forms have varying compositions of lipids and proteins (Betteridge and Morrell, 2003).

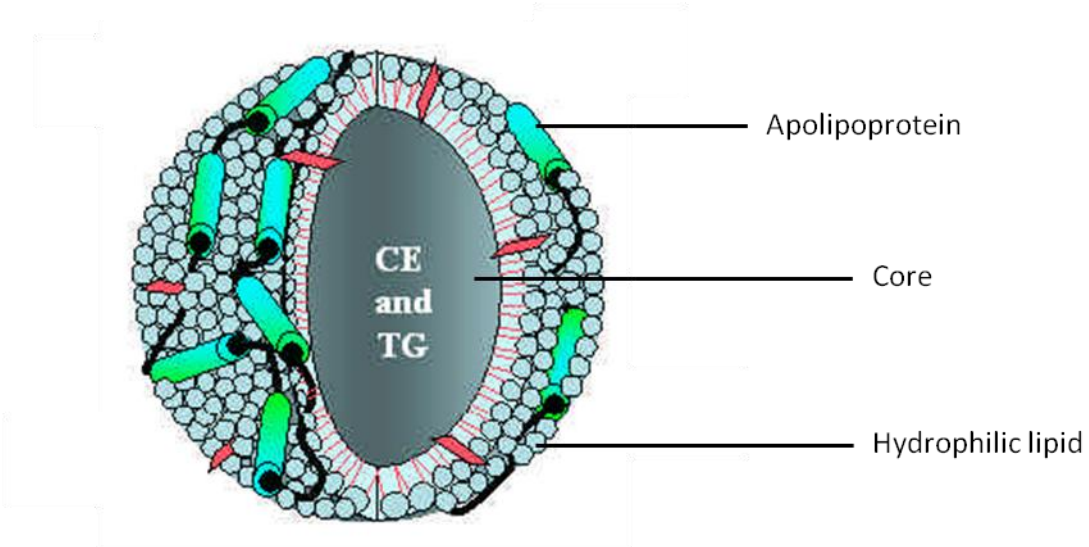

Figure 2.2. Lipoprotein particle structure

The polar lipids and apolipoproteins of the hydrophilic shell are represented. The core consists of cholesterol esters and hydrophobic lipids. This figure is adapted from Lund-Katz et al. (2003).

Dietary cholesterol and lipids are transported away from enterocytes in lipoprotein particles called chylomicrons. These particles have the lowest density of all lipoproteins due to approximately 99 % of

their composition being triacylglycerols. The amphipathic protein shell of chylomicrons is made up primarily of a 240 kD protein called apolipoprotein B-48 (apo B-48). These particles leave enterocytes by exocytosis and enter the circulation via intestinal lymphatics.

Once they reach the blood, chylomicrons bind to lipoprotein lipase enzymes on the surface of capillary endothelial cells. Lipoprotein lipase hydrolyses the chylomicron triacylglycerols to fatty acids and glycerol. This process allows fatty acids to be oxidised as fuel in muscle or be stored in adipose tissue after being re-esterified to triacylglycerol. The lipoprotein particles remaining after this hydrolysis are rich in cholesterol and are known as chylomicron remnants. These particles are less dense than chylomicrons and bind to the LDL-related protein (LRP) on the surface of liver cells before being internalised (Hey *et al.*, 1998). Once inside the liver, cholesterol is secreted into bile, converted to bile acids, esterified for storage or incorporated into new lipoproteins.

2.1.3 Cholesterol Biosynthesis

In addition to the absorption of dietary cholesterol, the human body also synthesises cholesterol *de novo*. Cholesterol synthesis occurs primarily in the liver although significant amounts are also synthesised in the intestine. A typical adult, eating a low-cholesterol diet, synthesises approximately 800 mg of cholesterol each day. Cholesterol is synthesised from acetoacetyl coenzyme A (acetoacetyl CoA) and acetyl CoA in a sequence of reactions involving 30 enzyme controlled steps, which is known as the mevalonate pathway. The pathway was first elucidated by Konrad Bloch who was awarded the Nobel Prize in Medicine for his work (Bloch, 1965). The first step in the mevalonate pathway is catalysed by an enzyme called 3-hydroxy-3-methylglutaryl coenzyme A (HMG-CoA) synthase and is shown in figure 2.3.

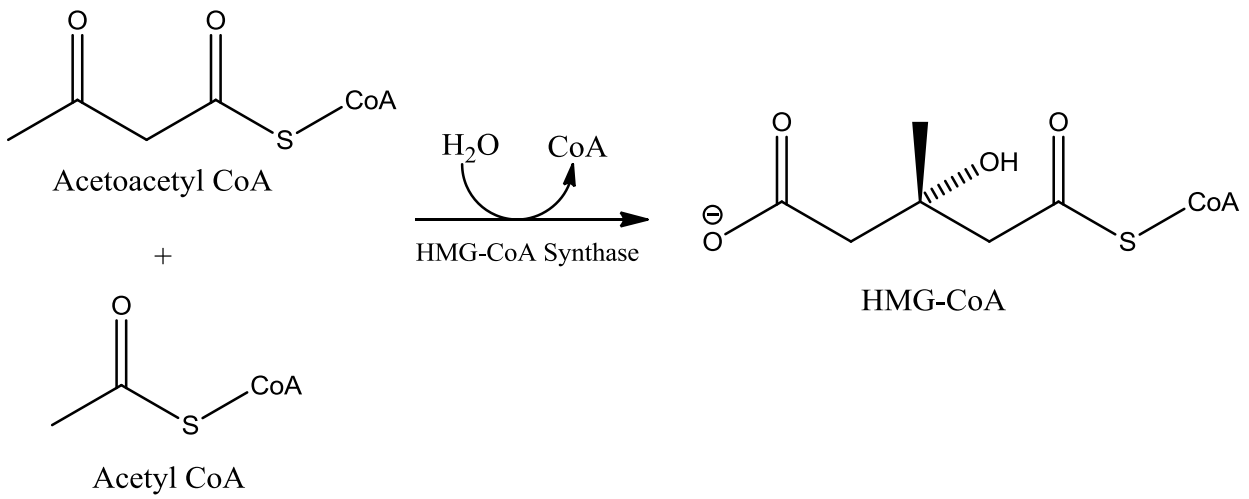

Figure 2.3. Synthesis of HMG-CoA by HMG-CoA synthase.

The second step in the pathway is catalysed by the enzyme HMG-CoA reductase and is the reduction of HMG-CoA to mevalonate. HMG-CoA reductase performs this four electron reduction using two molecules of NADPH as co-factors as shown in figure 2.4. Early studies in yeast determined this step in the biosynthetic pathway to be rate limiting (Bloch, 1965).

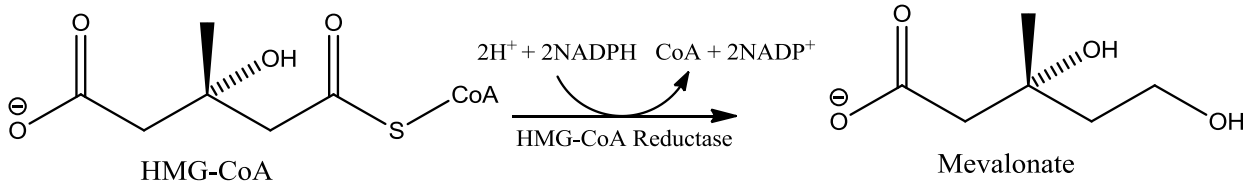

Figure 2.4. The reduction of HMG-CoA to mevalonate by HMG-CoA reductase.

Following the conversion of HMG-CoA to mevalonate, mevalonate is converted to 3-isopentenyl pyrophosphate. This conversion consists of three steps, each of which requires the hydrolysis of ATP, as shown in figure 2.5. Isopentenyl pyrophosphate is an activated molecule which acts as an essential building block for a number of biological molecules. The most notable of such molecules in humans is isopentenyl adenosine which is found in some transfer RNA (tRNA) molecules (Persson *et al.*, 1994).

Isopentenyl adenosine is a cytokinin; these are a group of molecules that are found in plants, where they regulate growth functions. It is also a precursor to a number of other compounds found in plants, for example terpenes, which are volatile compounds made up of two or three isoprene units and are responsible for plant fragrances (Berg *et al.*, 2002).

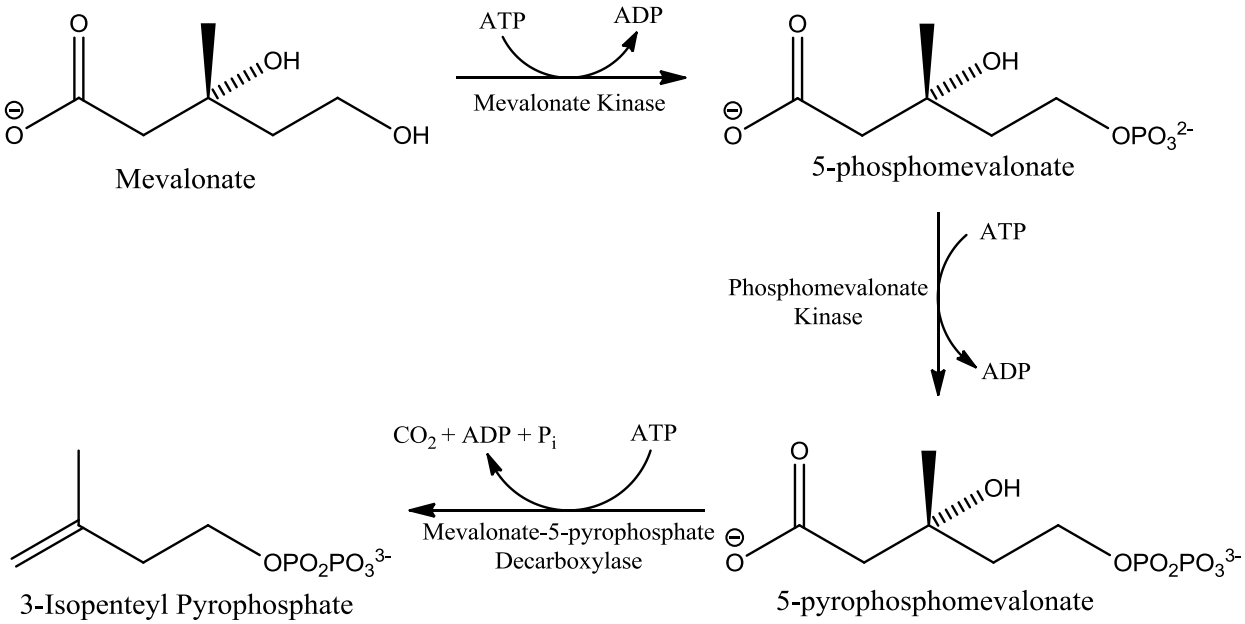

Figure 2.5. The three step conversion of mevalonate to 3-isopentenyl pyrophosphate.

Initially, mevalonate kinase phosphorylates mevalonate kinase to 5-phosphomevalonate. Phosphomevalonate kinase subsequently carries out a further phosphorylation to make 5-pyrophosphomevalonate. Finally, mevalonate-5-pyrophosphate decarboxylase carries out a decarboxylation reaction to leave 3-isopenteyl pyrophosphate.

The next stage in the biosynthesis of cholesterol is the condensation of six isopentenyl pyrophosphate molecules to form squalene. To allow this condensation reaction to occur, isopentenyl pyrophosphate must be converted to dimethylallyl pyrophosphate by the enzyme isopentenyl pyrophosphate isomerase, as shown in figure 2.6(A). Dimethylallyl pyrophosphate forms an allylic carbocation (figure 2.6(B)) which then undergoes a condensation reaction with a molecule of isopentenyl pyrophosphate to form geranyl pyrophosphate (figure 2.6(C)) (Berg *et al.*, 2002).

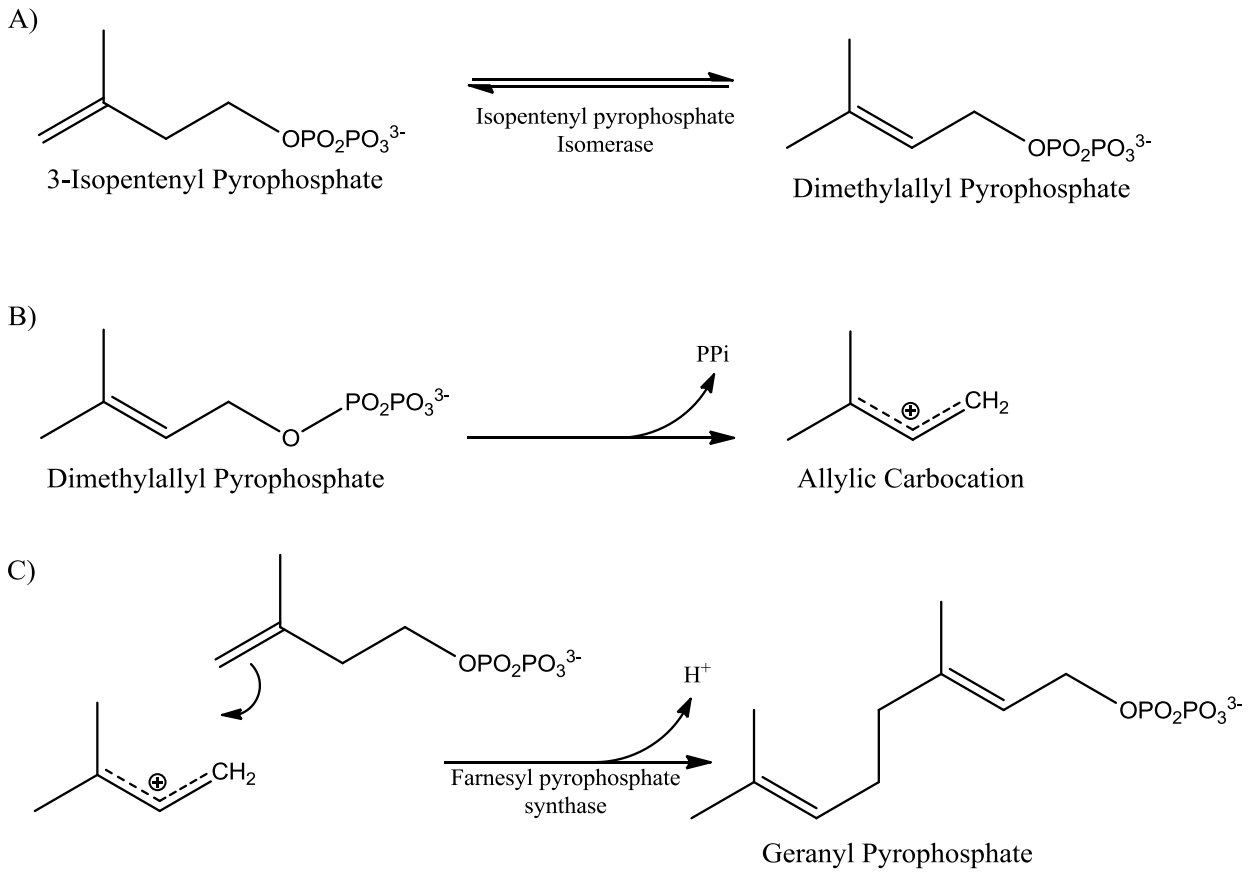

Figure 2.6. Synthesis of Geranyl Pyrophosphate from 3-Isopentyl Pyrophosphate

(A) *Isomerisation reaction carried out by isopentenyl pyrophosphate isomerase, converting 3-isopentenyl pyrophosphate to dimethylallyl pyrophosphate.* ***(B)*** *Formation of an allylic carbocation from dimethylallyl pyrophosphate through loss of pyrophosphate.* ***(C)*** *Condensation reaction between 3-isopentenyl pyrophosphate and the allylic carbocation to form geranyl pyrophosphate, as catalysed by the enzyme farnesyl pyrophosphate synthase.*

Geranyl pyrophosphate condenses with another molecule of isopentenyl pyrophosphate to form farnesyl pyrophosphate (figure 2.7). This reaction is also catalysed by farnesyl pyrophosphate synthase and takes place via the same mechanism of reaction as the synthesis of geranyl pyrophosphate, as shown in figure 2.6(C). Two molecules of farnesyl pyrophosphate then undergo a further condensation reaction to produce one molecule of squalene. This reductive coupling reaction requires the cofactor NADPH and is catalysed by squalene synthase. The synthesis of squalene from isopentenyl pyrophosphate is shown in figure 2.7.

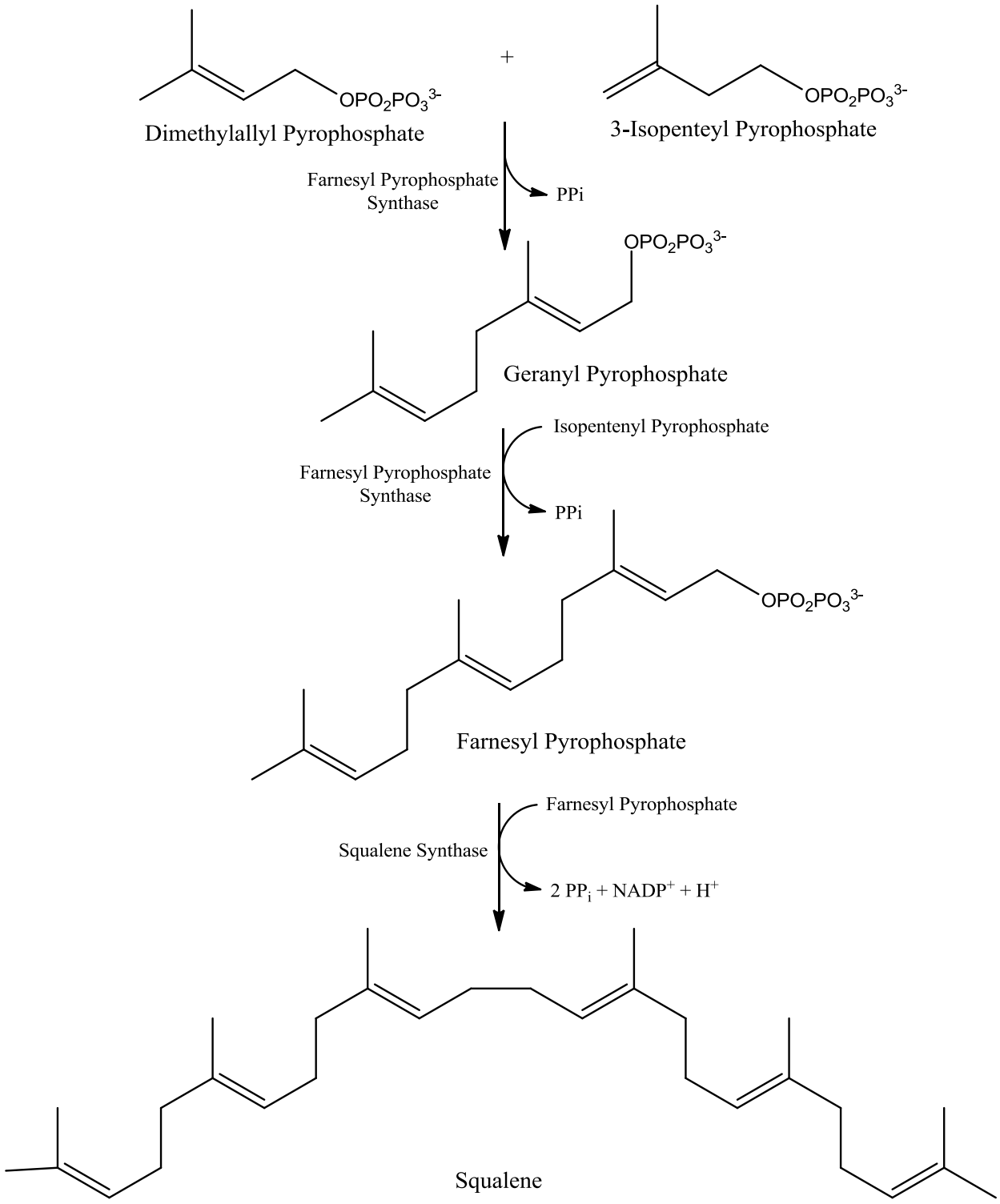

Figure 2.7. Synthesis of squalene from six molecules of isopentenyl pyrophosphate.

These reactions are catalysed by the enzymes farnesyl pyrophosphate synthase and squalene synthase.

Like isopentenyl pyrophosphate, farnesyl pyrophosphate is an important precursor for a number of biological molecules. Dolichols consist of up to twenty isoprene units and play an important role in the addition of oligosaccharides to glycoproteins (Swiezewska and Danikiewicz, 2005). Ubiquinone is an essential electron carrier in the electron transport chain of oxidative phosphorylation and also functions as an antioxidant (Kawamukai, 2002). Farnesyl pyrophosphate is also required for the synthesis of haem A, an iron-porphyrin complex found in the enzyme cytochrome c oxidase (Hederstedt, 2012). Like ubiquinone, cytochrome c plays an essential role in oxidative phosphorylation. Isoprenoid compounds are also often attached to the C-termini of proteins as a means of membrane targeting. The most common attachments are farnesyl or geranylgeranyl units, and their attachment to a protein confers hydrophobic character (Seabra, 1998).

Before squalene can cyclise to form the steroid nucleus of cholesterol it must be activated. Activation is achieved by the formation of squalene epoxide, a process which is catalysed by squalene epoxidase. This reaction requires a further molecule of NADPH as well as a molecule of oxygen. The activated squalene epoxidase is then able to cyclise to form a protosterol cation before a further rearrangement reaction produces lanosterol. The mechanism for the conversion of squalene to lanosterol is shown in figure 2.8. Biosynthesis of the complete cholesterol molecule from lanosterol is a complex process involving a further 19 steps (Risley, 2002).

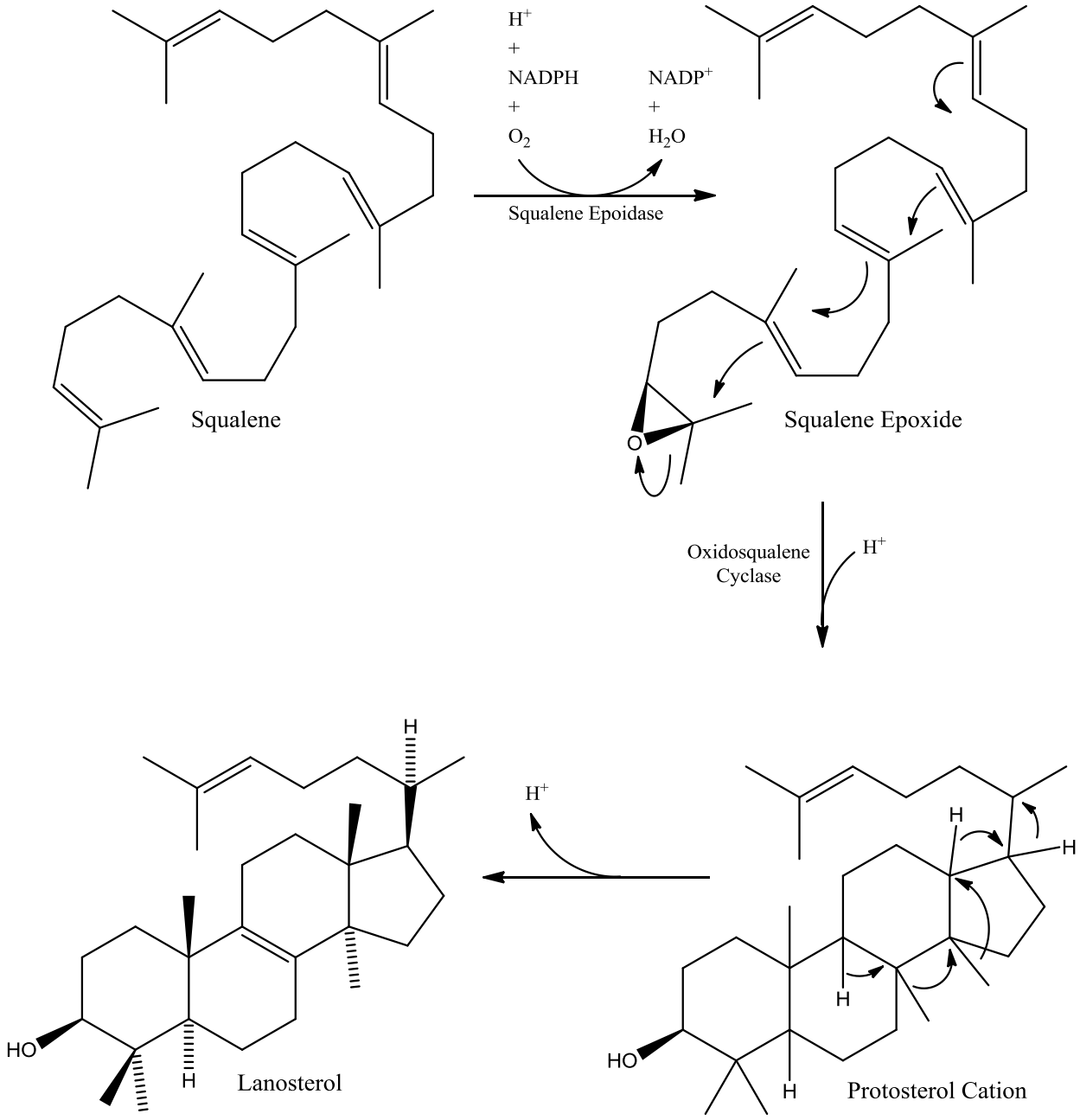

Figure 2.8. Cyclisation of squalene to form lanosterol.

First, squalene is activated by conversion to squalene epoxide as catalysed by squalene epoxidase. Oxidosqualene cyclase then catalyses the cyclisation and rearrangement of squalene epoxidase to lanosterol.

In addition to its role in regulating membrane fluidity, cholesterol is the starting point for the biosynthesis of a number of different compounds. One large group of such compounds is the steroid hormones. The synthesis of steroid hormones first requires the cleavage of the side chain from cholesterol to form pregnenolone. From pregnenolone, a wide range of hormones including progesterone, cortisol and testosterone are synthesised (Berg *et al.*, 2002). Another major type of compound synthesised from cholesterol is bile salt. Bile salts are excreted by the gall bladder in order to solubilise dietary lipids (section 2.1.2)(Mikov and Fawcett, 2006). The photolysis of 7-dehydrocholesterol by ultraviolet light produces previtamin D_3, of which a deficiency in childhood causes rickets or, in adulthood, causes osteomalacia (Holick *et al.*, 1977).

2.1.4 Cholesterol Transport

Cholesterol that has been synthesised in the liver and intestine is transported around the body in lipoprotein particles. As discussed in section 2.1.2, these particles consist of a lipid core surrounded by a hydrophilic shell made up of polar lipids and proteins. The particles are classified by density and the least dense forms, chylomicrons and chylomicron remnants, are responsible for the transport of dietary cholesterol and lipids to the liver.

Cholesterol is transported away from the liver as part of very low density lipoprotein (VLDL) particles. These particles are similar in density to chylomicron remnants but differ in the make-up of their protein shell. Whereas the protein shell of chylomicrons is primarily made up of apo B-48, the protein shell of VLDL contains apo B-100. Apo B-100 is a very large protein, 513 kD in size. Both apo B-48 and apo B-100 are encoded by the same gene but the transcribed mRNA undergoes alternative splicing in order to generate the two different proteins. Chylomicrons and VLDL also contain other apoproteins which are involved in receptor binding (Betteridge and Morrell, 2003).

VLDL particles are synthesised in the rough endoplasmic reticulum (ER) of hepatic cells which is the same location at which cholesterol synthesis occurs (Gordon *et al.*, 1995). They are excreted from the cell via the Golgi apparatus and behave in a similar way to chylomicrons in the blood. VLDL triacylglycerols are hydrolysed by lipoprotein lipase on the surface of endothelial cells, although the rate of hydrolysis is lower in VLDL than in chylomicrons probably due to the smaller size of VLDL (Betteridge and Morrell, 2003). After the hydrolysis of the triacylglycerol content of VLDL, cholesterol rich particles known as intermediate density lipoproteins (IDL) remain. Some IDL particles are taken up for processing by the liver via the low density lipoprotein (LDL) receptor. The triacylglycerol content of the remaining IDL particles is further hydrolysed by hepatic lipase to form low density lipoprotein particles.

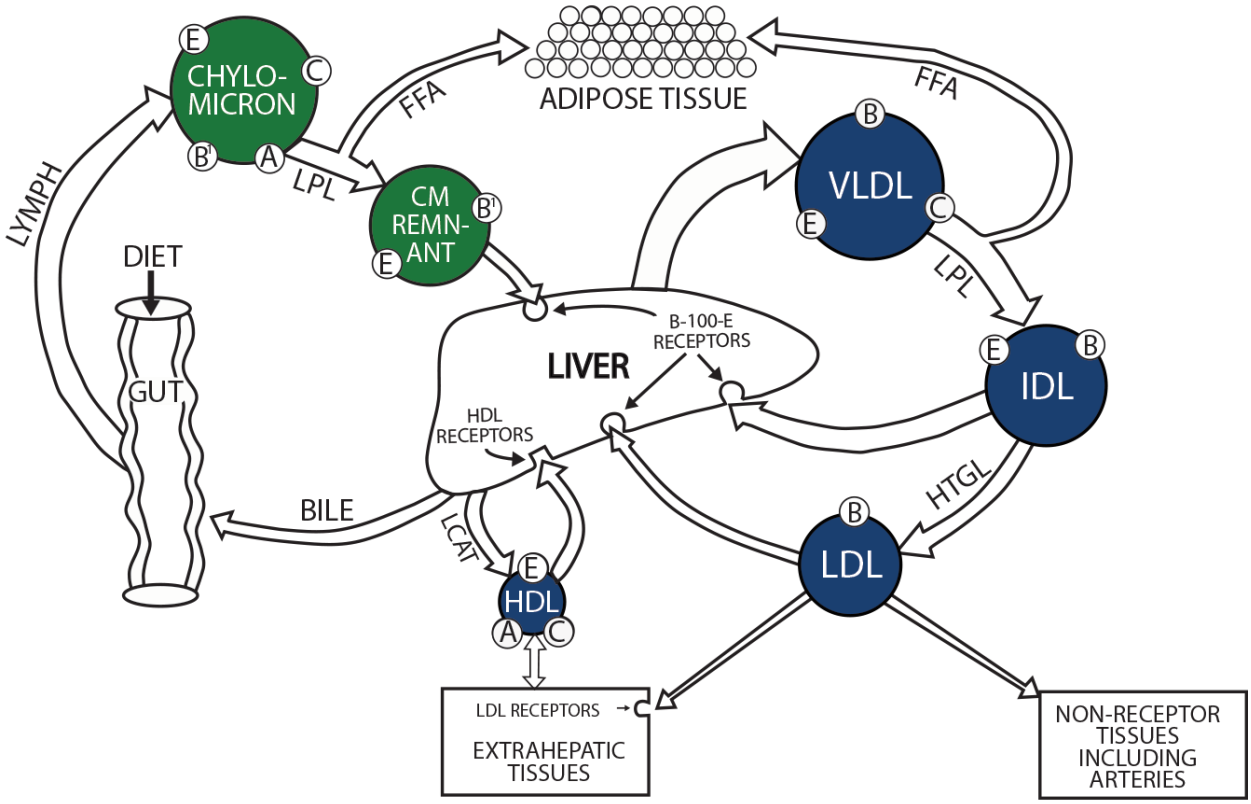

Figure 2.9. The lipoprotein pathway.

Dietary cholesterol is transported to the liver in chylomicrons and chylomicron remnants. Endogenous cholesterol leaves the liver in very low density lipoprotein particles which are converted to intermediate density and low density lipoprotein particles as they lose triglycerides.

LDL is the primary carrier of cholesterol in the blood. Like VLDL and IDL, the shell of LDL contains apo B-100 but LDL is lacking the other lipoproteins present in different lipoprotein particles. LDL is responsible for delivering cholesterol to peripheral tissues where it interacts with the LDL receptor and is internalised. LDL receptor molecules are found on the surface of the cell in areas called coated pits. When LDL particles interact with the receptor, the coated pits invaginate to form coated vesicles containing the lipoprotein particles. These vesicles then fuse with lysosomes in the cell where esterified cholesterol from LDL is hydrolysed to free cholesterol and the apoproteins are broken down to amino acids so that both can be used by the cell. The LDL receptor proteins are then recycled and return to the surface of the cell in new coated pits (Brown and Goldstein, 1986).

The final type of lipoprotein particle is high density lipoprotein (HDL). HDL is the densest of all of the lipoproteins and, instead of apo B-100 or apo B-48, contains apo A-I or apo A-II in its hydrophilic shell. Nascent HDL is secreted by the liver and intestine as bilayer discs containing apo A and phospholipids. The role of these particles is to take up free cholesterol from cell membranes undergoing turnover as well as taking up free cholesterol liberated from dead cells and other lipoproteins. An enzyme called lecithin cholesterol acyltransferase (LCAT), which circulates with HDL, is responsible for esterifying this free cholesterol so it can be incorporated into the lipid core of the mature HDL particle. The esterified cholesterol can then be shuttled to VLDL or LDL due to the action of a cholesterol ester transfer protein (CETP), which is contained within the HDL particle.

HDL is responsible for returning excess cholesterol from peripheral tissue to the liver for excretion in a process known as reverse cholesterol transport (Glomset, 1968). In this process, surplus cholesterol is absorbed from the plasma membrane by a low molecular weight type of HDL called prebeta-1 HDL. The efflux of cholesterol is dependent upon the action of a protein called cholesterol efflux regulatory protein (CERP). CERP is coded for by the gene ABCA1, a member of the ATP-binding cassette (ABC) family (Kane and Malloy, 2012). These genes typically encode proteins which transport substances across cell membranes using the energy produced by the hydrolysis of ATP. This excess, free cholesterol is esterified by LCAT in the prebeta-1 HDL particle and the majority is transferred to the lower density lipoproteins VLDL and LDL before eventually returning to the liver. The uptake of the remaining HDL particles by the liver is mediated by the scavenger receptor class B type 1 (SR-B1) (Liadaki *et al.*, 2000).

2.1.5 HMG-CoA Reductase

HMG-CoA is responsible for catalysing the second step in the mevalonate pathway. This is the reduction of HMG-CoA to mevalonate which requires two molecules of the cofactor NADPH. The reaction takes place in three stages: first HMG-CoA is reduced to mevaldyl-CoA; mevaldyl-CoA then decomposes to form mevaldehyde which is then reduced to mevalonate. It is a 97 kD enzyme containing 888 amino acid residues and is associated with the ER (Brown and Simoni, 1984) although it has also been found in the matrix of peroxisomes (Keller *et al.*, 1986). The N-terminal, ER bound domain consists of eight membrane-spanning helices separated by short loops and is encoded by amino acid residues 1-425 (Roitelman *et al.*, 1992). The remaining 462 residues make up the catalytic domain of the enzyme. This region is capable of catalysis without the presence of the ER binding domain. The main function of the N-terminal binding domain in the cell is in regulation of the half-life of the enzyme as will be discussed in section 2.1.6 (Gil *et al.*, 1985).

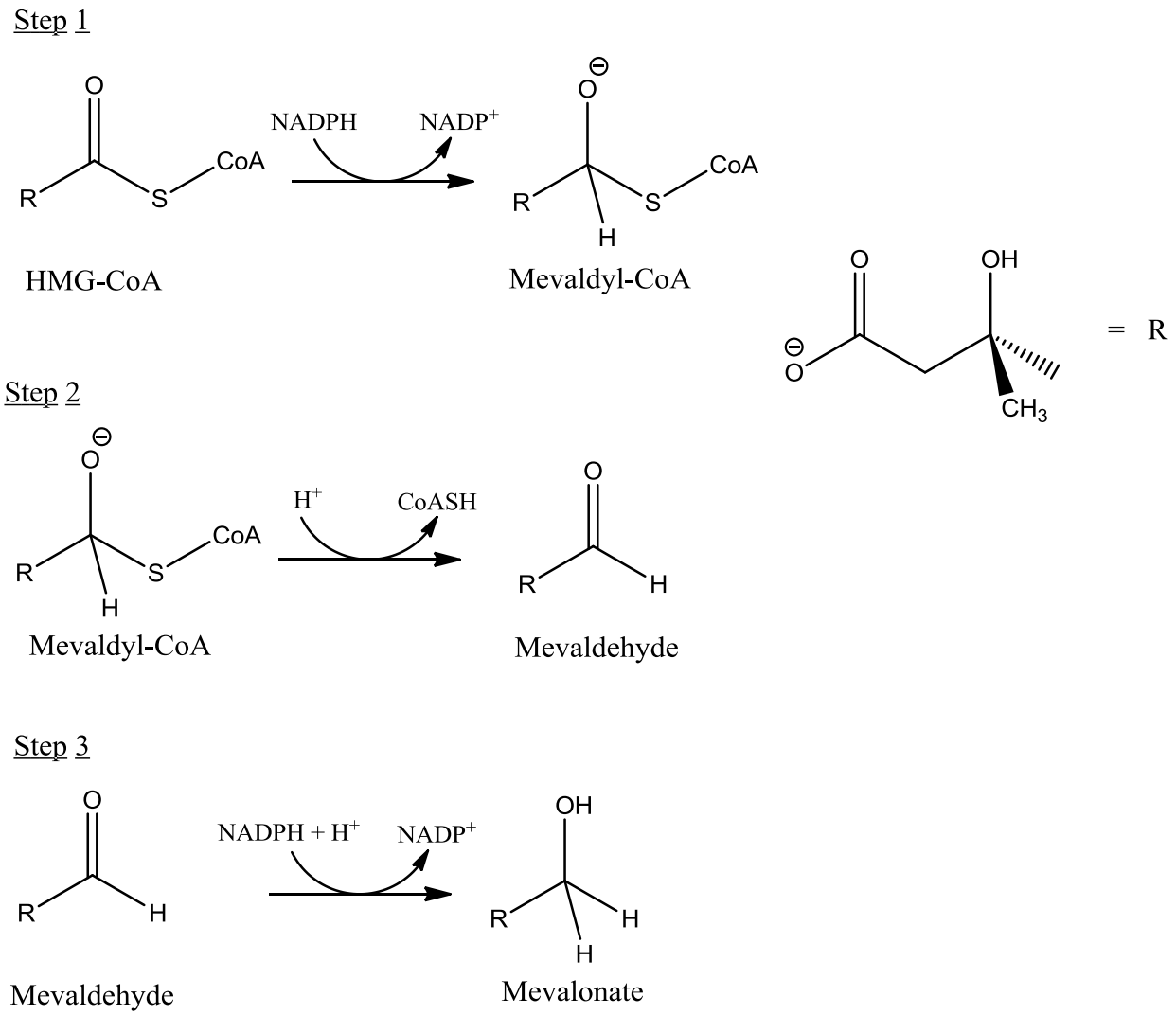

Figure 2.10. The reduction of HMG-CoA to mevalonate by HMG-CoA reductase.

In step one, NADPH transfers a hydride ion to HMG-CoA forming mevaldyl-CoA. In step two, mevaldyl-CoA decomposes, losing CoA thiol, to form mevaldehyde. In step three, a second hydride transfer reduces mevaldehyde to mevalonate.

The structure of the catalytic domain of HMG-CoA reductase has been solved by x-ray crystallography (Istvan *et al.*, 2000). In this structure, the catalytic domains form a tightly associated tetramer with the active sites of the enzyme located at the interface of two monomers. The catalytic region of the enzyme can be broken down into three different domains. The small N-domain is α-helical and acts as a linker between the catalytic domain and the ER bound N-terminal domain of the full enzyme. The large L-domain and small S-domain make up the enzyme's active site. The L-domain contains a fold which is

prism-shaped with a 27 residue α-helix at its core and unique to HMG-CoA reductase. The S-domain inserts into the L-domain to form the NADPH binding site. This creates an α/β sandwich fold that differs from the Rossman fold which is commonly found in NAD(P) dependent enzymes. All three of these domains are responsible for interacting with other monomers of HMG-CoA reductase when forming the active sites of the enzyme through dimerisation.

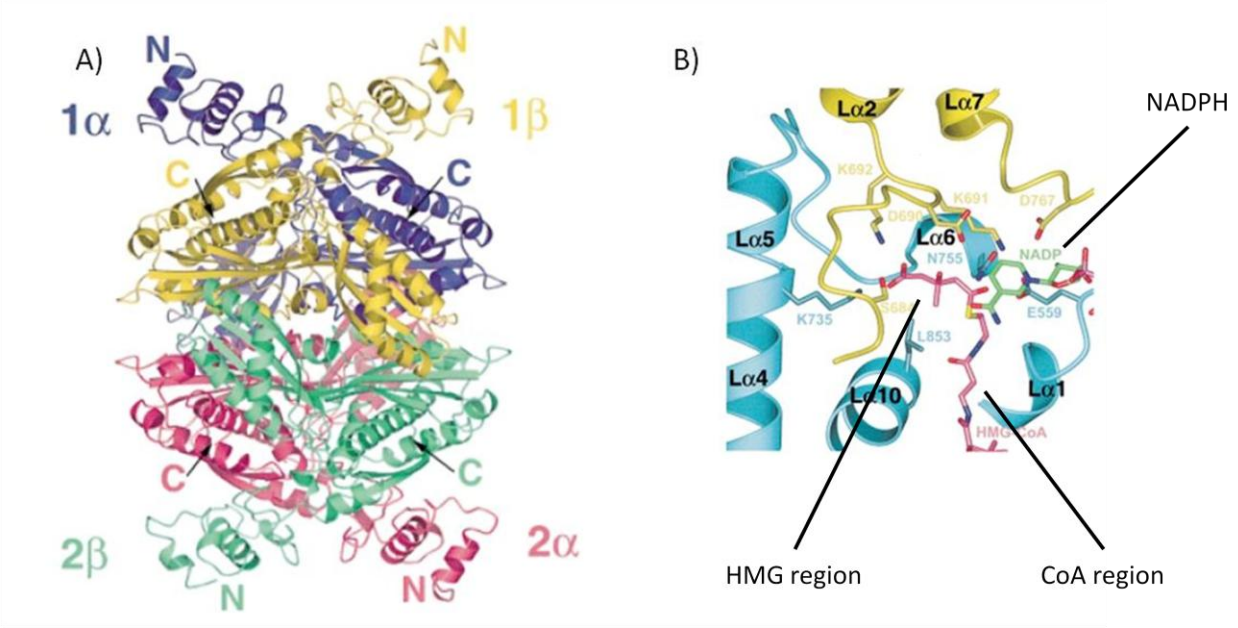

Figure 2.11. Ribbon diagrams of human HMG-CoA reductase.

(A) *The structure of the HMG-CoA reductase tetramer. Dimer 1 consists of monomers 1α (purple) and 1β (yellow) and dimer 2 consists of monomers 2α (pink) and 2β (green).* ***(B)*** *The active site of human HMG-CoA reductase. Residues from monomer α are in yellow and residues from monomer β are in blue. HMG-CoA is shown in magenta and NADPH is shown in green. This figure is taken from Istvan et al. (2000).*

The structure of the active site of HMG-CoA reductase has been solved with various combinations of substrates and products bound (Istvan *et al.*, 2000). The CoA portion of HMG-CoA binds to the active site in an extended conformation with the pantothenic acid region buried deep inside the structure of the enzyme, as can be seen in figure 2.11. The interactions between HMG-CoA reductase and CoA are all formed by the L-domain of a single monomer with the exception of one interaction with a tyrosine residue (Y479) from the N-domain of the adjacent monomer. This single interaction appears to be responsible for closing the extended binding site by forming a hydrophobic shield over the adenine base

of CoA. In contrast, the majority of the interactions between NADPH and the enzyme originate from the S-domain of the second monomer. The crystal structures obtained by Istvan *et al.* suggest that NADPH binding results in a conformational change in the c-terminus of the enzyme which completely closes the active site. The HMG domain of HMG-CoA binds to the enzyme in a pocket located between the L-domain of one monomer and the S-domain of another. It forms interactions with both monomers and most importantly binds to the '*cis*-loop' which bends over the top of the molecule, positioning key catalytic residues in their required positions.

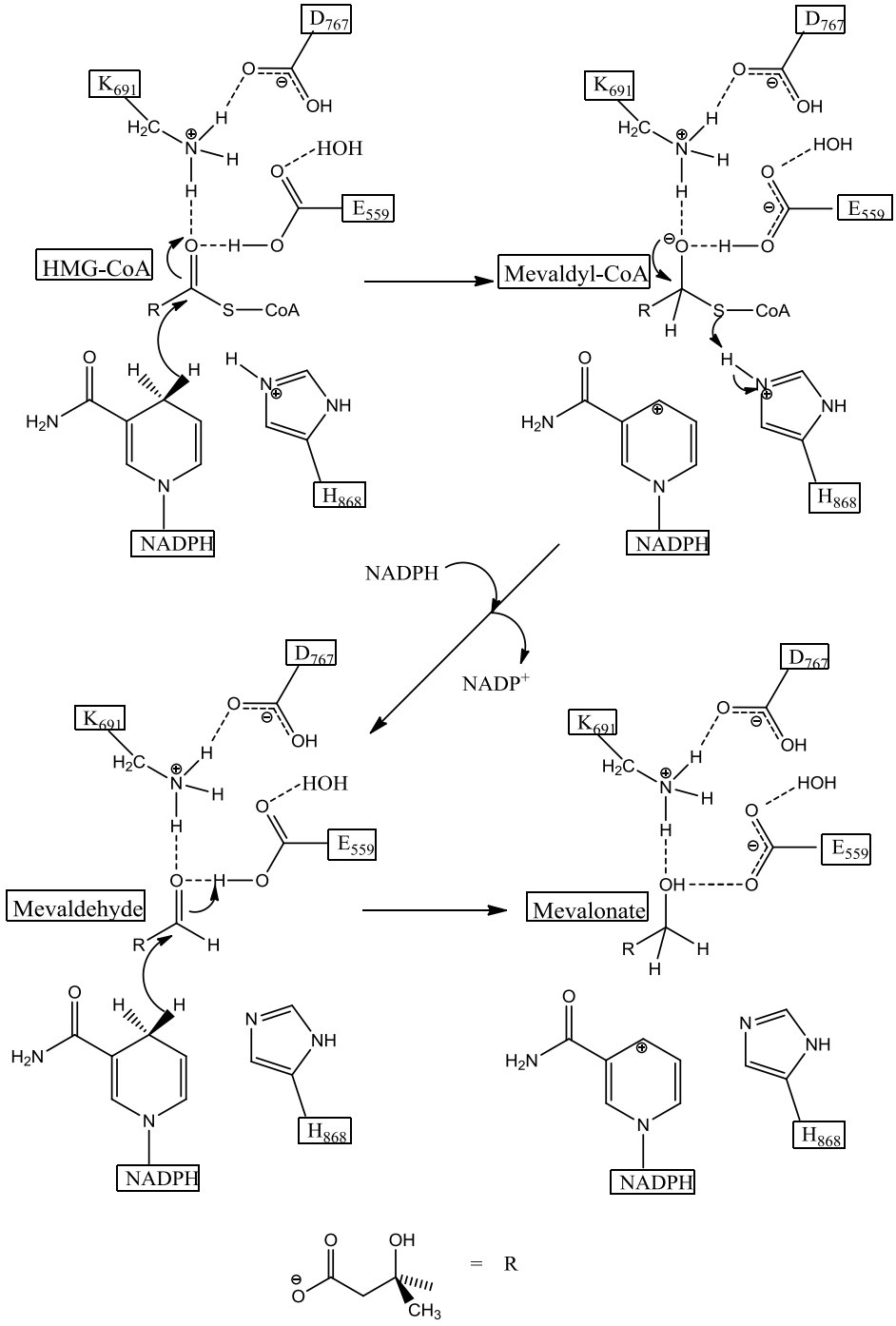

Figure 2.12. The proposed mechanism of catalysis by HMG-CoA reductase.

The negatively charged oxygen of mevaldyl-CoA is stabilised by the side chain of K691. The closing of the C-terminal flap of HMG-CoA reductase positions H866 close to the CoA thiol allowing it to donate a proton in the second step of the reaction. The proximity of E559 to D767 is likely to raise the pK_a of the glutamic acid sufficiently for its side chain to be protonated. This would allow E559 to act as a proton donor for mevaldehyde. D767 also acts to stabilise the side chain of K691 (Istvan and Deisenhofer, 2000).

2.1.6 Regulation of Cholesterol Homeostasis

Due to the potential threats that cholesterol can pose to the body, which will be discussed in section 2.1.7, cholesterol homeostasis is one of the most tightly regulated biological systems. As the rate-limiting enzyme in the mevalonate pathway, HMG-CoA reductase is itself one of the most highly regulated enzymes known (Goldstein and Brown, 1990). It is subject to control on several levels including over its rate of transcription, rate of translation, rate of degradation and level of activity. This control is mediated by a number of different molecules and enzymes which also exert control over other important proteins involved in cholesterol homeostasis, including HMG-CoA synthase and the LDL receptor. The different mechanisms involved have been studied in detail by Michael Brown and Joseph Goldstein who were awarded the Nobel Prize for Medicine for their work (Brown and Goldstein, 1986).

The rate of transcription of the HMG-CoA reductase gene is controlled by the sterol regulatory element binding protein (SREBP) pathway. The SREBP is a transcription factor that is associated with the ER or nuclear membrane in its inactive state (Wang *et al.*, 1994). The protein consists of an N-terminal transcription factor domain and a C-terminal regulatory domain, both cytosolic, separated by two membrane spanning helices and a hydrophilic loop projecting into the ER lumen (Nohturfft *et al.*, 1998). This means that, in order to enter the nucleus and initiate transcription of HMG-CoA reductase mRNA, the transcription factor domain of SREBP must be released from its membrane association. This release is controlled by a protein called SCAP (originally standing for SREBP cleavage-activating protein).

In the presence of cholesterol, SCAP and SREBP are both associated with the ER, with the cytosolic C-terminal domain of SCAP interacting with the regulatory domain of SREBP (Sakai *et al.*, 1997). However, when cellular cholesterol levels drop, the SCAP/SREBP complex moves to the Golgi complex. This movement is controlled by the interaction of SCAP with the copII coat protein complex. A sequence of six amino acids known as MELADL that is located on a cytosolic loop of the SCAP protein interacts with the sec24 component of the copII complex (Sun *et al.*, 2005). The copII complex then causes the formation of a vesicle containing the SCAP/SREBP complex by budding from the ER, this 'copII coated vesicle' then moves on to the Golgi (Rothman and Orci, 1992). Here, the luminal loop of SREBP is cleaved by a membrane associated protease called site-1 protease (S1P). This allows the release of the transcription factor domain by a second cleavage, in the membrane spanning helix, by site-2 protease (S2P) (Brown and Goldstein, 1997).

In the presence of cholesterol or oxysterol, the SCAP/SREBP complex does not interact with the copII complex and remains in the ER membrane. The disruption of SREBP export is mediated by ER retention proteins called insigs. When insigs bind to SCAP, the loop of SCAP containing the MELADL sequence, which interacts with the copII complex, undergoes a conformational change (Brown *et al.*, 2002). This change stops the copII complex from accessing the MELADL sequence and therefore blocks export of SCAP/SREBP to the Golgi. Cholesterol and oxysterol stimulate the binding of insigs to SCAP in different ways. Cholesterol binds directly to the membrane embedded domain of SCAP to stimulate insig binding whereas oxysterols bind to the insig stimulating it to bind to SCAP (Adams *et al.*, 2004).

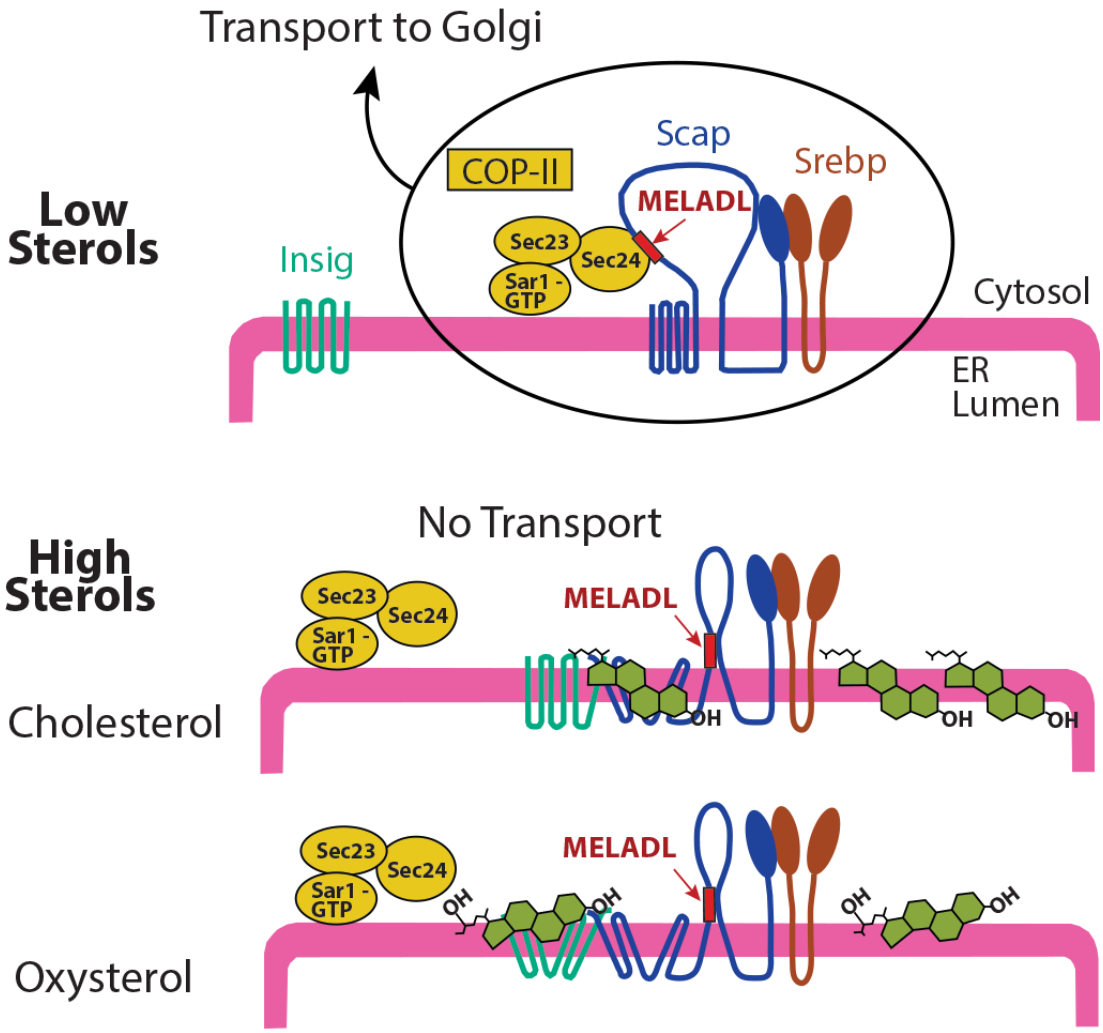

Figure 2.13. Mechanism of regulation of HMG-CoA reductase transcription.

When sterol concentration is low, the SCAP-SREBP complex moves to the golgi where the SREBP is cleaved enabling it to activate transcription. Cholesterol and oxysterol mediate insig binding to SCAP blocking the access of Cop-II to the MELADL region.

When SREBP enters the nucleus it binds to a short DNA sequence called a sterol regulatory element (SRE). The SRE is located on the 5' side of the HMG-CoA reductase gene and binding of SREBP activates transcription of the gene. SREs have also been identified downstream of the genes for the LDL receptor (Sudhof *et al.*, 1987), HMG-CoA synthase (Dooley *et al.*, 1998) and insig-1 (Yabe *et al.*, 2002). This results in both an increase in cholesterol biosynthesis and an increase in cholesterol uptake in response to a fall

in cellular cholesterol levels. The SREBP activation of insigs means that SREBPs trigger the synthesis of their own inhibitor, thus providing a further level of control.

HMG-CoA reductase and SCAP have similar topologies, each containing a cytosolic, C-terminal domain responsible for function as well as eight, membrane-spanning helices. In fact, the membrane spanning domains of both proteins bind to insigs in a sterol-controlled manner (Sever *et al.*, 2003b). However, whereas they act to stabilise SCAP, insigs are responsible for triggering the rapid degradation of HMG-CoA reductase. The sterol responsible for the binding of HMG-CoA to insig is 24,25-dihydrolanosterol, this is the first intermediate in the mevalonate pathway after lanosterol (see section 2.3). The insig molecules which bind to HMG-CoA reductase also associate with a membrane-bound ubiquitin ligase called gp78 that, in turn, associates with Ubc7, a ubiquitin conjugating enzyme (Song *et al.*, 2005). These two enzymes work together to initiate polyubiquitination of two cytosolic lysine residues in the N-terminal domain of HMG-CoA reductase. Ubiquitination of the reductase acts as a signal for the protein to be extracted from the ER membrane. This is carried out by an ATPase called VCP/p97, which is also associated with gp78, and a number of its cofactors (Kostova *et al.*, 2007). The mechanism by which this extraction occurs remains unclear although it is known that the nonsterol isoprenoid geranylgeraniol increases the rate of extraction (Sever *et al.*, 2003a). Geranylgeraniol is derived from farnesyl pyrophosphate which is an intermediate in the mevalonate pathway. Once extracted from the ER membrane, HMG-CoA reductase is transported to proteasomes where it is degraded.

In addition to mechanisms controlling the amount of HMG-CoA reductase present in the cell, the level of activity of the enzyme can also be controlled. The activity is controlled through the process of phosphorylation. HMG-CoA reductase phosphorylation is carried out by an enzyme called AMP-activated protein kinase (AMPK) (Omkumar *et al.*, 1994). AMPK is allosterically activated by AMP but not by ATP. Since AMP and ATP compete for the same binding site on AMPK, this means that the kinase is sensitive to the AMP:ATP ratio in the cell. This property of AMPK means that it becomes activated when the cell undergoes periods of metabolic stress (Hardie *et al.*, 2006). In these conditions, AMPK is responsible for the phosphorylation of serine 872 of HMG-CoA reductase. This phosphorylation inhibits the activity of the reductase and, although the mechanism of inhibition is not known, it is thought that this is achieved by either decreasing the NADPH affinity of the enzyme or by stopping the proper closure of the C-terminal flap over the active site (Tabernero *et al.*, 1999). When levels of ATP increase again, HMG-CoA reductase is dephosphorylated by the enzyme protein phosphatase 2A (PP2A) (Janssens and Goris, 2001). This dephosphorylation fully restores the catalytic activity of the reductase.

The rate of translation of HMG-CoA reductase mRNA is also tightly controlled. This control is known to be mediated by a nonsterol isoprenoid (Goldstein and Brown, 1990). However, the identity of this molecule and the mechanism by which the rate of translation is controlled is not known, although it is likely that the mechanism involves a complex, 5'-untranslated region of the reductase mRNA.

The combination of all of these mechanisms of control means that the HMG-CoA reductase activity in a cell can vary over a 200-fold range. Numerous other enzymes in the mevalonate pathway are controlled by the same or similar mechanisms ensuring the cholesterol needs of the cell can be met quickly when

required. Modulation of this control by a range of different metabolites found in, or derived from, the mevalonate pathway also helps to stop the build-up of undesirable intermediates.

2.1.7 Hypercholesterolemia, Atherosclerosis and Coronary Heart Disease

The insolubility of cholesterol is essential for its function in controlling plasma membrane fluidity. However, this insolubility means that cholesterol can be a potentially dangerous and even fatal molecule. Accumulation of cholesterol in the cell can have a number of negative consequences.

Excess free cholesterol can be incorporated into the cell membrane, reducing fluidity to below optimum levels. This can have negative effects on membrane proteins, which require a degree of conformational flexibility (Yeagle, 1991). This can affect proteins responsible for diverse cellular functions including transport and signalling. Reduced membrane fluidity can not only have negative effects for the cell membrane but can also affect the membranes of different organelles. High levels of free cholesterol can also result in the formation of intracellular cholesterol crystals (Kellner-Weibel *et al.*, 1999). These needle-shaped crystals are likely to physically disrupt intracellular structures. Finally, excess free cholesterol can be oxidised to oxysterols which may have cytotoxic effects (Brown and Jessup, 1999). All of these processes are toxic to the cell and can cause cell death.

Due to the dangers of the accumulation of free cholesterol, healthy cells are able to regulate their cholesterol content as discussed in section 2.6. This is achieved by the inhibition of cellular cholesterol synthesis, reduction in uptake of LDL cholesterol and the export of excess cholesterol via lipoprotein particles and reverse cholesterol transport. However, while this export of cholesterol from the cell to the blood stream is beneficial for the cell, the resulting increase in concentration of plasma LDL can have serious consequences.

Excess plasma LDL undergoes oxidation to form oxidised LDL (oxLDL). The oxLDL is taken up by macrophages which are unable to process it. This results in the formation of engorged, cholesterol rich foam cells. These foam cells become lodged in the walls of blood vessels leading to an accumulation of cholesterol in the lumen. This process is known as atherosclerosis (Levine *et al.*, 1995). The build up of cholesterol is called an atherosclerotic plaque and the sizes of these plaques increase over time in patients suffering from atherosclerosis. This leads to a narrowing of the blood vessel which can limit the blood supply to different tissues. In advanced cases this can lead to ischemia of different tissues and, even more seriously, coronary thrombosis of the coronary artery causing heart attacks. In some cases, parts of the atherosclerotic plaque can break off causing thromboembolisms such as strokes (Davies *et al.*, 1993).

While LDL is responsible for the negative consequences of high cholesterol levels, HDL plays a crucial role in minimising these effects. The primary cholesterol reducing role of HDL is in reverse cholesterol transport as discussed in section 2.1.4 (Kane and Malloy, 2012). However, it is also likely that HDL has antioxidant capabilities which can help to reduce the amount of oxLDL and therefore slow the

development of atherosclerotic plaques. This ability is thought to be conferred by the enzyme paraoxonase which is associated with the HDL particle and is able to hydrolyse oxidised phospholipids (Navab *et al.*, 1996). It is also possible that HDL has further atheroprotective abilities such as its ability to stop oxLDL inhibiting endothelial vasodilation (Stein and Stein, 1999). These protective capabilities mean that, as a marker for coronary heart disease risk, the LDL:HDL ratio is used rather than the total plasma cholesterol concentration.

While high cholesterol and atherosclerosis in most patients is caused by poor diet and lack of exercise, it can also have a genetic basis. Familial hypercholesterolemia (FH) is typically caused by a mutation in the gene encoding the LDL receptor (Brown and Goldstein, 1974), although it can also be caused by a mutation in the gene for apo B (Innerarity *et al.*, 1990). Heterozygous sufferers of the disease have one faulty copy of the LDL receptor and typically have plasma cholesterol levels of around 300 mg dl^{-1} (compared to < 200 mg dl^{-1} in healthy individuals) (Berg *et al.*, 2002). Heterozygous FH affects approximately 1 in 500 people around the world (Rader *et al.*, 2003). The elevated blood LDL levels in the disease lead to the deposition of cholesterol, causing nodules called xanthomas, in the skin and tendons. More seriously, excess LDL is oxidised to oxLDL leading to the development of atherosclerotic plaques and many sufferers of heterozygous FH experience premature cardiovascular disease. Homozygous FH is much rarer, affecting only around 1 in 1,000,000 people worldwide. Blood cholesterol levels in homozygotes are around 680 mg dl^{-1} and the majority of sufferers die of coronary artery disease as children.

Murray and Lopez estimated that, in 1990, ischaemic heart disease, i.e. heart disease caused by reduced blood flow to the heart muscle, was the leading cause of death worldwide (Murray and Lopez, 1997). In developed countries cardiovascular disease is a factor in 38-42 % of deaths (White, 1995), although this figure is closer to 15 % in developing nations (Murray and Lopez, 1997). Atherosclerosis caused by high cholesterol levels is a major contributor to these conditions and it has been shown that a ten percent reduction in cholesterol levels is associated with a reduction in the incidence of coronary heart disease of between twenty to thirty percent (Scandinavian Simvastatin Survival Group, 1994). Finding ways of successfully reducing the cholesterol levels of patients at risk of coronary heart disease is therefore extremely desirable.

The most effective way to maintain low cholesterol levels is through a healthy diet and regular exercise. Low fat diets in particular are recommended to patients with high cholesterol levels although there is evidence to suggest that diets rich in unsaturated fats and low in saturated and trans fats help to lower the LDL:HDL ratio in the blood (Mensink *et al.*, 2003). Administration of hypolipidaemic drugs has been shown as an alternative method of reducing cholesterol levels (Betteridge *et al.*, 1993). These drugs include: bile acid binding resins, fibric acid derivatives, HMG-CoA reductase inhibitors, nicotinic acid derivatives, probucol and omega-3 marine triglycerides. Inhibitors of HMG-CoA reductase, which are known as statins, are proven to reduce coronary heart disease and have fewer adverse effects than other hypolipidaemic agents (Scandinavian Simvastatin Survival Group, 1994).

2.1.8 Statins

The impact of high cholesterol levels on health has been known for some time. The fact that the majority of the cholesterol in the body is synthesised *de novo* means that inhibiting this synthesis is an ideal course of treatment for high cholesterol. The role of HMG-CoA reductase in catalysing the rate-limiting step in cholesterol synthesis made it a 'prime target for the development of a pharmacological intervention' (Endo, 1985). The first HMG-CoA reductase inhibitor was actually discovered by two groups independently in 1976 (Endo and Kuroda, 1976, Brown *et al.*, 1976). Compactin, as it was named, was isolated from the fungi *Penicillium citrinum* and *Penicillium brevicompactum*.

Compactin, like all statins, contains an HMG-like moiety connected to a ring system. It is a competitive inhibitor of HMG-CoA reductase although it has a 10,000-fold higher affinity for the enzyme than the natural substrate, HMG-CoA (Endo, 1985). This high potency and lack of effects on other enzymes made statins ideal as a potential treatment for high cholesterol. This led to the discovery of a range of other HMG-CoA reductase inhibitors, typically isolated from other species of fungus (Endo, 1979, Albers-Schonberg *et al.*, 1981). Compactin itself was never marketed as a drug due to adverse effects in animal studies. The first statin drug to be approved for use was lovastatin.

Statins are usually divided into two classes: type 1 statins are derived from fungi and resemble the substituted decalin ring structure of compactin whereas type 2 statins are completely synthetic and typically contain much larger cyclic groups attached to the HMG-like moiety. The structure of HMG-CoA reductase bound to a number of different statins has been solved by x-ray crystallography (Istvan and Deisenhofer, 2001). Statins bind to the reductase enzyme in the open, acid conformation rather than the lactone form. This conformation closely resembles the HMG region of HMG-CoA, the natural substrate of the enzyme.

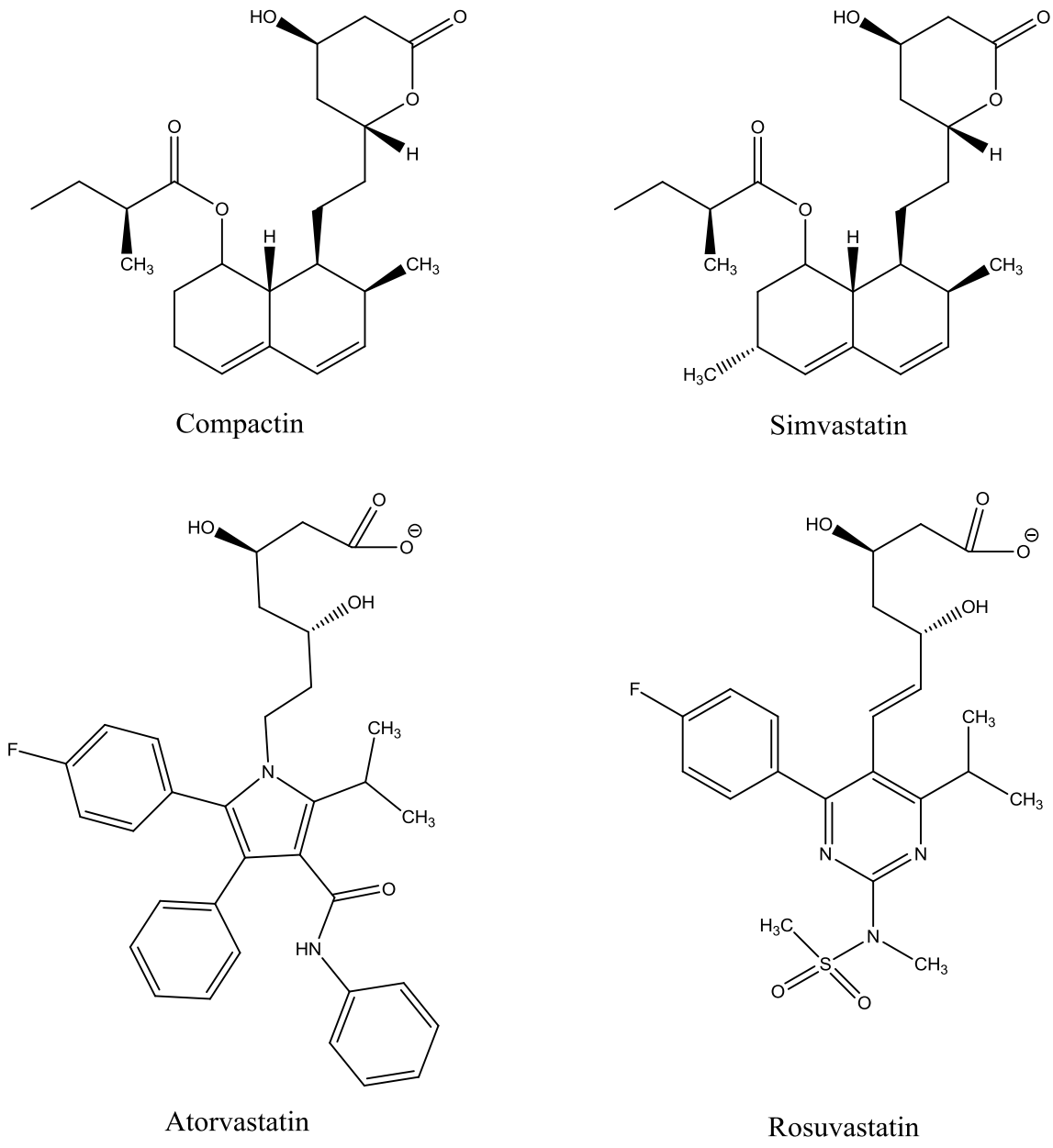

Figure 2.14. Structures of four statin compounds.

Compactin and simvastatin are type-I statins, both featuring the decalin ring structure. These are administered in the cyclic, lactone form. Atorvastatin and rosuvastatin are type-II statins with synthetic ring structures. These compounds are administered in an open, carboxylic acid form.

Kinetic studies show that statins are competitive inhibitors of HMG-CoA reductase with respect to HMG-CoA but not with respect to NADPH (Endo *et al.*, 1976). This finding is supported by the statin-bound

crystal structures that show the HMG-like moiety of each statin binding to the HMG binding site of the enzyme (Istvan and Deisenhofer, 2001). The bulky, hydrophobic regions of the statins do not resemble the structure of CoA and the crystal structures show that they do not bind to the CoA binding site. Instead, these regions occupy a 'shallow groove' which is created by a rearrangement of the C-terminal region of HMG-CoA in response to statin binding (Istvan, 2002). There is no interaction between statins and the NADPH binding site which further supports the earlier kinetic data. Statins form interactions with a number of key catalytic residues including a polar interaction with K691 and a hydrogen bond network with K691, E559 and D767.

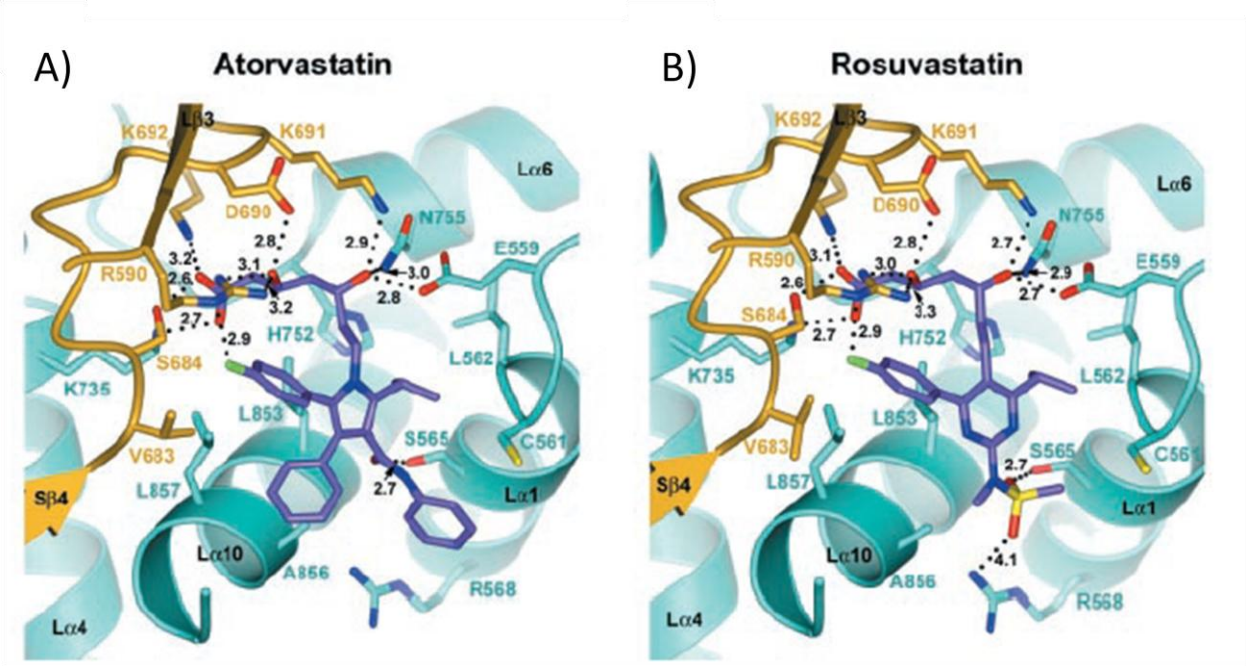

Figure 2.15. Mode of binding of (A) Atorvastatin and (B) Rosuvastatin to human HMG-CoA reductase.

The majority of interactions are ionic or polar and occur in the HMG binding region. Type 1 statins do not form the interactions with R590 that are seen in these type 2 statins. Both Atorvastatin and Rosuvastatin form interactions with S565 that are not observed with other statin compounds. Rosuvastatin also forms a unique interaction with R568. This figure is taken from Istvan & Deisenhofer (2001).

A number of statin compounds are available for doctors to prescribe. All perform well in clinical trials although the doses required vary for different drugs. The most potent statin compound marketed to date is cerivastatin, however, this was withdrawn from sale in 2001 due to an increased risk of serious

side effects compared to other statins (Furberg and Pitt, 2001). The most potent statins still available are atorvastatin and rosuvastatin. As can be seen in figure 2.15, these two statins form a greater number of interactions with the active site of HMG-CoA reductase which is likely to explain their increased binding affinity and therefore higher potency.

Statins are widely prescribed in developed countries. While primarily prescribed for patients suffering from high cholesterol levels they are also prescribed to those who have suffered from, or are deemed to be at risk of, heart attacks or cardiovascular disease (Ridker, 2003). In fact, in England in 2011, Simvastatin was the most widely prescribed medication (NHS, 2012). There were over 57 million prescriptions for statins in 2011, which the British Heart Foundation (BHF) estimates to mean that over 7 million people in the UK are taking statins (British Heart Foundation, 2011). Globally, atorvastatin is the biggest-selling pharmaceutical in history (Associated Press, 2011).

Statins have been proven to reduce mortality, coronary heart disease and strokes in both patients with a history of cardiovascular disease and those with raised cholesterol levels (Taylor *et al.*, 2011, Scandinavian Simvastatin Survival Group, 1994). However, there remain uncertainties regarding the cost-effectiveness of statins for primary prevention of cardiovascular disease, particularly for patients deemed to be at low risk (Taylor *et al.*, 2011). While statins are effective in lowering plasma LDL levels, it is likely that some of their success in reducing the incidence of cardiovascular disease is through pleiotropic effects (Zhou and Liao, 2009). These effects are caused because, by inhibiting HMG-CoA reductase, statins also inhibit the synthesis of isoprenoid compounds such as farnesyl pyrophosphate. As mentioned in section 2.1.3, isoprenoid compounds are important in post-translational modifications of many proteins, especially nuclear lamins such as Rac and Rho (Burridge and Wennerberg, 2004). Although the exact mechanisms involved are not understood, studies suggest that statins have a positive effect on many areas of the vascular system (Zhou and Liao, 2009). In particular, it is possible that statins have several pleiotropic effects on atherosclerotic plaques. These effects include: reduction of inflammation of the vascular wall (Vaughan *et al.*, 2000), lipid-independent inhibition of LDL oxidation (Wassmann *et al.*, 2001) and plaque stabilisation (Crisby *et al.*, 2001).

In addition to the suggested pleiotropic effects of statins on the cardiovascular system, there is also a possibility that statins have beneficial effects in treating or preventing a number of different conditions. These include dementia (Sparks *et al.*, 2006) and several types of cancer (Mandal *et al.*, 2011). However, further trials are needed to establish clearly whether or not statins are an appropriate treatment for other conditions (McGuinness *et al.*, 2010, Dellavalle *et al.*, 2005).

Despite the wide range of potential benefits to statin therapy, the drugs also have a number of associated side-effects. The most important of these is myopathy which occurs with a frequency of 1.2 per 10,000 treatment years (Sathasivam and Lecky, 2008). In serious cases, this can result in rhabdomyolysis which can be potentially life-threatening, although this is very rare, occurring with a frequency of approximately 0.1 per 10,000 treatment years. These negative effects on muscle function are due to the reduction in ubiquinone synthesis caused by the inhibition of HMG-CoA reductase (section 2.3). Another possible side-effect of statin therapy is liver failure which is dose dependent and

extremely rare, occurring with a frequency of 1 per 1,000,000 treatment years (Law and Rudnicka, 2006).

2.1.9 Potential New Inhibitors of HMG-CoA Reductase

A library of novel statin compounds have been synthesised (Lindsay *et al.*, 2010). These compounds are based around the structures of atorvastatin and rosuvastatin. These two statins were chosen as the parent compounds as they are the most potent LDL-lowering agents of the statins currently available (Shepherd *et al.*, 2003). The compounds are all synthesised with the HMG like moiety in a cyclic lactol form, this differs from the typical lactone form often seen in type 1 statins because the ketone is reduced to a hydroxyl group. This basic structure has then been modified to produce a library of potential HMG-CoA reductase inhibitors as shown in figure 2.16.

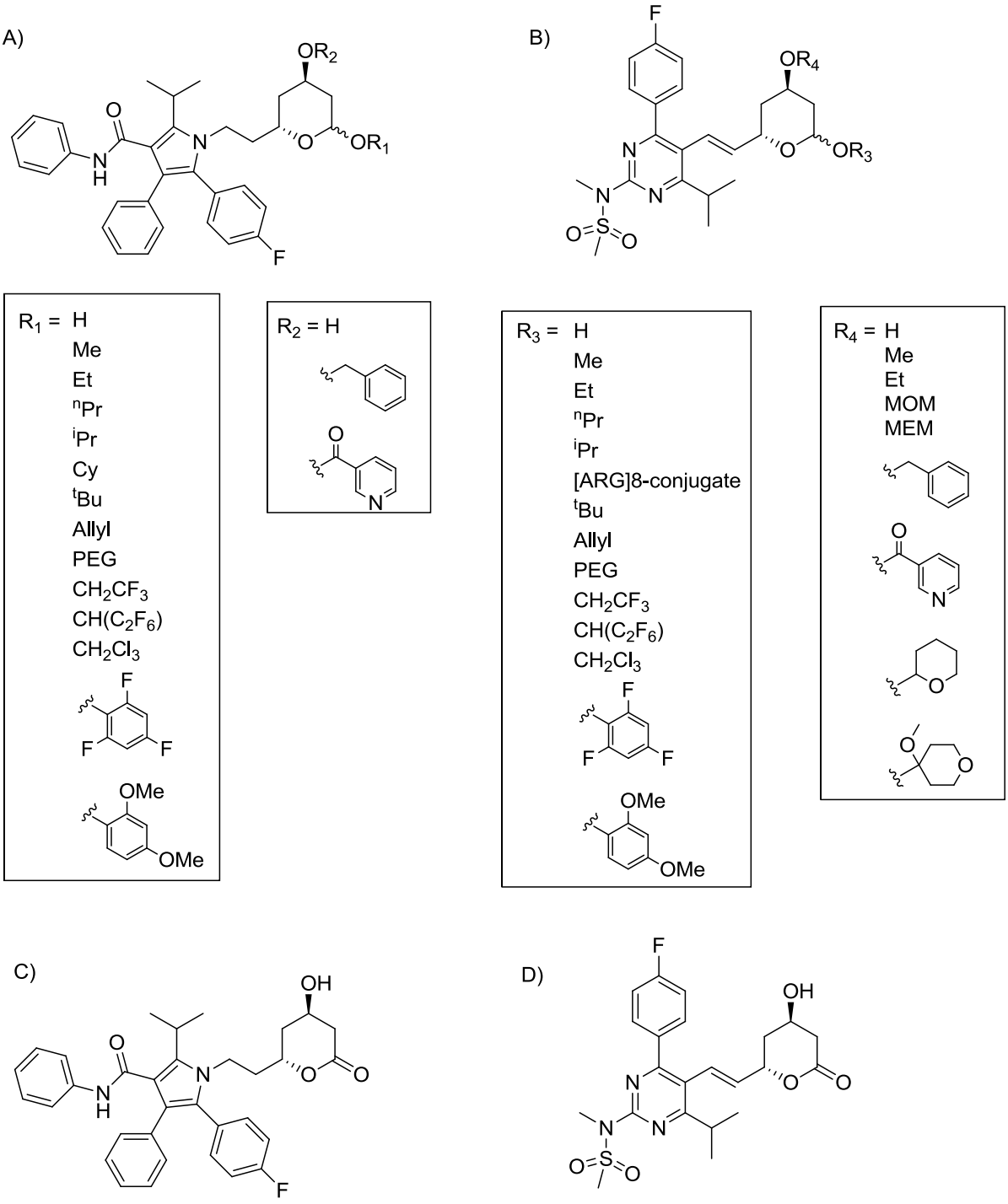

Figure 2.16. Structures of potential HMG-CoA reductase inhibitors synthesised by Redx Pharma.

*Structures are all based around the parent compounds **(A)** atorvastatin or **(B)** rosuvastatin. The structures of the wide range of lactol acetal compounds are indicated. The lactone derivatives of atorvastatin and rosuvastatin, **(C)** and **(D)** respectively, were also synthesised.*

All of the potential HMG-CoA reductase inhibitors contain a modification at the R_1/R_3 position indicated in figure 2.16, producing lactol acetal compounds. This modification ranges from a methyl group to a much larger polyether or substituted phenyl group. The R_2/R_4 position remains unmodified in many of the compounds. Modifications in both positions affect the steric and electronic properties of the original compounds which will alter the strength with which they bind to the active site of HMG-CoA reductase.

The aim of this work is to determine the ability of these new compounds to inhibit HMG-CoA reductase *in vitro*. The inhibitors that perform the best in enzyme assays will then be selected for animal trials in order to determine whether or not the inhibitory effects are replicated *in vivo*.

2.2 Results and Discussion

2.2.1 Initial Screening

The ability of the compounds described in section 2.1.9 to inhibit the activity of HMG-CoA reductase was measured using an enzyme assay. The assay showed the rate of conversion of HMG-CoA to mevalonate by measuring the conversion of the cofactor NADPH to NADP, at pH 7.2. The rate of reaction can be monitored due to the characteristic UV absorption of NADPH at 340 nm. For every molecule of HMG-CoA reduced to mevalonate, two molecules of NADPH are oxidised to NADP. NADP does not absorb UV light at 340 nm so the total absorption of the reaction mixture falls as the reaction proceeds. When the assay is carried out in the presence of an HMG-CoA reductase inhibitor, the rate of catalysis and therefore the fall in absorption at 340 nm is smaller, as can be seen in figure 2.17. More potent inhibitors of HMG-CoA reductase will produce lower rates of catalysis and therefore smaller decreases in absorption.

Through initial testing of the novel HMG-CoA inhibitors and the parent compounds, atorvastatin and rosuvastatin, it was determined that an inhibitor concentration of 50 nM was sufficient to differentiate between non-inhibitors and those compounds likely to inhibit HMG-CoA reductase to a similar degree to atorvastatin and rosuvastatin. The mean serum statin concentration of patients taking a 20 mg dose of atorvastatin is 15 nM (Bjorkhem-Bergman *et al.*, 2011) and statin concentrations in liver cells have been shown to be up to twice those in serum (Thelen *et al.*, 2006). 50 nM is therefore a reasonable approximation of *in vivo* concentrations.

The concentrations of HMG-CoA reductase, HMG-CoA and NADPH were adjusted in order to give a constant rate of catalysis over the ten minutes for which the absorption was measured. This ensures a more accurate calculation of the rate of reaction. All compounds were tested blind, *i.e.* the identity of each compound was unknown at the point of testing. A minimum of three biological repeats of each assay were carried out in a UV/vis microplate spectrophotometer. The assay is described in chapter 7.2.

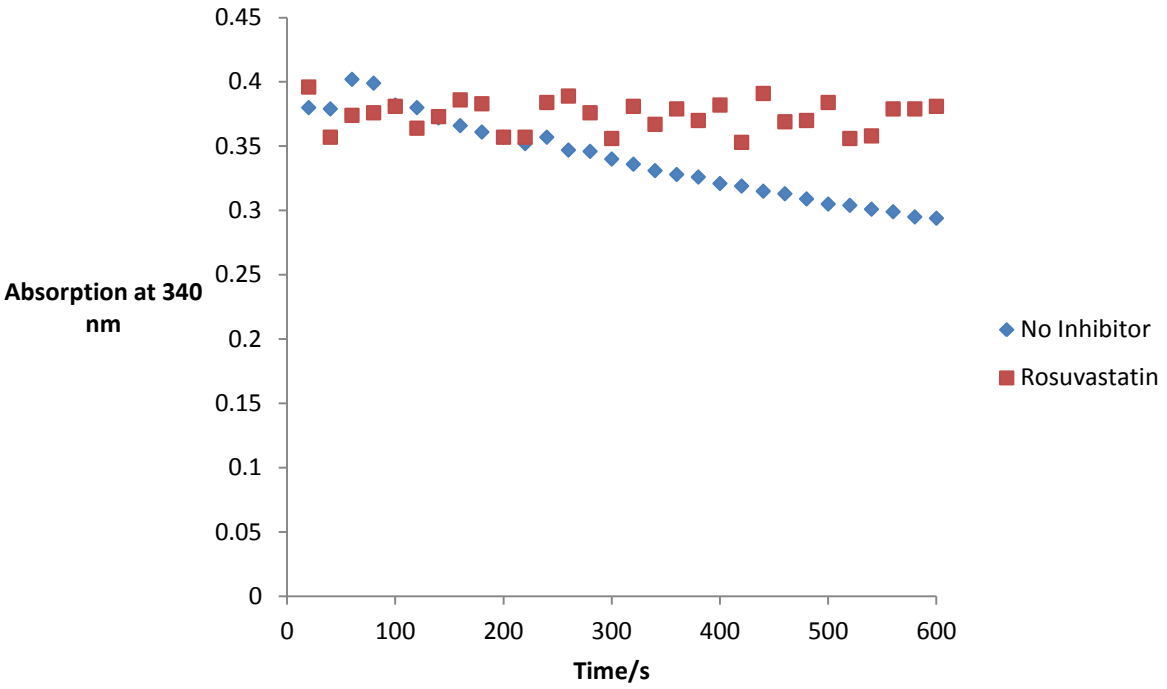

Figure 2.17. Effect of rosuvastatin on the change in UV absorption of the HMG-CoA reductase assay.

Change in UV absorption at 340 nm of the HMG-CoA reductase assay over time in the absence of an HMG-CoA reductase inhibitor and the presence of 50 nM rosuvastatin, a potent HMG-CoA reductase inhibitor. This plot shows the raw data from a single assay and negative control experiment.

The initial screening assays were carried out with inhibitor concentrations of 50 nM for a period of ten minutes. The average rates of reaction for all of the potential inhibitors tested are shown in figure 2.18. The rate of reaction was also measured at 50 nM concentrations of the parent compounds atorvastatin and rosuvastatin to serve as a comparison.

All of the organic compounds being tested are insoluble in water so 99.5 % DMSO was used to produce inhibitor solutions. As a result of this the initial test assays were carried out in 0.5 % DMSO. A control assay involving no inhibitor and a final DMSO concentration of 0.5 % was carried out to determine if the presence of DMSO had any significant effect on the rate of reaction compared to a second control containing no inhibitor and no DMSO. The results of these experiments are also shown in figure 2.18, which shows no significant change in the initial rate of reaction in the presence of 0.5 % DMSO. An additional control using denatured HMG-CoA reductase with each compound could also be included to confirm that the decrease in absorbance measured was due to the oxidation of NADPH to NADP by the enzyme and not directly by the inhibitor.

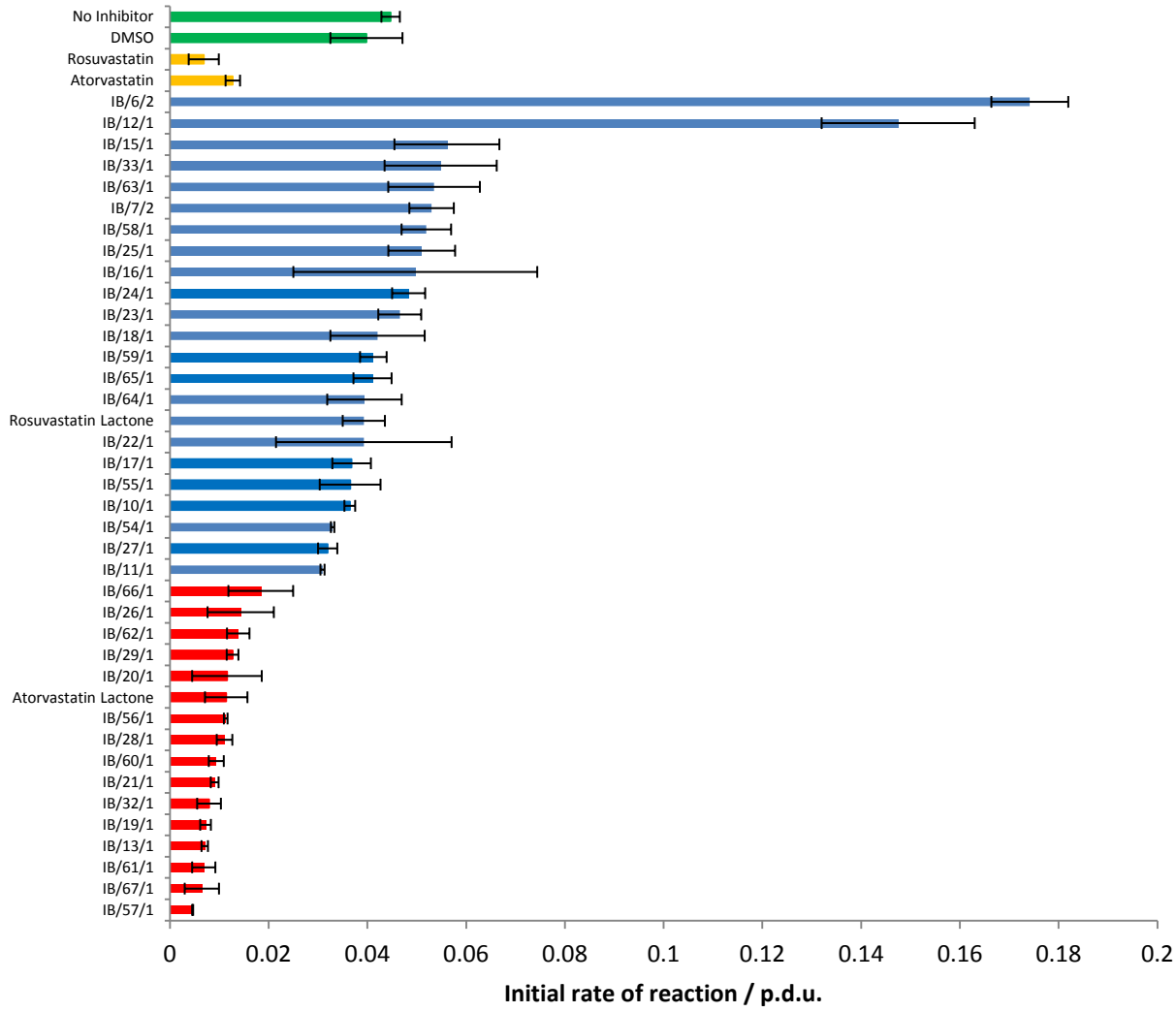

Figure 2.18. The initial rate of conversion of HMG-CoA to mevalonate by HMG-CoA reductase in the presence of 39 different potential inhibitor compounds.

Compounds which were not functional as inhibitors or showed poor inhibition are represented by blue bars. Compounds identified as good inhibitors are represented by red bars. The commercially available HMG-CoA reductase inhibitors atorvastatin and rosuvastatin are represented by orange bars. All inhibitors were tested at a final concentration of 50 nM and with a final DMSO concentration of 0.5 %. Negative controls, one containing no inhibitor and 0.5 % DMSO and one containing no inhibitor and no DMSO, are represented by green bars. Substrates HMG-CoA and NADPH both have a final concentration in the reaction of 200 µM and the HMG-CoA reductase concentration was 10 nM in all assays. Mean rates of reaction were calculated from a minimum of three biological repeats and error bars plotted show the standard error of the mean. Initial rate of reaction is shown in procedure defined units (p.d.u.) as it is calculated from absorption measurements which have no units.

Initially, 39 potential inhibitors were tested using the method outlined. Around 20 of these compounds appear to inhibit the activity of HMG-CoA reductase *in vitro*, as can be seen in figure 2.18. Of these 20 compounds, 16 caused inhibition of the enzyme at a concentration of 50 nM to a level at least approaching that caused by atorvastatin at the same concentration. These included eight atorvastatin lactol acetals and seven rosuvastatin lactol acetals in addition to the atorvastatin lactone.

The lactone forms of statin compounds are not expected to bind to the active site of HMG-CoA reductase in their cyclic form. Under physiological conditions they are hydrolysed enzymatically to form the extended, carboxylic acid conformation (Corsini *et al.*, 1995). This allows some statins to be administered in their lactone form as pro-drugs (Todd and Goa, 1990). The structures of atorvastatin and rosuvastatin bound to HMG-CoA reductase show the compounds binding in their acid conformation (Istvan and Deisenhofer, 2001). The fact that the atorvastatin lactone shows inhibition of the enzyme in this experiment was therefore not predicted. The assay was carried out at pH 7.2 which is not high enough to cause chemical hydrolysis of the lactone. If the result obtained from the assay is accurate then this suggests one of two things: either an interaction with the enzyme is in some way responsible for causing the opening of the lactone ring or atorvastatin is able to inhibit HMG-CoA reductase in its closed, lactone conformation.

Many of the lactol acetal variations were synthesised using both atorvastatin and rosuvastatin as the parent compounds. The results of the assay show that, in many cases, if an atorvastatin lactol acetal inhibits HMG-CoA reductase then its corresponding rosuvastatin lactol acetal will also inhibit the enzyme. The majority of the compounds lacking modifications in the R_2/R_4 position (as indicated in figure2.16) and containing only simple, alkyl substituents in the R_1/R_3 position showed no inhibition or poor inhibition at a concentration of 50 nM. Several compounds lacking R_2/R_4 modifications but with larger, cyclic substituents attached to the acetal oxygen showed inhibition in testing, although the presence of a substituent group in the R_2/R_4 position appears to be linked to *in vitro* inhibition. There was particularly good agreement between the ability of the equivalent atorvastatin and rosuvastatin lactol acetals to inhibit HMG-CoA reductase.

Some compounds with nicotinoyl esters in the R_2/R_4 position also appear to inhibit HMG-CoA reductase at concentrations of 50 nM. These compounds were designed with the nicotinoyl ester as it is known that, under physiological conditions, these groups are metabolised to form nicotinic acid (Salvi *et al.*, 1997). Nicotinic acid, or niacin as it is also known, has long been established to have lipid lowering effects which are achieved by inhibiting the breakdown of lipids stored in adipose tissue (Altschul *et al.*, 1955). A recent trial testing the effects of niacin therapy on patients already taking simvastatin indicated an increase in serum HDL levels and a decrease in serum LDL and triglyceride levels (Boden *et al.*, 2011). Unfortunately this trial was ended early due to an increase in the incidence of strokes which was subsequently shown to be statistically insignificant.

As previously mentioned, existing statin drugs are known to bind to HMG-CoA reductase with their HMG like moiety in the extended, acid conformation. In all of the compounds tested in this assay, the HMG like moiety is in a closed, lactol form. There is some evidence that, under physiological conditions, lactols are oxidised to form their corresponding lactones (Nicoll-Griffith *et al.*, 1999). In the case of statin

compounds the lactone ring would then undergo enzymatic ring opening allowing them to bind to HMG-CoA reductase in the extended form (Corsini *et al.*, 1995). However, the conditions under which this assay was carried out are unlikely to cause such reactions to occur. The assay lacks any of the enzymes which would be responsible for these conversions in the human body so these cannot cause oxidation or ring opening. In addition to that, the assay is carried out at pH 7.2 which is certainly too close to neutral to allow the ring opening of a lactone. This means that, either the lactol rings are opening via some other mechanism or the compounds are binding in their cyclic conformations.

Acetals are stable but exist in equilibrium with their corresponding hemiacetals in the presence of water. The lactol acetals tested in this work could, potentially, therefore form two different hemiacetals depending upon their relative stabilities. In one scenario the lactol form of the compound would be formed effectively removing the modification at the R position of all compounds, as shown in scheme (A) in figure 2.19. Following its formation, the lactol can then open to form a hydroxyaldehyde which is similar in structure to the open acid form taken by statin drugs but lacking a hydroxyl group. The practicalities of such ring opening would be that only the different R_2/R_4 substituents would have any effect upon the difference in inhibition caused between different compounds. However, only three different groups are present in that position across all of the compounds tested, namely hydroxyl, benzyl ether and nicotinoyl ester. While both of the nicotinoyl esters tested inhibited HMG-CoA reductase, only some of the hydroxyl and benzyl ether compounds were inhibitors while others were not. In addition to this, the lactol forms of the atorvastatin and rosuvastatin were also tested using the assay and neither compound inhibited HMG-CoA reductase. This result rules out the possibility of hydroxyaldehydes being the functional inhibitors in these compounds.

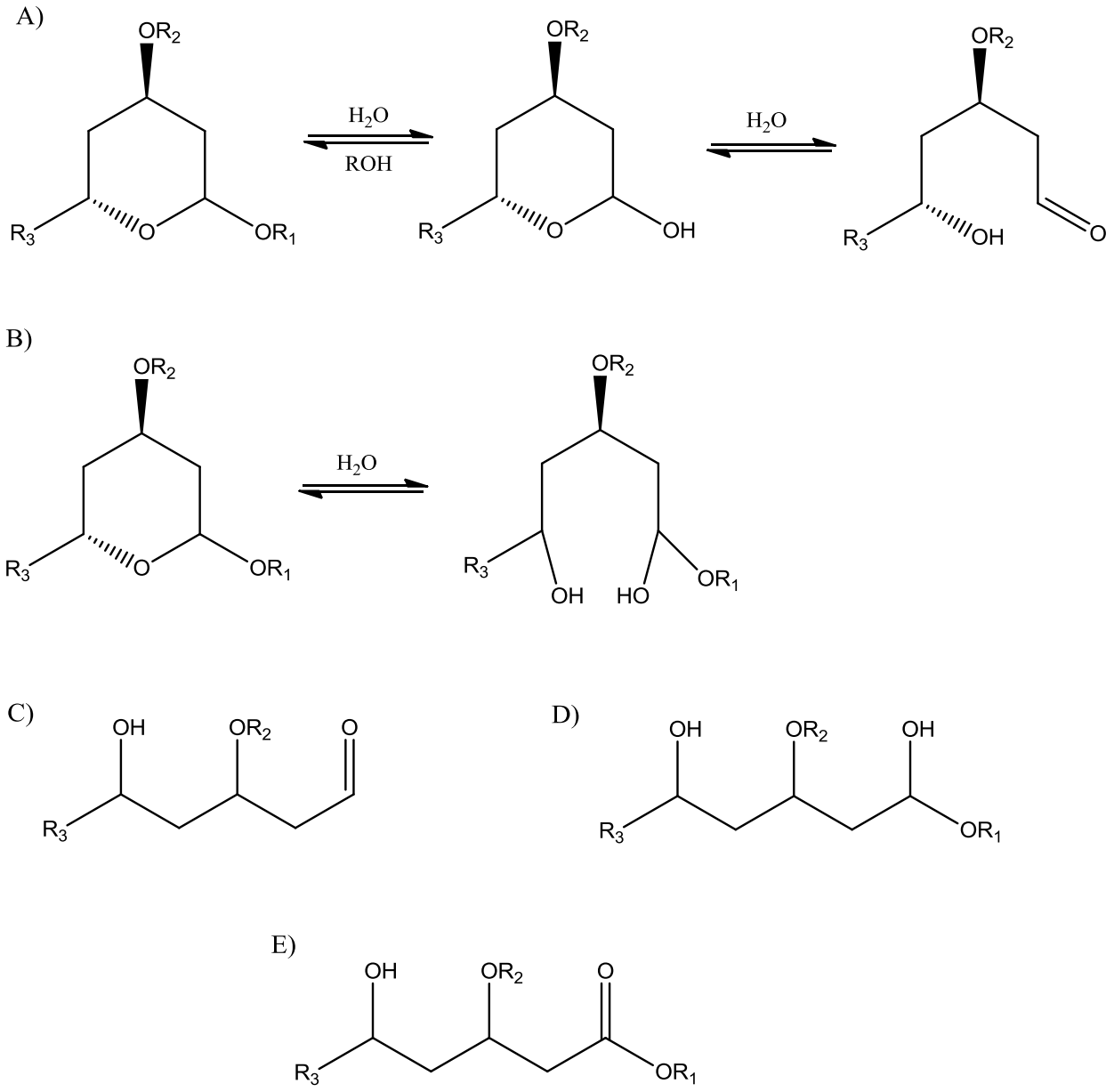

Figure 2.19. Potential ring opening reactions of lactol acetal compounds.

Acetals exist in equilibrium with their corresponding hemiacetal. In the case of the potential HMG-CoA reductase inhibitors tested here, this equilibrium could first result in the formation of ***(A)*** *the corresponding lactol or* ***(B)*** *the corresponding hydroxy-hemiacetal. Lactols often exist in equilibrium with their open, hydroxyacetone form as shown in scheme (A). The possible extended conformations are* ***(C)*** *hydroxyacetone produced by scheme (A) or* ***(D)*** *hydroxy-hemiacetal produced by scheme (B). The extended acid conformation of existing statin drugs is shown in* ***(E)****. R_3 is atorvastatin or rosuvastatin, R_1 and R_2 are the sites of variation in the compounds tested in this work.*

The other possible reaction that could take place involving formation of a hemiacetal results in the formation of a hydroxyhemiacetal. This reaction is shown in scheme (B) in figure 2.19 and causes the lactol ring to open. Again, this open form of the lactol ring is very similar to the open acid form of statin drugs, varying only in the presence of a hemiacetal functional group in place of the carboxylic acid. However, unlike the lactol ring opening discussed above, the modifications at both the R_1/R_3 and R_2/R_4 positions should be present in the open form. This could account for the inhibition results which do not support the hydroxyaldehyde being formed.

If the potential inhibitors do indeed form the hydroxyhemiacetal, then it is likely their modes of binding are similar to those observed for existing statin drugs in crystal structures with HMG-CoA reductase (Istvan and Deisenhofer, 2001). The significant difference between the hydroxyhemiacetals and the extended acid conformation of the statins is the replacement of the carboxylic acid group with a hemiacetal. This is likely to alter the interactions between the inhibitors and the enzyme active site although the hydroxyhemiacetals still contain polar oxygen atoms in similar positions so may still be able to form similar interactions with the enzyme. Any other differences in binding modes are likely to be due to the structural variation in the lactol acetal compounds.

If the inhibitors do bind in a conformation similar to that of the open acid statins, then any group added in the R_1/R_3 position is likely to be in close proximity to R590, S684, K692 and K735 in the active site of HMG-CoA reductase. However, the majority of the groups found at this position in the compounds showing inhibition are relatively large and are unlikely to fit easily into an area of the active site that would already be rather crowded. This means that any conformation of the inhibitors that does bind to HMG-CoA reductase would probably require any group in the R_1/R_3 position to be oriented away from the HMG binding region of the enzyme. This may allow new inhibitor-enzyme interactions not present in the binding of existing statin compounds. Such interactions may be stronger if the R_1/R_3 group of the inhibitor contains polar groups as present in the lactol 2,4-dimethoxyphenyl acetals and lactol 2,4,6-trifluorophenyl acetals, for example.

The role played by modifications in the R_2/R_4 position is less clear if the inhibitors are binding in the hydroxyhemiacetal form. All of the substituents present in this position contain large, six-membered aromatic rings. The size of these groups makes it unlikely that the hydroxyhemiacetals would be able to bind with this particular group in a similar conformation to that observed for the equivalent group in existing statins. Binding in such a conformation would almost certainly disrupt other interactions between the inhibitor and the HMG binding site. Any binding conformation would also have to minimise the interactions between the aromatic group substituent and the larger aromatic rings of the statin structure.

Another possibility is that the compounds are binding to HMG-CoA reductase in their cyclic, lactol conformations. This is possible as the relative distances between the oxygen atoms in the structure will not be too dissimilar to the distances between the carboxylic acid and hydroxyl groups in the extended acid conformation of the existing statin compounds. However, the ring structure limits the range of conformations that may be adopted by a given compound. This may explain the fact that the compounds with polar substituents are more likely to inhibit HMG-CoA reductase as their polar groups

are able to form stronger interactions with the active site of the enzyme. However, those compounds containing an additional benzyl or nicotinoyl group in the R_2/R_4 position would be unlikely to adopt a suitable binding conformation as any flexibility in their structures is limited.

Figure 2.18 appears to show that two of the compounds tested actually enhance the rate of catalysis by HMG-CoA reductase. Assuming that these results are accurate and that the compounds being tested are free of contamination which could account for this then the most likely explanation for this phenomenon would be allosteric enhancement of the enzyme. This would mean that the compounds are binding to a site in the enzyme that is distinct from the active site. Allosteric activators or inhibitors have been described for several enzymes (Volkman *et al.*, 2001, Chen *et al.*, 2010), although no allosteric activators have previously been described for HMG-CoA reductase. Further investigation of the nature of the interaction between the compounds which appear to show activation and the enzyme is needed, perhaps through crystallographic studies, in order to determine whether or not allosteric activation is truly occurring in these cases. This is discussed further in section 6.1.

A limitation of this assay is that these possible conformations of the compounds may not represent the forms that they take under physiological conditions. This is certainly true of the lactone compounds and the nicotinoyl compounds as they are known to undergo enzymatic modifications which would not be possible in the conditions of the assay. Similarly, benzyl ethers present in other compounds have been known to be removed by metabolic enzymes (Miller *et al.*, 2000). Additionally, there is a possibility that all of the lactol acetal compounds may be oxidised to form either the atorvastatin or rosuvastatin lactones that would then undergo an enzymatic ring-opening reaction. Effectively this would result in all of the potential inhibitors acting as prodrugs for their parent compounds, atorvastatin or rosuvastatin. It is therefore important that the mode of binding of the inhibitors is determined before drawing firm conclusions from the results of the assay. Should the compounds prove to be prodrugs for other, active compounds *in vivo*, they may possibly display improved pharmacokinetic properties compared to other statin compounds. This may allow lower doses to be used in treatment of high cholesterol which may result in lower costs or a reduction in side-effects.

The assay used seems to serve as an effective technique to assess whether or not the compounds are inhibitors of HMG-CoA reductase. Ideally, the initial rates of reaction for each compound could be used to identify trends within the library of compounds in order to gather further information about their modes of binding to the enzyme. This could potentially be used for more targeted inhibitor design if, for example, the addition of larger groups in certain positions caused an increase or decrease in the initial rate of catalysis at 50 nM inhibitor. Unfortunately no such trends can be identified in the data generated by this work. This is likely to be due to the limited sensitivity of the assay so other approaches would be required if such trends were to be identified. This is discussed in more detail in section 6.1.

2.2.2 Calculation of IC50 Values

Following the initial screening of potential HMG-CoA reductase inhibitors, IC50 values were calculated for those compounds selected as inhibitors. The IC50 of an inhibitor is the concentration of inhibitor that inhibits the activity of a process by 50 %. In the case of this assay, the IC50 is the concentration of inhibitor at which the initial rate of reaction is 50 % between its minimum and maximum values. In order to calculate this, the assay was repeated over a range of inhibitor concentrations from 1 nM to 50 nM. A graph of initial rate of reaction against inhibitor concentration was plotted for each inhibitor and a sigmoidal curve fitted to the data using a least squares regression method. Each curve was fitted to a Boltzman function in the form:

$$y = \frac{A_1 - A_2}{1 + e^{\frac{x - x0}{dx}}} + A_2$$

Where y is the initial rate of reaction, x is the inhibitor concentration, A_1 is the initial rate of reaction at minimal inhibition, A_2 is the initial rate of reaction at maximal inhibition, x_0 is the IC50 and dx is the concentration range over which inhibition changes from minimal to maximal. In each case the initial rate of reaction with no inhibitor was used as an estimate A_1. A_2 was estimated from a plot of the initial rates of reaction against the concentration of inhibitor. The estimated values of x_0 and dx were calculated by least squares regression.

IC50 values were calculated for the sixteen compounds identified as inhibitors by the initial screening assay carried out at 50 nM inhibitor. In addition to this, IC50 values were calculated for atorvastatin and rosuvastatin. The initial rates of reaction data and the fitted curves are shown in appendix A.

The IC50 values calculated for atorvastatin and rosuvastatin are 7 nM and 4 nM, respectively. The IC50 values found in the literature for these compounds are 8 nM for atorvastatin and 5 nM for rosuvastatin (Istvan and Deisenhofer, 2001). This shows that the method used for calculating IC50 values in this work provides reasonably accurate results although may slightly underestimate the true values. As can be seen in table 2.1 the IC50 values of the compounds tested vary although the majority of compounds have IC50 values lower than that of atorvastatin. Calculation of the IC50 values serves as a further level of screening before the compounds are put forward for use in *in vivo* testing.

Compounds with lower IC50 values are more desirable medicines as they require a smaller dose to achieve the same effects as a similar compound with a higher IC50 (Copeland, 2005). For many drugs this is particularly desirable as administering a lower dose can reduce the effects of any dose-dependent side effects. However, the majority of side effects of statin drugs are not dose dependent since they occur due to the reduction in synthesis of various molecules synthesised by the mevalonate pathway. Liver failure is the main dose-dependent side effect of statins although this is extremely rare so discovery of statins with IC50 values significantly lower than those already available is unlikely to have a significant effect upon its incidence.

Compound Number	IC50 / nM
IB/13/1	6
IB/19/1	1
IB/20/1	2
IB/21/1	2
IB/26/1	4
IB/28/1	1
IB/29/1	5
IB/32/1	4
IB/56/1	4
IB/57/1	1
IB/60/1	1
IB/61/1	2
IB/62/1	5
IB/66/1	12
IB/67/1	4
Atorvastatin Lactone	4
Atorvastatin	7
Rosuvastatin	4

Table 2.1. IC50 values of compounds identified to be inhibitors of HMG-CoA reductase after screening at 50 nM inhibitor.

Values are the concentration of inhibitor at which HMG-CoA reductase activity i is 50 % between its minimum and maximum values*, calculated over a range of inhibitor concentrations between 1 nM and 50 nM. Also included are the IC50 values of atorvastatin and rosuvastatin calculated by the same method.*

There are some limitations in these IC50 values. As discussed above, it is likely that these values are subject to an error of somewhere in the region of ±2 nM. This reduces the opportunity to identify trends within IC50 values and limits the application of the data beyond acting as a second level of screening. However, the IC50 values easily identify those compounds with an IC50 in the region of the IC50s of atorvastatin and rosuvastatin and those that clearly have a higher IC50 value. Part of the error is due to the range of concentrations of inhibitor that were tested. For example, in the case of the atorvastatin methyl nicotinoyl ester the IC50 value appears to be approximately 1 nM. However, the lowest inhibitor concentration used in the calculation is 1 nM. This means that the real IC50 may conceivably be one or more orders of magnitude lower and this could be determined by increasing the range of concentrations tested. The assay was not carried out at lower inhibitor concentrations as it was felt that the results obtained provided a good enough estimation of the IC50 value to identify the most suitable candidates for further testing. This is supported by the fact that the IC50 values calculated for atorvastatin and rosuvastatin using this method are with 1 nM of the published IC50 values. It is also possible that the *in*

vitro IC50 values will not necessarily be related to the *in vivo* IC50 values due to the likelihood of enzymatic modifications to the compounds as described in section 2.2.1.

2.2.3 Molecular Modelling of HMG-CoA Reductase Inhibitor Binding

Prior to the *in vitro* testing, the potential interactions between some of the compounds and HMG-CoA reductase had been modelled at the University of Liverpool. The results of this modelling suggested that the rosuvastatin analogues would have similar binding energies to rosuvastatin and that the atorvastatin analogues would bind with similar energies to atorvastatin. This modelling was carried out assuming that the inhibitors would be in the ring-open hemiacetal conformation and calculated two different docking energies, one for each enantiomer, for each compound. Of the compounds modelled, IB/6/2 and IB/7/2 were expected to bind poorly to HMG-CoA reductase and only one enantiomer of IB/21/1 was expected to bind to the enzyme. As the results in figure 2.18 show, IB/6/2 and IB/7/2 do not inhibit HMG-CoA reductase although IB/21/1 does. All of the other compounds modelled were predicted to bind to the enzyme although clearly several of them do not show inhibition in this assay.

Molecular modelling, such as that carried out for these compounds, has a number of limitations. In the case of these compounds, as has been discussed in section 2.2.1, the mode of binding is not known. The models assume that binding will occur in the hemiacetal conformation but binding may also be occurring in the cyclic, lactol acetal form. In addition to this, the modelling relies on existing structures of the enzyme when it is bound to existing statin drugs, particularly the parent compounds atorvastatin and rosuvastatin. As these compounds are almost certainly binding in a different conformation to the carboxylic acid forms observed in these structures, it is possible that the mode of binding and the shape of the active site will vary to some degree.

Despite the limitations of this modelling, it could be used, along with experimental data, in order to create more accurate models for other compounds. The results of this assay have some value in this as they show which compounds inhibit HMG-CoA reductase well and which do not appear to cause any inhibition. The IC50 values also provide a guide to the relative binding strength of each inhibitor. The most important step in improving molecular modelling would be to confirm the binding conformations of those compounds which inhibit the enzyme. In addition to this, determining the binding affinities of these compounds using a technique such as isothermal titration calorimetry would offer a direct experimental comparison for the calculated docking energies. This would allow refining of the model to enable more accurate prediction of the binding of other compounds and is discussed in more detail in section 6.1.

Accurate modelling is extremely useful as it allows the properties of compounds to be analysed before the compound itself has even been synthesised. This can save time and money as compounds predicted to show no interaction with the enzyme will not be synthesised or tested. Additionally, if the model is improved enough, molecular modelling could replace the need for carrying out *in vivo* studies in animals. This would also require accurate modelling of interactions with other molecules in order to

predict side-effects accurately. An effective molecular modelling system could potentially reduce the time and costs involved in drug discovery considerably.

2.2.4 Testing of Other Inhibitors

Following on from the initial inhibitor testing described in sections 2.2.1 and 2.2.2, a further group of compounds was synthesised (Lindsay *et al.*, 2010). These consisted of a number of new lactone acetal compounds not previously tested, as well as purified enantiomers of those compounds identified as inhibitors in the initial screening. The initial rate of catalysis by HMG-CoA reductase in the presence of 50 nM of inhibitor was calculated using the same method as described in section 2.2.1. The results of this are shown in figure 2.20.

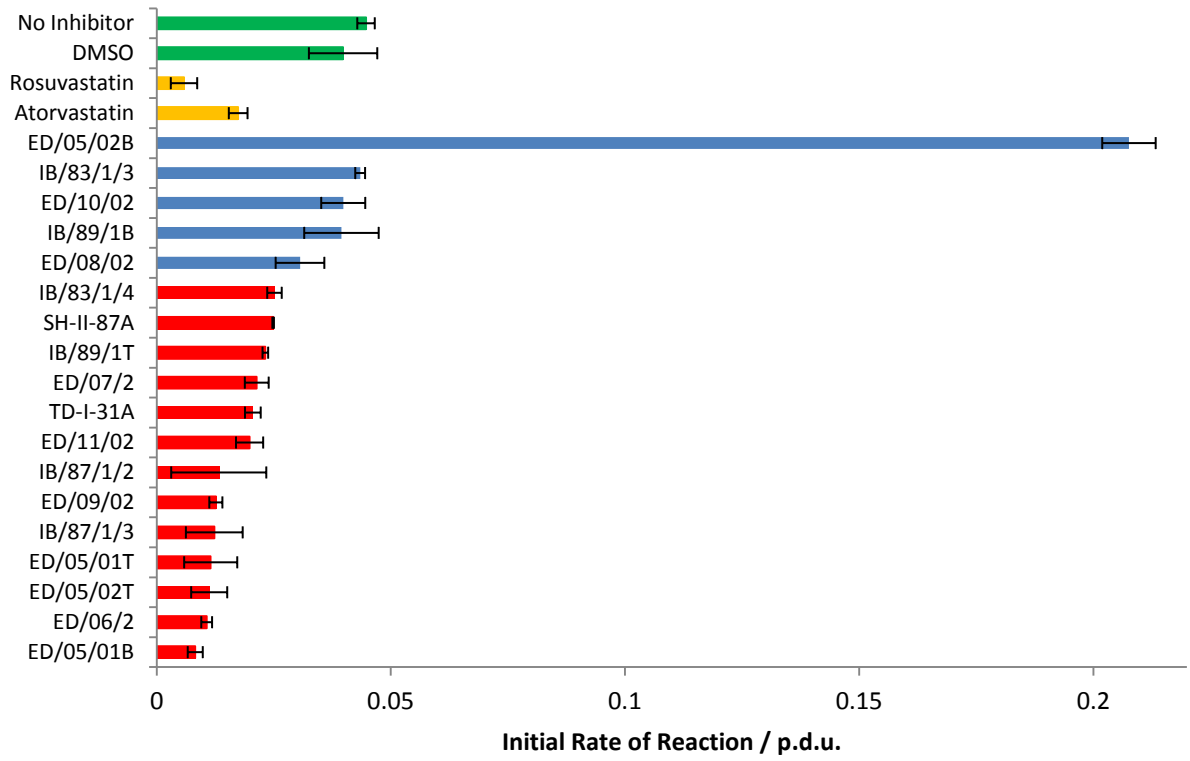

Figure 2.20. The initial rate of conversion of HMG-CoA to mevalonate by HMG-CoA reductase in the presence of 18 different potential inhibitor compounds.

Compounds which were not functional as inhibitors or showed poor inhibition are represented by blue bars. Compounds identified as inhibitors are represented by red bars. The commercially available HMG-CoA reductase inhibitors atorvastatin and rosuvastatin are represented by orange bars. All inhibitors were tested at a final concentration of 50 nM and with a final DMSO concentration of 0.5 %. Negative controls, one containing no inhibitor and 0.5 % DMSO and one containing no inhibitor and no DMSO, are represented by green bars. Substrates HMG-CoA and NADPH both have a final concentration in the reaction of 200 µM and the HMG-CoA reductase concentration was 10 nM in all assays. Mean rates of reaction were calculated from a minimum of three biological repeats and error bars plotted show the standard error of the mean. Initial rate of reaction is shown in procedure defined units (p.d.u.) as it is calculated from absorption measurements, which have no units.

Of the 18 new compounds tested, 13 of them were determined to inhibit HMG-CoA reductase to a similar degree to atorvastatin and rosuvastatin at concentrations of 50 nM. Six of these compounds are new compounds not tested in the earlier experiments and seven are purified enantiomers of compounds previously identified as inhibitors of HMG-CoA reductase. Interestingly, three of the ten purified enantiomers tested did not appear to inhibit HMG-CoA reductase. This suggests that the

compounds are binding to the enzyme in a manner which preserves their stereocentre. This means that they cannot be binding in the extended acid conformation or the extended aldehyde conformation as these forms are lacking the chiral carbon atom. Binding in the cyclic, lactol acetal, conformation or the extended hemiacetal conformation would both allow for the differences in inhibition between the stereoisomers.

Compound	IC50/nM
IB/83/1/4	3
IB/87/1/2	2
IB/87/1/3	7
IB/89/1T	8
ED/05/01B	13
ED/05/01T	5
ED/05/02T	10
ED/06/2	6
ED/07/2	8
ED/09/02	28
ED/11/02	3
SH/II/87A	34
TD/I/31A	9

Table 2.2. IC50 values of 13 HMG-CoA reductase inhibitors.

Values are the concentration of inhibitor at which HMG-CoA reductase activity is 50 % between its maximum and minimum values calculated over a range of inhibitor concentrations between 1 nM and 50 nM.

The IC50 values of the 13 compounds from this group which are inhibitors of HMG-CoA reductase are shown in table 2.2. As with the first group of compounds, the majority of these compounds have IC50 values similar to those of the parent compounds, atorvastatin and rosuvastatin. This suggests that they may be active in similar doses *in vivo*. Two pairs of separated enantiomers have had their IC50 values calculated in this work. In both cases, the IC50 value is different for each enantiomer further supporting the idea that the compounds are binding to the enzyme in a manner which preserves the differences in stereochemistry.

2.3 Conclusions

Many of the compounds tested inhibit HMG-CoA reductase at clinically useful concentrations (McTaggart *et al.*, 2001) having similar *in vitro* profiles to the currently used statins atorvastatin and rosuvastatin. The experiments were able to select a further batch of compounds for use in further testing. Had time allowed, *in vitro* testing of the toxicity of the compounds to cultured human cells could also have been carried out by assaying cell viability using a dye such as resazurin, as described in section 6.1. However, as *in vivo* animal testing experiments had already been arranged, it was not possible for such an experiment to be conducted

The animal testing that was carried out "demonstrated the potential for superiority over existing best-in-class drugs." This demonstrates that the testing carried out is an effective way of selecting effective inhibitors for further testing. A potential drawback of this type of assay is the possibility that modified versions of the compounds may be responsible for inhibition *in vivo*. However, the positive results obtained from the animal testing suggest that, even if this is the case, the experiments used are still a good indicator of such activity.

Chapter 3

3. Antibacterial Activity of Novel Fluoroquinolones

3.1 Introduction

3.1.1 Fluoroquinolones

The fluoroquinolones are a group of broad-spectrum, synthetic antibacterial compounds and are part of the wider, quinolone family. The first quinolone was discovered inadvertently as a by-product of the synthesis of chloroquine, an antimalarial agent. This compound, nalidixic acid, was discovered to have moderate antibacterial activity against gram-negative bacteria (Lesher *et al.*, 1962) and was first approved for medicinal use in 1967. In addition to its limited activity, nalidixic acid also proved to undergo high serum protein binding and caused rapid appearance of resistant bacteria (Hane and Wood, 1969). Further first generation quinolone compounds were developed including oxolinic acid, piramidic acid and pipemidic acid. These compounds typically have a greater potency against gram-negative bacteria and, in the case of pipemidic acid, activity against *Pseudomonas aeruginosa* which is not observed for nalidixic acid. The addition of the piperazine ring to form pipemidic acid was also shown to cause some activity against gram-positive bacteria (Jacoby and Hooper, 2012). The first fluoroquinolone, flumequine, was patented in 1973. This compound is a first generation quinolone compound which showed an even greater potency against gram-positive bacteria (Appelbaum and Hunter, 2000). These compounds, where still in use, are primarily used in treating urinary tract infections (UTIs) in humans and also have some veterinary uses.

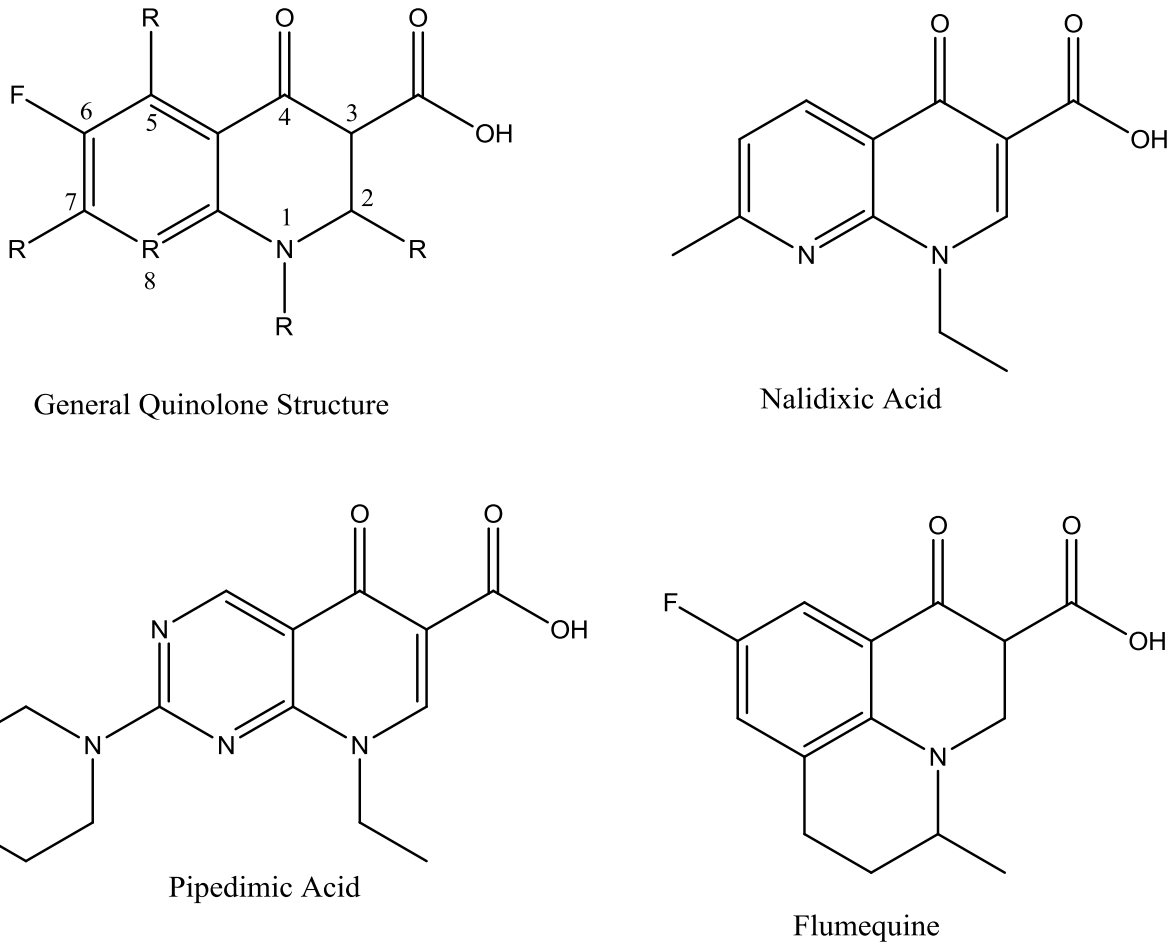

Figure 3.1. The general structure of quinolone compounds and the structures of three first generation quinolone antibacterial drugs.

All compounds contain the quinolone nucleus and the sites of potential structural variation are numbered in the general structure.

Norfloxacin was the first second generation quinolone to be produced. Like all later generation quinolone compounds, norfloxacin is a fluoroquinolone and combines the fluorine at position six found in flumequine with the piperazine ring found in pipedimic acid. The combination of these two structural features results in increased potency against both gram-negative and some gram-positive bacteria. Despite its improved potency, the pharmacokinetic profile of norfloxacin means that it is only used as a last resort in treating infections. However, following the patenting of norfloxacin in 1978 a large number of new fluoroquinolones were introduced. Many of these drugs, such as pefloxacin, ciprofloxacin and ofloxacin, are still in clinical use today. These other second generation fluoroquinolones are absorbed much more readily by the gastrointestinal tract, making them much more effective at fighting systemic infections. To this day, ciprofloxacin remains the most potent fluoroquinolone agent against gram-

negative bacteria. Despite their improvement upon first generation quinolones, these antibacterial drugs are still not potent enough against gram-positive bacteria to be used clinically against respiratory infections so are still used primarily in the treatment of UTIs (Appelbaum and Hunter, 2000). Ciprofloxacin can also be used in the treatment of gastrointestinal tract infections. However, while the development of resistance to these agents is not as rapid as development of resistance to nalidixic acid, resistance to second generation quinolones is still a problem in certain bacterial species, particularly *Staphylococcus aureus* and *P. aeruginosa*.

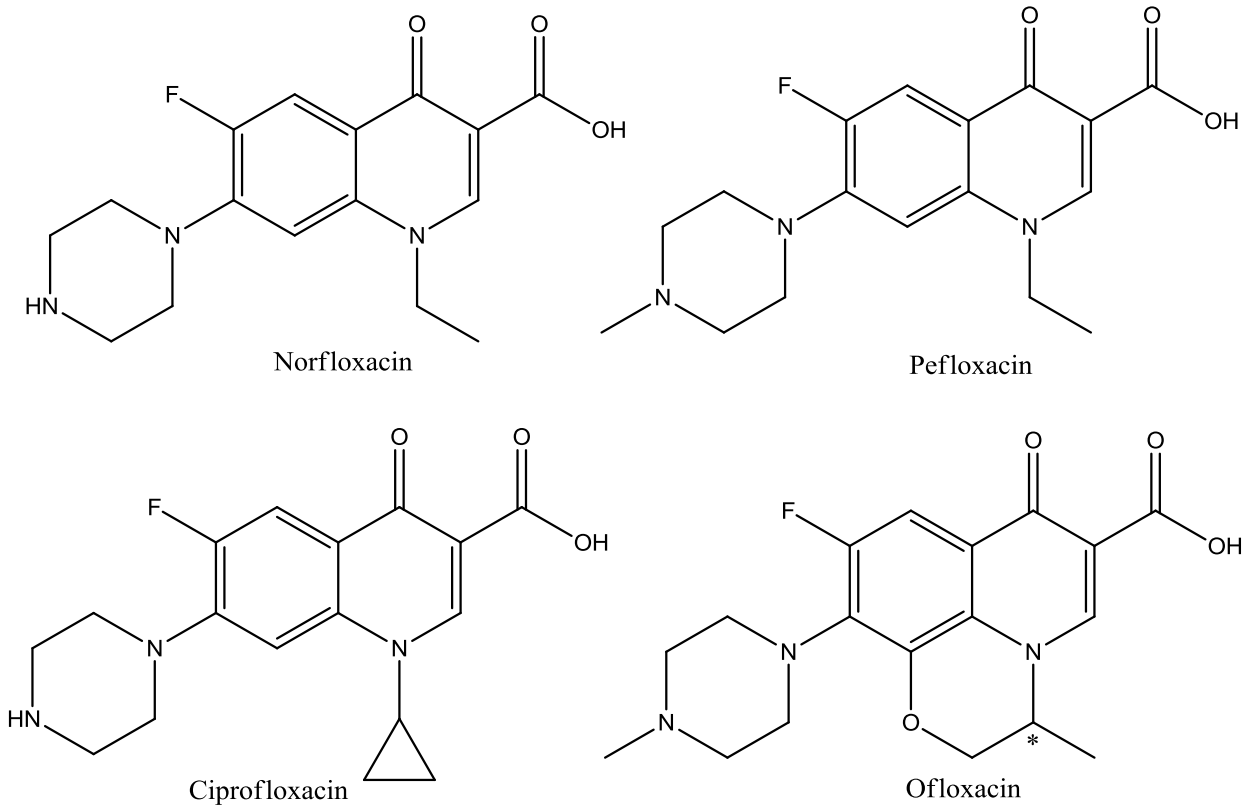

Figure 3.2. The structures of four second generation fluoroquinolone compounds.

All compounds contain the basic quinolone nucleus in addition to a fluorine at position 6 and a piperazine ring at position 7. Ofloxacin exists as a mixture of two enantiomers and its stereocentre is indicated.

The third generation, or 'respiratory', fluoroquinolones were developed specifically for increased activity against gram-positive bacteria. These compounds include levofloxacin, grepafloxacin and sparfloxacin. They typically have a much broader spectrum of activity which includes *Streptococci*, particularly

Streptococcus pneumoniae, as well as some anaerobes. However, the activity of third generation fluoroquinolones against *S. aureus* remains limited and their improvement in activity against fluoroquinolone-resistant *S. aureus* is not great enough to be clinically useful (Appelbaum and Hunter, 2000). Levofloxacin is the functional enantiomer of the second generation fluoroquinolone ofloxacin and shows improved activity when administered as the single enantiomer compared to the racemic mixture present in ofloxacin. The other third generation fluoroquinolones are similar in structure to the second generation compounds, often with very minor modifications responsible for their improved activity. Unlike the second generation drugs, the activity of these compounds is sufficient to treat respiratory tract infections.

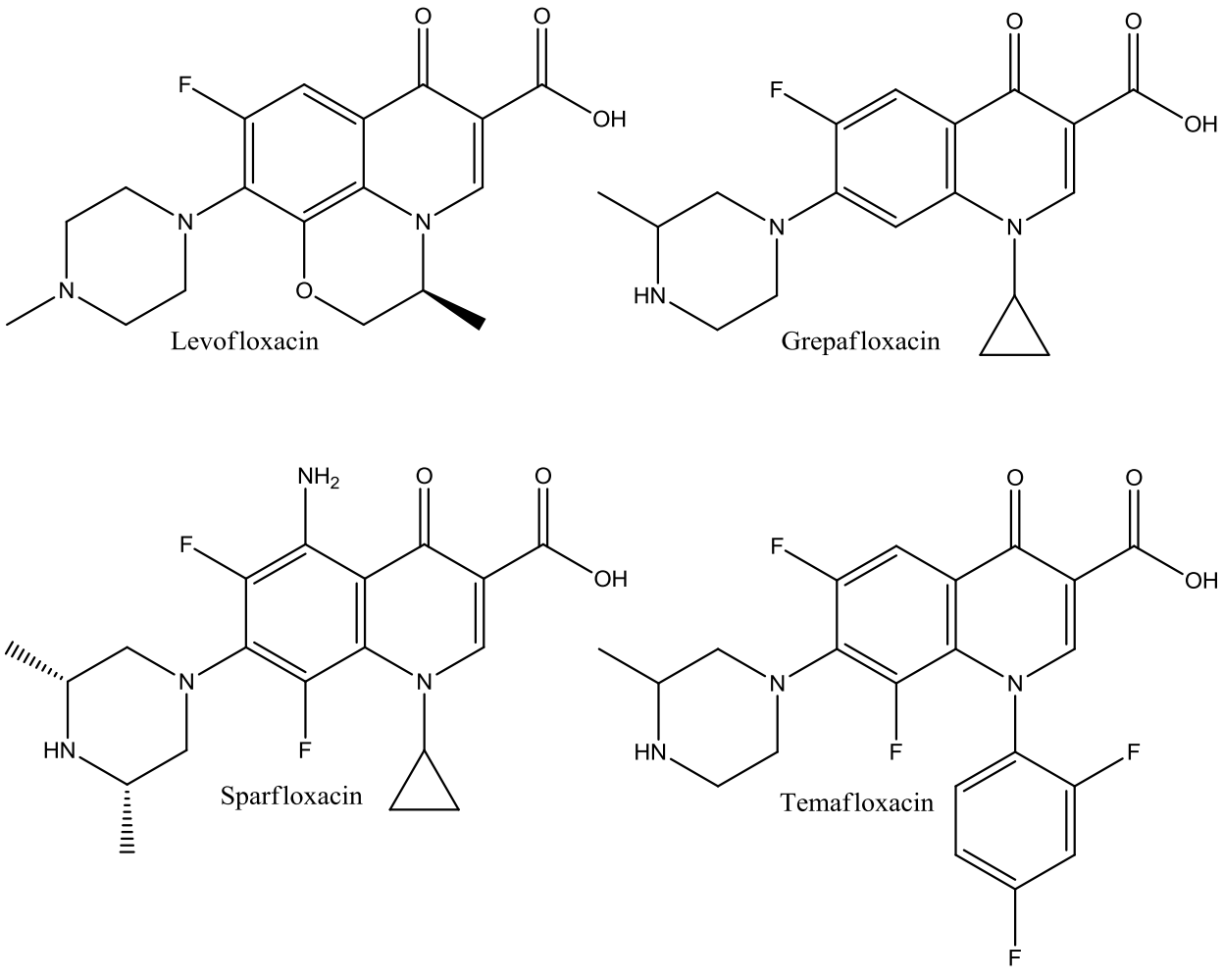

Figure 3.3. The structures of four third generation fluoroquinolones.

The fourth generation of fluoroquinolone compounds shows, perhaps, the greatest improvement over earlier generations. These compounds include clinafloxacin, gemifloxacin, sitafloxacin and moxifloxacin. All of these compounds show a similar level of activity against gram-negative bacteria to ciprofloxacin, making them some of the most effective fluoroquinolones at fighting infections caused by gram-negative species, although their activity against non-fermentative species such as *P. aeruginosa* remains poor. In addition to this activity, the fourth generation compounds show very good activity against a range of gram-positive bacteria including *S. pneumoniae*, *Haemophilus influenza* and *Chlamydia pneumoniae*. Many of the compounds, in particular sitafloxacin and clinafloxacin, also have increased activity against anaerobes. Another improvement seen in these compounds is the slower development of resistance to their action.

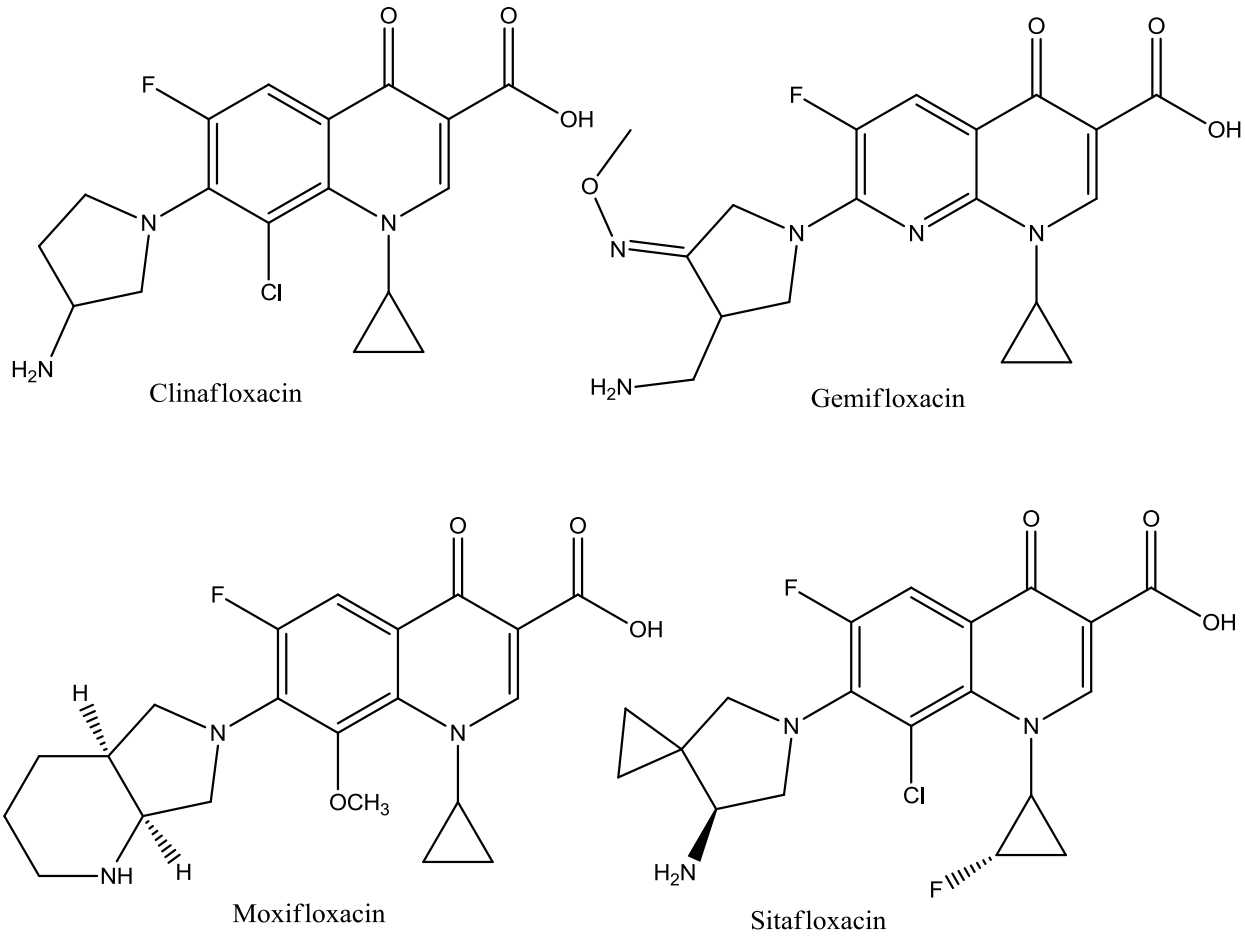

Figure 3.4. The structures of four fourth generation fluoroquinolones.

3.1.2 Type II DNA Topoisomerases

Fluoroquinolone antibiotics function by inhibiting the action of bacterial type II topoisomerases. These enzymes are essential for regulating DNA topology, especially during replication (Kubo *et al.*, 1979). There are two different types of type II topoisomerase: DNA gyrase and DNA topoisomerase IV. DNA gyrase is able to introduce negative supercoils into the bacterial chromosome and is also responsible for unwinding DNA at the replication fork (Brown and Cozzarelli, 1979). Topoisomerase IV, on the other hand, is responsible for decatenating the daughter chromosome from the parent prior to cell division (Peng and Marians, 1993) in addition to relaxing negative supercoils (Zechiedrich *et al.*, 2000). In order to achieve this, type II topoisomerases introduce and stabilise a double-strand break in the DNA allowing one strand to pass through the other in an ATP dependent manner. This is in contrast with type I topoisomerases which only break a single strand of DNA in order to regulate its topology (Lima *et al.*, 1994).

Type II topoisomerases are tetrameric with gyrase being made up of two GyrA subunits and two GyrB subunits and topoisomerase IV containing two ParE and two ParC subunits. The GyrB and ParE domains consist of a GHKL ATPase domain and a Toprim domain which is a Rossman fold capable of coordinating magnesium ions. The GyrA and ParC domains contain a 5Y-catabolite gene activator protein (5Y-CAP) domain as well as a variable C-terminal domain. Like domains form dimer interfaces which are known as gates and are responsible for controlling the movement of DNA by the enzyme. There is significant sequence homology between gyrase and topoisomerase IV enzymes and the two different type II topoisomerases of *Escherichia coli* share 40 % sequence identity (Ullsperger and Cozzarelli, 1996). Such identity is not seen in the C terminal domains of the enzymes which are likely to be responsible for substrate recognition (Corbett *et al.*, 2004). While the crystal structure of a complete type II topoisomerase has not been solved, several different partial structures exist which give a good insight into the structure and catalytic mechanism of the tetramer (Laponogov *et al.*, 2009, Bellon *et al.*, 2004, Morais Cabral *et al.*, 1997). A schematic representation of the different domains present in type II topoisomerases is shown in figure 3.5.

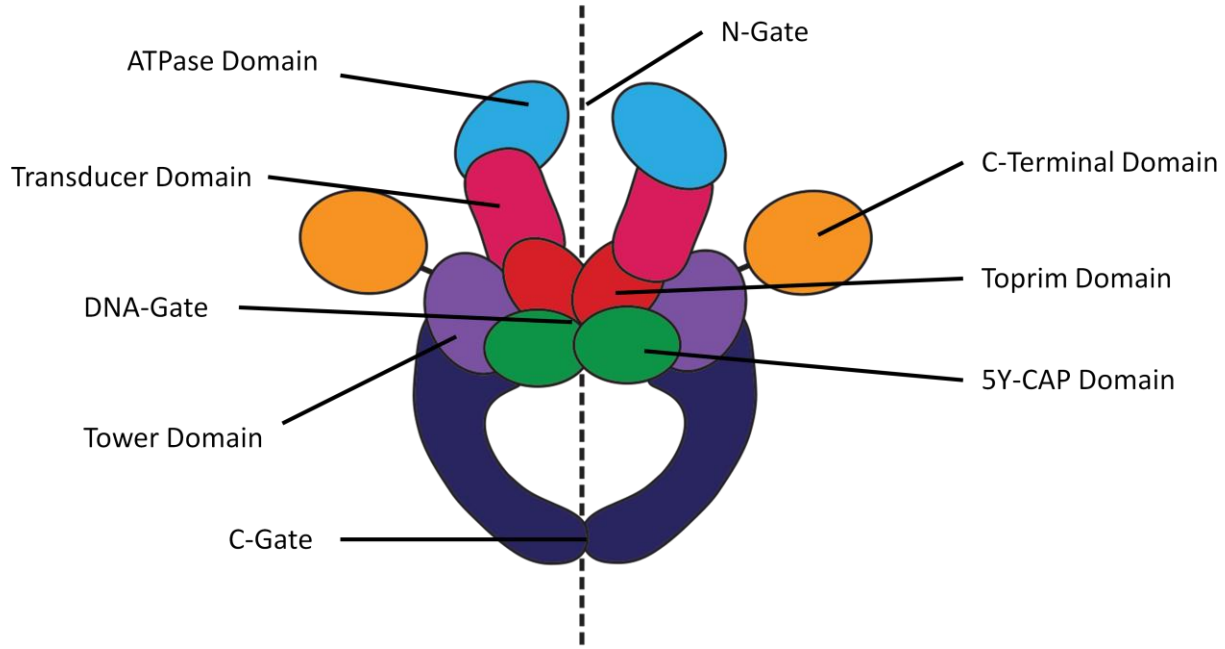

Figure 3.5. The domain structure of bacterial DNA gyrase.

The N-gate is formed by the ATPase domains, which are shown in light blue (GHKL subdomains) and pink (transducer subdomains). The DNA gate is formed by the Toprim domains, which are shown in red, and the 5Y-CAP domains, shown in green. The tower domains are shown in purple and the variable, C-terminal domains in orange and the C-gate is shown in dark blue.

Type II topoisomerases modify DNA via the 'two-gate mechanism' (Roca and Wang, 1994). The 'gates' involved are the N-gate which is created at the interface of the N-terminal domains of GyrB or ParE, the DNA gate which is formed by the GyrA-GyrB-DNA interface in gyrase and the ParC-ParE-DNA interface in topoisomerase IV and the C-gate or exit gate at the interface of the C-terminal region of GyrA or ParE. The gate (or 'G') segment of DNA associates with the enzyme at the interfaces of the N-termini of the GyrA dimer and the Toprim domain of GyrB (Bax *et al.*, 2010). During DNA association, approximately 130 base pairs wrap around the enzyme, particularly the variable C-terminal domains, supporting the hypothesis that these domains are involved in target recognition (Orphanides and Maxwell, 1994). Following association of the G segment, a second segment of DNA, the 'T' segment, associates with the N-gate of the enzyme. The primary role of gyrase is to introduce supercoils to a single DNA molecule so the T segment in such cases will be from the same DNA molecule as the G segment. Topoisomerase IV, in addition to a role in regulating supercoiling of DNA, is also responsible for decatenating daughter chromosomes from parent DNA, in which case the T segment and G segment would come from different DNA molecules. The N-gate is situated above the G segment, positioning the T segment in the optimum position to be passed through the G DNA strand (Heddle *et al.*, 2004).

Association of the DNA T segment to the N-gate of a type II topoisomerase enzyme facilitates ATP binding to the ATPase domain of GyrB or ParE. ATP binding triggers a conformational change in these subunits which effectively traps the T segment in position above the DNA G segment by closing the N-gate of the enzyme (Brino *et al.*, 2000). The closing of the N-gate triggers asymmetric double strand cleavage of the DNA G segment. The strands are cleaved four base pairs apart and the overhanging ends form phosphotyrosyl bonds with tyrosine residues in the GyrA or ParC breakage-reunion domains. These tyrosine residues are essential for catalysis and are highly conserved (Laponogov *et al.*, 2010, Morais Cabral *et al.*, 1997). At this point, the ATPase domain hydrolyses ATP, passing the DNA T segment through the double stranded break in the G segment. Once the T segment has passed through the break, the G segment is religated triggering the opening of the C gate and therefore release of DNA (Williams and Maxwell, 1999). In the absence of ATP, gyrase is able to catalyse DNA relaxation which is effectively the reverse of the supercoiling reaction (Gellert *et al.*, 1977).

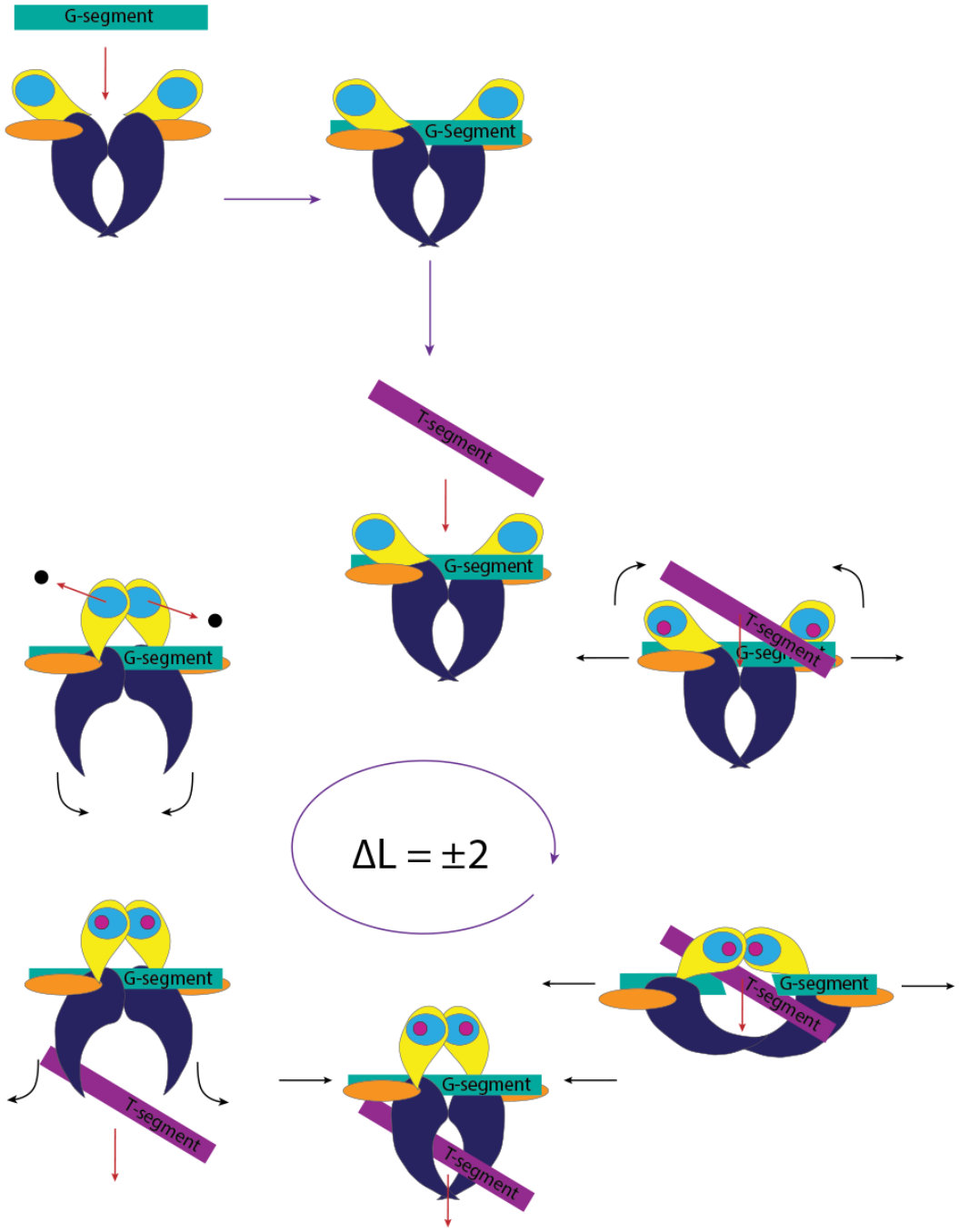

Figure 3.6.The reaction mechanism of type II topoisomerases.

The yellow subunit represents the GyrB/ParE domain, the dark blue subunit represents the N-terminal domain of GyrA/ParC and the orange subunit represents the C-terminal domain. The DNA G-segment is represented by the green bar and the DNA T-segment by the purple bar. The small circles represent bound ATP (red) and unbound ADP (black). The progression through the mechanism is indicated by blue arrows and direction of conformational change is indicated by black arrows. ΔL is the change in linking number of the substrate DNA.

The crystal structure of the ParC breakage-reunion domain and ParE Toprim domain of *S. pneumoniae* has been solved with levofloxacin, moxifloxacin and clinafloxacin bound (Laponogov *et al.*, 2009, Laponogov *et al.*, 2010). These structures all show the fluoroquinolone compounds intercalating between the nucleotides of the cleaved DNA G segment. Specifically, binding is in the gap adjacent to the nucleotides which are bound to Tyr188 in ParC. The structure with bound Moxifloxacin shows the cyclopropane group of the drug in close proximity to Ser79 and Asp83 in the active site of the enzyme. The bicyclic group at position seven of moxifloxacin stacks against the fourth nucleotide on the opposite DNA strand. The structure also shows the carboxylic acid and ketone groups, which are conserved across the vast majority of quinolones, in close proximity to Gly77, Asp78 and Arg117. However, despite its strong influence on the potency of the fluoroquinolones, the fluorine at position six of the structure is oriented away from both the protein and DNA, suggesting its influence on inhibition to be due to electronic effects (Laponogov *et al.*, 2009). The structure of topoisomerase IV with bound levofloxacin reveals a similar mode of binding, with the cyclic nucleus of the fluoroquinolone intercalating the cleaved DNA. However, in this structure the carboxylic acid group is seen to coordinate to Ser79 and Arg117 through a "highly-mobile" hydrogen-bonded water molecule (Laponogov *et al.*, 2010).

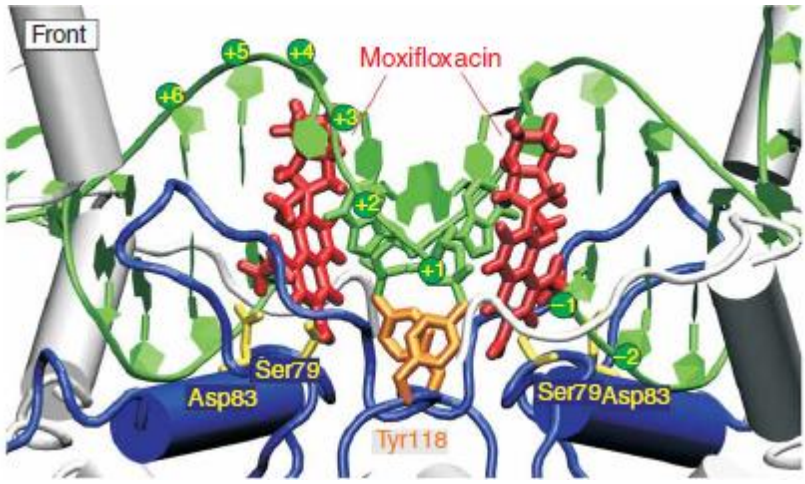

Figure 3.7. Moxifloxacin binding to DNA topoisomerase IV from S. pneumoniae.

The enzyme active site is shown in cartoon representation. Moxifloxacin is shown in red and the DNA G-segment is shown in green. The active site tyrosines which are bound to the cleaved DNA are shown in orange. Ser79 and Asp83, involved in quinolone binding, are shown in yellow. This image is taken from Laponogov et al.(2009).

The binding of fluoroquinolones to type II topoisomerases prevents religation of the DNA G segment, thus forming a stable quinolone-enzyme-DNA complex. This has a bacteriostatic effect as it blocks DNA replication and cell growth. Fluoroquinolones also have bactericidal effects which are not fully understood but act via different mechanisms depending upon the specific fluoroquinolone. The bactericidal effects of some quinolones can be blocked by the addition of the protein synthesis inhibitor chloramphenicol. This indicates that the quinolone-enzyme-DNA complex triggers the synthesis of a "suicide factor" which is responsible for cell death (Drlica *et al.*, 2008). Other fluoroquinolone compounds cause chloramphenicol insensitive cell death. This bactericidal mechanism is typically observed in compounds containing cyclopropyl and methoxy groups. It is likely that this mechanism requires the action of peroxide as the accumulation of hydroxyl radicals has been observed in cells undergoing this process (Wang and Zhao, 2009).

Fluoroquinolones are known to inhibit both DNA gyrase and DNA topoisomerase IV. However, which of these enzymes is the primary target depends upon the strain of bacteria and the fluoroquinolone in use. Typically, in gram negative bacteria, gyrase is the more susceptible enzyme, whereas, in gram positive bacteria, topoisomerase IV is more susceptible. This difference in preference goes some way to explaining why many fluoroquinolones tend to show high levels of potency against either gram negative or gram positive species but rarely both. The structure of a particular fluoroquinolone can have some influence on the target in a given bacterial strain. For example, *S. pneumoniae* is a gram positive bacterial species in which topoisomerase IV is the most susceptible target for fluoroquinolones. However, fluoroquinolones with a benzenesulfonylamido group at position seven show a preference for DNA gyrase in this organism. Addition of halogen or methoxy groups at position eight of the fluoroquinolone structure has also been observed to have a similar effect (Alovero *et al.*, 2000).

3.1.3 Structure Activity Relationships

Since the discovery of nalidixic acid, several thousand different quinolone compounds have been synthesised. This has led to a good understanding of the structure activity relationships for each part of the molecule. The carbonyl group in position 4, the carboxyl group in position 3 and the 2-3 double bond are all essential for antibacterial activity. The close proximity of these groups to the substituent in position 2 limits the range of modifications that can be made while still retaining activity and hydrogen has been shown to be by far the optimal group. These features are responsible for interactions with the topoisomerase DNA gates as shown in the structures described in section 2.2 (Laponogov *et al.*, 2010). The 3-carboxyl group is also important in bacterial uptake as it is ionised at physiological pH. The final essential structural feature of these drugs is the fluorine in position 6. The addition of this group to the first generation quinolone compounds was associated with a greater than ten-fold increase in DNA gyrase inhibition and up to a 100-fold improvement in minimum inhibitory concentration (MIC). As can be seen in figure 3.7, this group does not directly interact with the enzyme or the bound DNA. It is likely that the highly electronegative fluorine modulates the electron density of the aromatic quinolone ring allowing more effective base stacking when it is intercalating the cleaved DNA (Laponogov *et al.*, 2009).

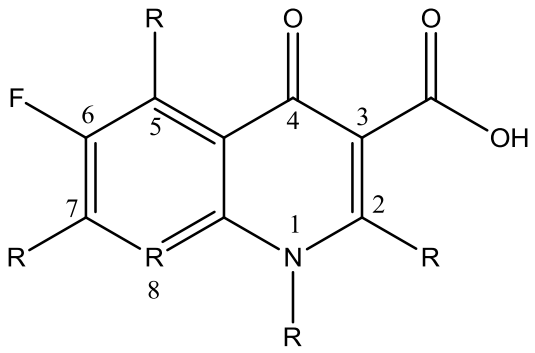

Figure 3.8. Core structure of quinolone compounds showing sites of modification.

The other positions of the quinolone structure are much more tolerant to modifications and this has enabled the huge range of structures and corresponding activities that can be seen in the quinolone family. Compounds with a number of different substituents in position 1 have been synthesised. These modifications have an effect on both the potency and pharmacokinetics of the compounds. One of the most commonly added groups in this position, particularly in later generation fluoroquinolones, is a cyclopropyl group. This group has been shown to provide optimum *in vitro* activity, with 2,4-diflurophenyl and *t*-butyl groups also improving activity to a lesser degree. The 2,4-difluorophenyl group, which is present in temafloxacin, also improves the *in vivo* efficacy of the compound and provides a slight improvement against gram positive bacteria and anaerobes. These groups are all more bulky than the ethyl groups found in nalidixic acid and other first generation quinolones and have been shown to interact directly with topoisomerase IV, which accounts for the improvement in activity against gram positive species (Laponogov *et al.*, 2009).

Substitutions at position 5 have been associated with improved activity against gram positive bacteria, although any improvements are minor if not present in addition to suitable substitutions in other positions, particularly position 1 (Domagala, 1994). Large, bulky substituents in position 5 cause a dramatic decrease in potency (Domagala *et al.*, 1993). This is likely to be due to the proximity of this position to the essential, enzyme binding groups in positions 3 and 4, with bulky groups likely to interfere with this binding. Small amino, hydroxyl and methyl groups in this position are associated with an increase in *in vitro* potency. Amino groups, as present in sparfloxacin are responsible for the greatest increase in potency. However, these groups also have a negative effect on the MIC of a compound, so many fluoroquinolones simply retain a hydrogen in this position.

The type of substituent in position 7 can have an influence on the potency, spectrum and pharmacokinetics of a quinolone compound. As discussed in section 3.1.1, the addition of a piperazine ring in this position in pipedimic acid was, along with the addition of fluorine in position 6, one of the key developments in producing clinically useful fluoroquinolones. The majority of later generation compounds contain either a piperazine or pyrrolidine ring in position 7, although these rings are often substituted. Piperazine rings, which are present in levofloxacin and sparfloxacin, are associated with improved potency against gram negative bacteria and also an increase in *in vivo* activity (Sanchez *et al.*,

1988). Amino pyrrolidine groups, found in clinafloxacin and sitafloxacin amongst others, are associated with improved potency against gram positive bacteria. The pyrrolidine ring in gemifloxacin is substituted with both a 3-aminomethyl group and a 4-methyloximino group. These substituents have been shown to increase further the potency of the compound against gram positive bacteria as well as improving the serum half life of the drug. It has also been shown that increasing the length of the alkyl chain in this compound increases the gram positive activity further although this is associated with a decrease in activity against gram negative bacteria (Appelbaum and Hunter, 2000). The presence of a basic nitrogen as the position 7 substituent is associated with an increase in membrane permeation of the compound. This is because, at physiological pH, the group will be protonated and therefore the fluoroquinolone will be zwitterionic.

The substituent at position 8 is important for the *in vivo* efficacy of the compound. Strictly speaking, quinolones have nitrogen in the aromatic ring in this position although the more common, pyridine-β-carboxylic acid derivatives are still described as quinolones. The optimum groups in this position for *in vivo* efficacy are N, CF and CCl, although CF, CCl and COMe groups also show improved activity against anaerobes (Domagala, 1994). Unfortunately, the presence of a halogen, particularly chlorine, at this position is strongly associated with phototoxicity which is an issue in compounds such as clinafloxacin and sparfloxacin. Methoxy groups in this position are also associated with an increase in activity against anaerobes but compounds with this group, such as moxifloxacin and gatifloxacin, do not appear to carry the risk of phototoxicity (Appelbaum and Hunter, 2000).

3.1.4 Side Effects of Fluoroquinolones

The majority of quinolones in clinical use produce adverse reactions in between two and ten percent of cases. The majority of these reactions are minor and affect the central nervous system (CNS), the gastrointestinal (GI) tract and the skin, although more serious reactions do occur in some cases. GI effects are the most common and are reported with all fluoroquinolones. These effects range from nausea and anorexia to abdominal pain, vomiting and diarrhoea. The exact cause of these effects is unknown although it is likely to be due to GI irritation or a CNS effect (Norrby, 1991). CNS effects are the second most common and can range from dizziness and headaches to sleep disorders, delirium and convulsions. Two possible pathways have been suggested to account for these effects. Some fluoroquinolones are known to bind to $GABA_A$ receptors in the brain. This stops gamma-aminobutyric acid (GABA), the natural ligand of the receptor, from binding and causes stimulation of the CNS. This effect is most common with fluoroquinolones containing piperazine rings in position 7 and also occurs when pyrrolidine rings are found in the same position. Substitution of these rings decreases the ability of the compounds to bind to $GABA_A$ and the degree of *in vivo* brain penetration also plays a role in the level of binding(Takayama *et al.*, 1995). Adverse skin reactions typically occur due to phototoxicity, which is discussed in section 3.1.3, or allergic reactions causing histamine release (Ball and Tillotson, 1995). More serious skin problems are extremely rare.

Many fluoroquinolone compounds have been withdrawn from clinical use due to side effects which are specific to or more common with particular drugs. In very rare cases, fluoroquinolones have been known to cause sudden cardiac death and a condition called torsades de pointes which is characterised by an increased QT interval. These effects are more common with the fluoroquinolone grepafloxacin which has subsequently been withdrawn from use (Ball, 2000). Gatifloxacin has been withdrawn from use due to an increased incidence of hypo- and hyperglycaemia (Park-Wyllie *et al.*, 2006) and levofloxacin has also been associated with dysglycaemia although it remains in use (Aspinall *et al.*, 2009). Temafloxacin and trovafloxacin are known to cause severe immunologically mediated adverse reactions. This is due to the 2,4-difluorophenyl groups present in position 1 of these compounds. These effects range from fever, jaundice and haemolysis to, in severe cases, renal failure and hepatitis. Trovafloxacin has also been known to cause eosinophilic hepatitis with liver necrosis and even the need for liver transplantation in the most extreme cases (Chen *et al.*, 2000). Neither of these two drugs remains in use. A final, rare class effect of fluoroquinolones is tendinitis, typically of the Achilles tendon. In some cases this can lead to the tendon rupturing although this effect is more common in the elderly and patients already taking corticosteroids (Dekens-Konter *et al.*, 1994).

Fluoroquinolones have also been shown to have some inhibitory activity against mammalian topoisomerase II. This activity is observed in all quinolones but each compound has a characteristic concentration above which inhibition occurs. The groups present in positions 1, 7 and 8 have been shown to be the most important in determining the degree of interaction with the mammalian enzyme (Elsea *et al.*, 1993). For position 1, the strongest interactions are observed in compounds with a cyclopropyl substituent although *t*-butyl groups also show high activity. Substitution of the cyclopropyl ring, as seen in sitafloxacin, is able to reduce this effect. In position 7, pyrrolidine rings are responsible for the greatest activity but any compounds containing cyclic, nitrogen containing groups show activity (Wentland *et al.*, 1993). In position 8, fluorine, chlorine or methoxy groups cause the greatest level of interaction with mammalian topoisomerase with a CH in that position causing the lowest activity. Interaction with the mammalian topoisomerase II enzyme is linked with cytotoxicity (Elsea *et al.*, 1993).

3.1.5 Mechanisms of Fluoroquinolone Resistance

A major problem for all antibacterial drugs is the development of bacterial resistance to their effects (Andersson and Levin, 1999). The emergence of strains resistant to many different types of drug is a particular concern in hospital environments as infections caused by such strains are becoming increasingly difficult to treat. Fluoroquinolones are no different to other antibacterials in this respect and several different mechanisms of resistance to these compounds have been identified (Drlica *et al.*, 2012).

Permeability based resistance to fluoroquinolones is an issue in gram negative bacteria. These bacteria contain protein channels called porins which are responsible for uptake of certain hydrophilic molecules. Fluoroquinolone resistance in certain gram negative bacteria has been associated with a deficiency in

certain porin proteins including OmpF in *E. coli* and D2 in *P. aeruginosa* (Michea-Hamzehpour *et al.*, 1991). In *E. coli*, permeability based quinolone resistance can also be associated with chloramphenicol and tetracycline resistance. This occurs because of a mutation in the *marA* gene of the multiple antibiotic system and leads to a downregulation of *ompF* mRNA and therefore a decrease in the number of OmpF porin channels (Cohen *et al.*, 1988).

Efflux based resistance is a significant issue for fluoroquinolones with many compounds acting as substrates for one or more different efflux pump proteins. Several different families of efflux pumps have been identified including the ATP-binding cassette (ABC) superfamily, the resistance-nodulation-division (RND) superfamily, the major facilitator (MF) superfamily, the small multidrug resistance (SMR) family and the multi-drug and toxic compound extrusion (MATE) family. Gram negative bacteria typically express several different efflux pumps, at least 37 different pumps have been identified in *E. coli*, for example, and virtually all species have at least one pump that is able to export certain quinolones. Due to the range of structural variation in fluoroquinolone compounds, generalising with regards to efflux mediated resistance can be difficult. Gatifloxacin has actually been shown to inhibit certain efflux pumps in ciprofloxacin resistant strains of *P. aeruginosa*. If both compounds are used together their synergistic effects produce antibacterial activity against the resistant strains (Pankey and Ashcraft, 2005). Many efflux pumps are known to play a role in the export of multiple drug types, for example the AcrAB-TolC system in *E. coli*. This RND system exports several different antibacterials including β-lactams, tetracycline and chloramphenicol. *E. coli* strains deficient in the AcrAB proteins of this system are known to be hypersensitive to some fluoroquinolones but many fluoroquinolone resistant strains overexpress AcrA (Hirakawa *et al.*, 2008). This results in decreased cellular accumulation of many antibacterials, potentially causing resistance to several different drugs. This phenomenon is also observed in certain resistant strains of *P. aeruginosa* where up to six different fluoroquinolone exporters from the RND superfamily are overexpressed leading to multidrug resistance (Kriengkauykiat *et al.*, 2005).

Efflux based resistance is also a common problem in gram positive bacteria. In these bacteria, the MF and SMR families are most commonly associated with fluoroquinolone resistance. In *S. aureus*, NorA, an MF family efflux pump, as well as certain MATE pumps are involved in quinolone export. These systems are regulated by the *mgrA* and *mepA* genes, respectively. In resistant strains, mutant alleles of these regulatory genes, leading to overexpression of the efflux pumps, are frequently found (Truong-Bolduc *et al.*, 2006, Kumaraswami *et al.*, 2009). The NorA equivalent in *S. pneumoniae*, PmrA, is known to export ciprofloxacin and norfloxacin although compounds with bulky substituents in position 7 of their structures, such as sitafloxacin and moxifloxacin, as well as substituents other than hydrogen in position 8, are less susceptible to efflux (Beyer *et al.*, 2000). It is possible to use fluoroquinolones in combination with efflux pump inhibitors such as reserpine; these inhibitors, however, are rarely broad enough in their spectrum of action to sufficiently increase MIC. The effects of efflux inhibitors are further limited due to the ability of fluoroquinolones to induce overexpression of certain ABC family exporter proteins (Marrer *et al.*, 2006).

Plasmid mediated fluoroquinolone resistance mechanisms have also been discovered in recent years. One such mechanism involves the role of topoisomerase protecting proteins. These proteins are known as Qnr (Quinolone resistance) proteins and were first identified in *Klebsiella pneumoniae*. QnrA from this

bacterium is a 218 amino acid protein characterised by pentapeptide repeats containing leucine or phenylalanine every fifth residue. A similar protein, MfpA, was discovered in *Mycobacterium smegmatis* and was shown to be similar in size, shape and electrostatics to B DNA (Hegde *et al.*, 2005). These proteins bind specifically to the GyrA and GyrB subunits of DNA gyrase and the ParC and ParE subunits of topoisomerase and reverse fluoroquinolone inhibition, even when fluoroquinolones are in a 1000-fold excess (Tran *et al.*, 2005a, Tran *et al.*, 2005b). This reversal of inhibition is likely to be due to an alteration of the DNA binding properties of topoisomerase enzymes rather than a direct effect upon quinolone binding and is able to increase the MIC of a compound up to 100-fold. Another mechanism of plasmid mediated resistance is via quinolone modifying enzymes such as aac(6')-lb-cr. This enzyme acetylates unsubstituted nitrogen atoms in the piperazinyl ring in position 7 of fluoroquinolones leading to an increase in MIC (Robicsek *et al.*, 2006).

The most common mechanism of quinolone resistance occurs via mutations in bacterial type II topoisomerase enzymes. Resistance causing mutations typically occur in a narrow region known as the quinolone-resistance-determining region. In *E. coli* gyrA the most effective mutations are of ser83 and asp87, two residues which are highly conserved across GyrA and ParC domains. As seen in the structure of *S. pneumoniae* these residues are heavily involved with quinolone binding (Laponogov *et al.*, 2010). Mutations have also been identified in gyrB and parE in fluoroquinolone resistant strains although these are less effective that gyrA/parC mutations. In gyrB these mutations are typically found in the GyrA recognition helix so may affect the activity of the enzyme rather than directly affecting quinolone binding (Fass *et al.*, 1999).

Selection of fluoroquinolone resistant mutants occurs in what is known as the mutant selection window. This is the fluoroquinolone concentration range between the MIC and the mutant prevention concentration (MPC). The MPC is defined as the MIC of the least fluoroquinolone susceptible mutant. If the fluoroquinolone concentration is within this window, growth of susceptible bacteria is inhibited but growth of resistant bacteria is not (Baquero and Negri, 1997). This effectively enriches the bacterial population with resistant mutants. In order for growth to occur above the MPC, two or more resistance mutations must be acquired, which is rare. Widespread quinolone resistance is likely to have been facilitated by prescription of the drugs for inappropriate infections and at doses that are within the mutant selection window (Lautenbach *et al.*, 2003). This is a particular problem with fluoroquinolone use in animals (Aarestrup *et al.*, 2000). Selection of mutants with efflux based resistance is a problem not only for future fluoroquinolone use but for the use of other antibiotics which are also exported from cells via the same mechanisms. In fact, one study has shown that an overall decrease in fluoroquinolone use in one hospital was associated with a significant decrease in the rates of methicillin-resistant *Staphylococcus aureus* (MRSA) (Parienti *et al.*, 2011).

3.1.6 New Fluoroquinolone Compounds

A number of novel fluoroquinolone derivatives have been synthesised (Murray *et al.*, 2012), the general structures of which are shown in figure 3.9 below. These compounds are based upon the existing fluoroquinolone compounds levofloxacin and pefloxacin. The only site of modification is in position 1 of the quinolone nucleus. The aim of the work undertaken here is to assess the *in vitro* activity of these compounds against a selection of non-fluoroquinolone resistant bacterial strains. These are *Enterococcus faecalis*, a gram positive bacterium found in the gastrointestinal tract, *S. aureus*, a gram positive bacterium found as part of the skin flora of many humans, and *P. aeruginosa*, a gram negative species found in soil and skin flora. All of these bacteria are capable of causing infections in humans that can, in some cases, be life threatening. The primary target of fluoroquinolones in *S. aureus* is topoisomerase IV whereas the primary target in *P. aeruginosa* is gyrase. Both gyrase and topoisomerase IV have been identified as fluoroquinolone targets in *E. faecalis* (Kanematsu *et al.*, 1998).

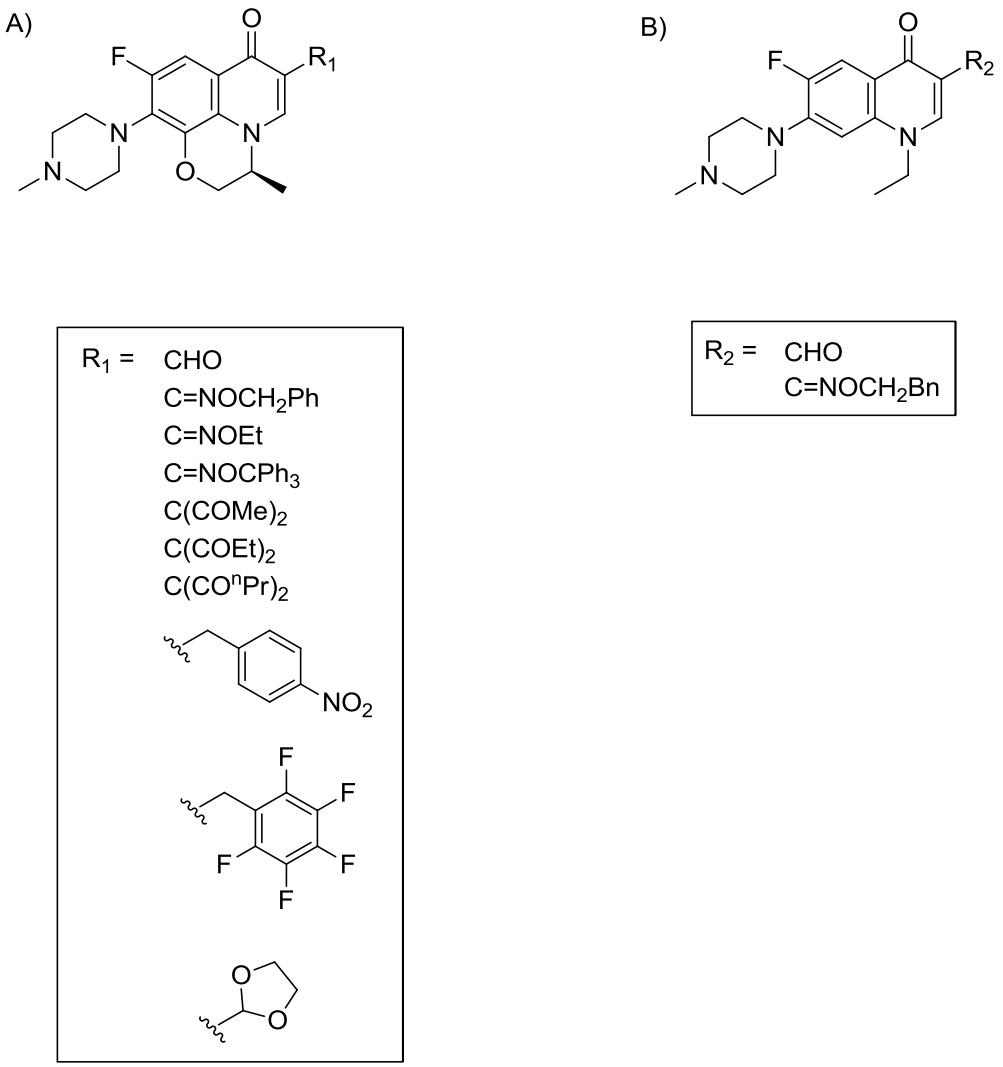

Figure 3.9. The structures of novel fluoroquinolone compounds synthesised by Redx Pharma Ltd.

Compounds are based upon (A) levofloxacin and (B) pefloxacin with variations all occurring at position 1 of the fluoroquinolone nucleus.

3.2 Results and Discussion

The potential antibacterial compounds were tested for their activity against a range of bacteria using the Kirby-Bauer disk diffusion technique (Bauer *et al.*, 1966). Different concentration solutions of each compound were applied to filter paper disks before being placed upon Mueller-Hinton agar plates which had been inoculated with Mueller-Hinton 'top' agar containing different bacterial culture to produce growth of a bacterial lawn. After being incubated at 37 °C for 18 hours, zones of activity could be

measured around the disks. These zones are regions of no bacterial growth and are easily identifiable as the agar in these zones is translucent rather than the opaque covering produced by the bacterial lawn.

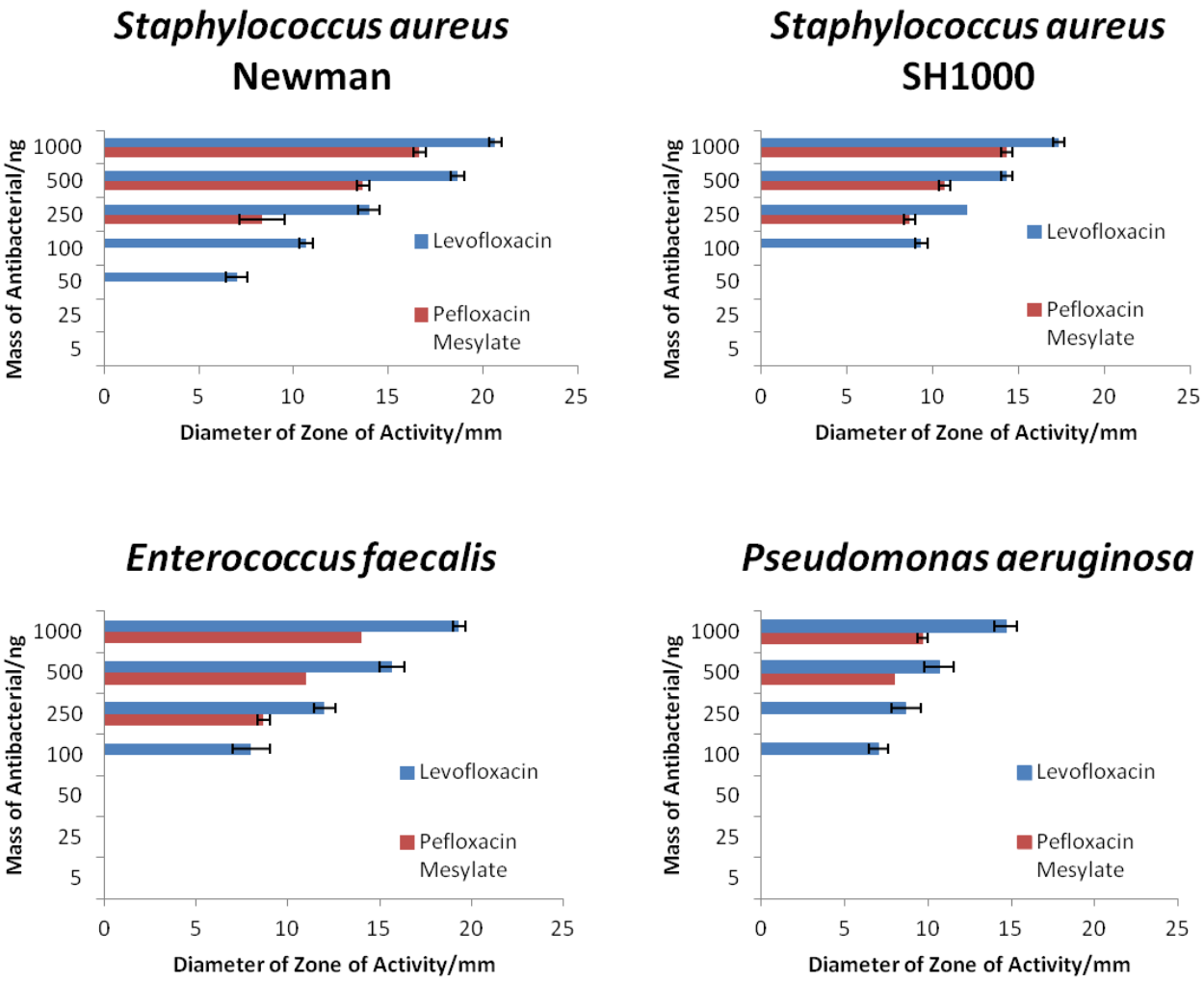

Figure 3.10. Size of zones of activity of levofloxacin and pefloxacin mesylate with four different bacterial strains.

Data was obtained using the Kirby-Bauer disk diffusion method with a range of different amounts of two commercially available fluoroquinolone compounds. Results for Levofloxacin are shown in blue and results for pefloxacin mesylate are shown in red. The diameters of zones of activity shown are the means of three biological replicates. Error bars are the standard error of the mean and results which lack error bars do so due to all replicates being identical to the nearest millimetre.

In initial testing, the parent compounds, levofloxacin and pefloxacin mesylate, showed clear zones of antibacterial activity around the discs containing higher amounts of the compounds. At the very lowest antibacterial concentrations no activity was observed, which suggests that the zones of no bacterial growth are due to the activity of the antibacterial compounds rather than any contamination introduced during the experiment. The results also show a clear decrease in the size of the zones of activity as the amount of antibacterial decreases. This can be seen in figure 3.11.

Based upon these initial results, it was decided to test the novel fluoroquinolone compounds using discs containing 10 ng, 100 ng, 1000 ng and 10000 ng of each. It was not possible to test significantly higher masses due to the small amounts of each compound that were provided. A positive control of 100 ng levofloxacin was included on each plate as this mass showed activity against all bacterial strains. Five novel fluoroquinolones and a 3-formyl levofloxacin derivative were tested by this method and the results are shown in tables 3.1 – 3.6. The plates produced during the experiments are shown in appendix B. Each compound was tested against each strain of bacteria twice and concordant results were obtained for all compounds.

	Diameter of Zone of No Bacterial Growth / mm							
	P. aeruginosa		*E. faecalis*		*S. aureus* SH1000		*S. aureus* Newman	
Mass of Compound / ng	Plate 1	Plate 2	Plate 1	Plate 2	Plate 1	Plate 2	Plate 1	Plate 2
10	0	0	0	0	0	0	0	0
100	0	0	0	0	0	0	0	0
1000	0	0	0	0	0	0	0	0
10000	7	7	7	8	7	8	8	8
Control	7	8	7	8	7	8	8	10

Table 3.1. Diameters of zones of no growth around discs of filter paper soaked in different masses of a 3-formyl levofloxacin derivative placed of plates inoculated with four different bacteria.

Discs of filter paper soaked with different masses of a 3-formyl levofloxacin derivative dissolved in 5 µl of DMSO are placed onto Mueller-Hinton agar (21 g l^{-1} Mueller-Hinton broth, 1.5 % (w/v) agar) plates inoculated with Mueller-Hinton top agar (21 g l^{-1} Mueller-Hinton broth, 0.7 % (w/v) agar) mixed with different strains of bacteria which are incubated at 37 °C for 18 hours. The control used is 100 ng of levofloxacin.

	Diameter of Zone of No Bacterial Growth / mm							
	P. aeruginosa		*E. faecalis*		*S. aureus* SH1000		*S. aureus* Newman	
Mass of Compound / ng	Plate 1	Plate 2	Plate 1	Plate 2	Plate 1	Plate 2	Plate 1	Plate 2
10	0	0	0	0	0	0	0	0
100	0	0	0	0	0	0	0	0
1000	0	0	0	0	0	0	0	0
10000	0	0	0	0	0	0	0	0
Control	8	7	8	7	7	7	11	8

Table 3.2. Diameters of zones of no growth around discs of filter paper soaked in different masses of fluoroquinolone derivative number one placed of plates inoculated with four different bacteria.

Discs of filter paper soaked with different masses of fluoroquinolone derivative number one dissolved in 5 µl of DMSO are placed onto Mueller-Hinton agar (21 g l^{-1} Mueller-Hinton broth, 1.5 % (w/v) agar) plates inoculated with Mueller-Hinton top agar (21 g l^{-1} Mueller-Hinton broth, 0.7 % (w/v) agar) mixed with different strains of bacteria which are incubated at 37 °C for 18 hours. The control used is 100 ng of levofloxacin.

	Diameter of Zone of No Bacterial Growth / mm							
	P. aeruginosa		*E. faecalis*		*S. aureus* SH1000		*S. aureus* Newman	
Mass of Compound / ng	Plate 1	Plate 2	Plate 1	Plate 2	Plate 1	Plate 2	Plate 1	Plate 2
10	0	0	0	0	0	0	0	0
100	0	0	0	0	0	0	0	0
1000	0	0	0	0	0	0	0	0
10000	0	0	0	0	0	0	0	0
Control	8	7	8	7	7	7	9	8

Table 3.3. Diameters of zones of no growth around discs of filter paper soaked in different masses of fluoroquinolone derivative number two placed of plates inoculated with four different bacteria.

Discs of filter paper soaked with different masses of fluoroquinolone derivative number two dissolved in 5 µl of DMSO are placed onto Mueller-Hinton agar (21 g l^{-1} Mueller-Hinton broth, 1.5 % (w/v) agar) plates inoculated with Mueller-Hinton top agar (21 g l^{-1} Mueller-Hinton broth, 0.7 % (w/v) agar) mixed with different strains of bacteria which are incubated at 37 °C for 18 hours. The control used is 100 ng of levofloxacin.

	Diameter of Zone of No Bacterial Growth / mm							
	P. aeruginosa		*E. faecalis*		*S. aureus* SH1000		*S. aureus* Newman	
Mass of Compound / ng	Plate 1	Plate 2	Plate 1	Plate 2	Plate 1	Plate 2	Plate 1	Plate 2
10	0	0	0	0	0	0	0	0
100	0	0	0	0	0	0	0	0
1000	0	0	0	0	0	0	0	0
10000	0	0	0	0	0	0	0	0
Control	8	8	7	7	7	8	9	8

Table 3.4. Diameters of zones of no growth around discs of filter paper soaked in different masses of fluoroquinolone derivative number three placed of plates inoculated with four different bacteria.

Discs of filter paper soaked with different masses of fluoroquinolone derivative number three dissolved in 5 µl of DMSO are placed onto Mueller-Hinton agar (21 g l^{-1} Mueller-Hinton broth, 1.5 % (w/v) agar) plates inoculated with Mueller-Hinton top agar (21 g l^{-1} Mueller-Hinton broth, 0.7 % (w/v) agar) mixed with different strains of bacteria which are incubated at 37 °C for 18 hours. The control used is 100 ng of levofloxacin.

	Diameter of Zone of No Bacterial Growth / mm							
	P. aeruginosa		*E. faecalis*		*S. aureus* SH1000		*S. aureus* Newman	
Mass of Compound / ng	Plate 1	Plate 2	Plate 1	Plate 2	Plate 1	Plate 2	Plate 1	Plate 2
10	0	0	0	0	0	0	0	0
100	0	0	0	0	0	0	0	0
1000	0	0	0	0	0	0	0	0
10000	0	0	0	0	0	0	0	0
Control	8	8	7	7	7	8	9	8

Table 3.5. Diameters of zones of no growth around discs of filter paper soaked in different masses of fluoroquinolone derivative number four placed of plates inoculated with four different bacteria.

Discs of filter paper soaked with different masses of fluoroquinolone derivative number four dissolved in 5 µl of DMSO are placed onto Mueller-Hinton agar (21 g l^{-1} Mueller-Hinton broth, 1.5 % (w/v) agar) plates inoculated with Mueller-Hinton top agar (21 g l^{-1} Mueller-Hinton broth, 0.7 % (w/v) agar) mixed with different strains of bacteria which are incubated at 37 °C for 18 hours. The control used is 100 ng of levofloxacin.

	Diameter of Zone of No Bacterial Growth / mm							
	P. aeruginosa		*E. faecalis*		*S. aureus* SH1000		*S. aureus* Newman	
Mass of Compound / ng	Plate 1	Plate 2	Plate 1	Plate 2	Plate 1	Plate 2	Plate 1	Plate 2
10	0	0	0	0	0	0	0	0
100	0	0	0	0	0	0	0	0
1000	0	0	0	0	0	0	0	0
10000	0	0	0	0	0	0	0	0
Control	8	8	7	7	7	7	8	8

Table 3.6. Diameters of zones of no growth around discs of filter paper soaked in different masses of fluoroquinolone derivative number five placed of plates inoculated with four different bacteria.

Discs of filter paper soaked with different masses of fluoroquinolone derivative number five dissolved in 5 µl of DMSO are placed onto Mueller-Hinton agar (21 g l^{-1} Mueller-Hinton broth, 1.5 % (w/v) agar) plates inoculated with Mueller-Hinton top agar (21 g l^{-1} Mueller-Hinton broth, 0.7 % (w/v) agar) mixed with different strains of bacteria which are incubated at 37 °C for 18 hours. The control used is 100 ng of levofloxacin.

One of the compounds tested, the 3-formyl levofloxacin derivative, showed a small zone of activity against each bacterial strain around the disc containing 10000 ng. These were significantly smaller than the zones of activity produced by the same mass of each of the parent compounds. This result is supported by previous work which showed that 3-formylquinolones display *in vitro* activity against *S. aureus* and *P. aeruginosa*. However, levofloxacin is expected to be over 100 times more potent than its 3-formyl derivative and pefloxacin is expected to be up to 30 times more potent than its 3-formyl derivative (Kondo *et al.*, 1988).

This study of 3-formylquinolone activity also investigated the *in vivo* activity of the levofloxacin and pefloxacin derivatives (Kondo *et al.*, 1988). The ED50 values calculated in this study show that the 3-formyl derivatives are approximately twice as effective *in vivo* as the parent fluoroquinolones. Under physiological conditions, 3-formylquinolones are oxidised to their corresponding carboxylic acid (Racker, 1955). This means that the 3-formyl derivatives of levofloxacin and pefloxacin will be converted to levofloxacin and pefloxacin *in vivo*. This means that the increase in *in vivo* activity must be due to improved pharmacokinetic properties of the 3-formyl compounds. It is likely that the improvement comes as a result of improved absorption of the drug when it is administered orally, which is supported by the serum concentration data produced (Kondo *et al.*, 1988).

As can be seen from tables 3.1 – 3.6, none of the remaining five compounds tested showed any activity against any of the bacterial strains at the quantities tested. This result is expected to some degree, due to the structures of the compounds. These compounds varied from the structures of the parent compounds levofloxacin and pefloxacin only by the group present in position 1 of the structure. In

nearly all known, functional fluoroquinolone compounds a carboxylic acid group is found in this position and this group is known to be heavily involved in binding to type II topoisomerases (Laponogov *et al.*, 2010, Laponogov *et al.*, 2009). With the exception of the aldehyde compounds, these new fluoroquinolones all contain groups that are substantially bulkier than a carboxylic acid group. These groups are likely to interfere with the interaction between the compound and the binding site serine or arginine residues involved in quinolone binding.

It is also possible that the other compounds tested would be metabolised to the parent compounds levofloxacin and pefloxacin under physiological conditions. This is certainly likely to be true for the compounds containing imine ether compounds which are known to be converted to carbonyl groups *in vivo* (Foley *et al.*, 2009). For the compounds tested in this experiment, this would result in the formation of the 3-formylquinolone compounds which would, of course, subsequently be oxidised to the carboxylic acids of the parent compounds. The metabolism of the other groups is less likely to result in formation of levofloxacin or pefloxacin. The β-diketone compounds are likely to be converted to alcohols via the actions of β-diketone hydrolases (Grogan, 2005) and carbonyl reductases. These possible products are unlikely to be active against topoisomerases as the remaining substituents in position 3 will be too bulky for enzyme binding to occur. In addition to this, β-diketone hydrolases are also found in bacteria including *Pseudomonas* species so if a metabolic product did have topoisomerase inhibiting activity then this may be seen in *in vitro* testing. The metabolic products of the compounds containing aromatic groups in position 3 are also likely to be too bulky for effective topoisomerase binding.

3.3 Conclusion

The lack of *in vitro* activity displayed by these compounds was deemed sufficient to end these trials. Despite this, further testing at higher concentrations may reveal that certain compounds do display *in vitro* activity. Unfortunately, due to the small amounts of each compound that were provided for these experiments, it was not possible to test the compounds at significantly higher amounts. However, any positive results obtained by such experiments would be limited in their usefulness because any fluoroquinolone-topoisomerase interactions causing the activity are unlikely to occur under physiological conditions. If these compounds were to be investigated further, the most useful approach would be to carry out *in vivo* testing, as described in section 6.2.

It is unlikely, however, that any of these compounds would offer an improvement in activity against fluoroquinolone resistant bacterial strains. Any improvement in activity over its parent compound offered by a compound would almost certainly be due to its pharmacokinetic properties. The pharmacodynamics of the compounds would be identical to those of the parent compounds, as the new fluoroquinolones are expected to behave as prodrugs. If metabolic reactions are able to form an active compound, then these must happen before the drug enters the bacterial cell. Effectively, the prodrug would be converted to its parent compound, either levofloxacin or pefloxacin, and its activity from that

point onwards would be the same as that parent. If a bacterial strain is resistant to levofloxacin or pefloxacin then, whatever the mechanism of that resistance, it will remain resistant to any prodrug which does not show activity *in vitro*.

Chapter 4

4. Development of a Biodegradable Shampoo Sachet

4.1 Introduction

4.1.1 Shampoo Packaging in Developing Countries

Developing countries with rapidly growing economies such as Brazil, Russia, India and China (BRIC countries) are potentially huge new markets for many global brands. These countries currently have a great imbalance in the distribution of wealth with large proportions of the population living in poverty. However, over this decade, it is estimated that the distribution of wealth in developing countries will change, resulting in a significant increase in the purchasing power of many people (Unilever, 2012a). This increase in disposable income means that people are more likely to consider purchasing cosmetic products, such as shampoos, in addition to other products which were not previously affordable for them. However, when large volume product sizes similar to those available in the UK were first introduced in India, they sold poorly as they still remained too expensive for the budgets of the majority of customers.

A solution to this problem was provided by Indian company CavinKare, who began selling shampoo in small sachets in 1983. These sachets allowed consumers to purchase shampoo as and when it was required, rather than having to make a comparatively expensive, one-off purchase for a large volume bottle. This is important in a country where almost one third of the population lives on less than $1.25 per day (World Bank Group, 2012). These sachets are sold for as little as 1 rupee (Unilever, 2012a) which is the equivalent of just over 1 penny in the UK. The contents of these sachets are often meted out very carefully by the customers and in some cases a single sachet of shampoo can last an entire family for a whole week. Not only are sachets an affordable solution for low income customers but they are also a more efficient way of packaging shampoo compared to larger bottles and produce less waste by weight per millilitre of product (Unilever, 2012b).

Unfortunately, the countries in which sachets are a popular product typically have poor infrastructure for waste removal and recycling. The majority of sachets sold end up in landfill, are discarded as litter or are washed into the sewage system. Sachets are typically manufactured from polyethylene coated with aluminium foil. These materials are degraded extremely poorly by the environment and can take decades to break down (Mumtaz *et al.*, 2010). This results in the production of large amounts of waste and can easily lead to blockages of sewers and water ways. As well as the clear environmental impact, the blockage of sewers can potentially cause public health issues. This is coupled with the embarrassment and negative commercial impact experienced by the shampoo manufacturers as large amounts of waste bearing their branding are created. A method of reducing this waste and its associated problems is therefore highly desirable from the point of view of both the manufacturer and consumer.

4.1.2 Initial Concept for a Biodegradable Shampoo Sachet

The work described in the next two chapters had the aim of creating a solution to the problems caused by shampoo sachet waste, specifically by producing a prototype of a biodegradable shampoo sachet. Ideally the prototype should lead to 0 % residual solid waste after degradation with all mass being eventually converted to carbon dioxide and water. In addition to being completely biodegradable, the sachet must also make use of existing, commercially available materials and be commercially viable. The initial concept for this work involves the use of a bilayer system of two different materials, with an enzyme contained between them. The outer layer will be made from cellulose, a biodegradable polysaccharide, and the enzyme used will be a cellulase in order to enhance the rate of cellulose breakdown. The inner layer of the bilayer will be made from polyvinyl alcohol (PVOH). This material will remain intact when the sachet contains shampoo but, once the contents have been used, the PVOH will break down when it comes into contact with water, activating the cellulase and triggering the breakdown of the outer layer.

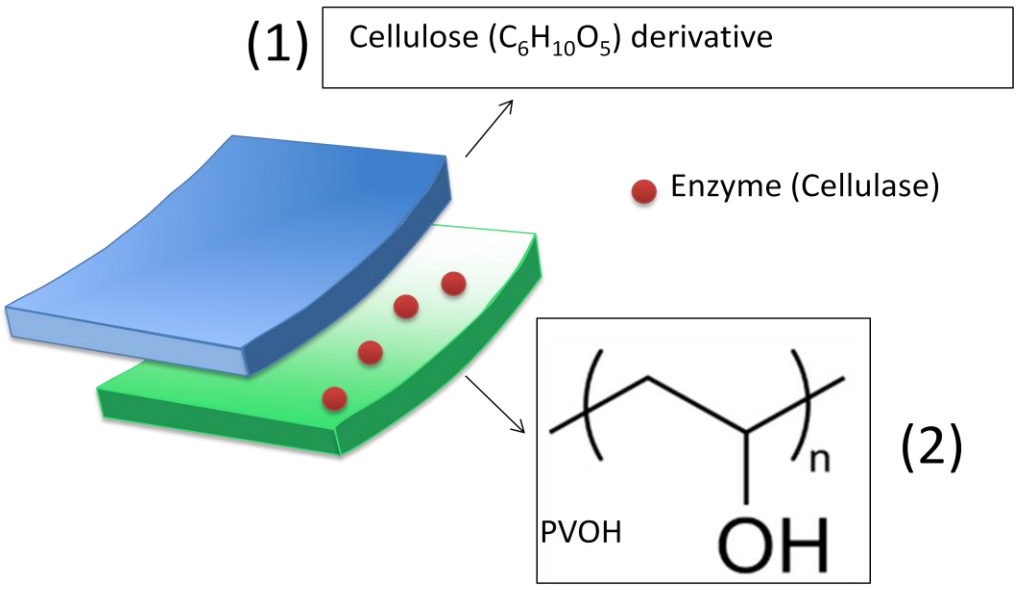

Figure 4.1. The initial bilayer concept for a biodegradable shampoo sachet.

The outer layer (1), shown in blue, will be made from a cellulose material and the inner layer (2), shown in green, will be made from PVOH. Cellulase enzyme will be held between the two layers and will be activated when the inner, PVOH, layer is broken down by water.

4.1.3 Cellulose

Cellulose is the most common organic molecule on Earth. It is found in plants, algae and oomycetes and is secreted by some bacteria. The cell walls of plant cells are synthesised from cellulose which makes up approximately 33 % of all plant matter. Cellulose has a host of different uses and is the major constituent of many fibres such as cotton and linen as well as synthetic cellulose fibres such as Rayon. Cellulose is used in many laboratory processes with microcrystalline cellulose being used as a medium for thin-layer chromatography as well as being used to manufacture filter paper. As well as these applications, cellulose can be made into films for use as packaging materials. These different cellulosic materials vary in their degree of crystallinity with cotton being 70 % crystalline and most commercially available celluloses being 30-70 % crystalline. The huge range of uses of cellulose means that an estimated 10^{10} to 10^{11} tonnes are synthesised and destroyed every year (Hon, 1994). Cellulose is insoluble in water but biodegradable via the action of cellulolytic enzymes.

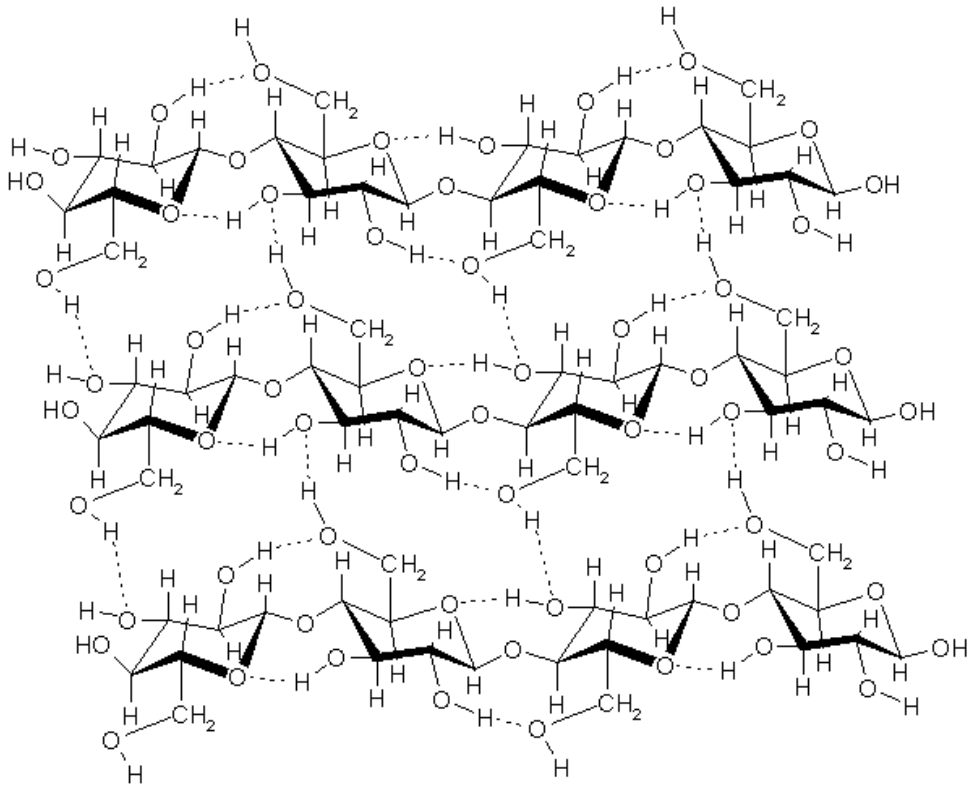

Figure 4.2. The structure of cellulose I.

Cellulose consists of chains of glucose molecules linked by β-1,4-glycosidic bonds. In the cellulose I allomorph, the glucose chains are organised in a parallel arrangement and extensive networks of hydrogen bonds can be seen between chains represented by dotted lines. In cellulose II, the chains are found in an antiparallel arrangement. The repeating unit of cellulose is cellobiose.

Research leading to the discovery of the structure of cellulose formed the foundation of the discipline of polymer science (Hon, 1994). The molecule consists of unbranched, linear chains of D-glucose molecules joined by β-1,4-glycosidic bonds. Each glucose residue in a cellulose chain is rotated through 180° with respect to the previous residue and an extensive network of hydrogen bonds is formed both within individual chains and between different chains. Cellulose exists as two different allomorphs, called I and II, the structure of cellulose I is shown in figure 3.2. In cellulose I, the chains of glucose residues are parallel with respect to each other (Koyama *et al.*, 1997) whereas, in cellulose II, the chains are antiparallel (Kuga *et al.*, 1993). There are two different suballomorphs of cellulose I known as Iα and Iβ. While these typically exist together in natural cellulose microfibrils, cellulose Iα is associated more with bacteria and algae whereas cellulose Iβ is more commonly produced by plants. Cellulose II is produced by solubilisation of cellulose I followed by reprecipitation (Brown Jr, 1999) and is the most stable allomorph (Ranby, 1952).

Cellulose is synthesised by enzymes called cellulose synthases. These synthases are plasma membrane associated proteins and, in plants, are found in hexameric "rosette" structures in the membrane (Kimura *et al.*, 1999). The active sites of the synthase monomers are found in the cytosolic portion of the protein. There, they are able to attach glucose molecules to the end of a growing microfibril which is translocated across the membrane as it extends (Pear *et al.*, 1996). Higher plants often contain multiple cellulose synthase genes which share conserved structures with each other and also bacterial cellulose synthases. Arabidopsis contains at least ten different cellulose synthase genes (Holland *et al.*, 2000).

4.1.4 Cellulolytic Enzymes

Cellulolytic enzymes are produced by a variety of fungi, bacteria and termites. Bacterial cellulases typically exist as multi-enzyme complexes containing enzymes with a range of different specificities (Bayer *et al.*, 1996). Fungi also secrete multiple different cellulolytic enzymes in order to achieve optimal cellulose breakdown (Tomme *et al.*, 1995). Different types of cellulolytic enzymes include endoglucanases, exoglucanases and β-glucosidases. Endoglucanases are able to cleave the β-1,4-glycosidic bonds within individual cellulose chains producing smaller cellulose fragments with more exposed ends. Exoglucanases, such as cellobiohydrolase, work processively from the end of an individual cellulose chain cleaving individual glucose molecules or small polysaccharides such as cellobiose or larger cellodextrins. These smaller molecules are then broken down into individual glucose molecules by the action of β-glucosidases such as cellobiase. The filamentous fungus *Trichoderma reesei* contains at least four cellulolytic enzymes including two cellobiohydrolases, four endoglucanases and one cellobiase (Medve *et al.*, 1998). In addition, many of these enzymes are also present in different isoforms due to differential glycosylation (Enari and Niku-Paavola, 1987).

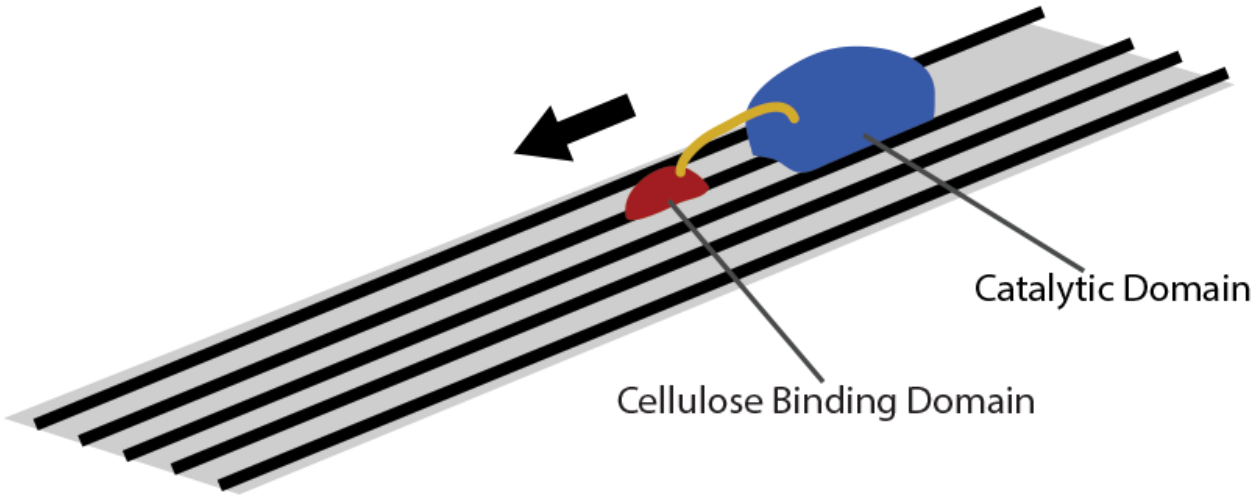

Figure 4.3. Domain structure of exoglucanases enzymes.

The cellulose binding domain (red) binds to an individual cellulose fibre and moves processively along it. The following catalytic domain (blue) cleaves cellobiose and cellodextrins from the end of the fibre. The linker region is shown in yellow and the direction of movement is shown by the arrow.

Cellulolytic enzymes typically contain two distinct domains separated by a flexible, glycosylated linker (Tomme *et al.*, 1995). One of the domains is a cellulose binding domain and the other contains the catalytic region of the enzyme. Strong adsorption of the cellulose binding domain onto the cellulose substrate is essential for a good rate of hydrolysis (Klyosov, 1990). Similar, two-domain structures have been observed in enzymes which hydrolyse other naturally occurring polysaccharides such as starch and chitin (Coutinho and Reilly, 1994, Blaak and Schrempf, 1995). The structures of cellulose binding domains are highly conserved within different taxonomic groups (Tomme *et al.*, 1995). In the case of exoglucanase enzymes, the cellulose binding domains move processively along the cellulose substrate (Teeri *et al.*, 1998).

The rate of cellulose hydrolysis by cellulolytic enzymes depends on a number of different factors, most of which impact on the ability of the enzymes to access the surface of the cellulose. These factors include surface area and degree of crystallinity (Mosier *et al.*, 2005). The rate of enzymatic hydrolysis has been observed to decrease over time as the reaction proceeds (Yang *et al.*, 2006). A number of different explanations have been suggested for this, including changes in the degree of crystallinity and polymerisation present in the cellulose (Eriksson *et al.*, 2002). Cellulolytic enzymes are also known to undergo product inhibition which would also explain this decrease in rate. A recent study has shown that hydrolysis can be halted due to exoglucanases blocking each others' progress along the tangled cellulose fibres (Igarashi *et al.*, 2011). These factors mean that it is often necessary for high concentrations of cellulolytic enzymes to be used in order to achieve a satisfactory rate of hydrolysis.

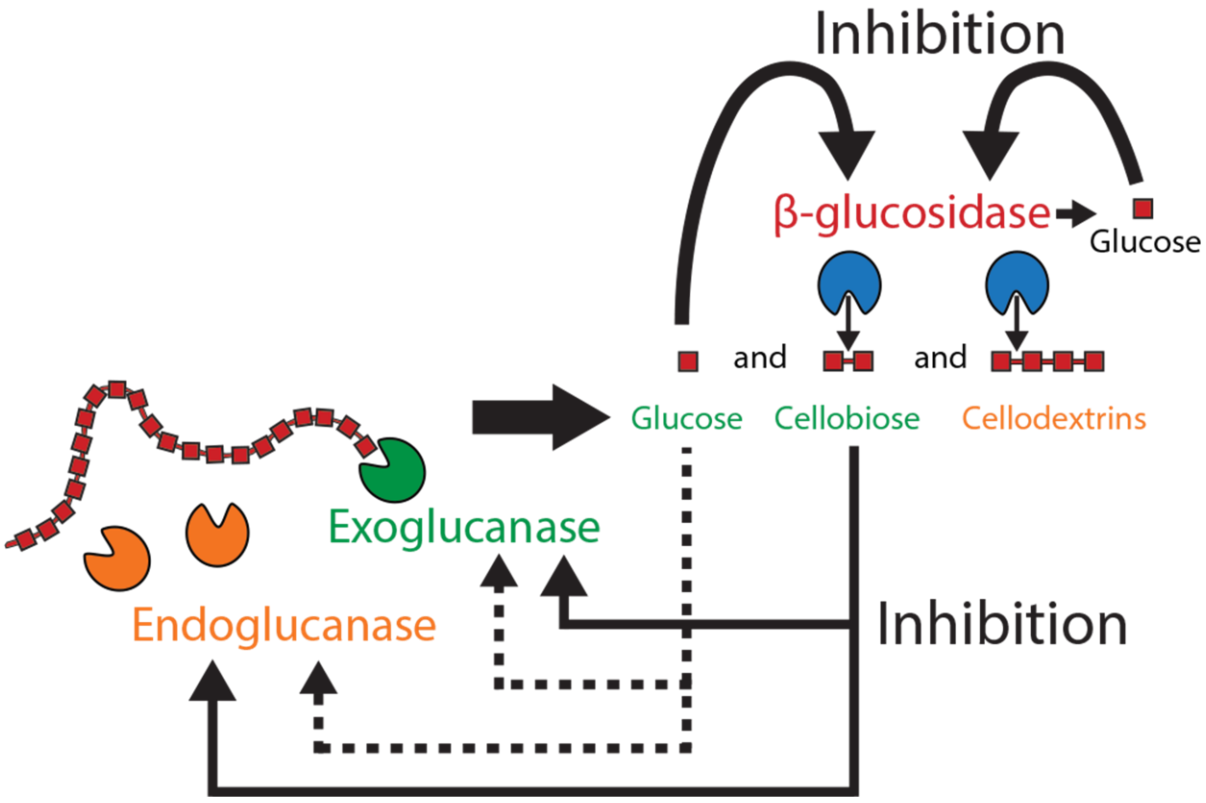

Figure 4.4. Enzymatic hydrolysis of cellulose.

Cellulose chains are broken down into smaller units by the actions of endoglucanases and exoglucanases. These units are further broken down into individual glucose molecules by the action of β-glucosidases. All enzymes are subject to product inhibition as indicated.

4.1.5 Problems with Cellulose as a Packaging Material

While cellulose can be broken down efficiently by cellulolytic enzymes, there are a number of other factors which must be considered regarding the suitability of cellulose as a packaging material for shampoo sachets. Not least of these is the method of sachet construction. Plastics made from fossil fuels, such as polyethylene, can be heat sealed. This allows an effective seal to be created by applying heat to a thin region around the edge of the sachet. This process, however, cannot be used on cellulose. Therefore, in order to construct a sachet from cellulose, an alternative method of sealing must be used.

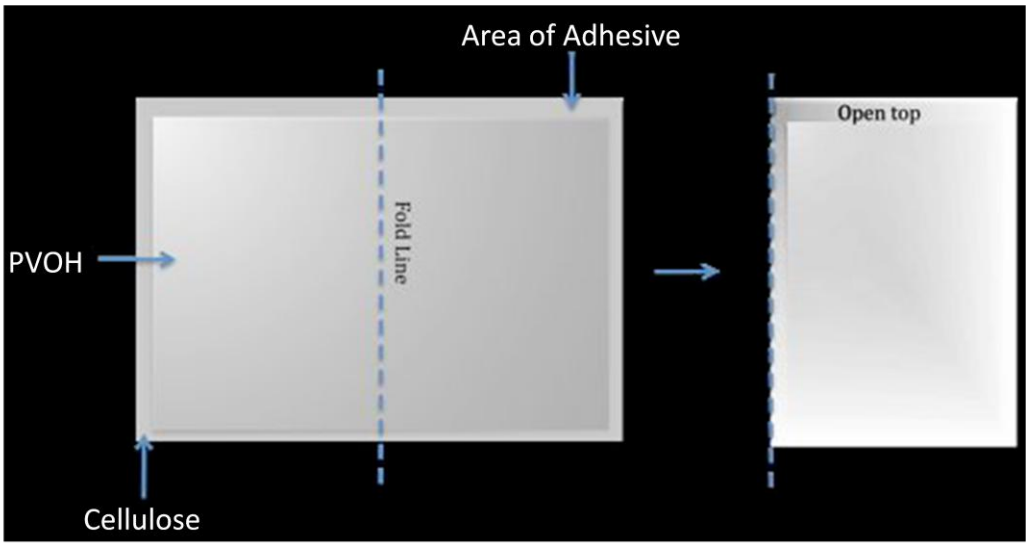

Figure 4.5. Method of construction for bilayer sachet.

A border of cellulose is left exposed around the sachet edge allowing the application of adhesive. The single sheet of material can then be folded over leaving a complete sachet. The top is left open to allow contents to be inserted. Sachet's were constructed by Joshua Swann at the University of Sheffield, Department of Chemistry.

Use of an adhesive is the best alternative for creating a sealed sachet from cellulose film. The construction of a completed bilayer sachet is shown in figure 4.5 although at this stage sachet construction used only the cellulose film with no PVOH applied. Use of an epoxy resin adhesive successfully sealed the cellulose sachet, however, further testing of the sachet by Joshua Swann at the University of Sheffield, Department of Chemistry revealed that the sachet leaked through both the edges of the construction and the surface of the cellulose. This is likely to be due to interactions between the epoxy and the cellulose. The cellulose film used became easily stress cracked and was

observed to be brittle around the regions of adhesive application. Further testing of other adhesives revealed that ST6093G, a polyurethane adhesive, had the most favourable interaction with the cellulose. This adhesive is also biodegradable which is essential for the manufacture of a fully biodegradable prototype.

Another problem with cellulose film is the degree of permeability. This is important as the sachet will be holding a liquid. The permeability is measured by the moisture vapour transmission rate (MVTR) which shows the rate at which water can evaporate through a material. The MVTR of simple cellulose film is approximately 360 g/ m^2/ 24 hrs which is equivalent to the loss of 0.75 g of water per day for a sachet 3 cm x 5 cm. This is much too high to be useful as the sachets must be stored for long periods of time in commercial use.

An alternative commercially available cellulose film consists of simple cellulose with the addition of an additional thin coating on one side. The intended purpose of the additional layer is to allow heat sealing of the cellulose. However, for the construction of a biodegradable sachet this cannot be used for heat sealing as it would result in a barrier being positioned between the cellulose and the cellulolytic enzymes. Instead, the heat seal layer will form the outer layer of the sachet, simply offering a barrier against the excess evaporation of water from within the sachet. Indeed, the MVTR of this material is approximately 30 g/ m^2/ 24 hrs which is around ten times lower than that of the simple cellulose film tested previously. However, a significant issue introduced by the use of the coated cellulose film as the heat seal layer is not biodegradable.

4.1.6 Polyvinyl Alcohol

PVOH is commercially produced by the hydrolysis of polyvinylacetate (PVA), as shown in figure 4.6. Fully hydrolysed PVOH is highly crystalline with strong hydrogen bonding and will only dissolve in temperatures exceeding 60 °C (Verall *et al.*, 2010). The hydrogen bonding present in partially hydrolysed PVOH is weaker, producing a less crystalline material which is soluble in water at temperatures below 10 °C. The difference in hydrogen bonding between fully hydrolysed and partially hydrolysed PVOH can be seen in figure 4.7. PVOH is used in a wide variety of commercial settings. In the health care sector, contaminated laundry in hospitals is stored in bags made from PVOH. This allows the bag and its contents to be placed into a washing machine where the bag will dissolve when it comes into contact with warm water. This reduces the exposure of laundry staff to the contaminated laundry. PVOH is used as a packaging material in the agricultural sector where it is used to store feedstock and fertiliser supplies. The PVOH packaging is contained within a further layer of polyethylene or polypropylene, however, meaning that the packaging is not biodegradable.

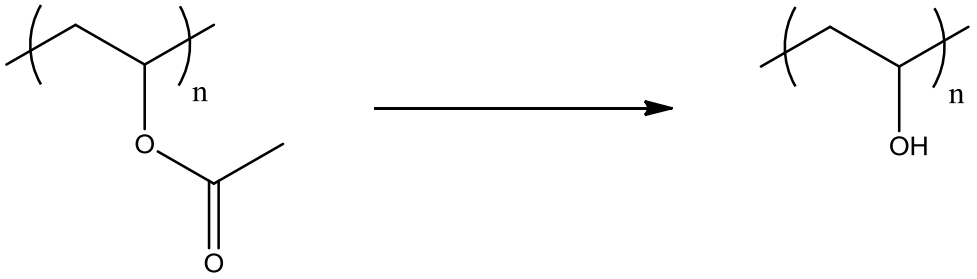

Figure 4.6. Synthesis of polyvinyl alcohol by hydrolysis of polyvinylacetate.

The majority of current uses for PVOH involve the storage of solids although one common product using PVOH to store a liquid is that of Persil 'capsules'. These 'capsules' contain laundry detergent and are placed directly into the washing machine drum where they dissolve during the wash cycle. As the only current PVOH material used commercially to store liquids, the detergent was removed from some Persil 'capsules' by Joshua Swann and replaced with a typical shampoo formulation. Within two minutes, the PVOH packaging began to lose its strength and after ten minutes shampoo was escaping from the damaged material. Closer investigation of the formulation of detergent intended for use in the 'capsules' revealed that it was approximately 97 % organic solvent. Typical shampoos contain closer to 75 % water explaining the rapid breakdown of PVOH. In order for PVOH to successfully store a liquid, that liquid must ideally contain less than 10 % water.

There are a number of proposed solutions to the problem of storing high water content liquids in PVOH. Modifications to the PVOH backbone are described in the patent literature as is the incorporation of wax into the PVOH film (Padget *et al.*, 2002, Verall *et al.*, 2010). However, these modifications to PVOH only serve to reduce the rate of breakdown by water rather than stopping it all together. In order for the bilayer concept to work properly, a PVOH film which is stable in the presence of shampoo but which breaks down in the presence of water is required. Additionally, PVOH with such modifications is not commercially available.

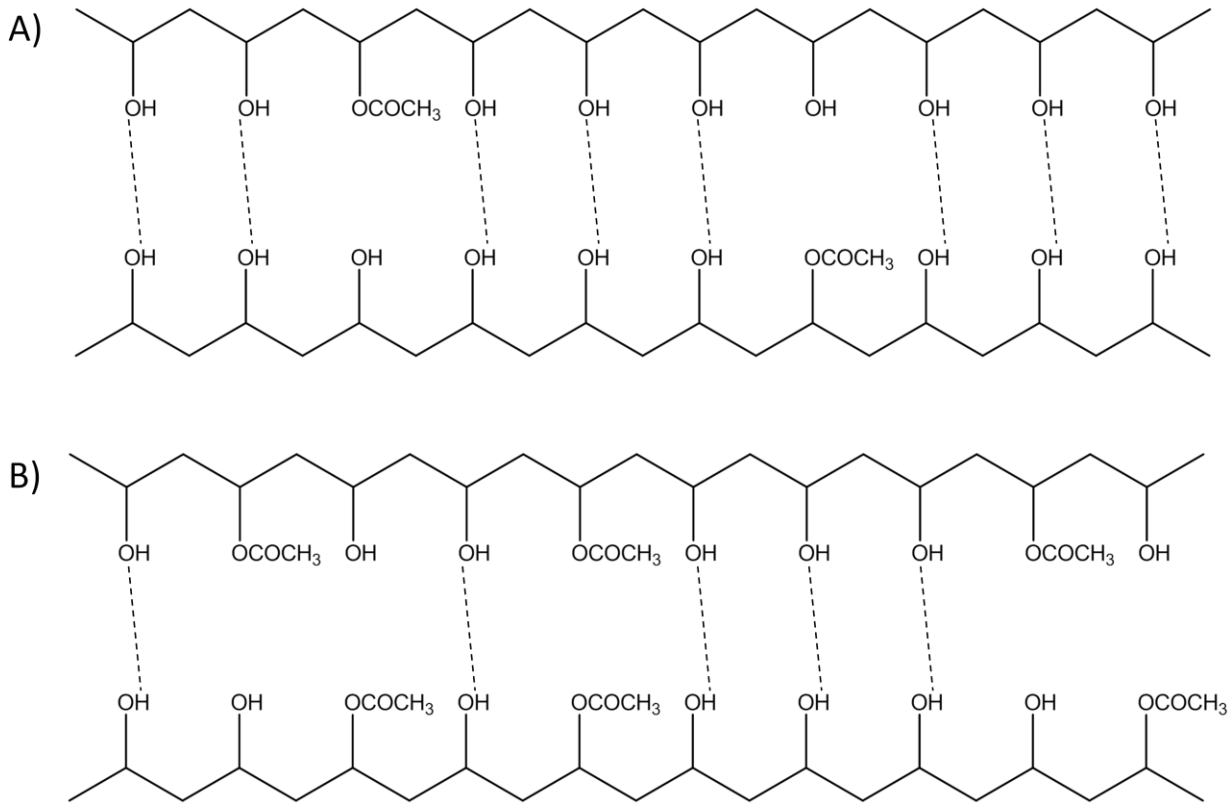

Figure 4.7. Intermolecular hydrogen bonding of polyvinyl alcohol.

Compound (A) has a higher degree of hydrolysis and forms a larger number of intermolecular hydrogen bonds compared to (B) which has a lower degree of hydrolysis. Breakdown of PVOH occurs when the strength of hydrogen bonding to water is greater than the strength of intermolecular hydrogen bonding.

A further possible method of increasing the stability of PVOH is by the addition of a salt to the shampoo formulation. The stability of PVOH depends upon intermolecular hydrogen bonding between polymer chains. When water is present, the hydrogen bonding network is disrupted as PVOH chains form hydrogen bonds with water molecules instead. Addition of a salt to the water encourages water molecules to form a hydration cage around the added ions which prevents them from disrupting the intermolecular hydrogen bonding. The effects of adding different concentrations of different salts have been further investigated by Joshua Swann and were found to reduce the rate of PVOH breakdown. However, the shampoo used in the tests became saturated with salt before breakdown could be stopped completely. In addition to this, some salts interacted directly with the PVOH causing alterations in its structural properties. Addition of salts to the shampoo formulation can have an effect on the properties of the shampoo, for example causing a reduction in the amount of lather produced, which is undesirable as it reduced the quality of the product.

One final solution for reducing the rate of breakdown of PVOH in the presence of liquids is to concentrate the shampoo formulation used. While this approach is effective in preventing breakdown of PVOH it has associated problems. In order to produce a shampoo formulation with a low enough water content to completely prevent PVOH breakdown, approximately 90 % of the water present must be removed. This is an issue for consumers in developing countries. As mentioned in section 4.1.1, customers often do not have sufficient income to purchase high volume products and, also, carefully regulate the use of a single sachet to last a family for several days. If the volume of a sachet was kept constant but contained concentrated shampoo, this would inevitably lead to a price increase which may well be out of the range that many customers can afford. Highly concentrated shampoo is, also, significantly more difficult to use sparingly which would be an issue for those families forced to make a single sachet last for a prolonged period of time.

4.1.7 Bilayer Films

Successful incorporation of cellulolytic enzymes into sachets is essential for the biodegradation of cellulose. In the initial concept outlined in section 4.1.2, the enzymes are placed between the PVOH and cellulose layers. The enzymes used in the cellulose breakdown assays described in section 4.2 are all in aqueous solution. This means that, were they to be placed between the two layers, they would instantly begin to degrade the outer, cellulose layer. These enzymes are also commercially available in solid form although incorporation of the solid enzyme between the layers would almost certainly result in an uneven distribution and therefore uneven breakdown. In order to avoid either of these problems, it was decided that the enzyme would be incorporated into an additional 'bonding' layer, as shown in figure 4.8.

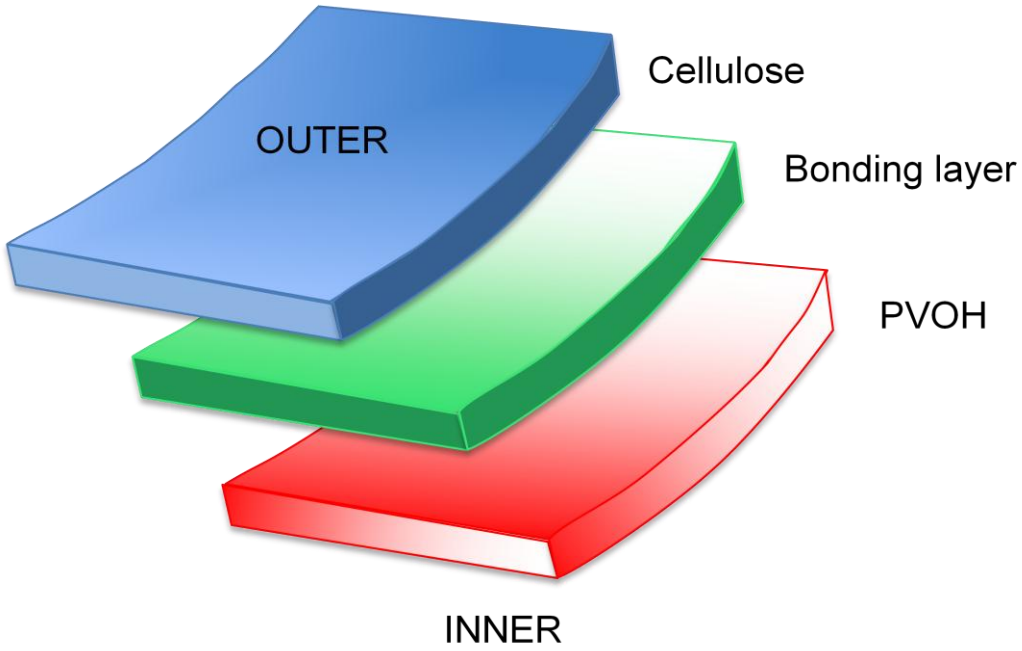

Figure 4.8. Structure of 'bilayer' packaging material with additional bonding layer.

Coated cellulose film is used for the outer layer and a PVOH which is insoluble in shampoo but soluble in water is used for the inner layer. The bonding layer is an additional layer of PVOH and acts as an adhesive between the inner and outer layers. The bonding layer incorporates cellulolytic enzymes.

Ideally, the bonding layer will break down slowly as this will increase the contact time between the cellulose and the cellulolytic enzymes resulting in more efficient degradation of cellulose. A further benefit of a slow rate of breakdown for this layer is the fact that it will act to keep the enzymes within the sachet for as long as possible. Were the bonding layer to break down quickly it would leave the cellulolytic enzymes free in solution where they could easily be lost were the open sachet to be inverted. The inner PVOH layer requires a material which is insoluble in the presence of shampoo but readily soluble in water.

A number of films were produced by Joshua Swann consisting of the outer layer of coated cellulose with an attached bonding layer. This is achieved by producing a solution of PVOH and adding cellulolytic enzymes before casting this mixture onto the non-coated surface of the cellulose film. The different types of PVOH used in the production of these films varied in both their degree of hydrolysis and their molecular weight. These properties affect the rate of breakdown of PVOH so should allow the slowest rate of breakdown to be determined. The different PVOH types used are shown in table 4.2.

4.2 Results and Discussion

4.2.1 Determination of Optimum Cellulolytic Enzymes

In order to measure the activity of different cellulolytic enzymes a two step assay was used. The methodology is described in section 7.4 but the basic steps involved are:

1. Digestion of 10 mg of cellulose substrate by cellulolytic enzymes for 20 hours at 37 °C.
2. Hexokinase/Glucose-6-phosphate Dehydrogenase assay with the supernatant from step one as substrate for one hour at 25 °C.

Glucose produced from cellulose in step one undergoes the following reaction in step two of the assay.

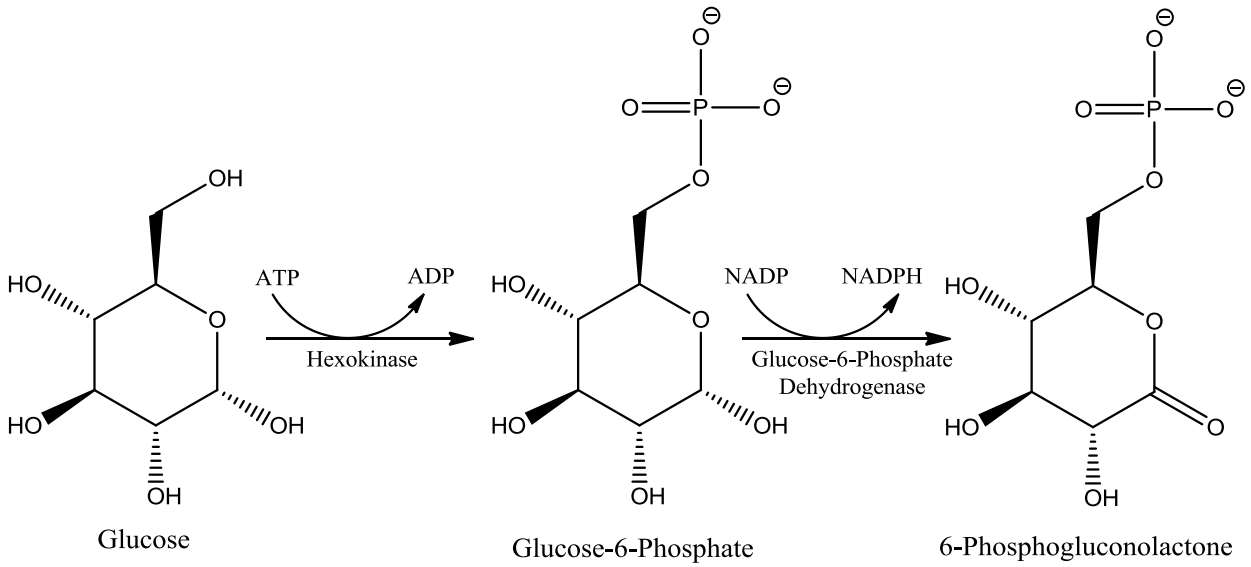

Figure 4.9. The conversion of glucose to 6-phosphoglucomo-δ-lactone.

The reaction proceeds via glucose-6-phosphate and is catalysed by hexokinase and glucose-6-phosphate dehydrogenase.

As shown in figure 4.9, the reaction in step two of the assay requires the conversion of NADP to NADPH. As with the assay used in chapter two, this allows the reaction to be monitored by UV spectroscopy as NADPH has a characteristic absorption at 340 nm while NADP does not. The number of moles of NADP converted to NADPH is equal to the number of moles of glucose converted to 6-phosphoglucomo-δ-lactone. The assay was allowed to proceed to its end point, i.e. until all glucose had been converted to 6-phosphoglucomo-δ-lactone.

Three different commercially available products were considered in this work: cellulase from *Trichoderma reesei*, cellulase from *Aspergillus* species and cellobiase from *Aspergillus niger*. These enzymes are crude extracts from the fungal cells and contain a mixture of different enzymes and isoforms. In order to determine the optimum combination of enzymes for the highest rate of degradation of cellulose, the assay was carried out using various enzyme combinations and 10 mg of Whatman filter paper as a substrate. Each enzyme was used individually as well as a number of different mixtures of two, or all three enzymes to determine the most efficient combination. The combinations tested are shown in table 4.1.

Enzyme Mixture	**Units of Cellulase from *Trichoderma reesei***	**Units of Cellulase from *Aspergillus* species**	**Units of Cellobiase from *Aspergillus niger***
A	10	0	0
B	0	63	0
C	0	0	3
D	5	32	0
E	5	0	2
F	0	32	2
G	3	21	1
H	4	25	1
I	7	16	0
J	2	47	0

Table 4.1. Combinations of cellulolytic enzymes used for optimization of cellulose breakdown.

For each enzyme mixture, two negative controls were carried out: one with no cellulolytic enzyme added to the reaction, and one with no filter paper added to the reaction. This ensured that any change in absorbance observed was due to the action of the enzyme or enzymes breaking down the cellulosic substrate. The absorbance values obtained are shown in appendix C.1.

In order to determine the extent of the breakdown of the substrate, the mass of glucose present in step two of the assay was calculated using the glucose standard curve in appendix C. Due to the large amounts of glucose produced by some of the reactions, it was necessary to dilute the supernatant from step one of the assay in some cases to ensure that the reactants in step two did not become limiting. All results shown in this chapter have been converted to masses of glucose using the following equation:

$$x = \frac{y - 1.97 \times 10^{-3}}{9.28 \times 10^{-4}}$$

Where x is the mass of glucose produced and y is the change in absorbance at 340 nm in step two of the assay.

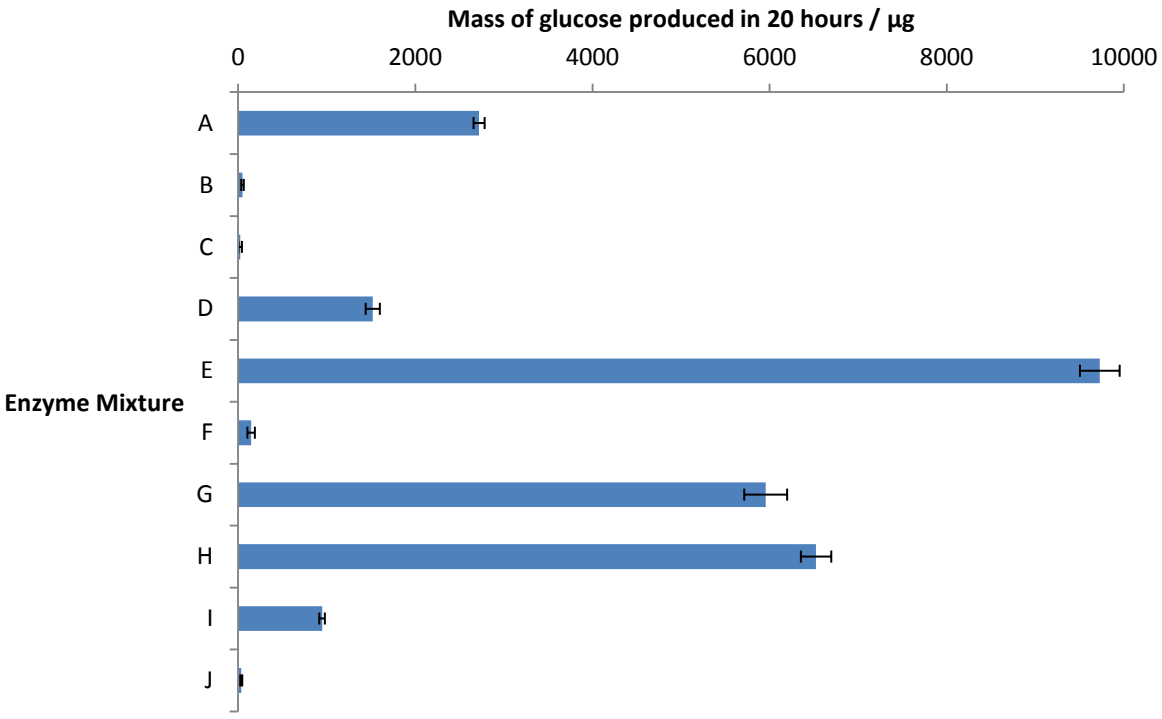

Figure 4.10. Mass of glucose produced after 20 hours from 10 mg of Whatman filter paper by different combinations of cellulolytic enzymes.

The composition of each enzyme mixture is given in table 4.1.

As can be seen in figure 4.10, when the different enzymes are used individually they breakdown only a small fraction of the cellulose present. Of the three individual enzymes, the cellulase from *T. reesei* is most effective. Cellobiase from *A. niger* causes virtually no breakdown of cellulose alone but when used in addition to the cellulase from *T. reesei*, as in enzyme mixtures E, G and H, the breakdown of cellulose is greatly enhanced. As these results show, a mixture of cellulase from *T. reesei* and cellobiase from *A. niger* is the most effective at breaking down cellulose from those tested. This enzyme mixture was selected for use in all further assays. The results suggest that close to complete digestion of the cellulose filter paper substrate is taking place within 20 hours with this enzyme mixture.

The number of units used is based upon the supplied concentrations of commercially available enzymes. Despite the concentrations of cellulose from *A. niger* in this experiment being significantly higher than that of the other two enzymes, the low rates of breakdown observed mean that it is unnecessary to test the enzyme at more similar concentrations.

4.2.2 Breakdown of Cellulose Films

The assay was repeated using the same conditions and enzyme mixture E but with alternative cellulosic substrates. The raw data and controls for this experiment are shown in appendix C.2 and the results shown in figure 4.11 have been converted to masses of glucose produced in 20 hours. These results also suggest complete, or near complete breakdown of the substrate into glucose is taking place within the time-frame. In the case of the cellulose film used, this is important as it will form the outer layer of the prototype biodegradable shampoo sachet.

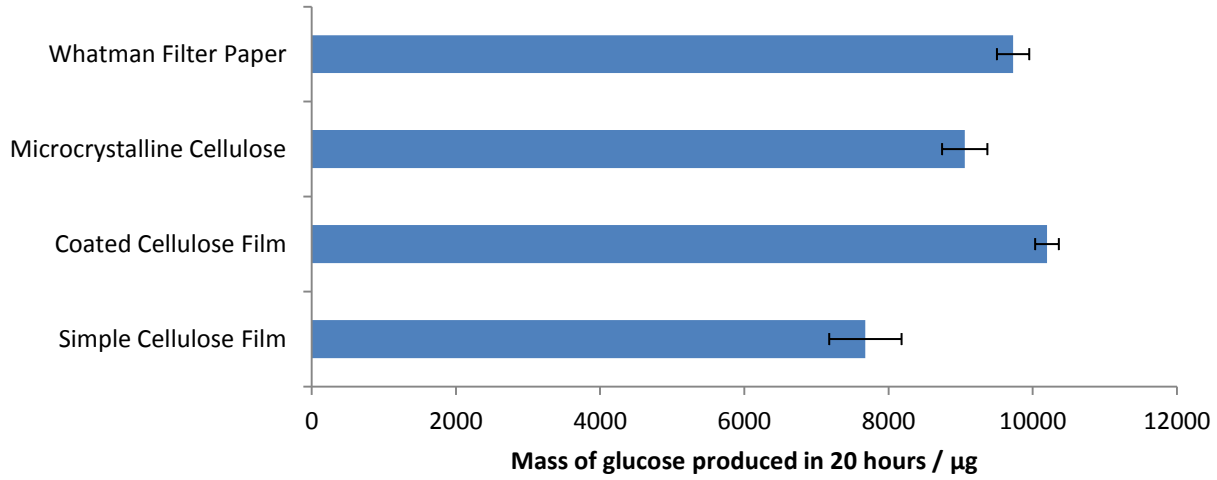

Figure 4.11. The mass of glucose produced from 10 mg of different cellulosic substrates after 20 hours digestion with cellulolytic enzymes.

The results of the digestion of other cellulosic substrates are included as a comparison. Assay conditions are identical to those outlined previously.

As these results show, the addition of the coating to the cellulose film has no significant impact on the level of breakdown taking place within 20 hours. As observed for the other substrates, the cellulose appears to break down completely in this time scale.

In order to confirm that complete breakdown was occurring within 20 hours, the time scale of the digestion (step one of the assay as outlined in section 4.2.1) was increased. The results of this are shown in figure 4.12 and confirm that no further glucose is produced by the digestion within this time frame.

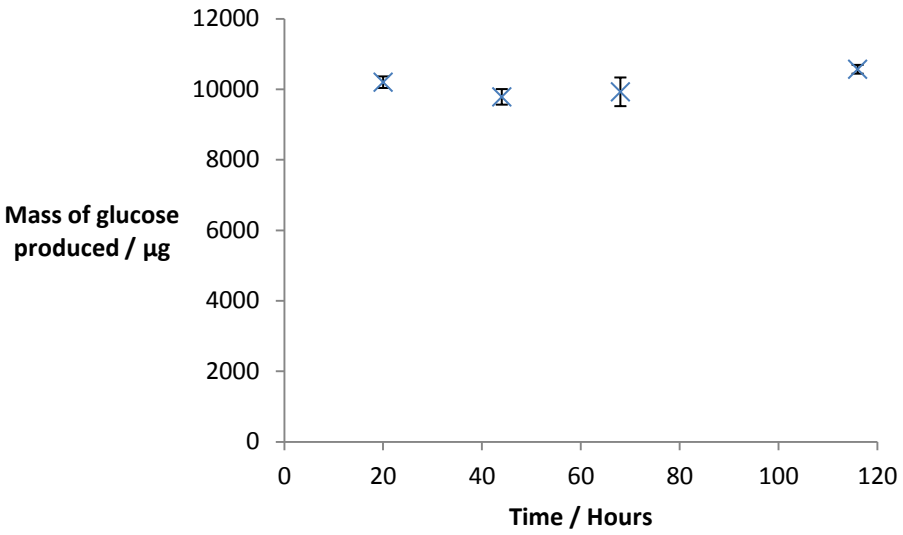

Figure 4.12. The mass of glucose produced from 10 mg of coated cellulose film after different periods of digestion with cellulolytic enzymes.

Following complete breakdown of the cellulose present in the film, the heat seal layer remains present in the enzyme solution. The layer is very thin compared to the overall thickness of the film and is not recognisable as a layer of film following cellulase digestion. While the remaining layer means that a shampoo sachet made from this film would not be entirely biodegradable, the small amount of waste produced by a sachet would still offer a considerable improvement upon the current situation. In addition to the reduction in total waste, the fragility of such a thin layer means that it would be unlikely to cause obstructions to water courses.

4.2.3 Breakdown of Bilayer Films

The breakdown of the films consisting of cellulose and a bonding layer of PVOH containing cellulolytic enzymes, as constructed by Joshua Swann, was measured using the assay outlined in section 4.2.1. Sections of these films contained 10 mg of cellulose in addition to the PVOH layer and the enzyme loading was 0.7 units of cellulolytic enzyme per mg of cellulose, as used in the earlier assays. One film was constructed with a lower enzyme concentration of 0.04 units of cellulolytic enzyme per mg of cellulose in the same ratio as described in section 4.2.1. For these experiments the negative control containing no cellulose substrate used a piece of PVOH film made from the same type of PVOH and with the same enzyme loading as the bilayer film being tested. The second negative control was a bilayer film containing no enzyme. The amount of degradation of these films in 20 hours at 37 °C is shown in figure 4.13.

Each film was constructed from the coated cellulose film that was tested in section 4.2.2. The differences between the bilayer films are caused by the different type of PVOH used for the bonding layer. These varied in both molecular weight and the percentage of hydrolysis as shown in table 4.2. In addition to creating films with each type individually, some mixtures of different types were also used.

Type	Molecular Weight / $gmol^{-1}$	Percentage Hydrolysis
4-88	31,000	88
8-88	67,000	88
40-88	205,000	88
4-98	27,000	98
6-98	47,000	98
10-98	61,000	98
20-98	125,000	98
28-99	145,000	99

Table 4.2. Different types of PVOH used for prototype bonding layers.

Types with 88 % hydrolysis are considered partially hydrolysed and types with 98 % hydrolysis and above are considered fully hydrolysed.

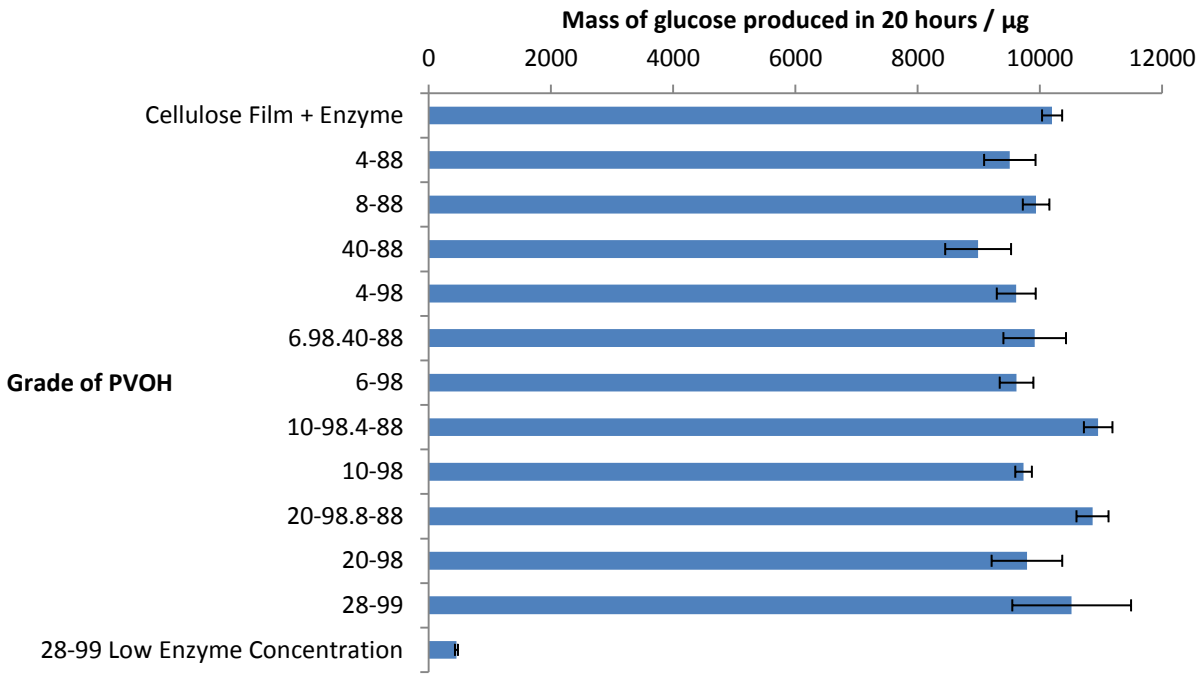

Figure 4.13. The mass of glucose produced from 10 mg of coated cellulose film in 20 hours when attached to a bonding layer of polyvinyl alcohol containing cellulolytic enzymes.

Each film contained a different type of PVOH in the bonding layer and three of the films contained a mixture of PVOH types. The mass of glucose produced in 20 hours from cellulose film is included by way of comparison. The concentration of enzyme was 0.7 units per mg of cellulose in all experiments except for '28-99 Low Enzyme Concentration' which had an enzyme concentration of 0.04 units per mg of cellulose.

The results show that all films containing the higher enzyme concentration undergo close to complete breakdown within 20 hours. This shows that all of the PVOH types are breaking down quickly enough to liberate the contained cellulolytic enzymes within a short enough time frame to allow the enzymes to fully digest the cellulose substrate. This conclusion is supported by experimental observations. Once the film is immersed in water and agitated, the appearance of the PVOH and enzyme layer begins to alter and the two layers (cellulose and bonding layer) delaminate. The enzymes used in producing the film have a distinct colour and this colour can be observed to transfer from the PVOH bonding layer into solution within a short time period. This means that none of the PVOH types tested fulfilled the aim of prolonging the contact time of the cellulolytic enzymes with cellulase.

4.2.4 Effect of Enzyme Concentration on Rate of Breakdown

While packaging materials such as cellulose and PVOH are relatively cheap, enzymes are comparatively expensive. Shampoo sachets are sold at prices lower than two pence in developing countries so an entire sachet and its contents cost significantly less than this in order to remain commercially viable for the manufacturer. Based upon the prices charged by Sigma-Aldrich, a 3 cm x 5 cm sachet with an enzyme loading of 0.7 units of enzyme per mg of cellulose would contain approximately ten pence worth of enzymes. This is clearly far too high for a commercially viable product so a lower enzyme loading must be used. The rate of breakdown of coated cellulose film by different concentrations of the cellulase/cellobiase mixture was monitored using the same assay, as described in section 7.5.

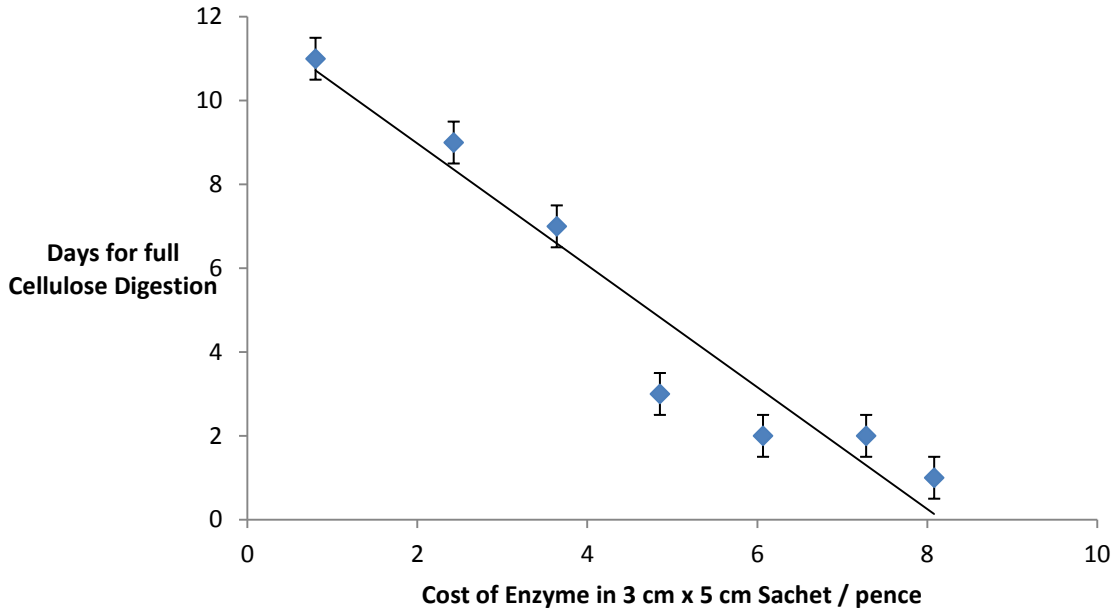

Figure 4.14. Number of days taken for complete degradation of coated cellulose film by different concentrations of cellulolytic enzymes.

Different concentrations are indicated by their cost when purchased from Sigma-Aldrich. The cellulolytic enzyme used was a mixture of five parts cellulase from T. reesei and 2 parts cellobiase from A. niger as described in section 4.2.1. Error bars displayed are ±0.5 days as samples were analysed after multiples of 24 hours.

Figure 4.14 shows the rates of breakdown of coated cellulase at different enzyme concentrations. When the cost of the enzyme is 1 penny for a 3 cm x 5 cm sachet the time for breakdown is approximately

eleven days. Purchasing of enzymes in bulk quantities can allow a decrease in cost to as little as 10 % of the cost of small scale purchases. If this is possible for these enzymes then this could lower the cost to around 0.1 pence per sachet for a degree of enzyme loading sufficient to break down all of the cellulose present in eleven days. However, this experiment was still carried out in a closed system with excess water ensuring the maximum possible rate of degradation and no loss of enzyme. In a real world situation, eleven days gives plenty of opportunity for enzyme to escape from the sachet thus increasing the time for complete breakdown.

4.3 Conclusions

The initial concept of this work, as outlined again in figure 4.15, involves the production of a bilayer material with a cellulosic outer layer and a PVOH inner layer with cellulolytic enzymes contained between the layers. Ideally, the PVOH inner layer would remain intact while in contact with shampoo but break down when in contact with water. This would allow the material to be used to construct a biodegradable shampoo sachet which is stable when full of shampoo. After the shampoo has been used the sachet can be filled with water, breaking down the PVOH and activating the cellulolytic enzymes which in turn break down the cellulose outer layer. As the work presented here shows, however, there are a number of barriers to this concept.

The cellulose outer layer itself proved to be a poor material for storage of liquids due to a high MVTR. This fact necessitated the addition of an extra, non-biodegradable coating to the outside of the sachet. This extra layer, although successful in significantly reducing the MVTR, did not reduce it sufficiently to make the cellulose film an appropriate packaging material for shampoo. Due to the layer being non-biodegradable, its addition also results in a failure to meet the aim of creating a completely biodegradable sachet.

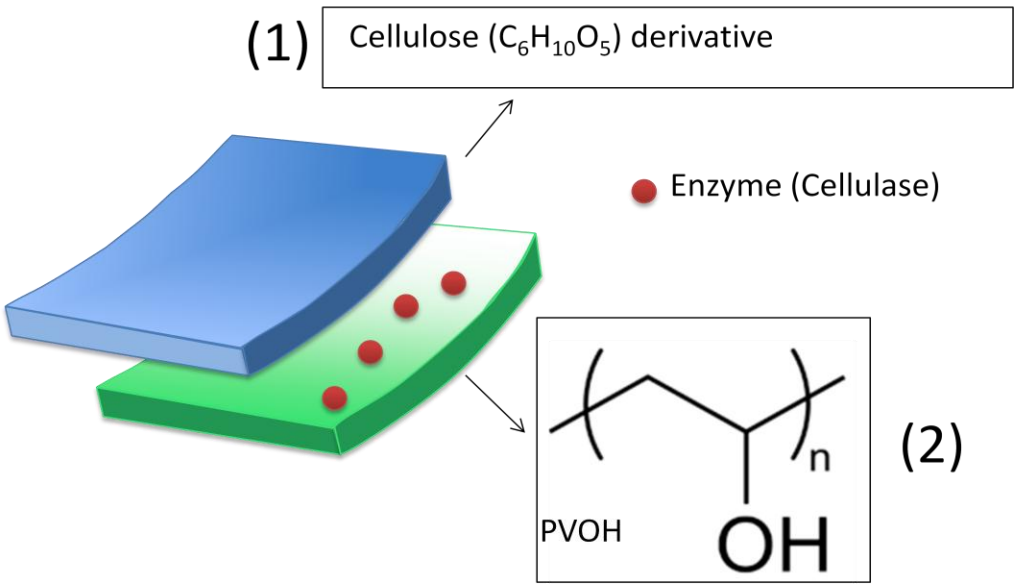

Figure 4.15. The initial bilayer concept for a biodegradable shampoo sachet.

The outer layer (1), shown in blue, will be made from a cellulose material and the inner layer (2), shown in green, will be made from PVOH. Cellulase enzyme will be held between the two layers and will be activated when the inner, PVOH, layer is broken down by water.

The internal PVOH layer also has associated issues. In order for the concept to work as intended, the internal layer must be completely stable when in contact with shampoo, but break down in contact with water at a rate high enough to facilitate the degradation of cellulose within an acceptable time frame. The high water content of shampoo, however, is sufficient to break down PVOH extremely rapidly. Potential modifications of the PVOH structure or shampoo formulation are able to reduce this rate of break down but not stop it completely. The only approach suitable for stopping the breakdown is that of concentrating the shampoo although this has issues from a commercial point of view as it affects the affordability of a sachet.

The most successful element of the initial concept was the cellulolytic enzymes. A combination of cellulase from *T. reesei* and cellobiase from *A. niger* was shown to break down cellulose rapidly at 37 °C. This temperature is higher than the temperatures likely to be experienced by discarded sachets although the rate of degradation at the concentration investigated is high enough to suggest degradation will still occur rapidly in cooler conditions. Experiments with lower enzyme concentrations demonstrate that cellulose can be broken down within an acceptable time-frame at an economically viable cost.

The main limitation of the assay used in estimating rates of degradation is the fact that the entire experiment is carried out in a closed system. This ensures that the enzyme, substrate and water remain in constant contact. When a complete sachet is filled with water and discarded, there are ample opportunities for the escape of these elements. The water could easily escape from the sachet before the PVOH has broken down and activated the cellulolytic enzymes, preventing degradation. Worse still, the PVOH could break down, liberating the enzymes followed by the resulting enzyme solution escaping from the sachet. This would remove any possibility of enzymatic degradation.

Another issue associated with the enzymes used was how best to contain them between the two layers. The use of a PVOH 'bonding layer' was intended to maximise contact time between the enzymes and the cellulose surface. However, the results show that this layer breaks down too quickly to achieve this effect. Importantly, the PVOH, almost instantly, delaminates from the cellulose film. This removes the contact between the enzymes and the surface which they are there to break down and, also, makes it easy for the enzymes to escape from the sachet environment completely.

While in theory the 'bilayer' concept could lead to the production of a completely biodegradable shampoo sachet, in practice there are too many problems preventing development of a successful prototype. Two simple layers swiftly become four layers that are not all biodegradable and are still too porous to store liquids. The biggest single issue though, is the requirement for a material for the inner layer which is soluble in water but stable in shampoo. Until such a material is developed a bilayer cellulosic sachet will remain merely an interesting concept.

While the experiments carried out represent an ideal environment for cellulose breakdown compared to the environmental conditions likely to face a discarded shampoo sachet, they still identify these issues which are inherent to the concept. Had the inherent issues not been identified, experiments testing the materials in environmental conditions would have been an important stage in the sachet development.

Despite these issues, a number of other biodegradable packaging materials are available, two of which are described in section 6.3. Of the two, the most likely candidate for the successful manufacture of a biodegradable shampoo sachet is polyhydroxyalkanoate (PHA) film. This is discussed in more detail in chapter 5.

Chapter 5

5. Suitability of Polyhydroxyalkanoates as Biodegradable Packaging Materials

5.1 Introduction

5.1.1 Polyhydroxyalkanoates

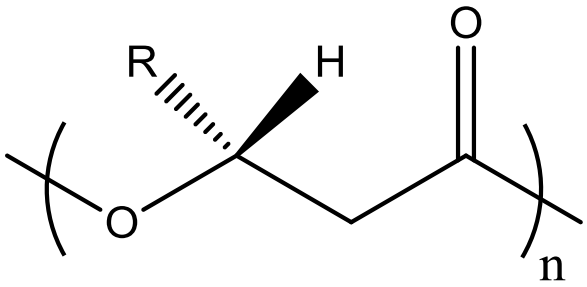

Figure 5.1. Structure of Polyhydroxyalkanoates.

When R is CH_3, the polymer is poly(3-hydroxybutyrate).

Polyhydroxyalkanoates (PHAs) are aliphatic polymers produced naturally by some bacterial cells. PHA production occurs in response to unbalanced growth conditions in which there is an excess carbon source but a lack of another nutrient, typically nitrogen. Depending upon the type of bacteria, the excess carbon is converted to either 3-, 4- or 5-hydroxyalkanoyl-CoA (Steinbuchel *et al.*, 1995). These monomers are then condensed into PHA polymers between 0.05 and 20 MDa via the action of PHA synthase enzymes. PHA is stored in water insoluble granules in the cytoplasm of the bacterial cell. Within 48 hours of synthesis beginning, these granules can account for up to 90 % of the dry weight of the cell and are clearly visible by phase contrast light microscopy (Sudesh and Abe, 2010).

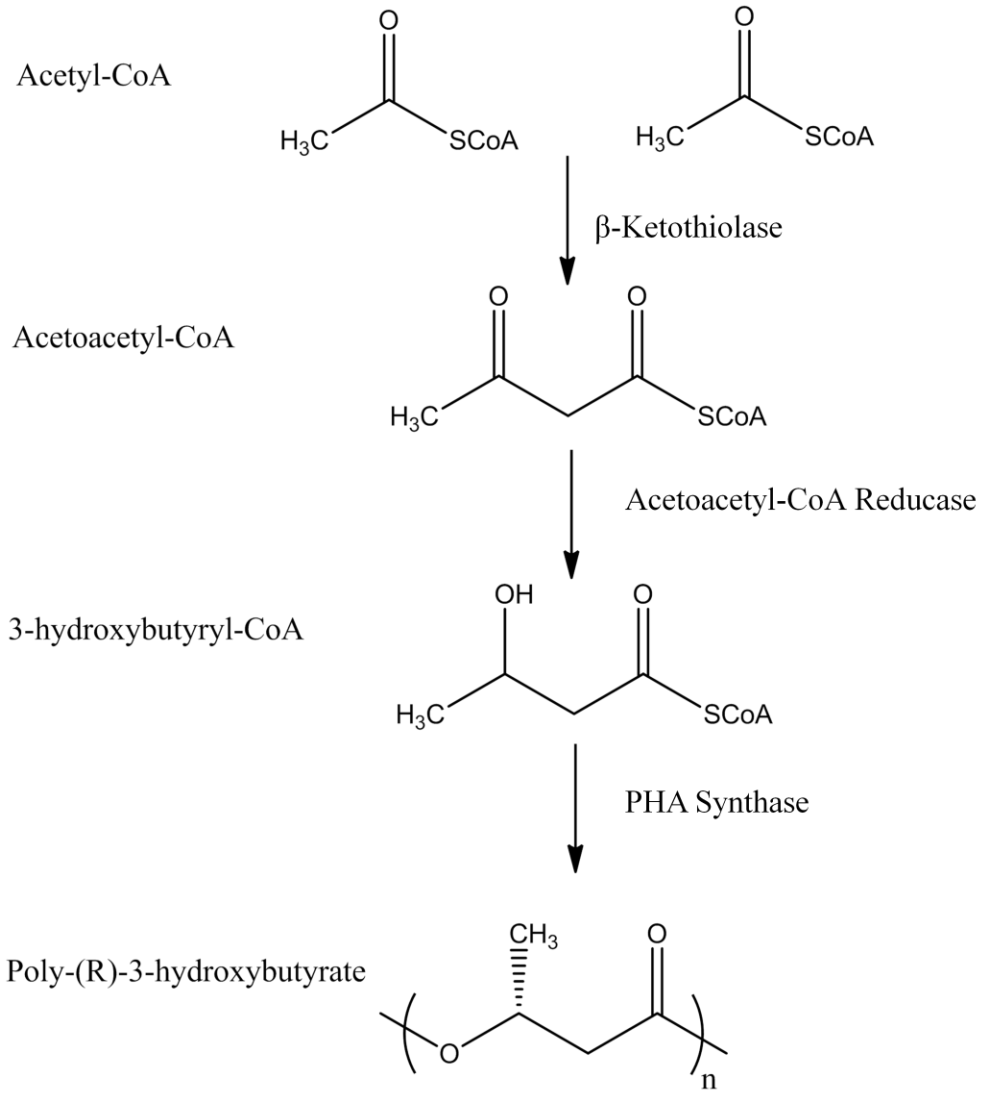

Figure 5.2. Bacterial synthesis of poly(3-hydroxybutyrate) from acetyl-CoA.

This pathway exists in many species of bacteria and all of the enzymes involved have been purified and characterised.

The most common type of PHA is poly(3-hydroxybutyrate) or P(3HB). This polymer is also commonly known simply as PHB as it was the first PHA to be discovered and remained the only known variant for some time (Lemoigne, 1926). Currently, over 150 different types of HA monomers are known to be incorporated into PHAs. This demonstrates the broad specificities of PHA synthase enzymes (Sudesh and Abe, 2010). The majority of these monomers are only found in what are termed 'unnatural PHAs'. Natural PHAs which, as the name suggests, occur naturally in bacteria, only ever contain a limited

number of different monomers. Most bacteria are only able to produce unnatural PHAs when they are grown in a medium containing a source of carbon structurally related to the unnatural HA monomer. Examples of monomers which are found exclusively in unnatural PHAs include: 4-hydroxybutyrate (4HB), 3-hydroxyvalerate (3HV) , 3-hydroxyhexanoate (3HHx) and 4-hydroxyoctanoate (Doi *et al.*, 1989). PHA synthases have even been demonstrated to polymerise polylactic acid monomers (Taguchi *et al.*, 2008). PHA synthase enzymes have thus far proven difficult to crystallise so their structure and exact mechanism of action are unknown. What is certain is their ability to polymerise insoluble, high molecular weight polymers at room temperature (Gerngross *et al.*, 1994).

PHAs are divided up into two categories depending upon the number of carbon atoms in their HA monomers. Monomers containing six carbon atoms or fewer are found in short chain length (SCL) PHAs and monomers containing between six and fourteen carbon atoms are found in medium chain length (MCL) PHAs. PHA synthase enzymes are always specific to either SCL or MCL PHAs. Typically a bacterial species will only produce either SCL or MCL polymers depending upon the synthase it contains. The scope for variation in the structure of a PHA allows the production of polymers with a wide variety of physical properties. Generally speaking, the longer the monomer carbon chain, the closer the properties of the polymer are to an elastomer (Rai *et al.*, 2011). PHA found in granules in bacterial cells is amorphous but commercially produced PHAs are highly crystalline. Electron micrographs of a commercially available PHA are shown in figure 5.3. The surface of the commercially produced PHA is highly regular and non-porous.

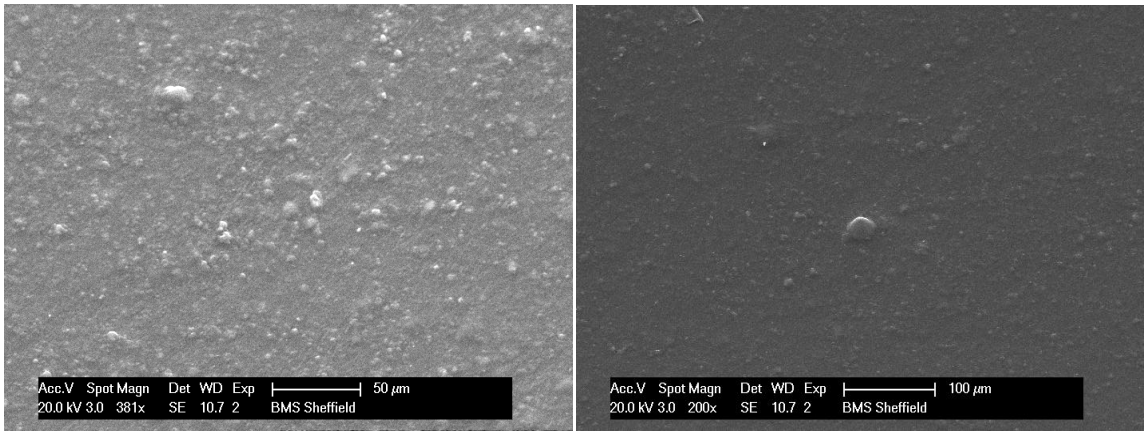

Figure 5.3. Scanning electron micrographs of a commercially produced polyhydroxyalkanoate.

The PHA shown is EM10020, produced by Ecomann films. Electron micrographs were produced by Chris Hill, University of Sheffield, Department of Biomedical Science.

5.1.2 Commercial Production of PHAs

The most common commercially available PHAs are P(3HB) and copolymers of 3HB. The most common monomers found in these copolymers with 3HB are 4HB, 3HV and 3HHx. Production typically requires growth of PHA producing bacteria in large bioreactors for between 24 and 96 hours (Chen *et al.*, 2001). This can be carried out via a two-stage cultivation in which the bacteria are grown on a nutrient rich medium before being transferred to a limited medium or, more commonly, for large scale production, a one stage cultivation with only a limited medium used. This process can be expensive and slow and also requires an abundant carbon source (Braunegg *et al.*, 2004). A range of different carbon sources has been used in the industrial production of PHAs. These include sugars, whey, molasses, triglycerols and starch. Selection of a suitable carbon source is essential to keep production costs as low as possible since this accounts for up to 50 % of the overall production costs (Lynd *et al.*, 1999). Glucose and sucrose are the most commonly used although plant oils and fatty acid derivatives were found to be cheaper, renewable and give a higher PHA yield (Loo *et al.*, 2005). Palm oil by-products and used cooking oil can also be used as carbon sources. Gram for gram, plant oils give almost double the yield of glucose when used as a carbon source (Akiyama *et al.*, 1995).

In order to further increase the efficiency of commercial PHA production a number of biotechnological approaches have been used. Over-expression of PHA synthase genes in natural PHA producers has little effect on the PHA yield (Suriyamongkol *et al.*, 2007, Wang and Lee, 1997a) and expression of PHA synthase genes in recombinant *E. coli* was also ineffective, as PHA yields tended to be lower than those in natural PHA producers (Lee, 1994, Wang and Lee, 1997b). PHA synthase genes have also been expressed in plants such as maize and Arabidopsis. Growing plants is considerably cheaper than growing bacteria by fermentation. However, high yields of PHA are often associated with growth defects which limit the commercial potential of PHA production (Poirier *et al.*, 1992). More recently, individual PHA synthetic enzymes have been purified. These may offer an alternative, *in vivo*, approach to PHA production. Production of the required substrate materials, however, is difficult and the enzymes are not very stable (Cho *et al.*, 2012).

Once PHA has accumulated in the bacterial cells it must be extracted. At the laboratory scale, solvent extraction is the method of choice. This requires large amounts of chlorinated solvents such as chloroform and isoamilic alcohols such as methanol (Nonato *et al.*, 2001). This process is hazardous to the environment and very expensive so unsuitable for use on an industrial scale. Cell solubilisers such as sodium hypochlorite can also be used to extract PHA although these methods can damage the polymer, causing as much as 50 % reduction of molecular weight. Mixtures of different chemicals and solvents have been investigated and all give varying yields, purities and reductions in PHA molecular weight (Choi and Lee, 1999). The most efficient way of extracting PHA from bacterial cells is by heat shock followed by enzymatic solubilisation of non-PHA biomass. This process achieves greater than 90 % purity and yield and causes no damage to the molecular weight of the PHA. As no chemicals are required for this method it also has a lower associated cost (Kapritchkoff *et al.*, 2006). Extraction of PHA from plants is complicated and often a combination of mechanical processes and solvent or enzyme extraction is required (Noda, 1997).

5.1.3 Enzymatic Degradation of PHAs

All PHA synthesising bacteria also produce two types of PHA depolymerase: intracellular and extracellular. Intracellular depolymerases allow the bacteria to liberate the carbon stored in intracellular PHA granules. *Legionella pneumophila* is able to survive for over 600 days with stored P(3HB) as its only available carbon source (James *et al.*, 1999). The majority of PHA producing organisms produce and store P(3HB) and P(3HB) depolymerases are known to break down P(3HB) into its constituent 3HB monomers. 3HB is converted to acetyl-CoA as shown in figure 5.4. Acetyl-CoA is subsequently able to enter the tricarboxylic acid (TCA) cycle where it serves as an energy source (Uchino *et al.*, 2007). Like PHA synthases, intracellular PHA depolymerases show specificity for certain PHAs and are always, at least, specific to either SCL- or MCL-PHA. Intracellular PHA depolymerases are active only against the amorphous PHAs found inside bacterial cells and are unable to break down crystalline, commercially produced PHAs.

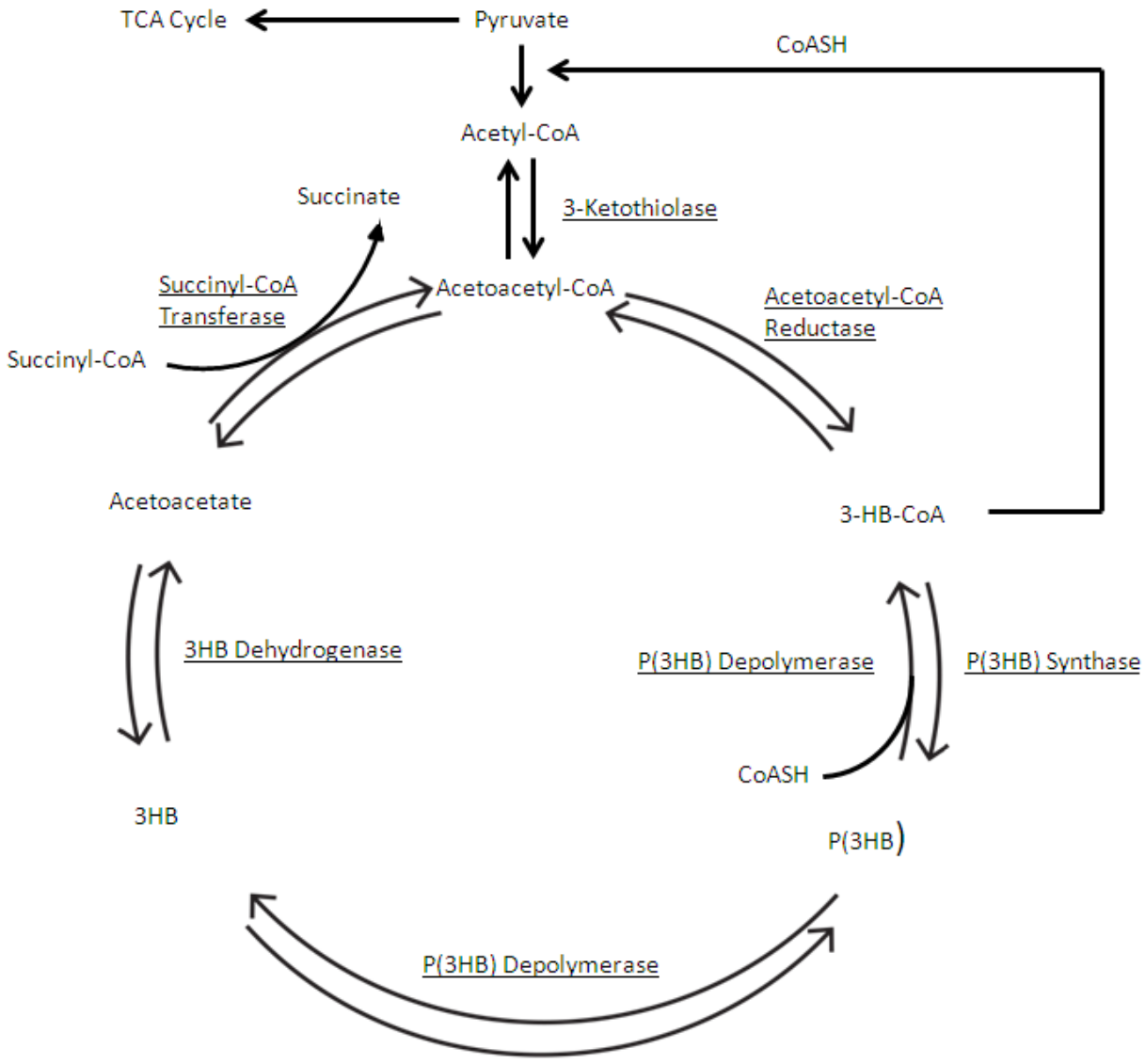

Figure 5.4. The P(3HB) cycle in bacteria as proposed by Uchino et al. (2007).

Enzymes involved are indicated by underlining.

PHA molecules are too large to enter bacterial cells so, in order to gain access to carbon from extracellular sources of PHA, PHA synthesising bacteria also produce extracellular PHA depolymerases. The rate of PHA breakdown by extracellular depolymerases depends on a number of factors. These include environmental factors such as temperature, moisture level, pH and nutrient supply. Such factors affect the growth of the degrading bacteria, the production and secretion of depolymerase enzymes and the activity of those enzymes. The nature of the PHA substrate also has a significant effect on rate of break down with polymer composition, degree of crystallinity and surface area all being important

factors (Sudesh and Abe, 2010). Extracellular PHA depolymerases, like intracellular depolymerases and synthases, are specific to either SCL- or MCL-PHAs. However, certain species of bacteria produce multiple extracellular depolymerases with different specificities. *Pseudomonas lemoignei* is known to produce six different depolymerase enzymes (Jendrossek, 2001). Production of PHA depolymerases is usually suppressed when suitable, soluble carbon sources are present, however, extracellular depolymerase expression is not dependent upon stored PHA suggesting that regulation does not occur via induction (Jendrossek *et al.*, 1993a).

Many extracellular PHA depolymerases have been purified and all consist of a single polypeptide chain between 26,000 and 63,000 Da in molecular weight. These enzymes all exhibit a high degree of stability over a range of temperature, ionic strength and pH although the optimum pH of depolymerase is typically between 7.5 and 9.8 (Jendrossek *et al.*, 1993b, Saito *et al.*, 1989). Many SCL-PHA depolymerases have been shown to have a similar two-domain structure to that observed in endoglucanases enzymes (discussed in section 4.1.4). The two domains are a catalytic domain and a PHA-binding domain joined by a flexible linker. Some depolymerases do not contain a PHA binding domain although the catalytic domains of all of these enzymes are highly conserved (Hisano *et al.*, 2006). The active site of the catalytic domain in PHA depolymerases contains a lipase box pentapeptide, [Gly-X_1-Ser-X_2-Gly]. This motif is found in almost all known serine hydrolases including lipases, esterase and serine-proteases (Jaeger *et al.*, 1999). In P(3HB) depolymerases, the serine of this motif forms a catalytic triad with highly conserved aspartate and histidine residues. It is proposed that, in addition to substrate binding, the PHA-binding domains and linker region may play a role in the disruption of the polymer structure in crystalline substrates (Sudesh and Abe, 2010). It is likely that PHA depolymerases have both endo and exohydrolase activity.

5.1.4 Biodegradation of PHAs

A range of data is available regarding the rate of biodegradation of various commercially produced PHA films. These are typically P(3HB) or copolymers of 3HB. Biodegradation is predominantly caused by bacteria although some fungi also produce PHA depolymerase enzymes (Kim et al., 2000). PHA degrading bacteria have been isolated from “soil, compost, aerobic and anaerobic sewage sludge, fresh and marine water, estuarine sediment and air” (Sudesh and Abe, 2010). These bacterial species include both aerobes and anaerobes and are present in almost every ecosystem both terrestrial and aquatic.

A study in Indonesia monitored the rate of breakdown of P(3HB) and a copolymer of 3-hydroxybutyric acid and hydroxyvaleric acid (P(3HB-co-HV)) in different conditions in the tropical climate (Akmal et al., 2003). The results can be seen in tables 5.1 and 5.2 and, as they show, there is considerable variation in the rate of degradation depending upon the type of PHA film and the conditions in which biodegradation is taking place. Other work provides further data on rates of biodegradation which, again, vary based upon the conditions used and the composition of the PHA (Luo and Netravali, 2003, Rudnik and Briassoulis, 2011, Gutierrez-Wing et al., 2010).

Medium	Average Weekly Percentage Mass Loss	Estimated Time for Complete Degradation/Weeks
Sewage Sludge	3.6	28
Soil	1.9	53
Lake Water	1.5	67
Sea Water	0.8	125

Table 5.1. Rate of mass loss of poly(3-hydroxybutyrate) in different environmental conditions.

Data taken from Akmal et al. (2003).

Medium	Average Weekly Percentage Mass Loss	Estimated Time for Complete Degradation/Weeks
Sewage Sludge	17.8	6
Soil	6.7	15
Lake Water	3.2	32
Sea Water	2.7	37

Table 5.2. Rate of mass loss of a copolymer of 3-hydroxybutyrate and 3-hydroxyvalerate in different environmental conditions.

Data taken from Akmal et al. (2003).

The work described in this chapter aims to assess the rate of breakdown of a commercially available PHA, EM10020, produced by Ecomann Films. This data will then be used to assess the suitability of this film as a packaging material for use in shampoo sachets sold in developing countries. A full analysis of the need for such materials can be found in section 4.1.1. The approach for development of a biodegradable sachet made from cellulose described in the previous chapter involved the use of cellulolytic enzymes. This had a number of problems associated with it so for PHAs the focus will be on its innate biodegradability rather than the use of depolymerase enzymes.

5.2 Results and Discussion

5.2.1 Breakdown of PHA films in Soil

The rate of breakdown of PHA film in different soils was determined by measuring the mass loss over time. A range of soils were used in these experiments in order to simulate a range of environmental conditions. The methods used in this experiment are described in section 7.6. An agricultural loam was collected from farmland in Lincolnshire as a general, fertile soil. In addition to this, sand was collected from the beach at Skegness as well as a sandy soil from sand dunes at near-by Gibraltar Point. In addition to this a saline soil was collected from a salt marsh also at Gibraltar Point.

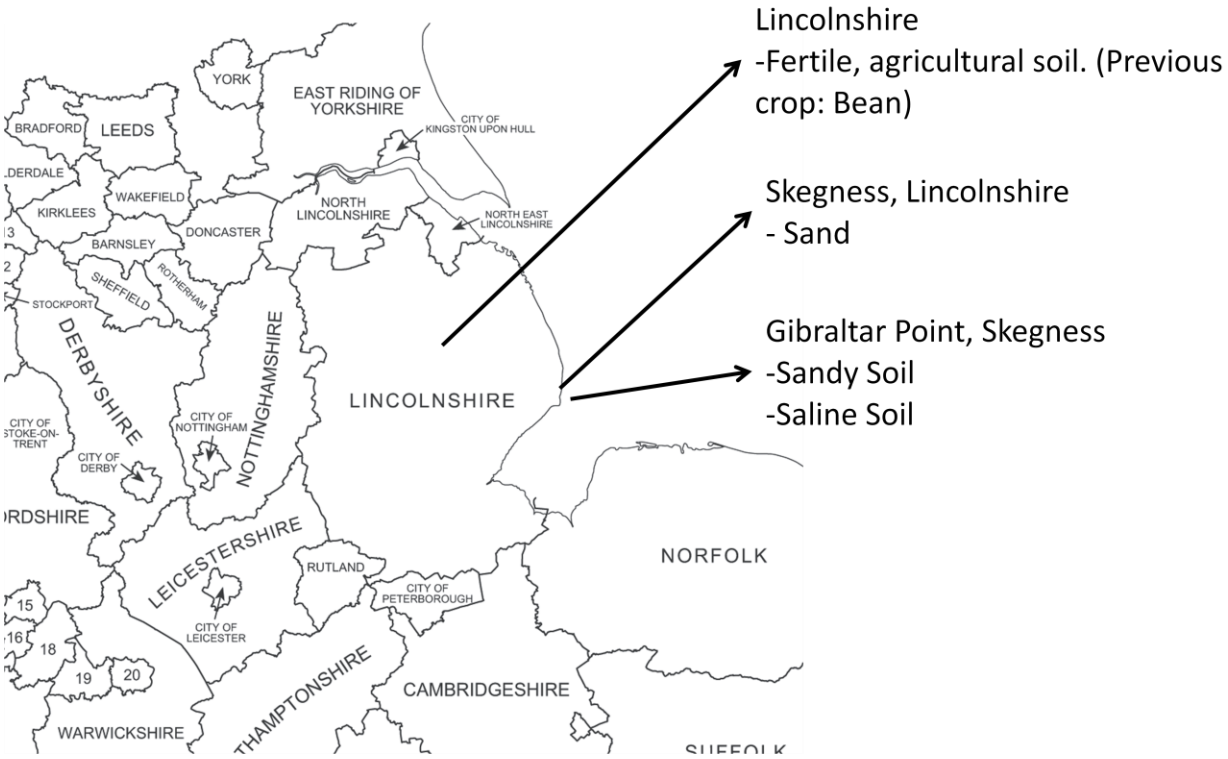

Figure 5.5. Locations of soil sample collection.

Reproduced from Ordnance Survey map data by permission of the Ordnance Survey © Crown copyright 2010.

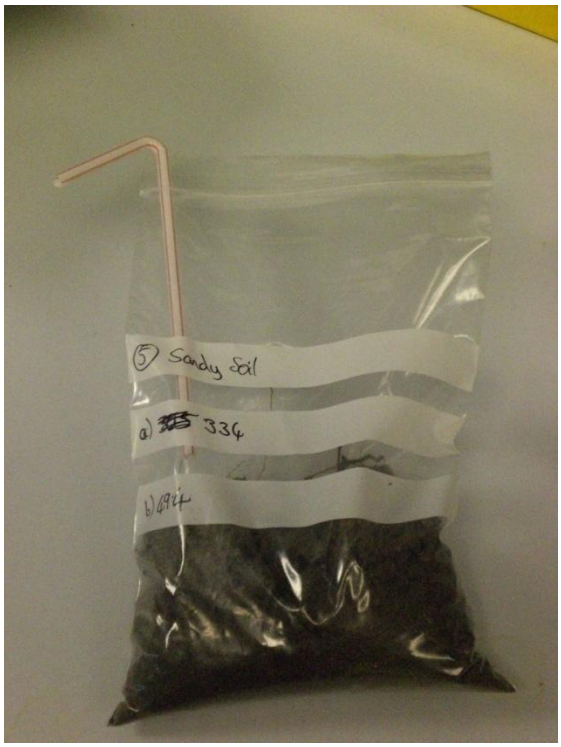

Figure 5.6. Experimental set-up for breakdown experiments.

Each bag contains 300 g of soil and a 3 cm x 3 cm piece of EM10020 PHA film. The straw allows aeration to the sample.

The soil was air-dried to constant mass and divided between several polythene bags before distilled water was added to achieve the desired moisture content. Each bag contained 300 g of soil and one 3 cm x 3 cm piece of EM10020 PHA film. Moisture contents of 9 %, 17 % and 20 % were used for each soil with each individual experiment carried out in triplicate. The samples were incubated at 25 °C and each week were removed from the soil, washed and dried to constant mass before being photographed. Any water lost from the soil due to evaporation was replaced and the pieces of PHA film replaced and returned to the incubator. The rate of degradation was measured by monitoring the percentage of mass lost from each PHA sample.

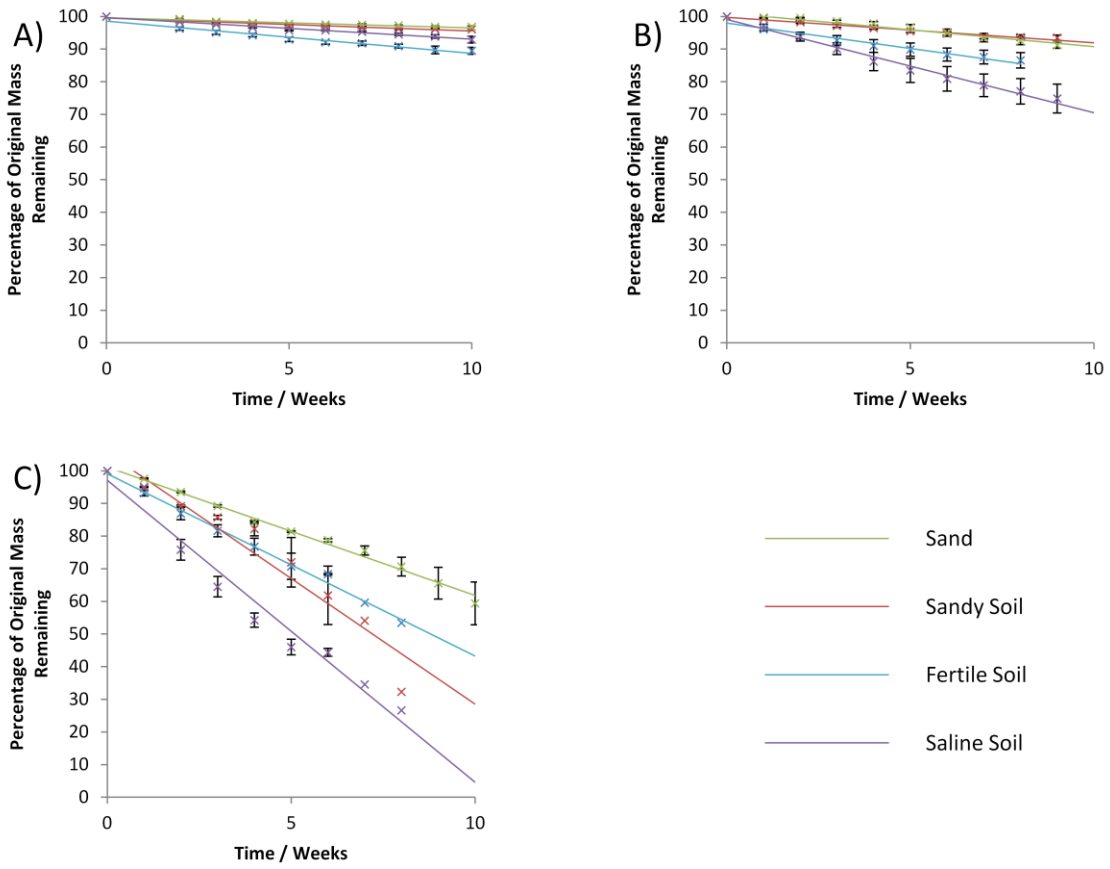

Figure 5.7. Mass loss of EM10020 samples over time in four different soils (fertile soil, sand, sandy soil and saline soil) with A) 9% moisture, B) 17% moisture and C) 20% moisture.

Samples were buried in soil and incubated at 25 °C with aeration. Samples were removed weekly, washed, dried and weighed before being returned to the soil and incubation. Each soil type was tested three times at each moisture content. Error bars show the standard error of the mean. Where error bars are missing, this is due to two of the samples in those conditions disintegrating to such a degree that it was no longer possible to recover them from the soil.

As can be seen in figure 5.7, the rate of degradation of PHA shows considerable variation based upon the soil type in which it is placed and the moisture content of that soil. As moisture content increases, so does the rate of degradation. The rates of degradation observed for all soils with 9 % moisture content are very low. Negative controls of sterilised soils would be required to determine whether the breakdown observed is biodegradation by bacteria and fungi, or is simply occurring due to chemical or physical degradation from the soil. However, the most rapid degradation takes place in fertile soil which would be expected if biodegradation was taking place due to the nutrient content of the soil being more supportive of bacterial and fungal growth and therefore greater production of PHA depolymerase

enzymes. However, PHA in this soil loses only around 10 % of its mass in 10 weeks, the equivalent of approximately two years for complete degradation. The slowest rate of degradation, for the soils with 9 % moisture content, was observed in sand. Samples in these conditions would not fully breakdown for approximately six years.

Soil Type	Percentage Moisture Content	Average Weekly Percentage Mass Loss	Estimated Time for Complete Degradation/Weeks
Fertile soil	9	1.0	102
Sandy Soil	9	0.4	250
Sand	9	0.3	324
Saline Soil	9	0.7	152
Fertile soil	17	1.6	65
Sandy Soil	17	0.8	128
Sand	17	1.0	97
Saline Soil	17	2.9	36
Fertile Soil	20	5.5	18
Sandy Soil	20	6.5	13
Sand	20	3.6	27
Saline Soil	20	9.6	11

Table 5.3. Estimated time for complete breakdown of EM10020 film in different soil types with varying moisture contents.

Estimates are based on the rate of breakdown calculated from the data in figure 5.7.

By photographing samples each week, it was possible to observe changes to the appearance of the films over time. Those samples in fertile soil appeared to have more localised areas of degradation. This effect was visible, after two or three weeks, as small, opaque, white, crystalline areas in the film samples, as can be seen in figure 5.8(A). Later in the experiments, as further degradation had occurred, these areas were more prone to split, leaving holes or tears in the material. This phenomenon was less apparent in the other soil types where a more even pattern of degradation was observed, as seen in figure 5.8(B). Samples placed in sandy soil were more prone to splitting than those in sand and saline soil.

For some samples which had lost a relatively large proportion of their masses, it became no longer possible to recover every piece of the sample where parts had broken away. Despite this, the area of the remaining pieces was never so small as to account for all of the recorded mass loss. It is possible to disregard the loss of very small pieces of PHA as these are unlikely to cause any of the environmental

issues associated with non-degradable packaging materials and will continue to break down at the same rate as the larger pieces.

An increase in soil moisture content was associated with an increase in rate of degradation for all soil types. If biodegradation is occurring, this is expected over the range of moisture contents investigated as an increase in water available in the environment would facilitate greater bacterial and fungal growth. Interestingly, the rate of breakdown in saline soil was observed to be faster than that in fertile soil at both 17 % moisture and 20 % moisture. This was surprising as it was assumed that soil with a high salt content would be less suitable for bacterial growth than nutrient-rich, agricultural soil. The reason for the higher-than-expected rate could be due to a number of factors. Firstly, the types of bacteria present in the saline soil could be different to those present in agricultural soil. If the saline soil naturally contains a higher percentage of PHA producing bacteria this would account for a difference in rate of biodegradation. This is possible as it is known that a number of halophilic bacteria produce PHA depolymerases (Rodriguez-Valera and Lillo, 1992). The result could also be explained if the bacteria responsible for PHA biodegradation were the same in both saline and fertile soils. Should this be the case it could be that the bacteria grow more successfully in saline conditions and thus produce more PHA depolymerase. An alternative explanation in this situation would be that similar amounts of PHA depolymerase were being produced in both soil types but the conditions in the saline soil were more favourable leading to a faster rate of breakdown. If biodegradation is not occurring, the differences in rate of breakdown between soils may be due to differences in the chemical composition of the soil.

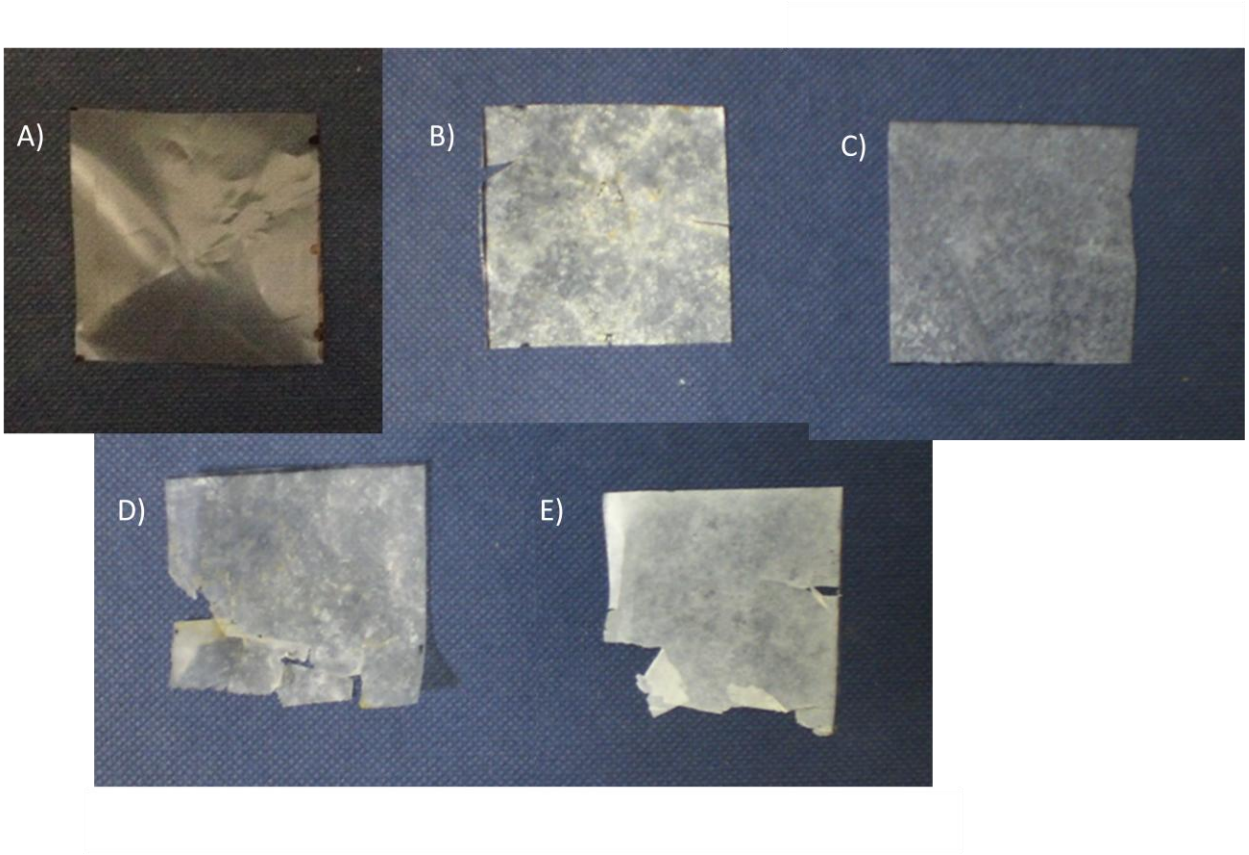

Figure 5.8. The appearance of samples of EM10020 after breakdown in different conditions.

A) Before any breakdown has occurred, B)Fertile soil with 17 % moisture, this sample has lost 20 % of its original mass, C)Sand with 17 % moisture, this sample has lost 10 % of its original mass, D)Saline soil with 17 % moisture, this sample has lost 33 % of its original mass, E)Lake Water 'B', this sample has lost 69 % of its original mass.

Samples in the soils with 17 % moisture content showed less evidence of the localised degradation observed in those samples with 9 % moisture. Tears and splits were still seen most frequently in the samples in fertile soil (figure 5.8(A)) but less frequently than in those samples in fertile soil with 9 % moisture content. This could be due to the higher moisture content ensuring more even bacterial growth throughout the sample rather than it being localised to particular areas.

Samples in soils with 20 % moisture content, however, were much more prone to tearing than samples at either of the lower moisture contents. This is almost certainly due to the much higher rates of degradation observed in these samples. In fact, after seven weeks six of the nine samples placed in fertile soil, sandy soil and saline soil had disintegrated into many small pieces. These pieces ranged from approximately 5 mm^2 to approximately 50 mm^2. Due to the small sizes of some of the fragments it was

subsequently impossible to effectively recover the entire sample from the soil. However, as described previously, due to the small sizes of the pieces which could not be recovered, the associated mass loss is not necessarily significant. After nine weeks, all of the samples in these three soil types had disintegrated. Previous work on the composting of PHA films suggests that disintegration is likely to occur when approximately 30 %, by mass, of the film is remaining (Luo and Netravali, 2003). However, the increased mechanical strain of repeated sample removal, washing, drying and reburying may account for why the samples in this experiment began to disintegrate even before this level of degradation was reached.

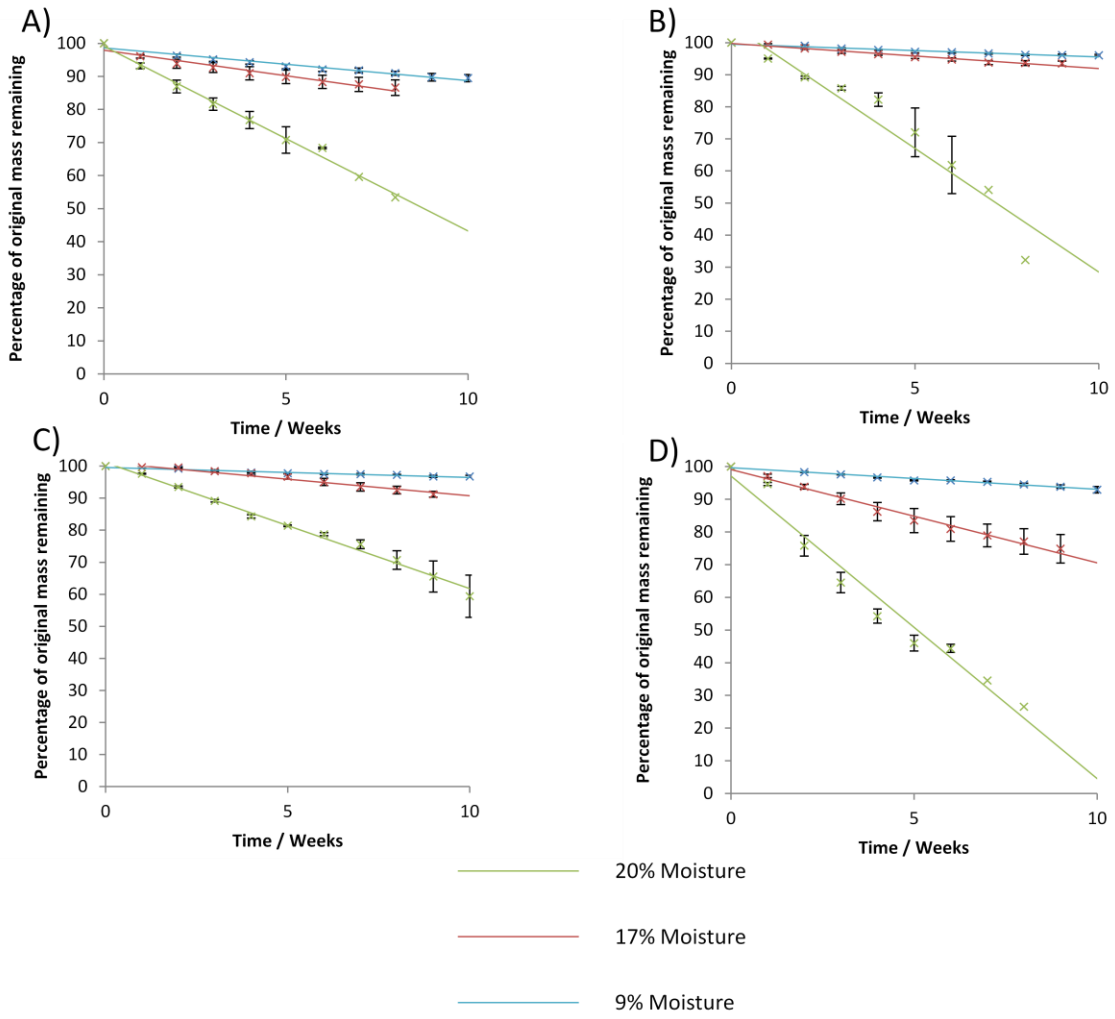

Figure 5.9. Mass loss of EM10020 samples over time in A) fertile soil, B) sandy soil, C) sand and D) saline soil with three different moisture contents (9 %, 17 % and 20 %).

Samples were buried in soil and incubated at 25 °C with aeration. Samples were removed weekly, washed, dried and weighed before being returned to the soil and incubation. Each soil type was tested three times at each moisture content. Error bars show the standard error of the mean. Where error bars are missing, this is due to two of the samples in those conditions disintegrating to such a degree that it was no longer possible to recover them from the soil. Data shown is the same as that shown in figure 5.7.

As can be seen in figure 5.9, the rate of degradation increased in each soil as moisture content increased. The extent of this increase was quite different for different soils and moisture contents. For example, the increase in rate of degradation in sandy soil when the moisture content increased from 9 % to 17 % is relatively small, equating to roughly a halving of the time for complete breakdown (table

5.3). In contrast, the equivalent increase in moisture content in saline soil (Figure 5.9) results in an almost five-fold increase in rate of degradation. Interestingly, the increase in rate between 17 % moisture and 20 % moisture in all soils was greater than the increase observed between 9 % moisture and 17 % moisture.

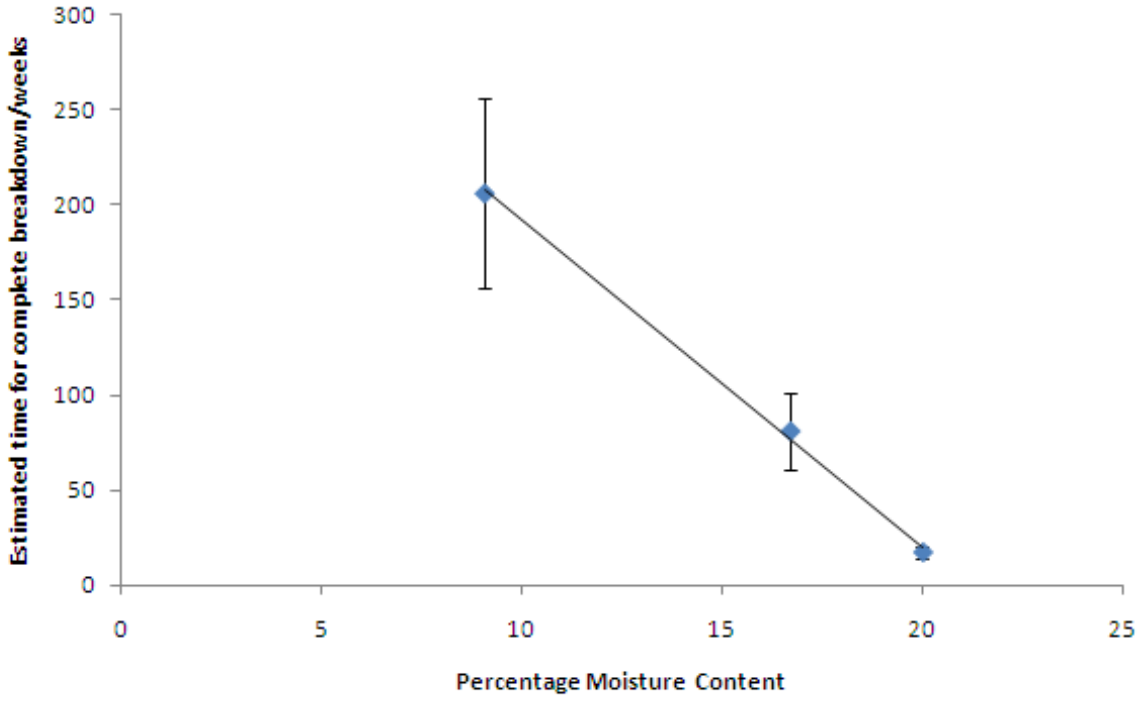

Figure 5.10. Mean estimated time for complete breakdown of EM10020 film at different moisture contents.

Points are the mean estimated time of breakdown for all samples at given moisture contents as shown in table 5.3.

Further analysis of the rates of breakdown in each individual soil reveals no obvious trends based upon the data collected so far. However, if the mean rate of breakdown for all soils at given moisture content is calculated then a clear trend can be seen (figure 5.10). Experiments which investigated a larger range of moisture contents would need to be gathered in order to make any firm conclusions about this relationship, in particular: how moisture content affects rate of breakdown outside the range investigated here.

5.2.2 Breakdown of PHA Films in Water

The breakdown of PHA film was monitored by following the loss of mass over time. A range of different water samples was used. Sea water, river water and lake water were collected as they represent the main sources of water in the environment. Water was also collected from a second lake in order to show possible variations in PHA breakdown. Two different samples were collected from the second lake (Lakeside). A negative control of boiled lake water from Lakeside was also tested. Experiments were carried out in 1 l sample jars each containing 500 ml of water and a 3 cm x 3 cm piece of PHA film (figure 5.12). The samples were incubated at 25 °C and every week were removed, washed and dried to constant mass. They were then photographed and replaced into the water samples before being returned to the incubator. The rate of degradation was measured by monitoring the percentage of mass lost from each PHA sample. The full methodology is described in section 7.7.

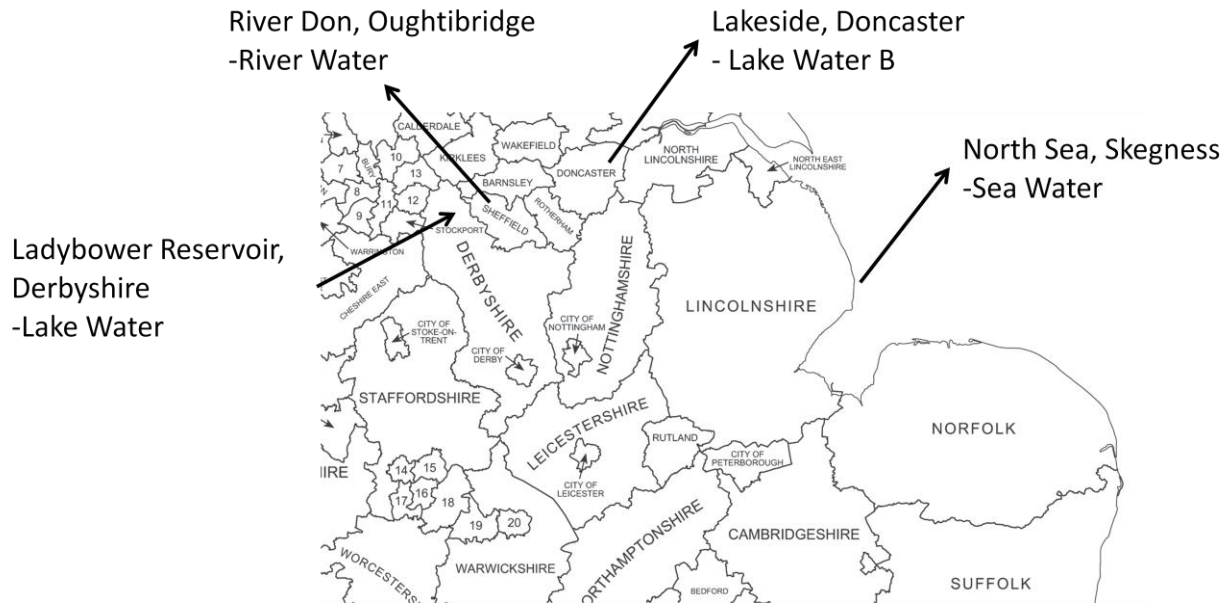

Figure 5.11. Locations of water sample collection.

Reproduced from Ordnance Survey map data by permission of the Ordnance Survey © Crown copyright 2010.

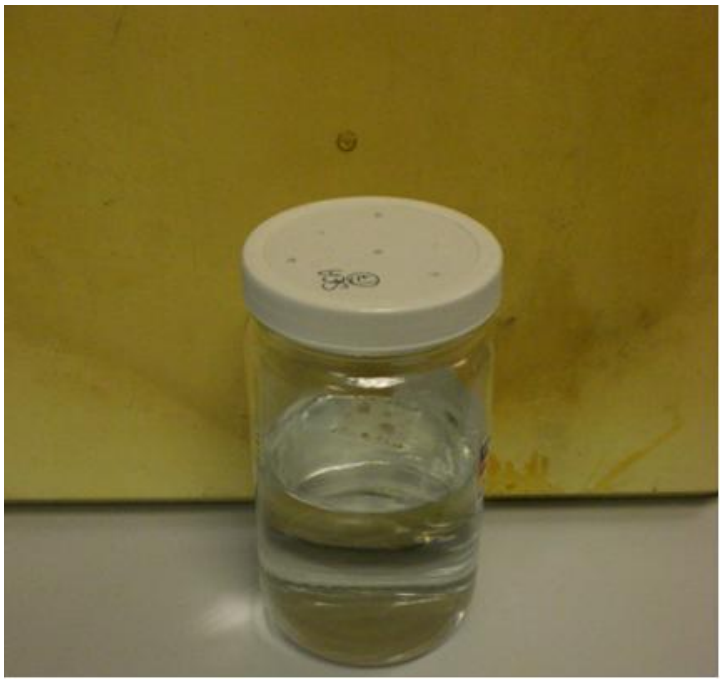

Figure 5.12. Experimental setup for breakdown experiments.

Each jar contained 500 ml of water and a 3 cm x 3 cm piece of EM10020 PHA film. Holes were drilled in the lid to allow aeration.

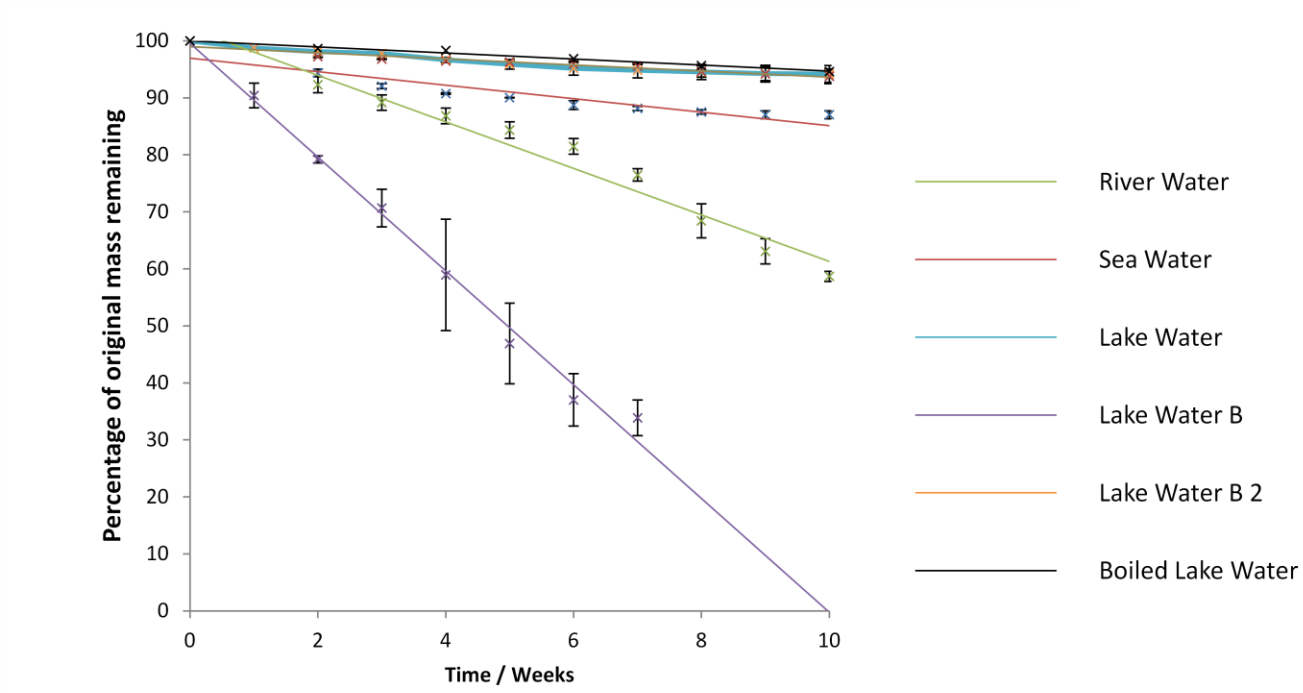

Figure 5.13. Mass loss of EM10020 samples over time in five different water samples (sea water, river water and three different lake water samples).

Samples were incubated at 25 °C with aeration. Samples were removed weekly, washed, dried and weighed before being returned to the water and incubation. Each water type was tested in triplicate. The error bars shown are the standard error of the mean.

As can be seen in figure 5.13, the rate of breakdown of PHA films varies greatly in different water types. Two of the three lake water samples showed extremely slow breakdown of the film, not significantly different to the breakdown observed in the negative control. These rates are equivalent to around three years for complete degradation to occur (table 5.4). In contrast, one of the lake water samples showed an extremely high rate of PHA breakdown, similar to that observed in saline soil with 20 % moisture (table 5.3). Samples in sea water showed a relatively slow rate of breakdown although this was still roughly twice as fast as the slowest rate observed in the lake water samples. Samples in river water are expected to breakdown completely within approximately six months. This result is interesting as previous work has suggested that PHAs should break down more rapidly in lake water than in sea water (Akmal et al., 2003).

Water Type	Average Weekly Percentage Mass Loss	Estimated Time for Complete Degradation/Weeks
Sea Water	1.2	85
River Water	4.1	25
Lake Water	0.5	187
Lake Water B	10.0	11
Lake Water B 2	0.7	156

Table 5.4. Estimated time for complete breakdown of EM10020 film in different soil types with varying moisture contents.

Estimates are based on the rate of breakdown calculated from the data in figure 5.13.

Degradation of PHA samples in water occurred very evenly. In contrast to the breakdown of the film in soils, samples placed in water remained largely intact even when they have lost a large proportion of their mass. When the samples have lost only a small proportion of their mass, they are almost indistinguishable from samples which have not started to biodegrade. As the extent of breakdown increases, the films become more translucent (figure 5.8(D)) but are noticeably not as fragile as films which have reached a similar level of breakdown in soil.

5.2.3 Mechanical Testing of Degraded PHA Films

A further experiment was planned to investigate the effects of degradation on the mechanical properties of the PHA film. Strips of PHA film approximately 2 cm x 5 cm were used in these experiments. Three different environments were chosen in which to carry out the breakdown of these strips. A new sample of agricultural soil was collected from Howbrook near Sheffield and water from Lakeside Doncaster was collected as this had produced a high rate of degradation in the previous studies. As a control, some of this lake water was boiled for 30 minutes to provide a third set of conditions. The strips of PHA were split between a number of bags and samples jars and incubated at 30 °C in order to maximise the rate of degradation. The methods used are described in section 7.8.

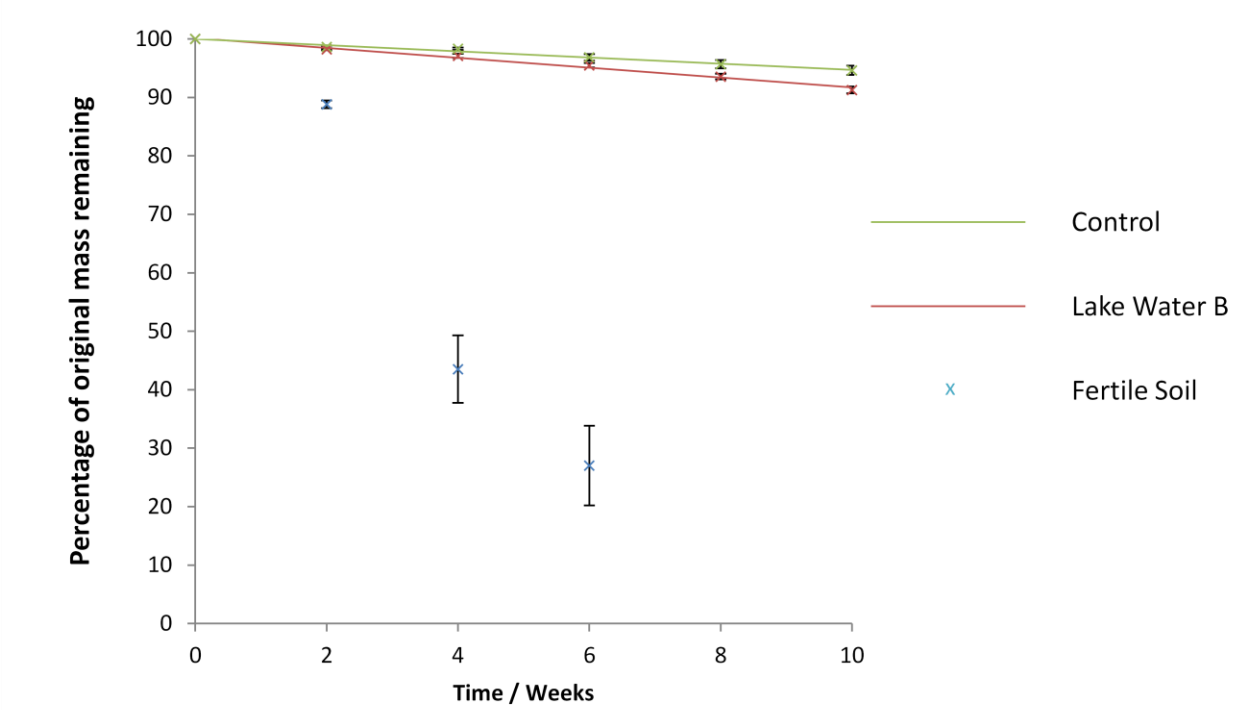

Figure 5.14. Mass loss of EM10020 samples over time in soil, lake water and boiled lake water.

Samples were buried in soil or submerged in water and incubated at 25 °C with aeration.

As shown in figure 5.14, the rate of degradation in soil was very high. In fact, after four weeks the strips had begun to break apart quite severely, as can be seen in figure 5.15(C). As a result of this, it is very likely that the PHA recovered after four and six weeks was not all that remained of each strip. As the strips were labelled only at each end, only those fragments which could be directly identified as belonging to a particular strip were dried and weighed. After eight weeks only very small fragments of PHA could be recovered from any of the bags of soil so the experiment was stopped. This result supports the previous results of composting studies which also showed that large-scale disintegration should occur when approximately 30 % of the original mass of PHA is remaining (Luo and Netravali, 2003).

Unfortunately, the higher than expected rate of breakdown of the samples in soil meant that mechanical testing was no longer possible. The photographs in figure 5.15 show the extent to which the PHA strips had broken down, even after two weeks. This amount of degradation would have meant that any force applied to the strips would have immediately resulted in them breaking apart.

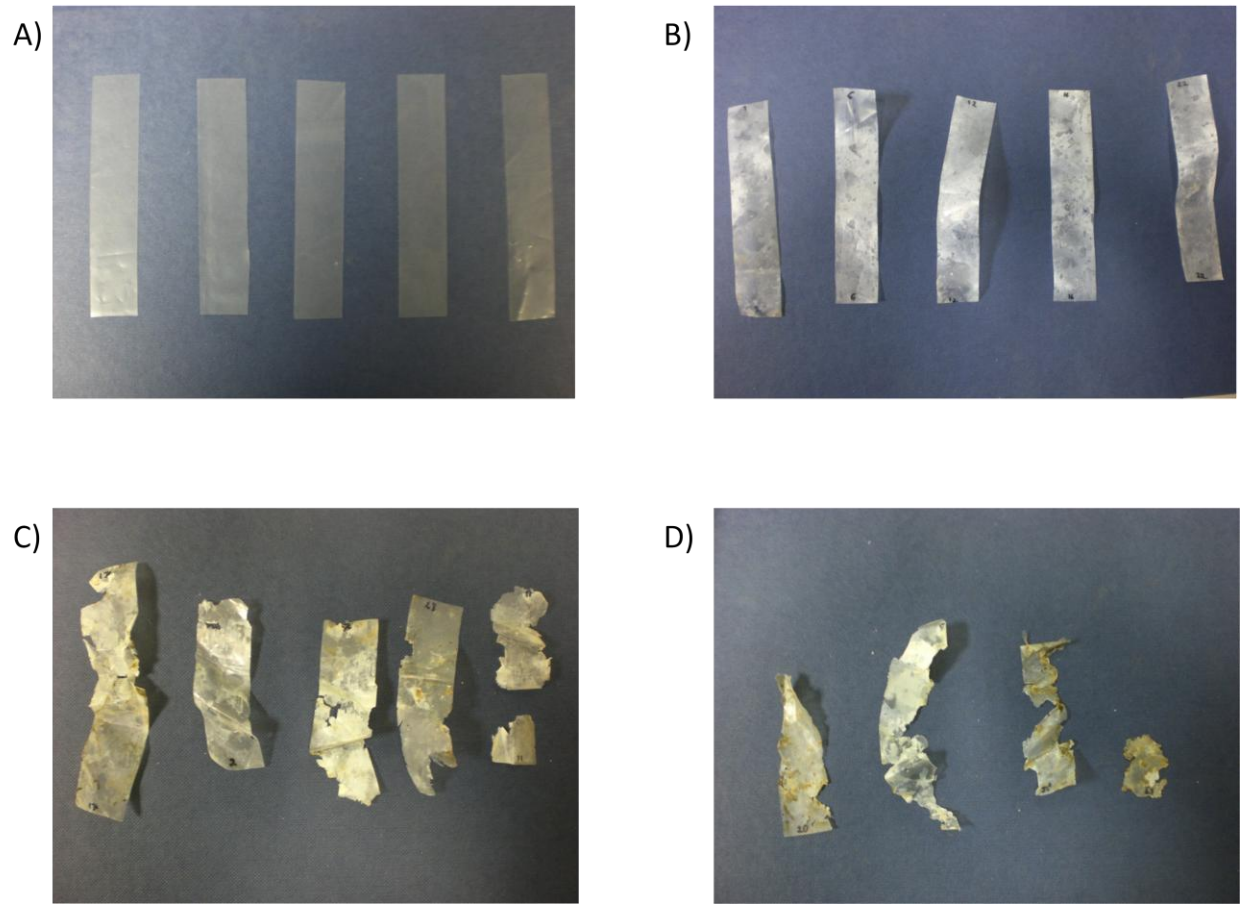

Figure 5.15. The breakdown of strips of EM10020 film after incubation at 30 °C in fertile soil with 20 % moisture content.

Samples were removed from the soil after A)0 weeks, B)2 weeks, C)4 weeks, D)6 weeks.

The samples incubated in lake water, conversely, broke down at a much slower rate than expected based upon the results in figure 5.13 ('Lake Water B'). In fact, the rate of degradation was only slightly greater than that in control experiment. Even after ten weeks the strips had lost, on average, less than 10 % of their mass. Again this limited any possible findings from mechanical testing as the range of breakdown was extremely small. However, this result did highlight the differences in rate of degradation between different environments, even if those environments are both found in the same lake.

5.2.4 Potential Use of PHA in Shampoo Packaging

There are a number of limitations in the experiments carried out in this work. First of all, the degradation was all carried out in the laboratory so could not be a true representation of environmental conditions. In real-world conditions bacterial growth nutrients would be constantly returned to soil or aquatic systems, whereas, in these experiments once any nutrients had been used up they would not be replenished. The amounts of soil used in the experiments were much larger than the amounts of PHA film buried in them in order to try to minimise this effect but for reasons of practicality (i.e. available incubator space and mass of large quantities of soil) the amount of soil that could be used was limited. This could cause a decrease in bacterial and fungal growth over the course of the experiment which could, in turn, lead to a decrease in the rate of breakdown of the PHA films. Such a phenomenon can possibly be seen occurring in some of the conditions investigated particularly 'sea water' in figure 5.13 and 'sandy soil' and 'sand' with 9 % moisture in figure 5.7. In order to confirm whether or not this is the case, an experiment in which samples would be buried in the natural environment or submerged directly in lake, sea or river water and monitored regularly, as described in section 6.4.

The process of removing, washing, drying and replacing the PHA samples also creates some issues with this work. First of all, the samples are out of the soil environment for approximately six hours every week while these processes are carried out. This means that for 3.6 % of the time the samples are not undergoing degradation. Additionally, the process of washing removes any bacteria or fungi that have built up on the surface of the film over the previous week. When the film is replaced in the soil, the population of bacteria and fungi must re-establish itself and begin to produce PHA depolymerases once more. This will, again, represent a period of time when degradation is either not taking place or is taking place at a lower rate. These limitations mean that the rate of degradation being observed is almost certainly lower than would take place in an equivalent environment. Repeating some of the experiments with more samples in a similar manner to the degradation for mechanical testing experiments described above could provide an estimate of exactly how much higher the rate of degradation could be.

The experiments were all carried out at a constant temperature and, in the case of the soils, constant moisture content. This does not take into account fluctuations that may occur in real-world conditions. Temperatures in India vary greatly throughout the country, as do levels of rainfall. It is likely that, rather than experiencing a constant rate of degradation, a shampoo sachet made from PHA would break down at a range of speeds depending on where it had been discarded and what time of year it was as well as a host of other factors. There is also no guarantee that a fertile agricultural soil in India would contain similar bacteria and fungi to the fertile soils used in this work. Extensive field studies would need to be carried out across India to determine what the true rates of degradation would be in the environment there. Even if these were carried out, however, it is extremely likely that a range of rates just as large as, if not larger than, the range observed in this work would be obtained.

The soil and water samples used for these experiments were collected in December. The typical environmental temperatures at this time of year are significantly lower than the 25 °C used for incubation in these experiments. It is possible that any microbes present in the soil may be better adapted to lower temperatures so will not grow optimally at 25 °C. However, it is also likely that this temperature will have the effect of increasing the rates of growth of many microbes present. It has also

been observed that soil microbe populations vary seasonally (Wolsing and Prieme, 2004) so it is possible that, at different times of the year, the microbe population present at the same sites at different times of year may be more effective at breaking down PHA. Despite these possibilities, the low rates of breakdown observed still suggest that PHA is an unsuitable material for the construction of a biodegradable sachet.

NMR spectroscopy experiments carried out by Joshua Swann at the University of Sheffield Department of Chemistry revealed that EM10020 is a copolymer of 3HB and 4HB containing approximately 20 % 4HB. P(3HB-co-4HB) is an interesting material as it has been shown that the rate of enzymatic degradation is highly dependent upon the proportion of 4HB present. The highest rate of degradation is observed for polymers containing approximately 15 % 4HB. The rate of degradation falls sharply at either side of this value and at 20 % 4HB, is reduced by roughly half (Sudesh and Abe, 2010). This suggests that just a small modification in the composition of the polymer could result in a significant increase in the rate of degradation.

The MVTR of EM10020 was also measured and was found to be 23 g/ m^2/ day at 25 °C. This is considerably lower than the MVTR of simple cellulose and even lower than the coated cellulose also investigated. Unfortunately, this value remains too high for the long term storage of liquids. The long term ultraviolet (UV) and humidity stability of EM10020 was investigated using a weathering simulation system. This revealed that, if exposed to UV light and humidity for a prolonged period, as is likely to be experienced by a shampoo sachet on display in a shop in India, the film begins to become brittle and crack. This again makes it unsuitable for the long term storage of liquids.

Ecomann film retails at £5000 per tonne. Based on a shampoo sachet size of 3 cm x 5 cm this works out at approximately 0.1 p per sachet. This would be considerably cheaper to produce than the previous, enzyme based proposal would have been, as it accounts for the entire cost of the sachet material. As the PHA film breaks down without any additional agents being present, it would also be much simpler to manufacture a complete sachet.

5.3 Conclusions

These experiments show that P(3HB-co-4HB) films break down in a range of different conditions. However, the rate of degradation varies greatly from 0.3 % per week to 10 % per week. While the higher rates of degradation would be ideal for a biodegradable shampoo sachet, the lower rates represent a time for total breakdown of up to six years. These timescales would offer little solution to many of the problems faced due to the current, non-biodegradable sachets.

Additional control experiments in sterilised samples of each soil and water type used are required to determine whether the degradation observed is true biodegradation or is occurring due to chemical or physical processes. However, should the final products of breakdown be biomass and water, the breakdown observed would still fulfil the initial requirements of the material as described in chapter 4.

It is important to note that the experiments described in this chapter were not carried out in environmental conditions. In particular, breakdown experiments were carried out at a constant temperature with limited quantities of soil and water. The results obtained are sufficient to show that the rate of breakdown of the EM10020 film investigated is too variable for it to be a suitable packaging material. The value of carrying out experiments in environmental conditions in the UK is limited as a biodegradable shampoo sachet would be sold in India or other developing countries in which environmental conditions would differ significantly.

There is the potential to produce a huge range of different PHA materials with different properties, all of which would degrade at different rates. This could be an area of further investigation and may produce materials with higher rates of degradation. As discussed in section 5.2.4, a small change such as adjusting the fraction of the second monomer in a copolymer could have a large effect on the rate of degradation. However, any such improvement in the rate of breakdown would also require an improvement in properties such as the MVTR and UV stability if PHAs were to be a suitable material for a shampoo sachet in the long term.

It is clear from the work undertaken investigating the properties of current biodegradable materials that no currently commercially available products are suitable for the production of shampoo sachets. In order to tackle the problem of sachet waste in the short term then an alternative solution must be used. One such solution may involve the creation of a partially biodegradable sachet. If the bulk of the sachet was made from a biodegradable film, such as a PHA, it could potentially be coated with a thin layer of a material such as aluminium foil which would reduce the MVTR and increase the UV stability of the sachet. Degradation of the bulk of the mass of the sachet would result in a decrease in waste mass and volume. Provided the coating layer could be made thin enough, this would be mechanically weak enough once the remainder of the sachet had degraded that it would not cause blockages of sewers and water courses. The downside of this approach if PHAs were used is that coating one side of the film would reduce the rate of degradation considerably by reducing access to the surface of the PHA for PHA depolymerases.

Another solution is to find a way to encourage people not to discard their waste sachets. Such an approach is currently in use by Unilever and relies upon the conversion of sachet waste into fuel via a process known as pyrolosis (Unilever, 2012b). This allows people to sell their used sachets back to Unilever who can then use the fuel produced to power their plants. This process recovers approximately 60 % of the energy stored within the sachet which is a significant improvement when the alternative is the entire sachet going to waste.

Chapter 6

6. Future Work

6.1 Small Molecule Inhibitors of HMG-CoA Reductase

While the method of calculation of IC50 values described in section 2.2.2 provided a sufficiently accurate estimate for this work, an increase in the range of concentrations of each compound investigated would improve the accuracy. A range of concentrations spanning a number of orders of magnitude both higher and lower than the concentrations investigated would produce data which could be plotted on a graph of initial rate of reaction against the logarithm of the inhibitor concentration. Using a least-squares regression method, this data could then be fitted to a sigmoidal curve in the form:

$$y = \frac{A_1 - A_2}{1 + 10^{(\log x_0 - x)p}} + A_2$$

Where y is the initial rate of reaction, x is the inhibitor concentration, A_1 is the initial rate of reaction at minimal inhibition, A_2 is the initial rate of reaction at maximal inhibition, x_0 is the IC50 and p is the gradient of the linear part of the curve.

Other further experiments could be carried out in order to better understand the mechanism of inhibition taking place in the assay. As mentioned in section 2.2.3, the use of isothermal titration calorimetry would enable binding energies to be calculated directly and accurately (McKinnon *et al.*, 1984). This technique is able to directly measure the energy change, at constant temperature, as an inhibitor is titrated against the enzyme. This data would be likely to be accurate enough to identify any correlation between gradations in structural properties, *i.e.* increasing size of groups added in the R_1/R_3 position, and binding energy. This could improve the selection of the most effective inhibitors as well as potentially allowing more targeted design and molecular modelling of future HMG-CoA reductase inhibitors.

In order to carry out isothermal titration calorimetry, or any of the other experiments described in this section, it would first be necessary to produce a supply of HMG-CoA reductase. This can be achieved by amplifying the catalytic portion of the human HMG-CoA reductase gene and cloning this into a plasmid containing a glutathione S-transferase (GST) protein. This plasmid can be transformed into *E. coli* leading to the production of a GST-fusion protein. The tagged protein can then be purified using affinity chromatography before the GST-tag is removed using a protease. HMG-CoA reductase can be further purified using anion-exchange chromatography (Istvan *et al.*, 2000).

Another important piece of further work would be to determine in what conformation the inhibitors bind to HMG-CoA reductase. One way of doing so would be to use ^{13}C-NMR, which would indicate changes in the environment of carbon atoms in the inhibitors under experimental conditions. An issue with this technique would be producing a clearly identifiable signal for the inhibitor. This may require a very high inhibitor concentration which may result in undesirable reactions occurring and thus producing less reliable results.

A more reliable method of determining the binding conformation of the inhibitors would be X-ray crystallography. For this technique, co-crystals of the catalytic portion of HMG-CoA reductase and each inhibitor would be produced. The diffraction pattern of these crystals could be used to calculate the structure of the inhibitor-enzyme complex (Istvan *et al.*, 2000). This would have the further advantage over ^{13}C-NMR of showing not only the inhibitor conformation but how each molecule interacts with the enzyme. This would also be very useful in identifying which structural features of the inhibitors were involved in binding, allowing better targeted design of future compounds. X-ray crystal structures would be particularly useful when refining molecular models of compound binding as this data could be used to further refine the current models that have been used.

As discussed in section 2.2.4, *in vitro* testing of the toxicity of the inhibitors tested would also be a useful further experiment to carry out. This can be done using the reagent resazurin, which fluoresces under reducing conditions. Viable cells maintain reducing conditions in the cytosol so when resazurin is added to cultured human cells and incubated at 37 °C it fluoresces. In order to test for the cytotoxicity of the inhibitors used in this experiment, cultured cells can be incubated in a solution of each different inhibitor before subsequently being incubated with resazurin. If the cultured cells do not fluoresce, or fluoresce to a lesser extent than cells that have not been incubated with the inhibitor, this would indicate that the inhibitor is cytotoxic (Fields and Lancaster, 1993).

Following elucidation of a compound's binding mechanism and confirmation that it is not toxic to human cells *in vitro*, the next stage of investigation would be to carry out *in vivo* testing in animals. Such experiments would allow an assessment of the pharmacokinetic and pharmacodynamic properties of a compound. Due to the nature of these compounds, as discussed in section 2.2.1, it is important to investigate the conformation that they take when they reach their sites of action. If the compounds are converted to the parent compounds, atorvastatin or rosuvastatin, by the time they reach cells then any improvement offered can only be in pharmacokinetic properties. This could be due to, for example, a longer elimination half-life or improved targeting to liver or intestinal cells which are the primary sites of cholesterol biosynthesis (Berg *et al.*, 2002). However, if the compounds reach cells in a different form and still inhibit cholesterol biosynthesis *in vivo*, this could be via a novel mechanism.

Initial testing of the compounds at concentrations of 50 nM in sections 2.2.1 and 2.2.4 identified three compounds that appear to enhance the initial rate of conversion of HMG-CoA to mevalonate (IB/6/2, IB/12/1 and ED/05/02B). Further investigation of these compounds would also be of interest. The assay used in chapter 2 could be repeated using a strong inhibitor such as rosuvastatin with one of the three rate enhancing compounds added to the reaction. If rosuvastatin has a similar effect on the rate of reaction as in the absence of the rate enhancing compound, this would suggest that any enhancement was due to allosteric effects. However, if the rate in the presence of both inhibitor and activator was higher than that in the presence of only inhibitor, this would suggest that the rate enhancement is caused by some interaction at the active site of the enzyme. This could be further investigated by carrying out x-ray crystallography on a complex of HMG-CoA reductase and a rate enhancing compound.

6.2 Antibacterial Activity of Novel Fluoroquinolones

It would be desirable to test the compounds investigated in chapter 3 using the same disc-diffusion technique but with larger amounts of each compound. However, as discussed in section 3.3, any positive results obtained would be of limited use as the mechanism of activity *in vitro* for these compounds is likely to differ from the *in vivo* mechanism of action.

As discussed in sections 3.2 and 6.1, the compounds used in these experiments are likely to be converted from their original conformation *in vivo*. Previous testing of 3-formyl fluoroquinolone analogues in mice has revealed improved pharmacokinetic properties compared to the equivalent fluoroquinolone parent compound (Kondo *et al.*, 1988). A similar experiment using the other novel fluoroquinolone analogues may also reveal an improvement in activity over existing, commercially available compounds, even when *in vitro* activity is not observed. As discussed in section 6.1, it would be preferable to carry out cytotoxicity testing on cultured human cells prior to carrying out animal work so as to avoid testing potentially dangerous compounds *in vivo*. The method employed for testing the toxicity of these compounds would be the same as the one described in that section.

Any antibacterial activity displayed in animal experiments is more likely to occur via the same mechanism as would occur when treating infections in humans. It would also reveal the pharmacokinetic properties of these novel compounds which would allow a direct comparison to the parent compounds levofloxacin and pefloxacin. Should any of the compounds offer improved activity *in vivo* then the equivalent substitution of the carboxylic acid group in position 1 of any existing fluoroquinolone compound could potentially also offer an improved treatment.

6.3 Alternative Biodegradable Materials for Shampoo Sachet Construction

Despite the shortcomings of cellulose as a material for a biodegradable shampoo sachet, there are a number of other biodegradable polymers which may yet offer a solution to the issues outlined in section 4.1. Like cellulose, starch is a polysaccharide made up of glucose monomers. It is made up of two different homopolymers of glucose: amylose contains glucose monomers exclusively linked by α-1,4-glycosidic bonds in a linear manner and amylopectin which resembles the linear structure of amylose but also contains branched chains connected by α-1,6-glycosidic bonds. Starch is produced by plants as an energy store and is a common component of the human diet.

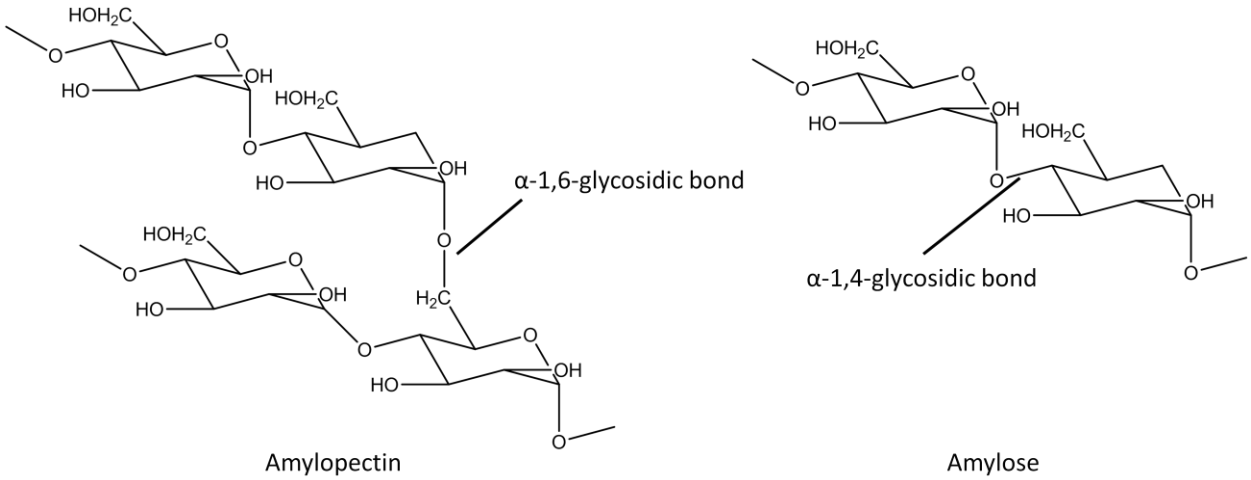

Figure 6.1. The structures of amylopectin and amylose, the two different homopolymer constituents of starch.

Starch is readily broken down by a number of different amylase enzymes (Reis and Cunha, 2001). However, compared to other materials, biodegradable products based on starch have several drawbacks, such as water sensitivity, brittleness and poor mechanical properties (Lu *et al.*, 2009) and is often used in blends with synthetic monomers such as vinyl alcohol. The MVTR of starch was measured, by Joshua Swann at the University of Sheffield, Department of Chemistry, as 140 g/ m^2/ day. This is lower than the MVTR of the simple cellulose film but for a film nearly seven times thicker. This fact alone is sufficient to discount starch as a suitable packaging material for shampoo.

Polylactic acid (PLA) is synthesised by condensation of lactic acid or by ring opening of lactide. The source of these starting materials is typically the fermentation of carbohydrates such as glucose. Degradation of PLA can occur either hydrolytically or enzymatically (Kikkawa *et al.*, 2002). The enzymes responsible for degradation of PLA are proteases rather than specific PLA depolymerases (Williams, 1981). Unfortunately, no commercially available PLAs are biodegradable and all rely on hydrolysis for degradation. This process is temperature dependent and will not occur without industrial composting maintaining a constant high temperature to initiate break down. This is unsuitable as the poor waste processing facilities in developing countries are one of the main reasons behind the requirement for a fully biodegradable solution.

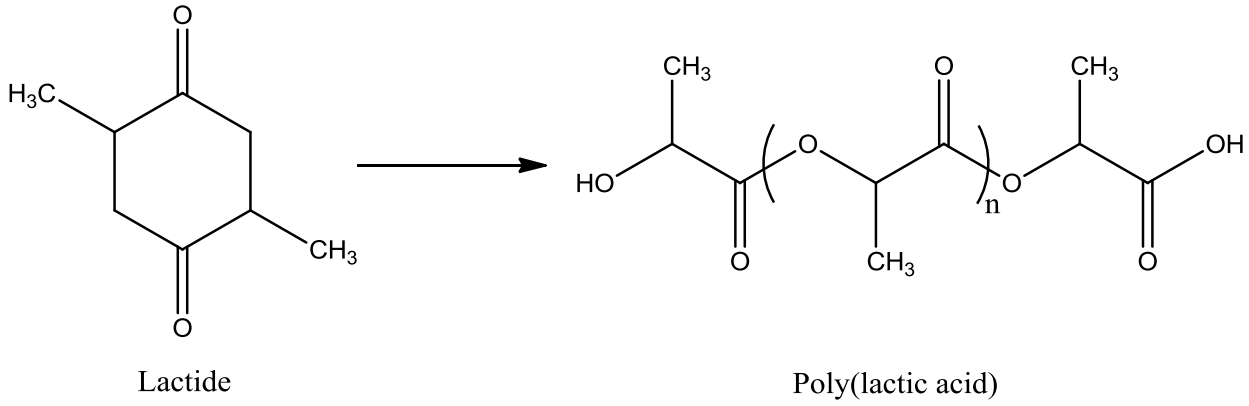

Figure 6.2. Polymerisation of PLA via the ring opening hydrolysis of lactide.

Polyhydroxyalkanoates (PHAs) are a type of linear polyesters which are synthesised by certain bacteria. The most common type of PHA is polyhydroxybutyrate (PHB) which is a polymer of butyric acid. PHAs are produced by bacteria in response to unbalanced growth conditions and serve as a stored carbon source until suitable growth conditions return. In order to utilise the stored carbon, PHA-producing bacteria produce PHA depolymerase enzymes. A wide range of different PHAs exist with several hundred different HA monomers known to be incorporated. PHAs are, therefore, a family of naturally occurring and fully biodegradable materials with a wide range of different properties. The suitability of PHAs as a packaging material for shampoo sachets is discussed in chapter 5.

6.4 Use of PHAs in Shampoo Sachet Construction

While the experiments carried out in chapter 5 demonstrate that the commercially available PHA tested is unsuitable as a material for the construction of a biodegradable shampoo sachet, there are a number of further experiments that could be carried out to better understand its breakdown. Initially, the negative control experiments discussed in section 5.2.1 should be carried out to determine whether the breakdown of the PHA film was due to the action of biological agents or simply the result of chemical or physical degradation. If biodegradation was taking place, an analysis of the bacteria and fungi present in each soil and water sample could be carried out to identify which species were causing the breakdown. This can be achieved by inoculating plates of minimal media containing PHA with a suspension of a soil or a sample of a water type. This should produce distinct strains of bacteria which can then be identified by sequencing their ribosomal RNA (Fierer *et al.*, 2005).

It would also be useful to carry out studies of the breakdown of PHAs in environmental conditions. This could be achieved by burying PHA samples directly in soil or submerging them in a fixed, porous

container in a lake, river or sea. The samples could then be retrieved after a fixed length of time and the extent of breakdown measured. This would confirm how good an estimation of the true rate of breakdown the experiments described in chapter 5 is.

The work described in chapters 4 and 5 shows that it is not possible to produce a functional, biodegradable shampoo sachet using commercially available materials. However, while beyond the scope of this work, it may be possible to produce a novel material suitable for this purpose. PHAs may be an ideal candidate due to the potential for variation in their structures, as discussed in section 5.1.1. A range of different copolymers of 3HB and other PHA monomers could be produced and their rates of breakdown investigated. As discussed in section 5.2.4, varying the proportion of a particular monomer in a copolymer by as little as 5 % can have a significant impact on the rate of breakdown (Sudesh and Abe, 2010).

If a PHA producing bacterium is grown in unbalanced growth conditions on a medium containing a carbon source that is structurally related to a particular HA monomer, it will produce crystals of the equivalent copolymer with 3HB. If these crystals are purified, they can be cast into films and their rates of breakdown in different environments measured. By varying the types and proportions of the carbon source during the initial bacterial growth, a range of different films could be investigated. If a polymer that broke down in an acceptable time-frame in a range of different conditions could be produced it may be a suitable candidate for use in shampoo sachets.

It is unlikely that a film produced by this method would have an MVTR low enough to be the sole component of a viable sachet. A further area for investigation would be the inclusion of an additional layer to a PHA sachet, similar to the coated cellulose used in chapter 4, to reduce its MVTR. It is unlikely that a biodegradable material would be suitable for this task unless it was so thick as to increase the time taken for the sachet to breakdown to above an acceptable level. Non-biodegradable alternatives would have to have a minimal impact on the rate of breakdown of the PHA and also a minimal impact on the environment following that breakdown.

Chapter 7

7. Materials and Methods

7.1 Materials and Equipment

All chemicals used in the experiments described here were of molecular biology grade. dH_2O was produced by a Millipore MilliQ system. ddH_2O was produced by autoclaving MilliQ dH_2O for a period of 20 minutes at 121 °C in acid-cleaned glass containers. ddH_2O was used in the preparation of all buffer solutions and in all experiments unless specified otherwise.

Description	**Supplier**	**Abbreviation**
3-Hydroxy-3-methylglutaryl-CoA Reductase Solution Human	Sigma-Aldrich	HMG-CoA Reductase
Agar Bacteriological	Oxoid	-
Albumin, from Bovine Serum	Sigma-Aldrich	BSA
Cellobiase from *Aspergillus niger*, liquid	Sigma-Aldrich	-
Cellulase from *Aspergillus* sp., aqueous solution	Sigma-Aldrich	-
Cellulase from *Trichoderma reesei* ATCC 26921, aqueous solution	Sigma-Aldrich	-
Cellulose, Microcrystalline Powder	Sigma-Aldrich	-
D(+)-Glucose Monohydrate	VWR BDH Prolabo	Glucose
Diaminoethanetetraacetic Acid Disodium Salt	Fisher Scientific	EDTA
Dimethyl Sulfoxide	Sigma-Aldrich	DMSO
Dimethyl Sulfoxide	Sigma-Aldrich	-
Dipotassium Hydrogen Orthophosphate	VWR BDH Prolabo	K_2HPO_4
DL-3-Hydroxy-3-methylglutaryl Coenzyme A Sodium Salt Hydrate	Sigma-Aldrich	HMG-CoA
EM10020 50 micron	A & O Film Pac	-
EM10020 60 micron	A & O Film Pac	-
Filter Paper Grade 1	Whatman	-
Mowiol 10-98	Mowiol	-
Mowiol 20-98	Mowiol	-
Mowiol 28-99	Mowiol	-
Mowiol 40-88	Mowiol	-
Mowiol 4-98	Mowiol	-
Mowiol 6-98	Mowiol	-
Mowiol 8-88	Mowiol	-

Mueller-Hinton Broth	Oxoid	-
Natureflex 22DNE	Innovia Films	Coated Cellulose Film
Natureflex NP21	Innovia Films	Simple Cellulose Film
Nutrient Broth	Oxoid	-
Potassium Chloride	Fisher Scientific	KCl
Potassium Dihydrogen Orthophosphate	VWR BDH Prolabo	KH_2PO_4
Tryptone Soya Broth	Oxoid	-
β-Nicotinamide Adenine Dinucleotide 2'-Phosphate Reduced Tetrasodium Salt Hydrate	Sigma-Aldrich	NADPH

Table 7.1. Materials used during experimental work.

Includes details of material supplier and, where applicable, the abbreviated description used in the text.

All disposable plastic used in this work were obtained from Star Labs, Bibby Sterelin and Anachem. Other equipment used is listed in table 7.2.

Equipment	**Supplier and Model**
Balances	Mettler 0-60 g model AJ100 and Mettler 0-800 g model K7
Microcentrifuge	MSE Microcentaur
Dry Heat Block	Grant Instruments
pH Meter	Denver Instruments Basic with Tris electrode
Pipettes	Gilson Pipetman P10, P20, P100, P200, P1000, P5000
Positive Displacement Pipette	Gilson Microman M10
UV/Vis Spectrophotometer	Perkin Elmer Lambda 12
Vortexer	Labnet
Microplate Reader	Biorad Model 550
96 Well EIA/RIA Plate	Costar

Table 7.2. Equipment used during experimental work including supplier information.

Staphylococcus aureus Newman, *S. aureus* SH1000, *Pseudomonas aeruginosa* and *Enterococcus faecalis* used in the testing of antibacterial compounds were provided by Professor Simon Foster.

7.2 *In vitro* Testing of HMG-CoA Reductase Inhibitors

The reaction buffer contained 100 mM potassium phosphate buffer at pH 7.2, 1 mM EDTA, 500 mM KCl and 2 mg/ ml BSA. HMG-CoA reductase was diluted to working concentration in the reaction buffer. NADPH and HMG-CoA were also dissolved in the reaction buffer. Potential inhibitor compounds were dissolved in 99.5 % DMSO, all to the same stock concentration. The assay was carried out in flat-bottomed 98-well microplates to a total volume of 200 µl. The final concentration of HMG-CoA reductase in each assay was 10 nM and the final concentrations of NADPH and HMG-CoA were both 200 µM. The reaction was activated by the addition of HMG-CoA reductase. The plate was transferred to a UV spectrophotometer which was set to a temperature of 37 °C and recorded the absorption at 340 nm every twenty seconds over a ten minute period. This cycle included 10 seconds of mixing prior to each of the first 10 absorption readings. All assays were carried out in triplicate as a minimum. All assays were carried out blind, i.e. the identity of each inhibitor was unknown when the experiments were carried out.

Initial screening assays were carried out with 50 nM inhibitor which resulted in a final DMSO concentration of 0.5 %. The following controls were also carried out: 0 nM inhibitor, 50 nM atorvastatin, 50 nM rosuvastatin and 0 nM inhibitor plus 0.5 % DMSO.

In order to calculate IC50 values for compounds, the assay was repeated with all conditions remaining constant except for the inhibitor concentration. Inhibitor concentrations of 1 nM, 2 nM, 5 nM, 10 nM, 20 nM, 30 nM and 40 nM were used for each compound along with the result of initial testing with 50 nM inhibitor. This allowed a graph of initial rate of catalysis against time to be plotted for each compound. This data was then fitted to a Boltzmann function using a least-squares regression method, which produced an estimate of the IC50 value.

7.3 *In vitro* Testing of Fluoroquinolone Compounds

The parent compounds, levofloxacin and pefloxacin mesylate, were dissolved in 99.5 % DMSO and solutions of 1 µg / ml, 5 µg / ml, 10 µg / ml, 20 µg / ml, 50 µg / ml, 100 µg / ml and 200 µg / ml were produced. 6 mm disks of Whatman filter paper number one were produced and placed in an oven overnight for sterilisation. Antibacterial disks were produced by applying 5 µl of a prepared solution to a filter paper disk and allowing the disk to dry. Mueller-Hinton agar plates were produced using 21 g l^{-1} Mueller-Hinton broth and 1.5 % (w/v) agar No 1. *P. aeruginosa* was grown in nutrient broth and *S. aureus* and *E. faecalis* were grown in tryptone soya broth all at 37 °C with shaking. All bacterial strains were grown to an optical density of between 0.07 and 0.1 at 625 nm. 100 µl of the bacterial culture was then mixed with 2 ml of Mueller-Hinton broth (21 g l^{-1}) containing 0.7 % (w/v) agar No 1. The mixture was then spread evenly onto a Mueller-Hinton agar plate and allowed to set.

Each bacterial strain was tested against both of the parent compounds. A single compound was tested on each agar plate. Disks containing different concentrations of an antibacterial compound were placed

onto the surface of the agar, each separated by a distance of at least 24 mm. The plates were incubated for 18 hours at 37 °C. Following incubation, the zone of inhibition for each disk was measured. Each concentration of each compound was tested three times.

Six novel compounds were tested using the method above but the solutions applied to the filter paper discs were 2 µg / ml, 20 µg / ml, 200 µg / ml and 2000 µg / ml. Each plate also contained a positive control of a disc with 5 µl of a 20 µg / ml solution of levofloxacin applied.

7.4 Degradation of Cellulose by Cellulolytic Enzymes

10 mg of cellulose substrate were added to 490 µl of ddH_2O and 10 µl of cellulolytic enzymes which were mixed at 25 revolutions per minute on a rotator at 37 °C for 20 hours. The reaction was stopped by placing the mixture on ice. The mixture was centrifuged at 14800 rpm for 5 minutes. 8.33 µl of the supernatant was added to 250 µl of glucose determination reagent containing 0.16 mM ATP, 0.09 mM NADP, 3.0 units of hexokinase and 2.4 units of glucose-6-phosphate dehydrogenase in 0.1 M Tris-HCl pH 7.2. The absorbance at 340 nm was measured every 30 seconds for one hour by UV spectroscopy and the final absorbance recorded.

A glucose standard curve was constructed using the same glucose determination reagent and 8.33 µl of solutions of glucose in ddH_2O. Thirteen different solutions were used with concentrations between 0 mM and 15 mM. The standard curve was then used to convert the final absorbances at 340 nm to the equivalent mass of glucose produced during the cellulose digestion.

10 mg of each different substrate was as follows: 10 mg of microcrystalline cellulose, two 6 mm diameter discs of Whatman Number 1 filter paper or 3 cm^2 of simple cellulose film and coated cellulose film. When measuring the breakdown of bilayer films, 3 cm^2 was also used. This represents a total mass of greater than 10 mg but a mass of cellulose of 10 mg. In addition to monitoring the breakdown of coated cellulose film over 20 hours, the assay was repeated with identical reagents but with increased incubation times of 44 hours, 68 hours and 116 hours.

Two negative controls were carried out for each assay. Firstly, the protocol outlined above with no enzyme present and, secondly, the protocol outlined above with no substrate. For experiments involving bilayer films, a cellulose-PVOH bilayer was used as one control and a PVOH film containing cellulolytic enzyme was used as a second control. All assays and controls were repeated a minimum of three times.

7.5 Degradation of Coated Cellulose by Different Enzyme Concentrations

A further experiment monitored the breakdown of coated cellulose film with varying concentrations of cellulolytic enzymes in solution. The concentrations used in addition to the 0.7 units of cellulolytic

enzyme per mg of cellulose used in other assays were: 0.63 units per mg, 0.525 units per mg, 0.42 units per mg, 0.315 units per mg, 0.21 units per mg and 0.07 units per mg. Multiple cellulolytic digestions were set up at each concentration and incubated at 37 °C with mixing at 25 revolutions per minute on a rotator. After 24 hours, three tubes of each concentration were removed from the incubator and the reaction stopped with ice. The tubes were centrifuged at 14800 rpm for 5 minutes. 8.33 µl of the supernatant from each tube was added to 250 µl of glucose determination reagent containing 0.16 mM ATP, 0.09 mM NADP, 3.0 units of hexokinase and 2.4 units of glucose-6-phosphate dehydrogenase in 0.1 M Tris-HCl pH 7.2. The absorbance at 340 nm was measured every 30 seconds for one hour by UV spectroscopy and the final absorbance recorded.

A further three tubes of each concentration were analysed in the same manner every 24 hours. The experiment was stopped after no change in final absorbance had been observed for three consecutive 24 hour periods. This was taken as an indication that complete digestion had taken place.

7.6 Breakdown of Polyhydroxyalkanoate Films in Soil

Samples of four different soils were collected as outlined in the table below. All soils were collected during December.

Soil Type	Location
Fertile Agricultural Soil	Lincolnshire (current crop: beans)
Sandy Soil	Gibraltar Point, Skegness, Lincolnshire
Sand	Skegness, Lincolnshire
Saline Soil	Gibraltar Point, Skegness, Lincolnshire

Table 7.3. Soil types used in breakdown experiments, the locations from which they were collected and a description of the soil.

Soils were air-dried to constant mass. Samples of approximately 300 g of each dried soil were placed into polythene bags before dH_2O was added to achieve the desired soil moisture content. A 3 cm x 3 cm piece of 50 micron EM10020 PHA film, of known mass, was then buried in each soil and the bags sealed, with straws inserted in order to provide ventilation. The bags were then incubated at 25 °C. At weekly intervals, the PHA samples were removed from the soil, washed with deionised water and dried in an incubator before being weighed. The samples were then returned to the bags and deionised water

added to maintain the soil moisture content before being returned to the 25 °C incubator. Degradation in each soil type was carried out in triplicate. The experiment was carried out for soil moisture contents of 9 %, 17 % and 20 %.

7.7 Breakdown of Polyhydroxyalkanoate Films in Water

Four different water samples were collected as outlined in the table below. All samples were collected during December, except for 'lake water B' which was collected during January.

Water Type	Location
River Water	River Don, Oughtibridge, South Yorkshire
Lake Water A	Lady Bower Reservoir, Derbyshire
Lake Water B	Doncaster, South Yorkshire
Sea Water	North Sea

Table 7.4. Water types used in breakdown experiments and the locations from which they were collected.

500 ml samples of each water type were placed into 1 litre glass sample jars. A 3 cm x 3 cm piece of 50 micron EM10020 PHA film, of known mass, was added to each jar. Holes were drilled into the lid of each sample jar to provide ventilation. The jars were incubated at 25 °C. At weekly intervals, the PHA samples were removed from the jars, washed with deionised water and dried in an incubator before being weighed. The samples were then returned to the jars and the jars returned to the 25 °C incubator. Experiments were carried out in triplicate for each water type.

7.8 Breakdown of Polyhydroxyalkanoate Films for Mechanical Testing

Soil was collected from a field planted with a grass ley, during March, and air-dried to constant mass. Ten polythene bags were each filled with approximately 750 g of the dry soil. dH_2O was added to each bag to give a soil moisture content of 20 %. 25 strips of 60 micron EM10020 PHA film, approximately 2 cm x 10 cm were buried in the soil with two or three strips in each bag. The bags were sealed, with a straw placed in each bag in order to provide ventilation. The bags were then incubated at 30 °C. dH_2O

was added to each bag weekly, in order to maintain constant soil moisture content. Every two weeks five PHA strips were removed, each one coming from a different bag. These strips were then washed and dried in an incubator before being weighed.

Five one-litre sample jars were each filled with 600 ml of ‘Lake Water B’ (see table 2) which was collected during March. Five 2 cm x 10 cm PHA strips were placed in each jar. Holes were drilled in the lid of each jar to provide ventilation. The jars were then incubated at 30 °C. Every two weeks one strip was removed from each jar. These strips were then washed and dried in an incubator before being weighed. This experiment was completed in duplicate using ‘Lake Water B’ which had been boiled for at least 30 minutes.

References

AARESTRUP, F. M., JENSEN, N. E., JORSAL, S. E. & NIELSEN, T. K. 2000. Emergence of resistance to fluoroquinolones among bacteria causing infections in food animals in denmark. *Veterinary Record,* 146**,** 76-8.

ADAMS, C. M., REITZ, J., DE BRABANDER, J. K., FERAMISCO, J. D., LI, L., BROWN, M. S. & GOLDSTEIN, J. L. 2004. Cholesterol and 25-hydroxycholesterol inhibit activation of srebps by different mechanisms, both involving scap and insigs. *Journal of Biological Chemistry,* 279**,** 52772-80.

AKIYAMA, M., TSUGE, T. & DOI, Y. 1995. Environmental life cycle comparison of polyhydroxyalkanoates produced from renewable carbon resources by bacterial fermentation. *Polymer Degradation and Stability,* 80**,** 183-194.

AKMAL, D., AZIZAN, M. N. & MAJID, M. I. A. 2003. Biodegradation of microbial polyesters p(3hb) and p(3hb-co-hv) under the tropical climate environment. *Polymer Degradation and Stability,* 80**,** 513-518.

ALBERS-SCHONBERG, G., JOSHUA, H., LOPEZ, M. B., HENSENS, O. D., SPRINGER, J. P., CHEN, J., OSTROVE, S., HOFFMAN, C. H., ALBERTS, A. W. & PATCHETT, A. A. 1981. Dihydromevinolin, a potent hypocholesterolemic metabolite produced by aspergillus terreus. *Journal of Antibiotics (Tokyo),* 34**,** 507-12.

ALOVERO, F. L., PAN, X. S., MORRIS, J. E., MANZO, R. H. & FISHER, L. M. 2000. Engineering the specificity of antibacterial fluoroquinolones: Benzenesulfonamide modifications at c-7 of ciprofloxacin change its primary target in streptococcus pneumoniae from topoisomerase iv to gyrase. *Antimicrobial Agents and Chemotherapy,* 44**,** 320-5.

ALTSCHUL, R., HOFFER, A. & STEPHEN, J. D. 1955. Influence of nicotinic acid on serum cholesterol in man. *Archives of Biochemistry and Biophysics,* 54**,** 558-9.

ANDERSSON, D. I. & LEVIN, B. R. 1999. The biological cost of antibiotic resistance. *Current Opinion in Microbiology,* 2**,** 489-93.

APPELBAUM, P. C. & HUNTER, P. A. 2000. The fluoroquinolone antibacterials: Past, present and future perspectives. *International Journal of Antimicrobial Agents,* 16**,** 5-15.

ASPINALL, S. L., GOOD, C. B., JIANG, R., MCCARREN, M., DONG, D. & CUNNINGHAM, F. E. 2009. Severe dysglycemia with the fluoroquinolones: A class effect? *Clinical Infectious Diseases,* 49**,** 402-8.

BALL, P. 2000. Quinolone-induced qt interval prolongation: A not-so-unexpected class effect. *Journal of Antimicrobial Chemotherapy,* 45**,** 557-9.

BALL, P. & TILLOTSON, G. 1995. Tolerability of fluoroquinolone antibiotics. Past, present and future. *Drug Safety,* 13**,** 343-58.

BAQUERO, F. & NEGRI, M. C. 1997. Strategies to minimize the development of antibiotic resistance. *Journal of Chemotherapy,* 9 Suppl 3**,** 29-37.

BAUER, A. W., KIRBY, W. M., SHERRIS, J. C. & TURCK, M. 1966. Antibiotic susceptibility testing by a standardized single disk method. *Am J Clin Pathol,* 45**,** 493-6.

BAX, B. D., CHAN, P. F., EGGLESTON, D. S., FOSBERRY, A., GENTRY, D. R., GORREC, F., GIORDANO, I., HANN, M. M., HENNESSY, A., HIBBS, M., HUANG, J., JONES, E., JONES, J., BROWN, K. K., LEWIS, C. J., MAY, E. W., SAUNDERS, M. R., SINGH, O., SPITZFADEN, C. E., SHEN, C., SHILLINGS, A., THEOBALD, A. J., WOHLKONIG, A., PEARSON, N. D. & GWYNN, M. N. 2010. Type iia topoisomerase inhibition by a new class of antibacterial agents. *Nature,* 466**,** 935-40.

BAYER, E. A., MORAG, E., SHOHAM, Y., TORMO, J. & LAMED, R. 1996. *The cellulosome: A cell surface organelle for the adhesion to and degradation of cellulose.,* Chichester, Wiley.

BELLON, S., PARSONS, J. D., WEI, Y., HAYAKAWA, K., SWENSON, L. L., CHARIFSON, P. S., LIPPKE, J. A., ALDAPE, R. & GROSS, C. H. 2004. Crystal structures of escherichia coli topoisomerase iv pare subunit (24 and 43 kilodaltons): A single residue dictates differences in novobiocin potency against topoisomerase iv and DNA gyrase. *Antimicrobial Agents and Chemotherapy,* 48**,** 1856-64.

BENNANI, Y. L. 2012. Drug discovery in the next decade: Innovation needed asap. *Drug Discovery Today,* 17 Suppl**,** S31-44.

BERG, J. M., TYMOCZKO, J. L. & STRYER, L. 2002. *Biochemistry,* New York, W. H. Freeman and Co. .

BETTERIDGE, D. J., DODSON, P. M., DURRINGTON, P. N., HUGHES, E. A., LAKER, M. F., NICHOLLS, D. P., REES, J. A., SEYMOUR, C. A., THOMPSON, G. R. & WINDER, A. F. 1993. Management of hyperlipidaemia: Guidelines of the british hyperlipidaemia association. *Postgraduate Medical Journal,* 69**,** 359-369.

BETTERIDGE, J. & MORRELL, J. M. 2003. *Clinicians' guide to lipids and coronary heart disease,* London, Arnold.

BEYER, R., PESTOVA, E., MILLICHAP, J. J., STOSOR, V., NOSKIN, G. A. & PETERSON, L. R. 2000. A convenient assay for estimating the possible involvement of efflux of fluoroquinolones by streptococcus pneumoniae and staphylococcus aureus: Evidence for diminished moxifloxacin, sparfloxacin, and trovafloxacin efflux. *Antimicrobial Agents and Chemotherapy,* 44**,** 798-801.

BJORKHEM-BERGMAN, L., LINDH, J. D. & BERGMAN, P. 2011. What is a relevant statin concentration in cell experiments claiming pleiotropic effects? *Br J Clin Pharmacol,* 72**,** 164-5.

BLAAK, H. & SCHREMPF, H. 1995. Binding and substrate specificities of a streptomyces olivaceoviridis chitinase in comparison with its proteolytically processed form. *European Journal of Biochemistry,* 229**,** 132-9.

BLOCH, K. 1965. The biological synthesis of cholesterol. *Science,* 150**,** 19-28.

BODEN, W. E., PROBSTFIELD, J. L., ANDERSON, T., CHAITMAN, B. R., DESVIGNES-NICKENS, P., KOPROWICZ, K., MCBRIDE, R., TEO, K. & WEINTRAUB, W. 2011. Niacin in patients with low hdl cholesterol levels receiving intensive statin therapy. *New England Journal of Medicine,* 365**,** 2255-67.

BRAUNEGG, G., BONA, R. & KOLLER, M. 2004. Sustainable polymer production. *Polymer-Plastics Technology and Engineering,* 43**,** 1779-1793.

BRINO, L., URZHUMTSEV, A., MOUSLI, M., BRONNER, C., MITSCHLER, A., OUDET, P. & MORAS, D. 2000. Dimerization of escherichia coli DNA-gyrase b provides a structural mechanism for activating the atpase catalytic center. *Journal of Biological Chemistry,* 275**,** 9468-75.

BROWN, A. G., SMALE, T. C., KING, T. J., HASENKAMP, R. & THOMPSON, R. H. 1976. Crystal and molecular structure of compactin, a new antifungal metabolite from penicillium brevicompactum. *Journal of the Chemical Society, Perkin Transactions 1***,** 1165-70.

BROWN, A. J. & JESSUP, W. 1999. Oxysterols and atherosclerosis. *Atherosclerosis,* 142**,** 1-28.

BROWN, A. J., SUN, L., FERAMISCO, J. D., BROWN, M. S. & GOLDSTEIN, J. L. 2002. Cholesterol addition to er membranes alters conformation of scap, the srebp escort protein that regulates cholesterol metabolism. *Molecular Cell,* 10**,** 237-45.

BROWN, D. A. & SIMONI, R. D. 1984. Biogenesis of 3-hydroxy-3-methylglutaryl-coenzyme a reductase, an integral glycoprotein of the endoplasmic reticulum. *Proceedings of the National Academy of Sciences of the United States of America,* 81**,** 1674-8.

BROWN JR, R. M. 1999. Cellulose structure and biosynthesis. *Pure and Applied Chemistry,* 71**,** 767-775.

BROWN, M. S. & GOLDSTEIN, J. L. 1974. Expression of the familial hypercholesterolemia gene in heterozygotes: Mechanism for a dominant disorder in man. *Science,* 185**,** 61-3.

BROWN, M. S. & GOLDSTEIN, J. L. 1986. A receptor-mediated pathway for cholesterol homeostasis. *Science,* 232**,** 34-47.

BROWN, M. S. & GOLDSTEIN, J. L. 1997. The srebp pathway: Regulation of cholesterol metabolism by proteolysis of a membrane-bound transcription factor. *Cell,* 89**,** 331-40.
BROWN, P. O. & COZZARELLI, N. R. 1979. A sign inversion mechanism for enzymatic supercoiling of DNA. *Science,* 206**,** 1081-3.
BURRIDGE, K. & WENNERBERG, K. 2004. Rho and rac take center stage. *Cell,* 116**,** 167-79.
CHANDRAPPA, R. & DAS, D. B. 2012. Waste quantities and characteristics. *In:* CHANDRAPPA, R. & DAS, D. B. (eds.) *Solid waste management.* Springer.
CHEN, G. Q., ZHANG, G., PARK, S. J. & LEE, S. Y. 2001. Industrial scale production of poly(3-hydroxybutyrate-co-3-hydroxyhexanoate). *Applied Microbiology and Biotechnology,* 57**,** 50-5.
CHEN, H., RICKLIN, D., HAMMEL, M., GARCIA, B. L., MCWHORTER, W. J., SFYROERA, G., WU, Y. Q., TZEKOU, A., LI, S., GEISBRECHT, B. V., WOODS, V. L., JR. & LAMBRIS, J. D. 2010. Allosteric inhibition of complement function by a staphylococcal immune evasion protein. *Proceedings of the National Academy of Sciences of the United States of America,* 107**,** 17621-6.
CHEN, H. J., BLOCH, K. J. & MACLEAN, J. A. 2000. Acute eosinophilic hepatitis from trovafloxacin. *New England Journal of Medicine,* 342**,** 359-60.
CHO, M., BRIGHAM, C. J., SINSKEY, A. J. & STUBBE, J. 2012. Purification of polyhydroxybutyrate synthase from its native organism, ralstonia eutropha: Implications for the initiation and elongation of polymer formation in vivo. *Biochemistry,* 51**,** 2276-2288.
CHOI, J. & LEE, S. Y. 1999. Efficient and economical recovery of poly(3-hydroxybutyrate) from recombinant escherichia coli by simple digestion with chemicals. *Biotechnology and Bioengineering,* 62**,** 546-53.
COHEN, S. P., MCMURRY, L. M. & LEVY, S. B. 1988. Mara locus causes decreased expression of ompf porin in multiple-antibiotic-resistant (mar) mutants of escherichia coli. *Journal of Bacteriology,* 170**,** 5416-22.
COMMISSION, E. 2012. *Packaging waste statistics - statistics explained* [Online]. Available: http://epp.eurostat.ec.europa.eu/statistics_explained/index.php/Packaging_waste_statistics# [Accessed 07/11/2012 2012].
COPELAND, R. A. 2005. *Evaluation of enzyme inhibitors in drug discovery : A guide for medicinal chemists and pharmacologists,* Hoboken, N.J. ; Chichester, John Wiley.
CORBETT, K. D., SHULTZABERGER, R. K. & BERGER, J. M. 2004. The c-terminal domain of DNA gyrase a adopts a DNA-bending beta-pinwheel fold. *Proceedings of the National Academy of Sciences of the United States of America,* 101**,** 7293-8.
CORSINI, A., MAGGI, F. M. & CATAPANO, A. L. 1995. Pharmacology of competitive inhibitors of hmg-coa reductase. *Pharmacology Research,* 31**,** 9-27.
COUTINHO, P. M. & REILLY, P. J. 1994. Structure-function relationships in the catalytic and starch binding domains of glucoamylase. *Protein Engineering,* 7**,** 393-400.
CRISBY, M., NORDIN-FREDRIKSSON, G., SHAH, P. K., YANO, J., ZHU, J. & NILSSON, J. 2001. Pravastatin treatment increases collagen content and decreases lipid content, inflammation, metalloproteinases, and cell death in human carotid plaques: Implications for plaque stabilization. *Circulation,* 103**,** 926-33.
DAVIES, M. J., RICHARDSON, P. D., WOOLF, N., KATZ, D. R. & MANN, J. 1993. Risk of thrombosis in human atherosclerotic plaques: Role of extracellular lipid, macrophage, and smooth muscle cell content. *British Heart Journal,* 69**,** 377-81.
DAVIS, H. R., ZHU, L. J., HOOS, L. M., TETZLOFF, G., MAGUIRE, M., LIU, J. J., YAO, X. R., IYER, S. P. N., LAM, M. H., LUND, E. G., DETMERS, P. A., GRAZIANO, M. P. & ALTMANN, S. W. 2004. Niemann-pick c1 like 1 (npc1l1) is the intestinal phytosterol and cholesterol transporter and a key modulator of whole-body cholesterol homeostasis. *Journal of Biological Chemistry,* 279**,** 33586-33592.

DEKENS-KONTER, J. A., KNOL, A., OLSSON, S., MEYBOOM, R. H. & DE KONING, G. H. 1994. [tendinitis of the achilles tendon caused by pefloxacin and other fluoroquinolone derivatives]. *Nederlands Tijdschrift voor Geneeskunde,* 138**,** 528-31.

DELLAVALLE, R., DRAKE, A., GRABER, M., HEILIG, L., HESTER, E., JOHNSON, L., MCNEALY, K. & SCHILLING, L. 2005. Statins and fibrates for preventing melanoma. *Cochrane Database of Systematic Reviews* [Online]. Available: http://onlinelibrary.wiley.com/doi/10.1002/14651858.CD003697.pub2/abstract.

DOI, Y., KAWAGUCHI, Y., NAKAMURA, Y. & KUNIOKA, M. 1989. Nuclear magnetic resonance studies of poly(3-hydroxybutyrate) and polyphosphate metabolism in alcaligenes eutrophus. *Applied and Environmental Microbiology,* 55**,** 2932-8.

DOMAGALA, J. M. 1994. Structure-activity and structure-side-effect relationships for the quinolone antibacterials. *Journal of Antimicrobial Chemotherapy,* 33**,** 685-706.

DOMAGALA, J. M., HAGEN, S. E., JOANNIDES, T., KIELY, J. S., LABORDE, E., SCHROEDER, M. C., SESNIE, J. A., SHAPIRO, M. A., SUTO, M. J. & VANDERROEST, S. 1993. Quinolone antibacterials containing the new 7-[3-(1-aminoethyl)-1- pyrrolidinyl] side chain: The effects of the 1-aminoethyl moiety and its stereochemical configurations on potency and in vivo efficacy. *Journal of Medicinal Chemistry,* 36**,** 871-82.

DOOLEY, K. A., MILLINDER, S. & OSBORNE, T. F. 1998. Sterol regulation of 3-hydroxy-3-methylglutaryl-coenzyme a synthase gene through a direct interaction between sterol regulatory element binding protein and the trimeric ccaat-binding factor/nuclear factor y. *Journal of Biological Chemistry,* 273**,** 1349-1356.

DRLICA, K., MALIK, M., KERNS, R. J. & ZHAO, X. 2008. Quinolone-mediated bacterial death. *Antimicrobial Agents and Chemotherapy,* 52**,** 385-92.

DRLICA, K., ZHAO, X., MALIK, M., SALZ, T. & KERNS, R. 2012. Fluoroquinolone resistance: Mechanisms, restrictive dosing, and anti-mutant screening strategies for new compounds. *In:* DOUGHERTY, T. J. & PUCCI, M. J. (eds.) *Antibiotic discovery and development.* New York: Springer.

ELSEA, S. H., MCGUIRK, P. R., GOOTZ, T. D., MOYNIHAN, M. & OSHEROFF, N. 1993. Drug features that contribute to the activity of quinolones against mammalian topoisomerase ii and cultured cells: Correlation between enhancement of enzyme-mediated DNA cleavage in vitro and cytotoxic potential. *Antimicrobial Agents and Chemotherapy,* 37**,** 2179-86.

ENARI, T. M. & NIKU-PAAVOLA, M. L. 1987. Enzymatic hydrolysis of cellulose: Is the current theory of the mechanisms of hydrolysis valid? *Critical Reviews in Biotechnology,* 5**,** 67-87.

ENDO, A. 1979. Monacolin k, a new hypocholesterolemic agent produced by a monascus species. *Journal of Antibiotics (Tokyo),* 32**,** 852-4.

ENDO, A. 1985. Compactin (ml-236b) and related compounds as potential cholesterol-lowering agents that inhibit hmg-coa reductase. *Journal of Medicinal Chemistry,* 28**,** 401-5.

ENDO, A. & KURODA, M. 1976. Citrinin, an inhibitor of cholesterol synthesis. *Journal of Antibiotics (Tokyo),* 29**,** 841-3.

ENDO, A., KURODA, M. & TANZAWA, K. 1976. Competitive inhibition of 3-hydroxy-3-methylglutaryl coenzyme a reductase by ml-236a and ml-236b fungal metabolites, having hypocholesterolemic activity. *FEBS Letters,* 72**,** 323-6.

ERIKSSON, T., KARLSSON, J. & TJERNELD, F. 2002. A model explaining declining rate in hydrolysis of lignocellulose substrates with cellobiohydrolase i (cel7a) and endoglucanase i (cel7b) of trichoderma reesei. *Applied Biochemistry and Biotechnology,* 101**,** 41-60.

FASS, D., BOGDEN, C. E. & BERGER, J. M. 1999. Quaternary changes in topoisomerase ii may direct orthogonal movement of two DNA strands. *Nature Structural Biology,* 6**,** 322-6.

FIELDS, R. D. & LANCASTER, M. V. 1993. Dual-attribute continuous monitoring of cell proliferation/cytotoxicity. *Am Biotechnol Lab,* 11**,** 48-50.

FIERER, N., JACKSON, J. A., VILGALYS, R. & JACKSON, R. B. 2005. Assessment of soil microbial community structure by use of taxon-specific quantitative pcr assays. *Appl Environ Microbiol,* 71**,** 4117-20.
FOLEY, D., BAILEY, P., PIERI, M. & MEREDITH, D. 2009. Targeting ketone drugs towards transport by the intestinal peptide transporter, pept1. *Organic and Biomolecular Chemistry,* 7**,** 1064-7.
FOUNDATION, B. H. 2011. *Statin prescriptions* [Online]. London. [Accessed 16th September 2012].
FURBERG, C. D. & PITT, B. 2001. Withdrawal of cerivastatin from the world market. *Current Controlled Trials in Cardiovascular Medicine,* 2**,** 205-207.
GELLERT, M., MIZUUCHI, K., O'DEA, M. H., ITOH, T. & TOMIZAWA, J. I. 1977. Nalidixic acid resistance: A second genetic character involved in DNA gyrase activity. *Proceedings of the National Academy of Sciences of the United States of America,* 74**,** 4772-6.
GERNGROSS, T. U., SNELL, K. D., PEOPLES, O. P., SINSKEY, A. J., CSUHAI, E., MASAMUNE, S. & STUBBE, J. 1994. Overexpression and purification of the soluble polyhydroxyalkanoate synthase from alcaligenes eutrophus: Evidence for a required posttranslational modification for catalytic activity. *Biochemistry,* 33**,** 9311-20.
GIL, G., FAUST, J. R., CHIN, D. J., GOLDSTEIN, J. L. & BROWN, M. S. 1985. Membrane-bound domain of hmg coa reductase is required for sterol-enhanced degradation of the enzyme. *Cell,* 41**,** 249-58.
GLOMSET, J. A. 1968. The plasma lecithins:Cholesterol acyltransferase reaction. *Journal of Lipid Research,* 9**,** 155-67.
GOLDSTEIN, J. L. & BROWN, M. S. 1990. Regulation of the mevalonate pathway. *Nature,* 343**,** 425-30.
GORDON, D. A., WETTERAU, J. R. & GREGG, R. E. 1995. Microsomal triglyceride transfer protein: A protein complex required for the assembly of lipoprotein particles. *Trends in Cell Biology,* 5**,** 317-21.
GROGAN, G. 2005. Emergent mechanistic diversity of enzyme-catalysed beta-diketone cleavage. *Biochemical Journal,* 388**,** 721-30.
GROUP, S. S. S. S. 1994. Randomised trial of cholesterol lowering in 4444 patients with coronary heart disease: The scandinavian simvastatin survival study (4s). *Lancet,* 344**,** 1383-9.
GROUP, W. B. 2012. *Poverty headcount ratio at $1.25 a day (ppp) (% of population)* [Online]. Available: http://data.worldbank.org/indicator/SI.POV.DDAY?order=wbapi_data_value_2011+wbapi_data_value+wbapi_data_value-last&sort=asc [Accessed 04/11/2012 2012].
GUTIERREZ-WING, M. T., STEVENS, B. E., THEEGALA, C. S., NEGULESCU, I. I. & RUSCH, K. A. 2010. Anaerobic biodegradation of polyhydroxybutyrate in municipal sewage sludge. *Journal of Environmental Engineering-Asce,* 136**,** 709-718.
HANE, M. W. & WOOD, T. H. 1969. Escherichia coli k-12 mutants resistant to nalidixic acid: Genetic mapping and dominance studies. *Journal of Bacteriology,* 99**,** 238-41.
HARDIE, D. G., HAWLEY, S. A. & SCOTT, J. W. 2006. Amp-activated protein kinase--development of the energy sensor concept. *Journal of Physiology,* 574**,** 7-15.
HARVEY, A. L. 2008. Natural products in drug discovery. *Drug Discovery Today,* 13**,** 894-901.
HEDDLE, J. G., MITELHEISER, S., MAXWELL, A. & THOMSON, N. H. 2004. Nucleotide binding to DNA gyrase causes loss of DNA wrap. *Journal of Molecular Biology,* 337**,** 597-610.
HEDERSTEDT, L. 2012. Heme a biosynthesis. *Biochimica et Biophysica Acta,* 1817**,** 920-7.
HEGDE, S. S., VETTING, M. W., RODERICK, S. L., MITCHENALL, L. A., MAXWELL, A., TAKIFF, H. E. & BLANCHARD, J. S. 2005. A fluoroquinolone resistance protein from mycobacterium tuberculosis that mimics DNA. *Science,* 308**,** 1480-3.
HEY, P. J., TWELLS, R. C., PHILLIPS, M. S., YUSUKE, N., BROWN, S. D., KAWAGUCHI, Y., COX, R., GUOCHUN, X., DUGAN, V., HAMMOND, H., METZKER, M. L., TODD, J. A. & HESS, J. F. 1998. Cloning of a novel member of the low-density lipoprotein receptor family. *Gene,* 216**,** 103-11.

HIRAKAWA, H., TAKUMI-KOBAYASHI, A., THEISEN, U., HIRATA, T., NISHINO, K. & YAMAGUCHI, A. 2008. Acrs/envr represses expression of the acrab multidrug efflux genes in escherichia coli. *Journal of Bacteriology,* 190**,** 6276-9.

HISANO, T., KASUYA, K., TEZUKA, Y., ISHII, N., KOBAYASHI, T., SHIRAKI, M., OROUDJEV, E., HANSMA, H., IWATA, T., DOI, Y., SAITO, T. & MIKI, K. 2006. The crystal structure of polyhydroxybutyrate depolymerase from penicillium funiculosum provides insights into the recognition and degradation of biopolyesters. *Journal of Molecular Biology,* 356**,** 993-1004.

HOLICK, M. F., FROMMER, J. E., MCNEILL, S. C., RICHTAND, N. M., HENLEY, J. W. & POTTS, J. T., JR. 1977. Photometabolism of 7-dehydrocholesterol to previtamin d3 in skin. *Biochemical and Biophysical Research Communications,* 76**,** 107-14.

HOLLAND, N., HOLLAND, D., HELENTJARIS, T., DHUGGA, K. S., XOCONOSTLE-CAZARES, B. & DELMER, D. P. 2000. A comparative analysis of the plant cellulose synthase (cesa) gene family. *Plant Physiology,* 123**,** 1313-24.

HON, D. N.-S. 1994. Cellulose: A random walk along its historical path. *Cellulose,* 1**,** 1-25.

IGARASHI, K., UCHIHASHI, T., KOIVULA, A., WADA, M., KIMURA, S., OKAMOTO, T., PENTTILA, M., ANDO, T. & SAMEJIMA, M. 2011. Traffic jams reduce hydrolytic efficiency of cellulase on cellulose surface. *Science,* 333**,** 1279-82.

INNERARITY, T. L., MAHLEY, R. W., WEISGRABER, K. H., BERSOT, T. P., KRAUSS, R. M., VEGA, G. L., GRUNDY, S. M., FRIEDL, W., DAVIGNON, J. & MCCARTHY, B. J. 1990. Familial defective apolipoprotein b-100: A mutation of apolipoprotein b that causes hypercholesterolemia. *Journal of Lipid Research,* 31**,** 1337-49.

ISTVAN, E. S. 2002. Structural mechanism for statin inhibition of 3-hydroxy-3-methylglutaryl coenzyme a reductase. *American Heart Journal,* 144**,** S27-32.

ISTVAN, E. S. & DEISENHOFER, J. 2000. The structure of the catalytic portion of human hmg-coa reductase. *Biochimica et Biophysica Acta,* 1529**,** 9-18.

ISTVAN, E. S. & DEISENHOFER, J. 2001. Structural mechanism for statin inhibition of hmg-coa reductase. *Science,* 292**,** 1160-4.

ISTVAN, E. S., PALNITKAR, M., BUCHANAN, S. K. & DEISENHOFER, J. 2000. Crystal structure of the catalytic portion of human hmg-coa reductase: Insights into regulation of activity and catalysis. *EMBO Journal,* 19**,** 819-30.

JACOBY, G. A. & HOOPER, D. C. 2012. Review of the quinolone family. *In:* DOUGHERTY, T. J. & PUCCI, M. J. (eds.) *Antibiotic discovery and development.* New York: Springer.

JAEGER, K. E., DIJKSTRA, B. W. & REETZ, M. T. 1999. Bacterial biocatalysts: Molecular biology, three-dimensional structures, and biotechnological applications of lipases. *Annual Review of Microbiology,* 53**,** 315-51.

JAMES, B. W., MAUCHLINE, W. S., DENNIS, P. J., KEEVIL, C. W. & WAIT, R. 1999. Poly-3-hydroxybutyrate in legionella pneumophila, an energy source for survival in low-nutrient environments. *Applied and Environmental Microbiology,* 65**,** 822-7.

JANSSENS, V. & GORIS, J. 2001. Protein phosphatase 2a: A highly regulated family of serine/threonine phosphatases implicated in cell growth and signalling. *Biochemical Journal,* 353**,** 417-39.

JENDROSSEK, D. 2001. Transfer of [pseudomonas] lemoignei, a gram-negative rod with restricted catabolic capacity, to paucimonas gen. Nov. With one species, paucimonas lemoignei comb. Nov. *International Journal of Systematic and Evolutionary Microbiology,* 51**,** 905-8.

JENDROSSEK, D., KNOKE, I., HABIBIAN, R. B., STEINBUCHEL, A. & SCHLEGEL, H. G. 1993a. Degradation of poly(3-hydroxybutyrate), phb, by bacteria and purification of a novel phb depolymerase from *comamonas* sp. *Journal of Polymers and the Environment,* 1**,** 53-63.

JENDROSSEK, D., MULLER, B. & SCHLEGEL, H. G. 1993b. Cloning and characterization of the poly(hydroxyalkanoic acid)-depolymerase gene locus, phaz1, of pseudomonas lemoignei and its gene product. *European Journal of Biochemistry,* 218**,** 701-10.

KANE, J. P. & MALLOY, M. J. 2012. Prebeta-1 hdl and coronary heart disease. *Current Opinion in Lipidology,* 23**,** 367-71.

KANEMATSU, E., DEGUCHI, T., YASUDA, M., KAWAMURA, T., NISHINO, Y. & KAWADA, Y. 1998. Alterations in the gyra subunit of DNA gyrase and the parc subunit of DNA topoisomerase iv associated with quinolone resistance in enterococcus faecalis. *Antimicrobial Agents and Chemotherapy,* 42**,** 433-5.

KAPRITCHKOFF, F. M., VIOTTI, A. P., ALLI, R. C., ZUCCOLO, M., PRADELLA, J. G., MAIORANO, A. E., MIRANDA, E. A. & BONOMI, A. 2006. Enzymatic recovery and purification of polyhydroxybutyrate produced by ralstonia eutropha. *Journal of Biotechnology,* 122**,** 453-62.

KAWAMUKAI, M. 2002. Biosynthesis, bioproduction and novel roles of ubiquinone. *Journal of Bioscience and Bioengineering,* 94**,** 511-7.

KELLER, G. A., PAZIRANDEH, M. & KRISANS, S. 1986. 3-hydroxy-3-methylglutaryl coenzyme a reductase localization in rat liver peroxisomes and microsomes of control and cholestyramine-treated animals: Quantitative biochemical and immunoelectron microscopical analyses. *Journal of Cell Biology,* 103**,** 875-86.

KELLNER-WEIBEL, G., YANCEY, P. G., JEROME, W. G., WALSER, T., MASON, R. P., PHILLIPS, M. C. & ROTHBLAT, G. H. 1999. Crystallization of free cholesterol in model macrophage foam cells. *Arteriosclerosis, Thrombosis and Vascular Biology,* 19**,** 1891-8.

KIKKAWA, Y., ABE, H., IWATA, T., INOUE, Y. & DOI, Y. 2002. Crystallization, stability, and enzymatic degradation of poly(l-lactide) thin film. *Biomacromolecules,* 3**,** 350-6.

KIM, M. N., LEE, A. R., YOON, J. S. & CHIN, I. J. 2000. Biodegradation of poly(3-hydroxybutyrate), sky-green (r) and mater-bi (r) by fungi isolated from soils. *European Polymer Journal,* 36**,** 1677-1685.

KIMURA, S., LAOSINCHAI, W., ITOH, T., CUI, X., LINDER, C. R. & BROWN, R. M., JR. 1999. Immunogold labeling of rosette terminal cellulose-synthesizing complexes in the vascular plant vigna angularis. *Plant Cell,* 11**,** 2075-86.

KLYOSOV, A. A. 1990. Trends in biochemistry and enzymology of cellulose degradation. *Biochemistry,* 29**,** 10577-85.

KONDO, H., SAKAMOTO, F., KAWAKAMI, K. & TSUKAMOTO, G. 1988. Studies on prodrugs. 7. Synthesis and antimicrobial activity of 3-formylquinolone derivatives. *Journal of Medicinal Chemistry,* 31**,** 221-5.

KOSTOVA, Z., TSAI, Y. C. & WEISSMAN, A. M. 2007. Ubiquitin ligases, critical mediators of endoplasmic reticulum-associated degradation. *Seminars in Cell and Developmental Biology,* 18**,** 770-9.

KOYAMA, M., HELBERT, W., IMAI, T., SUGIYAMA, J. & HENRISSAT, B. 1997. Parallel-up structure evidences the molecular directionality during biosynthesis of bacterial cellulose. *Proceedings of the National Academy of Sciences of the United States of America,* 94**,** 9091-5.

KRIENGKAUYKIAT, J., PORTER, E., LOMOVSKAYA, O. & WONG-BERINGER, A. 2005. Use of an efflux pump inhibitor to determine the prevalence of efflux pump-mediated fluoroquinolone resistance and multidrug resistance in pseudomonas aeruginosa. *Antimicrobial Agents and Chemotherapy,* 49**,** 565-70.

KUBO, M., KANO, Y., NAKAMURA, H., NAGATA, A. & IMAMOTO, F. 1979. In vivo enhancement of general and specific transcription in escherichia coli by DNA gyrase activity. *Gene,* 7**,** 153-71.

KUGA, S., TAKAGI, S. & BROWN JR, R. M. 1993. Native folded-chain cellulose ii. *Polymer,* 34**,** 3293-3297.

KUMARASWAMI, M., SCHUMAN, J. T., SEO, S. M., KAATZ, G. W. & BRENNAN, R. G. 2009. Structural and biochemical characterization of mepr, a multidrug binding transcription regulator of the staphylococcus aureus multidrug efflux pump mepa. *Nucleic Acids Research,* 37**,** 1211-24.

LAPONOGOV, I., PAN, X. S., VESELKOV, D. A., MCAULEY, K. E., FISHER, L. M. & SANDERSON, M. R. 2010. Structural basis of gate-DNA breakage and resealing by type ii topoisomerases. *Plos One,* 5**,** e11338.

LAPONOGOV, I., SOHI, M. K., VESELKOV, D. A., PAN, X. S., SAWHNEY, R., THOMPSON, A. W., MCAULEY, K. E., FISHER, L. M. & SANDERSON, M. R. 2009. Structural insight into the quinolone-DNA cleavage complex of type iia topoisomerases. *Nature Structural and Molecular Biology,* 16**,** 667-9.

LAUTENBACH, E., LAROSA, L. A., KASBEKAR, N., PENG, H. P., MANIGLIA, R. J. & FISHMAN, N. O. 2003. Fluoroquinolone utilization in the emergency departments of academic medical centers: Prevalence of, and risk factors for, inappropriate use. *Archives of Internal Medicine,* 163**,** 601-5.

LAW, M. & RUDNICKA, A. R. 2006. Statin safety: A systematic review. *American Journal of Cardiology,* 97**,** 52C-60C.

LEE, S. Y. 1994. Suppression of filamentation in recombinant escherichia-coli by amplified ftsz activity. *Biotechnology Letters,* 16**,** 1247-1252.

LEMOIGNE, M. 1926. Produits de deshydration et de polymerisation de l'acide beta-oxybutyrique. *Bulletin de la Societe de Chimie,* 8**,** 770-782.

LESHER, G. Y., FROELICH, E. J., GRUETT, M. D., BAILEY, J. H. & BRUNDAGE, R. P. 1962. 1,8-naphthyridine derivatives. A new class of chemotherapeutic agents. *Journal of Medicinal and Pharmaceutical Chemistry,* 91**,** 1063-5.

LEVINE, G. N., KEANEY, J. F., JR. & VITA, J. A. 1995. Cholesterol reduction in cardiovascular disease. Clinical benefits and possible mechanisms. *New England Journal of Medicine,* 332**,** 512-21.

LI, J. W. & VEDERAS, J. C. 2009. Drug discovery and natural products: End of an era or an endless frontier? *Science,* 325**,** 161-5.

LIADAKI, K. N., LIU, T., XU, S., ISHIDA, B. Y., DUCHATEAUX, P. N., KRIEGER, J. P., KANE, J., KRIEGER, M. & ZANNIS, V. I. 2000. Binding of high density lipoprotein (hdl) and discoidal reconstituted hdl to the hdl receptor scavenger receptor class b type i. Effect of lipid association and apoa-i mutations on receptor binding. *Journal of Biological Chemistry,* 275**,** 21262-71.

LIMA, C. D., WANG, J. C. & MONDRAGON, A. 1994. Three-dimensional structure of the 67k n-terminal fragment of e. Coli DNA topoisomerase i. *Nature,* 367**,** 138-46.

LINDSAY, D., JACKSON, P., HINDLEY, S. & BHAMRA, I. 2010. *Rosuvastatin and atorvastatin derivatives*. European Patent EP 2405910.

LOO, C. Y., LEE, W. H., TSUGE, T., DOI, Y. & SUDESH, K. 2005. Biosynthesis and characterization of poly(3-hydroxybutyrate-co-3- hydroxyhexanoate) from palm oil products in a wautersia eutropha mutant. *Biotechnology Letters,* 27**,** 1405-10.

LU, D. R., XIAO, C. M. & XU, S. J. 2009. Starch-based completely biodegradable polymer materials. *Polymer Letters,* 3**,** 366-375.

LUND-KATZ, S., LIU, L., THUAHNAI, S. T. & PHILLIPS, M. C. 2003. High density lipoprotein structure. *Frontiers in Bioscience,* 8**,** d1044-54.

LUO, S. & NETRAVALI, A. N. 2003. A study of physical and mechanical properties of poly(hydroxybutyrate-co-hydroxyvalerate) during composting. *Polymer Degradation and Stability,* 80**,** 59-66.

LYND, L. R., WYMAN, C. E. & GERNGROSS, T. U. 1999. Biocommodity engineering. *Biotechnology Progress,* 15**,** 777-793.

MANDAL, C. C., GHOSH-CHOUDHURY, N., YONEDA, T. & CHOUDHURY, G. G. 2011. Simvastatin prevents skeletal metastasis of breast cancer by an antagonistic interplay between p53 and cd44. *Journal of Biological Chemistry,* 286**,** 11314-27.

MARRER, E., SCHAD, K., SATOH, A. T., PAGE, M. G., JOHNSON, M. M. & PIDDOCK, L. J. 2006. Involvement of the putative atp-dependent efflux proteins pata and patb in fluoroquinolone resistance of a

multidrug-resistant mutant of streptococcus pneumoniae. *Antimicrobial Agents and Chemotherapy,* 50**,** 685-93.
MASTERS, J. J., LINK, J. T., SNYDER, L. B., YOUNG, W. B. & DANISHEFSKY, S. J. 1995. A total synthesis of taxol. *Angewandte Chemie International Edition in English,* 34**,** 1723-1726.
MCGUINNESS, B., O'HARE, J., CRAIG, D., BULLOCK, R., MALOUF, R. & PASSMORE, P. 2010. Statins for the treatment of dementia. *Cochrane Database of Systematic Reviews* [Online]. Available: http://onlinelibrary.wiley.com/doi/10.1002/14651858.CD007514.pub2/abstract.
MCKINNON, I. R., FALL, L., PARODY-MORREALE, A. & GILL, S. J. 1984. A twin titration microcalorimeter for the study of biochemical reactions. *Analytical Biochemistry,* 139**,** 134-9.
MCTAGGART, F., BUCKETT, L., DAVIDSON, R., HOLDGATE, G., MCCORMICK, A., SCHNECK, D., SMITH, G. & WARWICK, M. 2001. Preclinical and clinical pharmacology of rosuvastatin, a new 3-hydroxy-3-methylglutaryl coenzyme a reductase inhibitor. *American Journal of Cardiology,* 87**,** 28B-32B.
MEDVE, J., KARLSSON, J., LEE, D. & TJERNELD, F. 1998. Hydrolysis of microcrystalline cellulose by cellobiohydrolase i and endoglucanase ii from trichoderma reesei: Adsorption, sugar production pattern, and synergism of the enzymes. *Biotechnology and Bioengineering,* 59**,** 621-34.
MENSINK, R. P., ZOCK, P. L., KESTER, A. D. M. & KATAN, M. B. 2003. Effects of dietary fatty acids and carbohydrates on the ratio of serum total to hdl cholesterol and on serum lipids and apolipoproteins. *The American Journal of Clinical Nutrition,* 77**,** 1146-1155.
MICHEA-HAMZEHPOUR, M., FURET, Y. X. & PECHERE, J. C. 1991. Role of protein d2 and lipopolysaccharide in diffusion of quinolones through the outer membrane of pseudomonas aeruginosa. *Antimicrobial Agents and Chemotherapy,* 35**,** 2091-7.
MIKOV, M. & FAWCETT, J. P. 2006. Chemistry, biosynthesis, analysis, chemical & metabolic transformations and pharmacology. *European Journal of Drug Metabolism and Pharmacokinetics,* 31**,** 133-4.
MILLER, V. P., STRESSER, D. M., BLANCHARD, A. P., TURNER, S. & CRESPI, C. L. 2000. Fluorometric high-throughput screening for inhibitors of cytochrome p450. *Annals of the New York Academy of Sciences,* 919**,** 26-32.
MORAIS CABRAL, J. H., JACKSON, A. P., SMITH, C. V., SHIKOTRA, N., MAXWELL, A. & LIDDINGTON, R. C. 1997. Crystal structure of the breakage-reunion domain of DNA gyrase. *Nature,* 388**,** 903-6.
MOSIER, N., WYMAN, C., DALE, B., ELANDER, R., LEE, Y. Y., HOLTZAPPLE, M. & LADISCH, M. 2005. Features of promising technologies for pretreatment of lignocellulosic biomass. *Bioresource Technology,* 96**,** 673-86.
MUMTAZ, T., KHAN, M. R. & HASSAN, M. A. 2010. Study of environmental biodegradation of ldpe films in soil using optical and scanning electron microscopy. *Micron,* 41**,** 430-8.
MURRAY, C. J. & LOPEZ, A. D. 1997. Mortality by cause for eight regions of the world: Global burden of disease study. *Lancet,* 349**,** 1269-76.
MURRAY, C. J., RICHARDS, M. A., NEWTON, J. N., FENTON, K. A., ANDERSON, H. R., ATKINSON, C., BENNETT, D., BERNABE, E., BLENCOWE, H., BOURNE, R., BRAITHWAITE, T., BRAYNE, C., BRUCE, N. G., BRUGHA, T. S., BURNEY, P., DHERANI, M., DOLK, H., EDMOND, K., EZZATI, M., FLAXMAN, A. D., FLEMING, T. D., FREEDMAN, G., GUNNELL, D., HAY, R. J., HUTCHINGS, S. J., OHNO, S. L., LOZANO, R., LYONS, R. A., MARCENES, W., NAGHAVI, M., NEWTON, C. R., PEARCE, N., POPE, D., RUSHTON, L., SALOMON, J. A., SHIBUYA, K., VOS, T., WANG, H., WILLIAMS, H. C., WOOLF, A. D., LOPEZ, A. D. & DAVIS, A. 2013. Uk health performance: Findings of the global burden of disease study 2010. *Lancet,* 381**,** 997-1020.
MURRAY, N., PALIN, R., LINDSAY, D. & CRAIGHEAD, M. 2012. *Antibacterial drug derivatives*. WO2013072703 (A1).
NAVAB, M., BERLINER, J. A., WATSON, A. D., HAMA, S. Y., TERRITO, M. C., LUSIS, A. J., SHIH, D. M., VAN LENTEN, B. J., FRANK, J. S., DEMER, L. L., EDWARDS, P. A. & FOGELMAN, A. M. 1996. The yin and

yang of oxidation in the development of the fatty streak. A review based on the 1994 george lyman duff memorial lecture. *Arteriosclerosis, Thrombosis and Vascular Biology,* 16**,** 831-42.
NHS 2012. Prescription cost analysis england 2011. *In:* NHS (ed.). Health and Social Care Information Centre.
NICOLL-GRIFFITH, D. A., FALGUEYRET, J. P., SILVA, J. M., MORIN, P. E., TRIMBLE, L., CHAN, C. C., CLAS, S., LEGER, S., WANG, Z., YERGEY, J. A. & RIENDEAU, D. 1999. Oxidative bioactivation of the lactol prodrug of a lactone cyclooxygenase-2 inhibitor. *Drug Metabolism and Disposition,* 27**,** 403-9.
NODA, I. 1997. *Solvent extraction of polyhydroxyalkanoates from biomass*. WO number 97/07230 patent application.
NOHTURFFT, A., BROWN, M. S. & GOLDSTEIN, J. L. 1998. Topology of srebp cleavage-activating protein, a polytopic membrane protein with a sterol-sensing domain. *Journal of Biological Chemistry,* 273**,** 17243-50.
NONATO, R. V., MANTELATTO, P. E. & ROSSELL, C. E. 2001. Integrated production of biodegradable plastic, sugar and ethanol. *Applied Microbiology and Biotechnology,* 57**,** 1-5.
NORRBY, S. R. 1991. Side-effects of quinolones: Comparisons between quinolones and other antibiotics. *European Journal of Clinical Microbiology and Infectious Disease,* 10**,** 378-83.
OMKUMAR, R. V., DARNAY, B. G. & RODWELL, V. W. 1994. Modulation of syrian hamster 3-hydroxy-3-methylglutaryl-coa reductase activity by phosphorylation. Role of serine 871. *Journal of Biological Chemistry,* 269**,** 6810-4.
ORPHANIDES, G. & MAXWELL, A. 1994. Evidence for a conformational change in the DNA gyrase-DNA complex from hydroxyl radical footprinting. *Nucleic Acids Research,* 22**,** 1567-75.
PADGET, J. C., YEATES, T. & HINDE, D. C. 2002. *Soluble sachet for water based compositions*. European Patent EP0942875.
PANKEY, G. A. & ASHCRAFT, D. S. 2005. In vitro synergy of ciprofloxacin and gatifloxacin against ciprofloxacin-resistant pseudomonas aeruginosa. *Antimicrobial Agents and Chemotherapy,* 49**,** 2959-64.
PARIENTI, J. J., CATTOIR, V., THIBON, P., LEBOUVIER, G., VERDON, R., DAUBIN, C., DU CHEYRON, D., LECLERCQ, R. & CHARBONNEAU, P. 2011. Hospital-wide modification of fluoroquinolone policy and meticillin-resistant staphylococcus aureus rates: A 10-year interrupted time-series analysis. *Journal of Hospital Infection,* 78**,** 118-22.
PARK-WYLLIE, L. Y., JUURLINK, D. N., KOPP, A., SHAH, B. R., STUKEL, T. A., STUMPO, C., DRESSER, L., LOW, D. E. & MAMDANI, M. M. 2006. Outpatient gatifloxacin therapy and dysglycemia in older adults. *New England Journal of Medicine,* 354**,** 1352-61.
PEAR, J. R., KAWAGOE, Y., SCHRECKENGOST, W. E., DELMER, D. P. & STALKER, D. M. 1996. Higher plants contain homologs of the bacterial cela genes encoding the catalytic subunit of cellulose synthase. *Proceedings of the National Academy of Sciences of the United States of America,* 93**,** 12637-42.
PENG, H. & MARIANS, K. J. 1993. Decatenation activity of topoisomerase iv during oric and pbr322 DNA replication in vitro. *Proceedings of the National Academy of Sciences of the United States of America,* 90**,** 8571-5.
PERSSON, B. C., ESBERG, B., OLAFSSON, O. & BJORK, G. R. 1994. Synthesis and function of isopentenyl adenosine derivatives in trna. *Biochimie,* 76**,** 1152-60.
POIRIER, Y., DENNIS, D. E., KLOMPARENS, K. & SOMERVILLE, C. 1992. Polyhydroxybutyrate, a biodegradable thermoplastic, produced in transgenic plants. *Science,* 256**,** 520-523.
PRESS, A. 2011. Lipitor becomes world's top-selling drug. *Crain's New York Business*.
RACKER, E. 1955. [83] liver aldehyde dehydrogenase. *Methods in Enzymology,* 1**,** 514-517.
RADER, D. J., COHEN, J. & HOBBS, H. H. 2003. Monogenic hypercholesterolemia: New insights in pathogenesis and treatment. *Journal of Clinical Investigation,* 111**,** 1795-803.

RAI, R., KSHAVARZ, T., ROETHER, J., BOCCACCINI, A. R. & ROY, I. 2011. Medium chain length polyhydroxyalkanoates, promising new biomedical materials for the future. *Materials Science and Engineering: R: reports,* 72**,** 29-47.

RANBY, B. G. 1952. The mercerisation of cellulose. *Acta Chemica Scandinavica,* 6**,** 116-127.

REIS, R. L. & CUNHA, A. M. 2001. Starch and starch based thermoplastics. *In:* BUSCHOW, K. H. J. (ed.) *Encyclopedia of materials : Science and technology.* Amsterdam ; London: Elsevier.

RIDKER, P. M. 2003. Rosuvastatin in the primary prevention of cardiovascular disease among patients with low levels of low-density lipoprotein cholesterol and elevated high-sensitivity c-reactive protein: Rationale and design of the jupiter trial. *Circulation,* 108**,** 2292-7.

RISLEY, J. M. 2002. Cholesterol biosynthesis: Lanosterol to cholesterol. *Journal of Chemical Education,* 79**,** 377-384.

ROBICSEK, A., JACOBY, G. A. & HOOPER, D. C. 2006. The worldwide emergence of plasmid-mediated quinolone resistance. *Lancet Infectious Disease,* 6**,** 629-40.

ROCA, J. & WANG, J. C. 1994. DNA transport by a type ii DNA topoisomerase: Evidence in favor of a two-gate mechanism. *Cell,* 77**,** 609-16.

RODRIGUEZ-VALERA, F. & LILLO, J. A. G. 1992. Halobacteria as producers of polyhydroxyalkanoates. *Fems Microbiology Letters,* 103**,** 181-186.

ROITELMAN, J., OLENDER, E. H., BAR-NUN, S., DUNN, W. A., JR. & SIMONI, R. D. 1992. Immunological evidence for eight spans in the membrane domain of 3-hydroxy-3-methylglutaryl coenzyme a reductase: Implications for enzyme degradation in the endoplasmic reticulum. *Journal of Cell Biology,* 117**,** 959-73.

ROTHMAN, J. E. & ORCI, L. 1992. Molecular dissection of the secretory pathway. *Nature,* 355**,** 409-15.

RUDNIK, E. & BRIASSOULIS, D. 2011. Comparative biodegradation in soil behaviour of two biodegradable polymers based on renewable resources. *Journal of Polymers and the Environment,* 19**,** 18-39.

SAITO, T., SUZUKI, K., YAMAMOTO, J., FUKUI, T., MIWA, K., TOMITA, K., NAKANISHI, S., ODANI, S., SUZUKI, J. & ISHIKAWA, K. 1989. Cloning, nucleotide sequence, and expression in escherichia coli of the gene for poly(3-hydroxybutyrate) depolymerase from alcaligenes faecalis. *Journal of Bacteriology,* 171**,** 184-9.

SAKAI, J., NOHTURFFT, A., CHENG, D., HO, Y. K., BROWN, M. S. & GOLDSTEIN, J. L. 1997. Identification of complexes between the cooh-terminal domains of sterol regulatory element-binding proteins (srebps) and srebp cleavage-activating protein. *Journal of Biological Chemistry,* 272**,** 20213-21.

SALVI, A., CARRUPT, P. A., MAYER, J. M. & TESTA, B. 1997. Esterase-like activity of human serum albumin toward prodrug esters of nicotinic acid. *Drug Metabolism and Disposition,* 25**,** 395-8.

SANCHEZ, J. P., DOMAGALA, J. M., HAGEN, S. E., HEIFETZ, C. L., HUTT, M. P., NICHOLS, J. B. & TREHAN, A. K. 1988. Quinolone antibacterial agents. Synthesis and structure-activity relationships of 8-substituted quinoline-3-carboxylic acids and 1,8-naphthyridine-3-carboxylic acids. *Journal of Medicinal Chemistry,* 31**,** 983-91.

SATHASIVAM, S. & LECKY, B. 2008. Statin induced myopathy. *British Medical Journal,* 337**,** a2286.

SEABRA, M. C. 1998. Membrane association and targeting of prenylated ras-like gtpases. *Cell Signaling,* 10**,** 167-72.

SEVER, N., SONG, B. L., YABE, D., GOLDSTEIN, J. L., BROWN, M. S. & DEBOSE-BOYD, R. A. 2003a. Insig-dependent ubiquitination and degradation of mammalian 3-hydroxy-3-methylglutaryl-coa reductase stimulated by sterols and geranylgeraniol. *Journal of Biological Chemistry,* 278**,** 52479-90.

SEVER, N., YANG, T., BROWN, M. S., GOLDSTEIN, J. L. & DEBOSE-BOYD, R. A. 2003b. Accelerated degradation of hmg coa reductase mediated by binding of insig-1 to its sterol-sensing domain. *Molecular and Cellular Biology,* 11**,** 25-33.

SHEPHERD, J., HUNNINGHAKE, D. B., BARTER, P., MCKENNEY, J. M. & HUTCHINSON, H. G. 2003. Guidelines for lowering lipids to reduce coronary artery disease risk: A comparison of rosuvastatin with atorvastatin, pravastatin, and simvastatin for achieving lipid-lowering goals. *American Journal of Cardiology,* 91**,** 11C-17C; discussion 17C-19C.

SONG, B. L., SEVER, N. & DEBOSE-BOYD, R. A. 2005. Gp78, a membrane-anchored ubiquitin ligase, associates with insig-1 and couples sterol-regulated ubiquitination to degradation of hmg coa reductase. *Molecular and Cellular Biology,* 19**,** 829-40.

SPARKS, D. L., CONNOR, D. J., SABBAGH, M. N., PETERSEN, R. B., LOPEZ, J. & BROWNE, P. 2006. Circulating cholesterol levels, apolipoprotein e genotype and dementia severity influence the benefit of atorvastatin treatment in alzheimer's disease: Results of the alzheimer's disease cholesterol-lowering treatment (adclt) trial. *Acta Neurologica Scandinavica Supplementum,* 185**,** 3-7.

STEIN, O. & STEIN, Y. 1999. Atheroprotective mechanisms of hdl. *Atherosclerosis,* 144**,** 285-301.

STEINBUCHEL, A., AERTS, K., BABEL, W., FOLLNER, C., LIEBERGESELL, M., MADKOUR, M. H., MAYER, F., PIEPER-FURST, U., PRIES, A., VALENTIN, H. E. & ET AL. 1995. Considerations on the structure and biochemistry of bacterial polyhydroxyalkanoic acid inclusions. *Canadian Journal of Microbiology,* 41 Suppl 1**,** 94-105.

SUDESH, K. & ABE, H. 2010. *Practical guide to microbial polyhydroxyalkanoates,* Shawbury, iSmithers.

SUDHOF, T. C., RUSSELL, D. W., BROWN, M. S. & GOLDSTEIN, J. L. 1987. 42 bp element from ldl receptor gene confers end-product repression by sterols when inserted into viral tk promoter. *Cell,* 48**,** 1061-9.

SUN, L. P., LI, L., GOLDSTEIN, J. L. & BROWN, M. S. 2005. Insig required for sterol-mediated inhibition of scap/srebp binding to copii proteins in vitro. *Journal of Biological Chemistry,* 280**,** 26483-90.

SURIYAMONGKOL, P., WESELAKE, R., NARINE, S., MOLONEY, M. & SHAH, S. 2007. Biotechnological approaches for the production of polyhydroxyalkanoates in microorganisms and plants - a review. *Biotechnology Advances,* 25**,** 148-175.

SWIEZEWSKA, E. & DANIKIEWICZ, W. 2005. Polyisoprenoids: Structure, biosynthesis and function. *Progress in Lipid Research,* 44**,** 235-58.

TABERNERO, L., BOCHAR, D. A., RODWELL, V. W. & STAUFFACHER, C. V. 1999. Substrate-induced closure of the flap domain in the ternary complex structures provides insights into the mechanism of catalysis by 3-hydroxy-3-methylglutaryl-coa reductase. *Proceedings of the National Academy of Sciences of the United States of America,* 96**,** 7167-71.

TAGUCHI, S., YAMADA, M., MATSUMOTO, K., TAJIMA, K., SATOH, Y., MUNEKATA, M., OHNO, K., KOHDA, K., SHIMAMURA, T., KAMBE, H. & OBATA, S. 2008. A microbial factory for lactate-based polyesters using a lactate-polymerizing enzyme. *Proceedings of the National Academy of Sciences of the United States of America,* 105**,** 17323-7.

TAKAYAMA, S., HIROHASHI, M., KATO, M. & SHIMADA, H. 1995. Toxicity of quinolone antimicrobial agents. *Journal of Toxicology and Environmental Health,* 45**,** 1-45.

TAYLOR, F., WARD, K., MOORE, T. H. M., BURKE, M., DAVEY SMITH, G., CASAS, J. P. & EBRAHIM, S. 2011. Statins for the primary prevention of cardiovascular disease. *Cochrane Database of Systematic Reviews* [Online], Issue 1.

TEERI, T. T., KOIVULA, A., LINDER, M., WOHLFAHRT, G., DIVNE, C. & JONES, T. A. 1998. Trichoderma reesei cellobiohydrolases: Why so efficient on crystalline cellulose? *Biochemical Society Transactions,* 26**,** 173-8.

THELEN, K. M., RENTSCH, K. M., GUTTECK, U., HEVERIN, M., OLIN, M., ANDERSSON, U., VON ECKARDSTEIN, A., BJORKHEM, I. & LUTJOHANN, D. 2006. Brain cholesterol synthesis in mice is affected by high dose of simvastatin but not of pravastatin. *J Pharmacol Exp Ther,* 316**,** 1146-52.

TODD, P. A. & GOA, K. L. 1990. Simvastatin. A review of its pharmacological properties and therapeutic potential in hypercholesterolaemia. *Drugs,* 40**,** 583-607.
TOMME, P., WARREN, R. A. & GILKES, N. R. 1995. Cellulose hydrolysis by bacteria and fungi. *Advances in Microbial Physiology,* 37**,** 1-81.
TRAN, J. H., JACOBY, G. A. & HOOPER, D. C. 2005a. Interaction of the plasmid-encoded quinolone resistance protein qnr with escherichia coli DNA gyrase. *Antimicrobial Agents and Chemotherapy,* 49**,** 118-25.
TRAN, J. H., JACOBY, G. A. & HOOPER, D. C. 2005b. Interaction of the plasmid-encoded quinolone resistance protein qnra with escherichia coli topoisomerase iv. *Antimicrobial Agents and Chemotherapy,* 49**,** 3050-2.
TRUONG-BOLDUC, Q. C., STRAHILEVITZ, J. & HOOPER, D. C. 2006. Norc, a new efflux pump regulated by mgra of staphylococcus aureus. *Antimicrobial Agents and Chemotherapy,* 50**,** 1104-7.
UCHINO, K., SAITO, T., GEBAUER, B. & JENDROSSEK, D. 2007. Isolated poly(3-hydroxybutyrate) (phb) granules are complex bacterial organelles catalyzing formation of phb from acetyl coenzyme a (coa) and degradation of phb to acetyl-coa. *Journal of Bacteriology,* 189**,** 8250-6.
ULLSPERGER, C. & COZZARELLI, N. R. 1996. Contrasting enzymatic activities of topoisomerase iv and DNA gyrase from escherichia coli. *Journal of Biological Chemistry,* 271**,** 31549-55.
UNILEVER. 2012a. *Affordable products* [Online]. Available: http://www.unilever.com/sustainable-living/betterlivelihoods/affordable/ [Accessed 04/11/2012 2012].
UNILEVER. 2012b. *Tackling sachet waste* [Online]. Available: http://www.unilever.com/sustainable-living/news/news/Tacklingsachetwaste.aspx [Accessed 04/11/2012 2012].
VANE, J. R. 1971. Inhibition of prostaglandin synthesis as a mechanism of action for aspirin-like drugs. *Nature New Biology,* 231**,** 232-5.
VAUGHAN, C. J., GOTTO, A. M., JR. & BASSON, C. T. 2000. The evolving role of statins in the management of atherosclerosis. *Journal of the American College of Cardiology,* 35**,** 1-10.
VERALL, A. P., BENING, P. S. & KUGLER, K. A. 2010. *Polyvinyl alcohol copolymer film for packaging liquid products and having improved shelf-life*. US Patent 2004008231.
VOLKMAN, B. F., LIPSON, D., WEMMER, D. E. & KERN, D. 2001. Two-state allosteric behavior in a single-domain signaling protein. *Science,* 291**,** 2429-33.
WANG, D. Q. H. 2007. Regulation of intestinal cholesterol absorption. *Annual Review of Physiology,* 69**,** 221-248.
WANG, D. Q. H., LAMMERT, F., COHEN, D. E., PAIGEN, B. & CAREY, M. C. 1999. Cholic acid aids absorption, biliary secretion, and phase transitions of cholesterol in murine cholelithogenesis. *American Journal of Physiology-Gastrointestinal and Liver Physiology,* 276**,** G751-G760.
WANG, F. L. & LEE, S. Y. 1997a. Poly(3-hydroxybutyrate) production with high productivity and high polymer content by a fed-batch culture of alcaligenes latus under nitrogen limitation. *Applied and Environmental Microbiology,* 63**,** 3703-3706.
WANG, F. L. & LEE, S. Y. 1997b. Production of poly(3-hydroxybutyrate) by fed-batch culture of filamentation-suppressed recombinant escherichia coli. *Applied and Environmental Microbiology,* 63**,** 4765-4769.
WANG, X., SATO, R., BROWN, M. S., HUA, X. & GOLDSTEIN, J. L. 1994. Srebp-1, a membrane-bound transcription factor released by sterol-regulated proteolysis. *Cell,* 77**,** 53-62.
WANG, X. & ZHAO, X. 2009. Contribution of oxidative damage to antimicrobial lethality. *Antimicrobial Agents and Chemotherapy,* 53**,** 1395-402.
WASSMANN, S., LAUFS, U., BAUMER, A. T., MULLER, K., KONKOL, C., SAUER, H., BOHM, M. & NICKENIG, G. 2001. Inhibition of geranylgeranylation reduces angiotensin ii-mediated free radical production in vascular smooth muscle cells: Involvement of angiotensin at1 receptor expression and rac1 gtpase. *Molecular Pharmacology,* 59**,** 646-54.

WENTLAND, M. P., LESHER, G. Y., REUMAN, M., GRUETT, M. D., SINGH, B., ALDOUS, S. C., DORFF, P. H., RAKE, J. B. & COUGHLIN, S. A. 1993. Mammalian topoisomerase ii inhibitory activity of 1-cyclopropyl-6,8- difluoro-1,4-dihydro-7-(2,6-dimethyl-4-pyridinyl)-4-oxo-3-quinolinecarb oxylic acid and related derivatives. *Journal of Medicinal Chemistry,* 36**,** 2801-9.

WHITE, A. A. 1995. Mapping and geographic display of data. *Statistics in Medicine,* 14**,** 697-9.

WILLIAMS, D. F. 1981. Enzymatic hydrolysis of polylactic acid. *Medical Engineering and Physics,* 10**,** 5-7.

WILLIAMS, N. L. & MAXWELL, A. 1999. Locking the DNA gate of DNA gyrase: Investigating the effects on DNA cleavage and atp hydrolysis. *Biochemistry,* 38**,** 14157-64.

WOLSING, M. & PRIEME, A. 2004. Observation of high seasonal variation in community structure of denitrifying bacteria in arable soil receiving artificial fertilizer and cattle manure by determining t-rflp of nir gene fragments. *Fems Microbiology Ecology,* 48**,** 261-71.

YABE, D., BROWN, M. S. & GOLDSTEIN, J. L. 2002. Insig-2, a second endoplasmic reticulum protein that binds scap and blocks export of sterol regulatory element-binding proteins. *Proceedings of the National Academy of Sciences of the United States of America,* 99**,** 12753-8.

YANG, B., WILLIES, D. M. & WYMAN, C. E. 2006. Changes in the enzymatic hydrolysis rate of avicel cellulose with conversion. *Biotechnology and Bioengineering,* 94**,** 1122-8.

YEAGLE, P. L. 1991. Modulation of membrane function by cholesterol. *Biochimie,* 73**,** 1303-10.

ZECHIEDRICH, E. L., KHODURSKY, A. B., BACHELLIER, S., SCHNEIDER, R., CHEN, D., LILLEY, D. M. & COZZARELLI, N. R. 2000. Roles of topoisomerases in maintaining steady-state DNA supercoiling in escherichia coli. *Journal of Biological Chemistry,* 275**,** 8103-13.

ZHOU, Q. & LIAO, J. K. 2009. Statins and cardiovascular diseases: From cholesterol lowering to pleiotropy. *Current Pharmaceutical Design,* 15**,** 467-78.

Appendix A

A. Raw Data and Plots for IC50 Calculations

	Initial Rate of Reaction / p.d.u.									
[Inhibitor] / nM	Assay 1	Assay 2	Assay 3	Assay 4	Assay 5	Assay 6	Assay 7	Assay 8	Mean	Error
0	0.047	0.046	0.041	0.043	0.043	0.042	0.042	0.045	0.044	0.001
1	0.044	0.042	0.035	0.033	0.044	0.044	0.034	0.040	0.039	0.002
2	0.032	0.030	0.036		0.038			0.036	0.034	0.001
5	0.030	0.029	0.029		0.028		0.030		0.029	0.000
10	0.018		0.022	0.023	0.017	0.016	0.023	0.020	0.020	0.001
15		0.026	0.015	0.002	0.021				0.016	0.005
20	0.020	0.011	0.025	0.011	0.008	0.004	0.013	0.019	0.014	0.002
30	0.010	0.008	0.017	0.012	0.013	0.021	0.016	0.009	0.013	0.002
40	0.007	0.009	0.015	0.015	0.012	0.012	0.012	0.009	0.012	0.001
50	0.015	0.019	0.013	0.011	0.014	0.015	0.008	0.007	0.013	0.001

Table A.1. The initial rate of conversion of HMG-CoA to mevalonate by HMG-CoA reductase in the presence of different concentrations of Atorvastatin.

Substrates HMG-CoA and NADPH both have a final concentration in the reaction of 200 µM and the HMG-CoA reductase concentration was 10 nM in all assays. All assays were biological repeats and errors are standard error of the mean. Initial rate of reaction is shown in procedure defined units as it is calculated from absorption measurements which have no units.

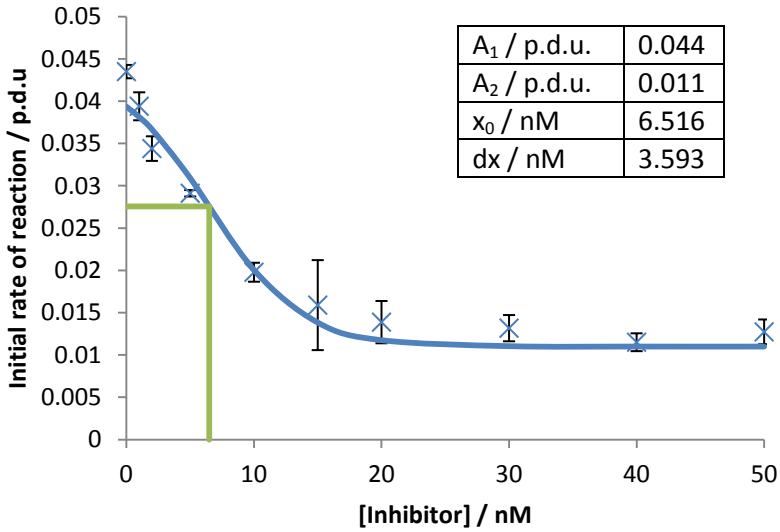

Figure A.1. The initial rate of conversion of HMG-CoA to mevalonate by HMG-CoA reductase in the presence of different concentrations of Atorvastatin.

Data plotted are those shown in table A.1. The curve fitted is a Boltzmann function with the parameters shown, where A_1 is the initial rate of reaction at minimal inhibition, A_2 is the initial rate of reaction at maximal inhibition, x_0 is the IC50 and dx is the concentration range over which inhibition changes from minimal to maximal.

	Initial Rate of Reaction / p.d.u.									
[Inhibitor] / nM	Assay 1	Assay 2	Assay 3	Assay 4	Assay 5	Assay 6	Assay 7	Assay 8	Mean	Error
0	0.047	0.046	0.041	0.043	0.043	0.042	0.042	0.045	0.044	0.001
1	0.021	0.051	0.054	0.042	0.032				0.040	0.006
2	0.041	0.024	0.032						0.032	0.005
5	0.021	0.021	0.034		0.019				0.024	0.003
10	0.016	0.011		0.011					0.013	0.002
15	0.000	0.016	0.010						0.009	0.005
20	0.005	0.007	0.008						0.007	0.001
30	0.000	0.016	0.009						0.008	0.005
40	0.004	0.007	0.009						0.007	0.001
50	0.009	0.004	0.008						0.007	0.002

Table A.2. The initial rate of conversion of HMG-CoA to mevalonate by HMG-CoA reductase in the presence of different concentrations of Rosuvastatin.

Substrates HMG-CoA and NADPH both have a final concentration in the reaction of 200 µM and the HMG-CoA reductase concentration was 10 nM in all assays. All assays were biological repeats and errors are standard error of the mean. Initial rate of reaction is shown in procedure defined units as it is calculated from absorption measurements which have no units.

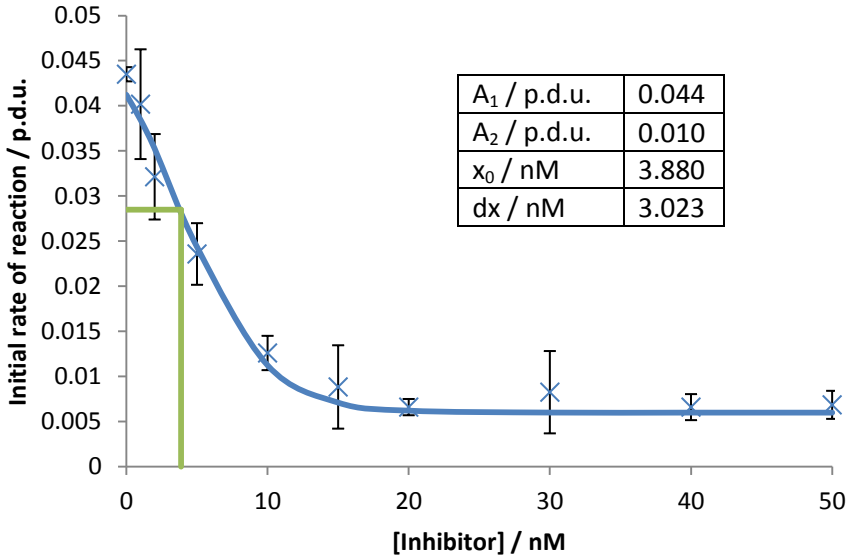

Figure A.2. The initial rate of conversion of HMG-CoA to mevalonate by HMG-CoA reductase in the presence of different concentrations of Rosuvastatin.

Data plotted are those shown in table A.2. The curve fitted is a Boltzmann function with the parameters shown, where A_1 is the initial rate of reaction at minimal inhibition, A_2 is the initial rate of reaction at maximal inhibition, x_0 is the IC50 and dx is the concentration range over which inhibition changes from minimal to maximal.

	Initial Rate of Reaction / p.d.u.									
[Inhibitor] / nM	Assay 1	Assay 2	Assay 3	Assay 4	Assay 5	Assay 6	Assay 7	Assay 8	Mean	Error
0	0.047	0.046	0.041	0.043	0.043	0.042	0.042	0.045	0.044	0.001
1	0.049	0.040	0.047						0.045	0.003
2	0.045	0.042	0.039						0.042	0.002
5	0.017	0.037	0.026						0.026	0.006
10	0.020	0.005	0.007						0.011	0.005
20	0.013	0.003	0.023						0.013	0.006
30	0.010	0.014	0.013						0.012	0.001
40	0.022	0.005	0.011						0.012	0.005
50	0.010	0.004	0.001						0.011	0.004

Table A.3. The initial rate of conversion of HMG-CoA to mevalonate by HMG-CoA reductase in the presence of different concentrations of atorvastatin lactone.

Substrates HMG-CoA and NADPH both have a final concentration in the reaction of 200 µM and the HMG-CoA reductase concentration was 10 nM in all assays. All assays were biological repeats and errors are standard error of the mean. Initial rate of reaction is shown in procedure defined units as it is calculated from absorption measurements which have no units.

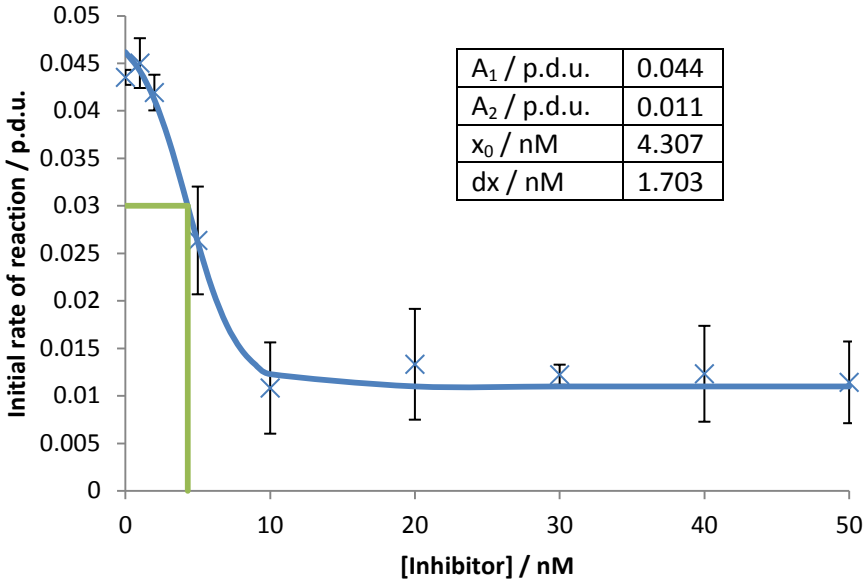

Figure A.3. The initial rate of conversion of HMG-CoA to mevalonate by HMG-CoA reductase in the presence of different concentrations of atorvastatin lactone.

Data plotted are those shown in table A.3. The curve fitted is a Boltzmann function with the parameters shown, where A_1 is the initial rate of reaction at minimal inhibition, A_2 is the initial rate of reaction at maximal inhibition, x_0 is the IC50 and dx is the concentration range over which inhibition changes from minimal to maximal.

	Initial Rate of Reaction / p.d.u.									
[Inhibitor] / nM	Assay 1	Assay 2	Assay 3	Assay 4	Assay 5	Assay 6	Assay 7	Assay 8	Mean	Error
0	0.047	0.046	0.041	0.043	0.043	0.042	0.042	0.045	0.044	0.001
1	0.025	0.037	0.038						0.033	0.004
2	0.032	0.032	0.025						0.029	0.002
5	0.025	0.014	0.021						0.020	0.003
10	0.023	0.016	0.020						0.019	0.002
20	0.011	0.008	0.014						0.011	0.002
30	0.004	0.012	0.006						0.007	0.002
40	0.005	0.008	0.014						0.009	0.003
50	0.008	0.008	0.005						0.007	0.001

Table A.4. The initial rate of conversion of HMG-CoA to mevalonate by HMG-CoA reductase in the presence of different concentrations of IB/13/1.

Substrates HMG-CoA and NADPH both have a final concentration in the reaction of 200 µM and the HMG-CoA reductase concentration was 10 nM in all assays. All assays were biological repeats and errors are standard error of the mean. Initial rate of reaction is shown in procedure defined units as it is calculated from absorption measurements which have no units.

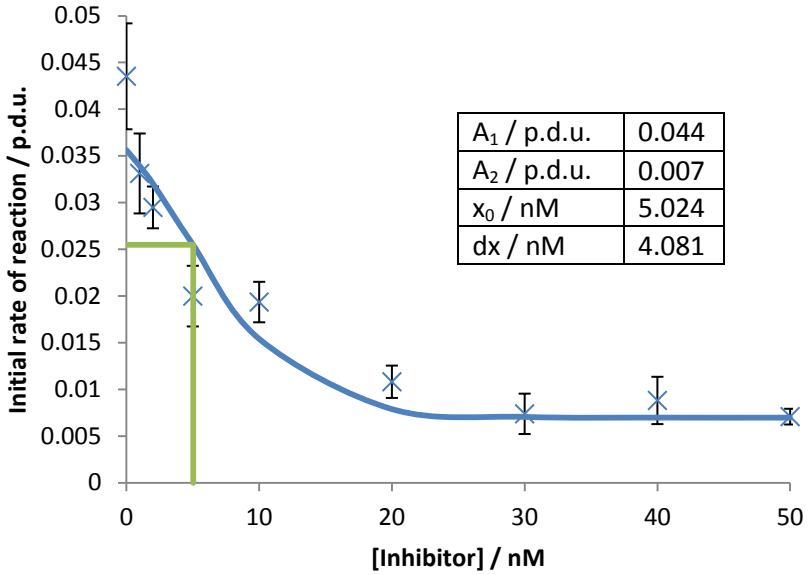

Figure A.4. The initial rate of conversion of HMG-CoA to mevalonate by HMG-CoA reductase in the presence of different concentrations of IB/13/1.

Data plotted are those shown in table A.4. The curve fitted is a Boltzmann function with the parameters shown, where A_1 is the initial rate of reaction at minimal inhibition, A_2 is the initial rate of reaction at maximal inhibition, x_0 is the IC50 and dx is the concentration range over which inhibition changes from minimal to maximal.

	Initial Rate of Reaction / p.d.u.									
[Inhibitor] / nM	Assay 1	Assay 2	Assay 3	Assay 4	Assay 5	Assay 6	Assay 7	Assay 8	Mean	Error
0	0.047	0.046	0.041	0.043	0.043	0.042	0.042	0.045	0.044	0.001
1	0.038	0.031	0.032	0.023	0.018	0.029	0.021	0.034	0.028	0.002
2	0.017	0.017	0.023	0.025	0.024	0.023	0.024	0.022	0.022	0.001
5	0.013			0.017	0.017	0.013	0.022	0.024	0.017	0.002
10	0.011	0.010	0.014	0.010	0.011	0.015	0.018	0.013	0.013	0.001
20	0.025	0.007	0.006	0.019	0.007	0.015	0.010	0.009	0.012	0.002
30	0.012	0.010	0.004	0.008	0.013	0.011	0.010	0.006	0.009	0.001
40	0.022	0.000	0.008	0.012	0.011	0.013	0.008	0.008	0.010	0.002
50	0.008	0.003	0.013	0.008	0.008	0.006	0.008	0.005	0.011	0.003

Table A.5. The initial rate of conversion of HMG-CoA to mevalonate by HMG-CoA reductase in the presence of different concentrations of IB/19/1.

Substrates HMG-CoA and NADPH both have a final concentration in the reaction of 200 µM and the HMG-CoA reductase concentration was 10 nM in all assays. All assays were biological repeats and errors are standard error of the mean. Initial rate of reaction is shown in procedure defined units as it is calculated from absorption measurements which have no units.

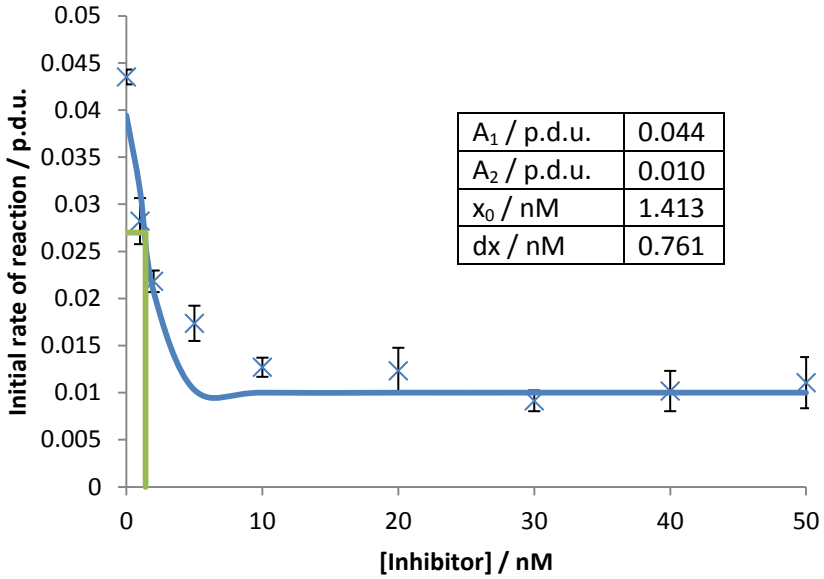

Figure A.5. The initial rate of conversion of HMG-CoA to mevalonate by HMG-CoA reductase in the presence of different concentrations of IB/19/1.

Data plotted are those shown in table A.5. The curve fitted is a Boltzmann function with the parameters shown, where A_1 is the initial rate of reaction at minimal inhibition, A_2 is the initial rate of reaction at maximal inhibition, x_0 is the IC50 and dx is the concentration range over which inhibition changes from minimal to maximal.

	Initial Rate of Reaction / p.d.u.									
[Inhibitor] / nM	Assay 1	Assay 2	Assay 3	Assay 4	Assay 5	Assay 6	Assay 7	Assay 8	Mean	Error
0	0.047	0.046	0.041	0.043	0.043	0.042	0.042	0.045	0.044	0.001
1	0.051	0.040	0.029						0.040	0.006
2	0.043	0.009	0.029						0.027	0.010
5	0.019	0.009	0.029						0.019	0.006
10	0.018	0.010	0.026						0.018	0.005
20	0.009	0.015	0.007						0.010	0.003
30	0.005	0.006	0.002						0.004	0.001
40	0.013	0.005	0.021						0.013	0.005
50	0.012	0.005	0.019						0.012	0.004

Table A.6. The initial rate of conversion of HMG-CoA to mevalonate by HMG-CoA reductase in the presence of different concentrations of IB/20/1.

Substrates HMG-CoA and NADPH both have a final concentration in the reaction of 200 µM and the HMG-CoA reductase concentration was 10 nM in all assays. All assays were biological repeats and errors are standard error of the mean. Initial rate of reaction is shown in procedure defined units as it is calculated from absorption measurements which have no units.

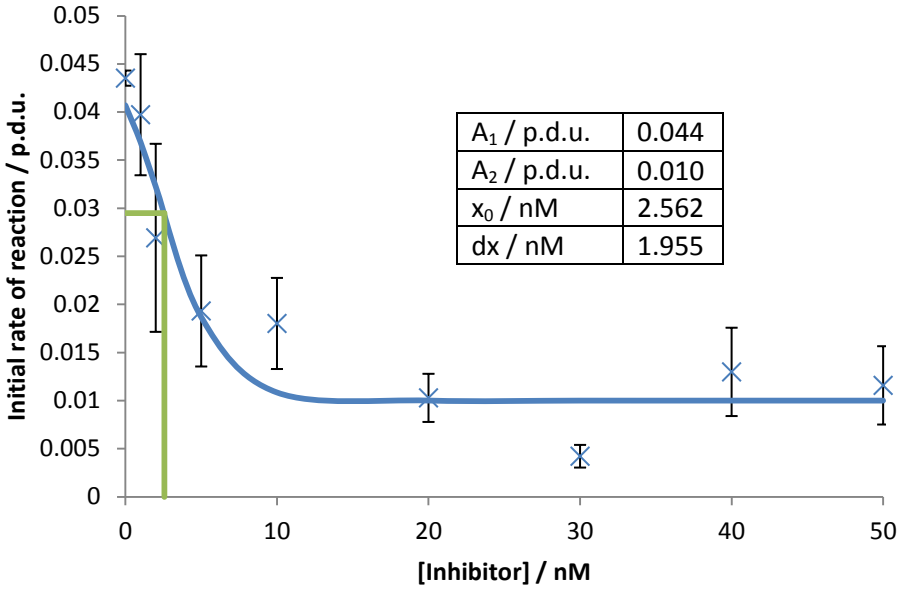

Figure A.6. The initial rate of conversion of HMG-CoA to mevalonate by HMG-CoA reductase in the presence of different concentrations of IB/20/1.

Data plotted are those shown in table A.6. The curve fitted is a Boltzmann function with the parameters shown, where A_1 is the initial rate of reaction at minimal inhibition, A_2 is the initial rate of reaction at maximal inhibition, x_0 is the IC50 and dx is the concentration range over which inhibition changes from minimal to maximal.

	Initial Rate of Reaction / p.d.u.									
[Inhibitor] / nM	Assay 1	Assay 2	Assay 3	Assay 4	Assay 5	Assay 6	Assay 7	Assay 8	Mean	Error
0	0.047	0.046	0.041	0.043	0.043	0.042	0.042	0.045	0.044	0.001
1	0.041	0.029	0.030	0.035	0.036	0.024	0.028	0.030	0.031	0.002
2	0.023	0.029	0.028	0.023	0.027	0.024	0.025	0.025	0.025	0.001
5	0.017	0.012	0.024	0.026	0.017	0.016	0.020	0.023	0.019	0.002
10	0.011	0.013	0.015	0.015	0.021		0.016	0.021	0.016	0.001
20	0.015	0.012	0.013	0.014	0.013	0.013	0.019	0.008	0.013	0.001
30	0.010	0.010	0.014	0.015	0.016	0.011	0.010	0.012	0.012	0.001
40	0.013	0.013	0.012	0.014	0.010	0.010	0.011	0.013	0.012	0.001
50	0.010	0.008	0.005	0.009	0.010	0.008	0.012	0.011	0.010	0.002

Table A.7. The initial rate of conversion of HMG-CoA to mevalonate by HMG-CoA reductase in the presence of different concentrations of IB/21/1.

Substrates HMG-CoA and NADPH both have a final concentration in the reaction of 200 µM and the HMG-CoA reductase concentration was 10 nM in all assays. All assays were biological repeats and errors are standard error of the mean. Initial rate of reaction is shown in procedure defined units as it is calculated from absorption measurements which have no units.

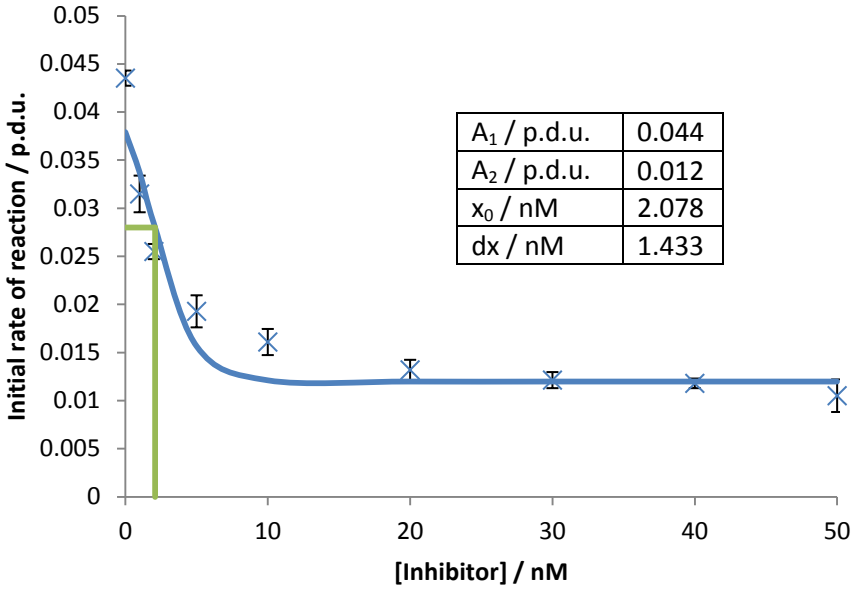

Figure A.7. The initial rate of conversion of HMG-CoA to mevalonate by HMG-CoA reductase in the presence of different concentrations of IB/21/1.

Data plotted are those shown in table A.7. The curve fitted is a Boltzmann function with the parameters shown, where A_1 is the initial rate of reaction at minimal inhibition, A_2 is the initial rate of reaction at maximal inhibition, x_0 is the IC50 and dx is the concentration range over which inhibition changes from minimal to maximal.

	Initial Rate of Reaction / p.d.u.									
[Inhibitor] / nM	Assay 1	Assay 2	Assay 3	Assay 4	Assay 5	Assay 6	Assay 7	Assay 8	Mean	Error
0	0.047	0.046	0.041	0.043	0.043	0.042	0.042	0.045	0.044	0.001
1	0.054	0.040	0.033						0.042	0.006
2	0.025	0.031	0.037						0.031	0.003
5	0.042	0.028	0.015						0.028	0.008
10	0.024	0.026	0.015						0.021	0.003
20	0.010	0.016	0.016						0.014	0.002
30	0.020	0.014	0.022						0.019	0.002
40	0.032	0.003	0.017						0.017	0.008
50	0.028	0.010	0.006						0.014	0.007

Table A.8. The initial rate of conversion of HMG-CoA to mevalonate by HMG-CoA reductase in the presence of different concentrations of IB/26/1.

Substrates HMG-CoA and NADPH both have a final concentration in the reaction of 200 µM and the HMG-CoA reductase concentration was 10 nM in all assays. All assays were biological repeats and errors are standard error of the mean. Initial rate of reaction is shown in procedure defined units as it is calculated from absorption measurements which have no units.

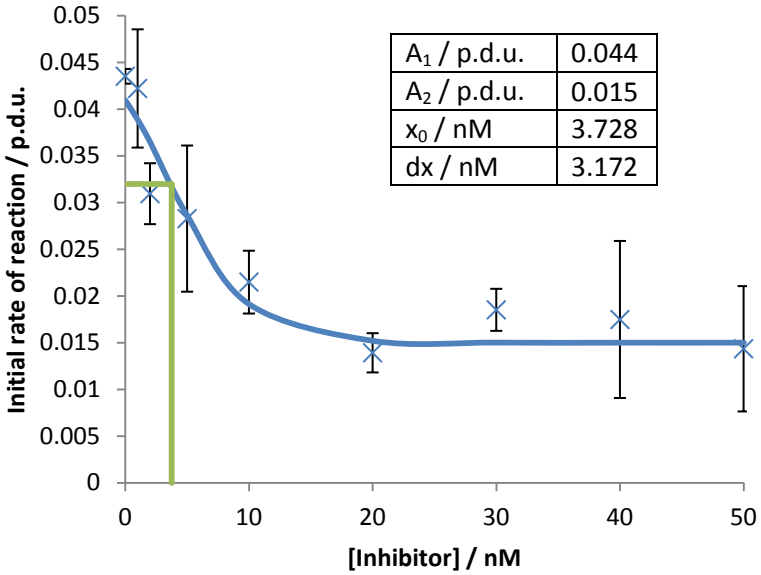

Figure A.8. The initial rate of conversion of HMG-CoA to mevalonate by HMG-CoA reductase in the presence of different concentrations of IB/26/1.

Data plotted are those shown in table A.8. The curve fitted is a Boltzmann function with the parameters shown, where A_1 is the initial rate of reaction at minimal inhibition, A_2 is the initial rate of reaction at maximal inhibition, x_0 is the IC50 and dx is the concentration range over which inhibition changes from minimal to maximal.

	Initial Rate of Reaction / p.d.u.									
[Inhibitor] / nM	Assay 1	Assay 2	Assay 3	Assay 4	Assay 5	Assay 6	Assay 7	Assay 8	Mean	Error
0	0.047	0.046	0.041	0.043	0.043	0.042	0.042	0.045	0.044	0.001
1				0.035	0.032	0.025	0.023		0.029	0.003
2	0.017	0.013	0.018	0.016	0.018	0.025	0.020	0.017	0.018	0.001
5	0.012				0.018	0.018	0.014	0.011	0.015	0.001
10	0.011		0.019	0.016		0.012		0.016	0.015	0.002
20	0.013	0.014	0.019	0.011	0.011	0.008	0.012	0.012	0.012	0.001
30	0.014	0.020	0.013	0.008	0.010	0.020	0.014	0.012	0.014	0.001
40	0.009	0.010	0.017	0.008	0.012	0.012	0.016	0.013	0.012	0.001
50	0.012	0.009	0.014	0.007	0.006	0.020	0.010	0.011	0.011	0.002

Table A.9. The initial rate of conversion of HMG-CoA to mevalonate by HMG-CoA reductase in the presence of different concentrations of IB/28/1.

Substrates HMG-CoA and NADPH both have a final concentration in the reaction of 200 µM and the HMG-CoA reductase concentration was 10 nM in all assays. All assays were biological repeats and errors are standard error of the mean. Initial rate of reaction is shown in procedure defined units as it is calculated from absorption measurements which have no units.

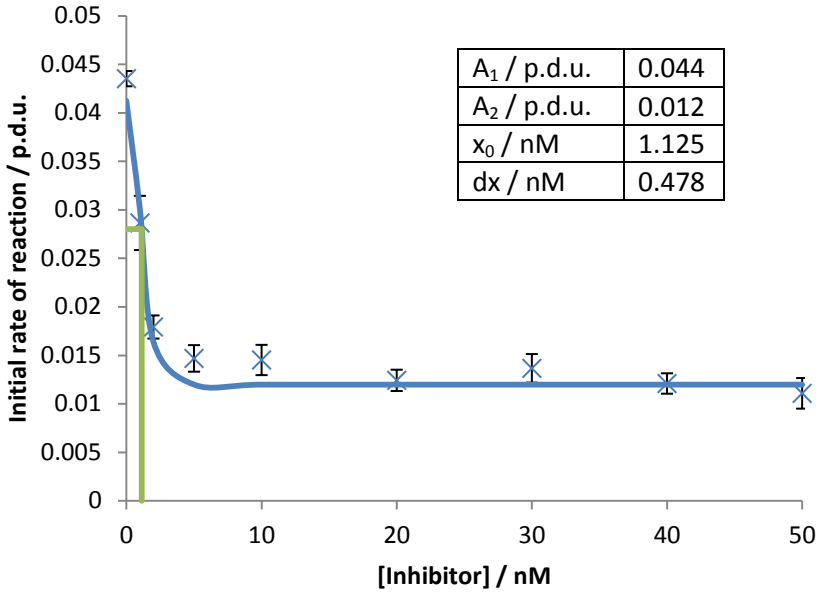

Figure A.9. The initial rate of conversion of HMG-CoA to mevalonate by HMG-CoA reductase in the presence of different concentrations of IB/28/1.

Data plotted are those shown in table A.9. The curve fitted is a Boltzmann function with the parameters shown, where A_1 is the initial rate of reaction at minimal inhibition, A_2 is the initial rate of reaction at maximal inhibition, x_0 is the IC50 and dx is the concentration range over which inhibition changes from minimal to maximal.

	Initial Rate of Reaction / p.d.u.									
[Inhibitor] / nM	Assay 1	Assay 2	Assay 3	Assay 4	Assay 5	Assay 6	Assay 7	Assay 8	Mean	Error
0	0.047	0.046	0.041	0.043	0.043	0.042	0.042	0.045	0.044	0.001
1	0.037	0.044	0.037	0.036	0.042	0.046	0.042	0.036	0.040	0.001
2	0.030	0.038	0.030	0.028	0.034	0.041	0.028	0.035	0.033	0.002
5	0.025	0.022	0.026	0.021	0.030	0.022	0.029	0.028	0.025	0.001
10	0.015	0.010	0.017	0.014	0.019	0.018	0.017	0.017	0.016	0.001
20	0.010	0.012	0.011	0.013	0.011	0.010	0.012	0.010	0.011	0.000
30	0.016	0.008	0.001	0.010	0.010	0.004		0.016	0.009	0.002
40	0.007	0.007	0.007	0.010	0.010	0.011	0.012	0.008	0.009	0.001
50	0.015	0.016	0.015	0.010	0.015	0.007	0.014	0.009	0.013	0.001

Table A.10. The initial rate of conversion of HMG-CoA to mevalonate by HMG-CoA reductase in the presence of different concentrations of IB/29/1.

Substrates HMG-CoA and NADPH both have a final concentration in the reaction of 200 µM and the HMG-CoA reductase concentration was 10 nM in all assays. All assays were biological repeats and errors are standard error of the mean. Initial rate of reaction is shown in procedure defined units as it is calculated from absorption measurements which have no units.

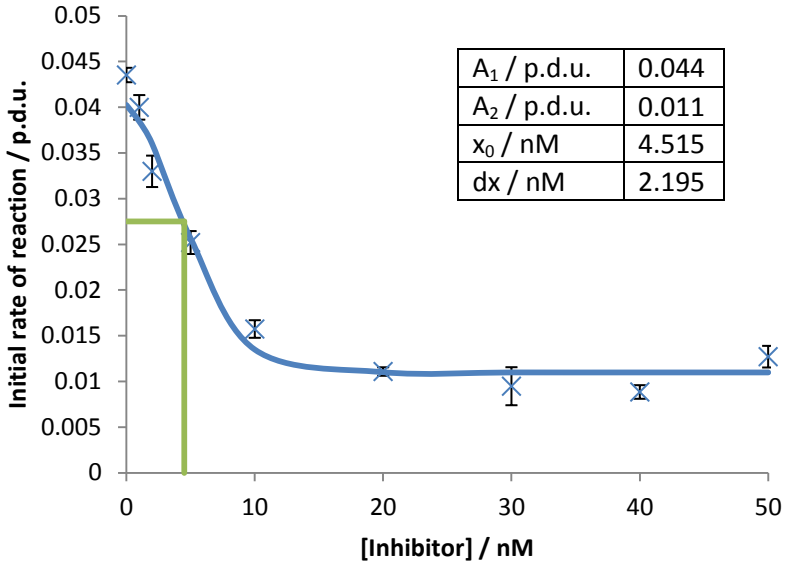

Figure A.10. The initial rate of conversion of HMG-CoA to mevalonate by HMG-CoA reductase in the presence of different concentrations of IB/29/1.

Data plotted are those shown in table A.10. The curve fitted is a Boltzmann function with the parameters shown, where A_1 is the initial rate of reaction at minimal inhibition, A_2 is the initial rate of reaction at maximal inhibition, x_0 is the IC50 and dx is the concentration range over which inhibition changes from minimal to maximal.

	Initial Rate of Reaction / p.d.u.									
[Inhibitor] / nM	Assay 1	Assay 2	Assay 3	Assay 4	Assay 5	Assay 6	Assay 7	Assay 8	Mean	Error
0	0.047	0.046	0.041	0.043	0.043	0.042	0.042	0.045	0.044	0.001
1	0.046	0.039	0.040						0.042	0.002
2	0.033	0.039	0.027						0.033	0.003
5	0.036	0.025	0.014						0.025	0.006
10	0.019	0.007	0.018						0.015	0.004
20	0.021	0.006	0.006						0.011	0.005
30	0.007	0.011	0.006						0.008	0.002
40	0.003	0.013	0.007						0.008	0.003
50	0.010	0.003	0.001						0.008	0.002

Table A.11. The initial rate of conversion of HMG-CoA to mevalonate by HMG-CoA reductase in the presence of different concentrations of IB/32/1.

Substrates HMG-CoA and NADPH both have a final concentration in the reaction of 200 µM and the HMG-CoA reductase concentration was 10 nM in all assays. All assays were biological repeats and errors are standard error of the mean. Initial rate of reaction is shown in procedure defined units as it is calculated from absorption measurements which have no units.

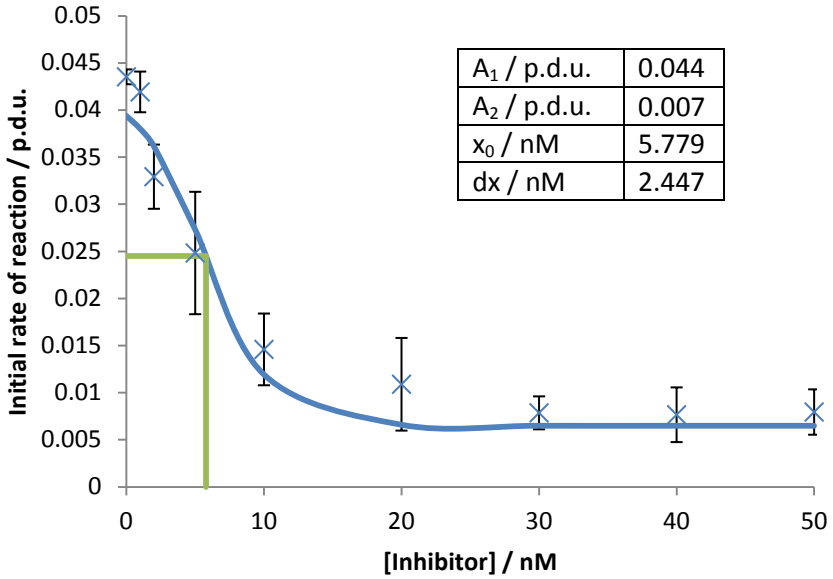

Figure A.11. The initial rate of conversion of HMG-CoA to mevalonate by HMG-CoA reductase in the presence of different concentrations of IB/32/1.

Data plotted are those shown in table A.11. The curve fitted is a Boltzmann function with the parameters shown, where A_1 is the initial rate of reaction at minimal inhibition, A_2 is the initial rate of reaction at maximal inhibition, x_0 is the IC50 and dx is the concentration range over which inhibition changes from minimal to maximal.

	Initial Rate of Reaction / p.d.u.									
[Inhibitor] / nM	Assay 1	Assay 2	Assay 3	Assay 4	Assay 5	Assay 6	Assay 7	Assay 8	Mean	Error
0	0.047	0.046	0.041	0.043	0.043	0.042	0.042	0.045	0.044	0.001
1	0.040	0.039	0.031	0.028	0.041	0.043	0.028	0.035	0.036	0.002
2	0.032	0.031	0.032	0.030	0.031	0.037	0.024	0.033	0.031	0.001
5	0.021	0.012	0.017	0.027	0.030	0.029	0.016	0.027	0.022	0.002
10	0.016	0.018	0.013	0.024	0.023	0.011	0.015	0.013	0.017	0.002
20	0.016	0.011	0.014	0.018	0.010	0.017	0.015	0.015	0.014	0.001
30	0.011		0.018	0.014	0.007	0.018	0.020		0.014	0.002
40	0.008	0.014	0.011	0.012	0.012	0.011	0.014	0.014	0.012	0.001
50			0.012		0.012	0.011	0.011	0.011	0.011	0.000

Table A.12. The initial rate of conversion of HMG-CoA to mevalonate by HMG-CoA reductase in the presence of different concentrations of IB/56/1.

Substrates HMG-CoA and NADPH both have a final concentration in the reaction of 200 µM and the HMG-CoA reductase concentration was 10 nM in all assays. All assays were biological repeats and errors are standard error of the mean. Initial rate of reaction is shown in procedure defined units as it is calculated from absorption measurements which have no units.

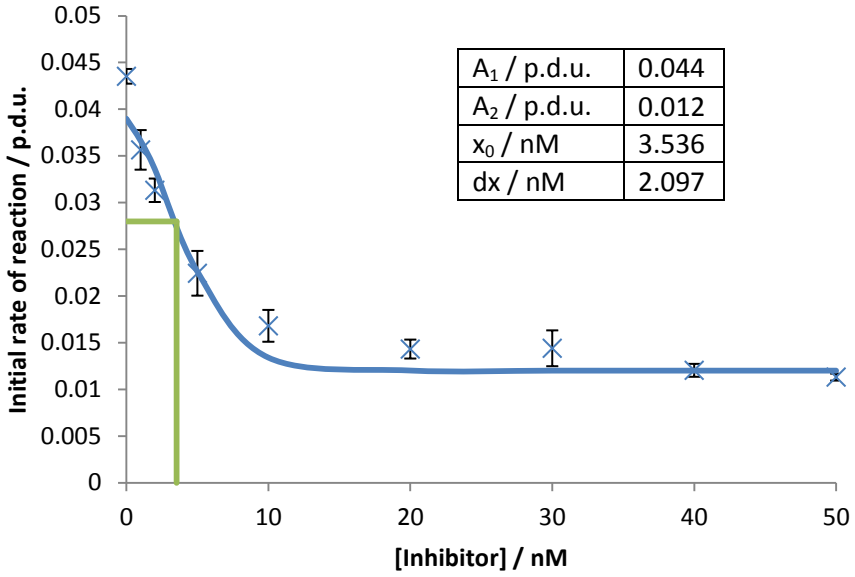

Figure A.12. The initial rate of conversion of HMG-CoA to mevalonate by HMG-CoA reductase in the presence of different concentrations of IB/56/1.

Data plotted are those shown in table A.12. The curve fitted is a Boltzmann function with the parameters shown, where A_1 is the initial rate of reaction at minimal inhibition, A_2 is the initial rate of reaction at maximal inhibition, x_0 is the IC50 and dx is the concentration range over which inhibition changes from minimal to maximal.

	Initial Rate of Reaction / p.d.u.									
[Inhibitor] / nM	Assay 1	Assay 2	Assay 3	Assay 4	Assay 5	Assay 6	Assay 7	Assay 8	Mean	Error
0	0.047	0.046	0.041	0.043	0.043	0.042	0.042	0.045	0.044	0.001
1	0.002	0.003	0.004						0.003	0.001
2	0.006	0.011	0.008						0.008	0.001
5	0.010	0.007	0.005						0.007	0.001
10	0.006	0.001	0.015						0.007	0.004
20	0.002	0.009	0.007						0.006	0.002
30	0.004	0.005	0.002						0.004	0.001
40	0.005	0.007	0.002						0.005	0.002
50	0.005	0.005	0.007						0.005	0.001

Table A.13. The initial rate of conversion of HMG-CoA to mevalonate by HMG-CoA reductase in the presence of different concentrations of IB/57/1.

Substrates HMG-CoA and NADPH both have a final concentration in the reaction of 200 µM and the HMG-CoA reductase concentration was 10 nM in all assays. All assays were biological repeats and errors are standard error of the mean. Initial rate of reaction is shown in procedure defined units as it is calculated from absorption measurements which have no units.

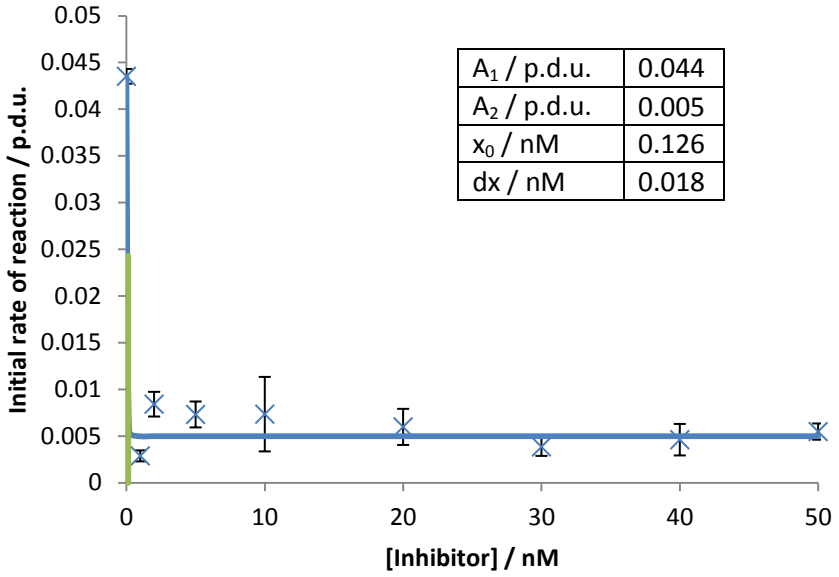

Figure A.13. The initial rate of conversion of HMG-CoA to mevalonate by HMG-CoA reductase in the presence of different concentrations of IB/57/1.

Data plotted are those shown in table A.13. The curve fitted is a Boltzmann function with the parameters shown, where A_1 is the initial rate of reaction at minimal inhibition, A_2 is the initial rate of reaction at maximal inhibition, x_0 is the IC50 and dx is the concentration range over which inhibition changes from minimal to maximal.

	Initial Rate of Reaction / p.d.u.									
[Inhibitor] / nM	Assay 1	Assay 2	Assay 3	Assay 4	Assay 5	Assay 6	Assay 7	Assay 8	Mean	Error
0	0.047	0.046	0.041	0.043	0.043	0.042	0.042	0.045	0.044	0.001
1	0.019	0.026	0.031	0.021		0.016	0.038	0.019	0.024	0.003
2	0.025	0.014	0.021	0.013	0.032	0.018	0.018	0.012	0.019	0.002
5		0.017	0.011		0.015	0.012	0.016	0.015	0.014	0.001
10	0.012	0.020		0.017	0.014	0.018	0.010	0.018	0.016	0.001
20	0.010	0.008	0.010	0.008	0.012	0.008	0.009	0.013	0.010	0.001
30	0.014	0.005	0.010	0.013	0.012	0.008	0.014	0.010	0.011	0.001
40	0.011	0.012	0.007	0.014	0.008	0.015	0.009	0.011	0.011	0.001
50	0.007	0.009	0.006	0.010	0.011	0.016	0.014	0.003	0.009	0.002

Table A.14. The initial rate of conversion of HMG-CoA to mevalonate by HMG-CoA reductase in the presence of different concentrations of IB/60/1.

Substrates HMG-CoA and NADPH both have a final concentration in the reaction of 200 µM and the HMG-CoA reductase concentration was 10 nM in all assays. All assays were biological repeats and errors are standard error of the mean. Initial rate of reaction is shown in procedure defined units as it is calculated from absorption measurements which have no units.

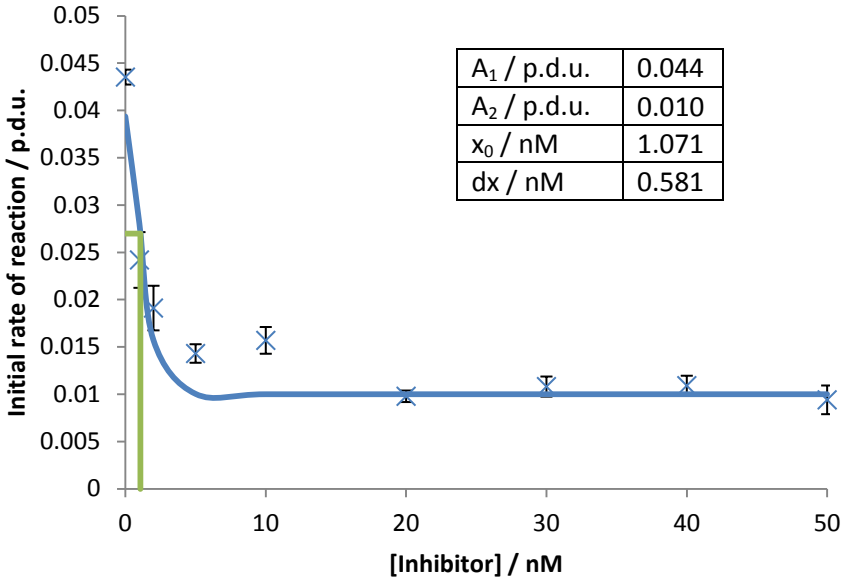

Figure A.14. The initial rate of conversion of HMG-CoA to mevalonate by HMG-CoA reductase in the presence of different concentrations of IB/60/1.

Data plotted are those shown in table A.14. The curve fitted is a Boltzmann function with the parameters shown, where A_1 is the initial rate of reaction at minimal inhibition, A_2 is the initial rate of reaction at maximal inhibition, x_0 is the IC50 and dx is the concentration range over which inhibition changes from minimal to maximal.

	Initial Rate of Reaction / p.d.u.									
[Inhibitor] / nM	Assay 1	Assay 2	Assay 3	Assay 4	Assay 5	Assay 6	Assay 7	Assay 8	Mean	Error
0	0.047	0.046	0.041	0.043	0.043	0.042	0.042	0.045	0.044	0.001
1	0.033	0.025	0.048						0.035	0.007
2	0.021	0.022	0.030						0.024	0.003
5	0.012	0.008	0.011						0.010	0.001
10	0.009	0.013	0.005						0.009	0.002
20	0.005	0.008	0.010						0.008	0.001
30	0.007	0.005	0.008						0.006	0.001
40	0.002	0.010	0.010						0.008	0.003
50	0.007	0.009	0.005						0.007	0.001

Table A.15. The initial rate of conversion of HMG-CoA to mevalonate by HMG-CoA reductase in the presence of different concentrations of IB/61/1.

Substrates HMG-CoA and NADPH both have a final concentration in the reaction of 200 µM and the HMG-CoA reductase concentration was 10 nM in all assays. All assays were biological repeats and errors are standard error of the mean. Initial rate of reaction is shown in procedure defined units as it is calculated from absorption measurements which have no units.

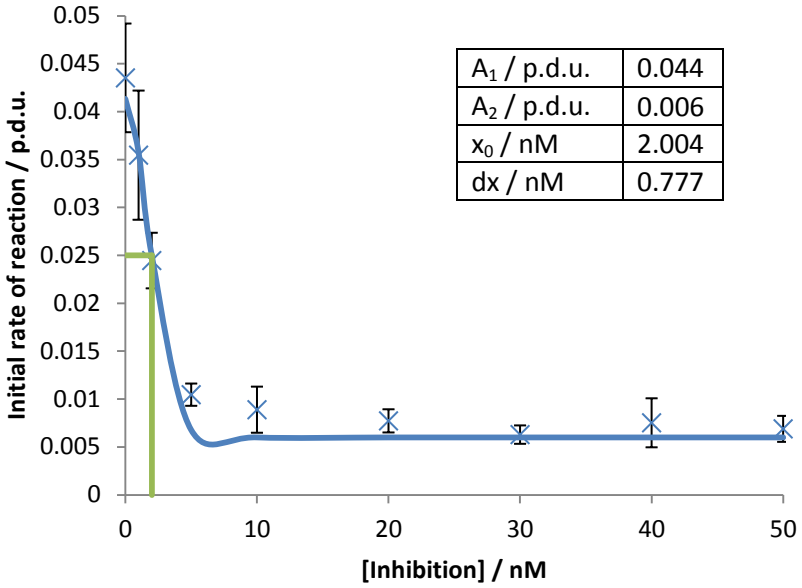

Figure A.15. The initial rate of conversion of HMG-CoA to mevalonate by HMG-CoA reductase in the presence of different concentrations of IB/61/1.

Data plotted are those shown in table A.15. The curve fitted is a Boltzmann function with the parameters shown, where A_1 is the initial rate of reaction at minimal inhibition, A_2 is the initial rate of reaction at maximal inhibition, x_0 is the IC50 and dx is the concentration range over which inhibition changes from minimal to maximal.

	Initial Rate of Reaction / p.d.u.									
[Inhibitor] / nM	Assay 1	Assay 2	Assay 3	Assay 4	Assay 5	Assay 6	Assay 7	Assay 8	Mean	Error
0	0.047	0.046	0.041	0.043	0.043	0.042	0.042	0.045	0.044	0.001
1	0.051	0.028	0.027						0.035	0.008
2	0.045	0.037	0.046						0.043	0.003
5	0.037	0.032	0.037						0.035	0.002
10	0.022	0.009	0.003						0.011	0.006
20	0.028	0.012	0.008						0.016	0.006
30	0.038	0.010	0.014						0.021	0.009
40	0.023	0.008	0.019						0.017	0.004
50	0.051	0.000	0.003						0.014	0.002

Table A.16. The initial rate of conversion of HMG-CoA to mevalonate by HMG-CoA reductase in the presence of different concentrations of IB/62/1.

Substrates HMG-CoA and NADPH both have a final concentration in the reaction of 200 µM and the HMG-CoA reductase concentration was 10 nM in all assays. All assays were biological repeats and errors are standard error of the mean. Initial rate of reaction is shown in procedure defined units as it is calculated from absorption measurements which have no units.

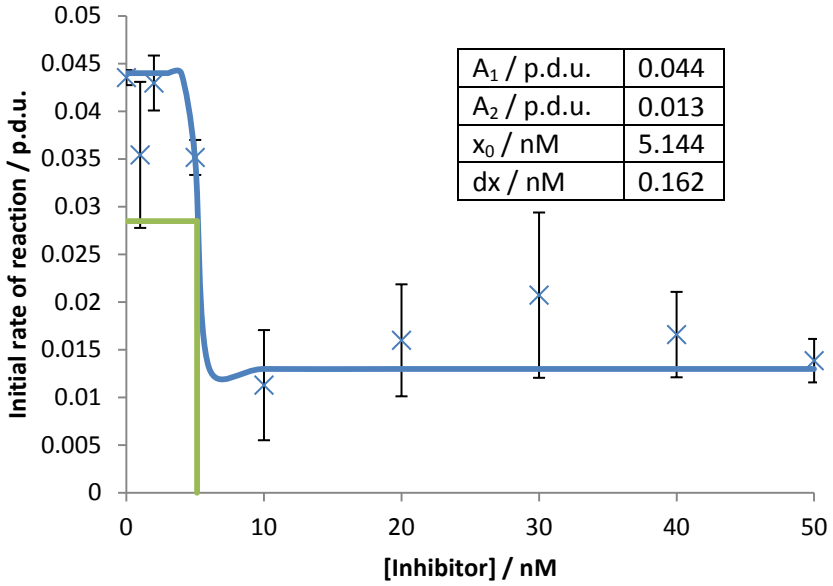

Figure A.16. The initial rate of conversion of HMG-CoA to mevalonate by HMG-CoA reductase in the presence of different concentrations of IB/62/1.

Data plotted are those shown in table A.16. The curve fitted is a Boltzmann function with the parameters shown, where A_1 is the initial rate of reaction at minimal inhibition, A_2 is the initial rate of reaction at maximal inhibition, x_0 is the IC50 and dx is the concentration range over which inhibition changes from minimal to maximal.

	Initial Rate of Reaction / p.d.u.									
[Inhibitor] / nM	Assay 1	Assay 2	Assay 3	Assay 4	Assay 5	Assay 6	Assay 7	Assay 8	Mean	Error
0	0.047	0.046	0.041	0.043	0.043	0.042	0.042	0.045	0.044	0.001
1	0.035	0.068	0.040						0.047	0.010
2	0.028	0.062	0.043						0.045	0.010
5	0.064	0.029	0.032						0.042	0.011
10	0.058	0.038	0.028						0.042	0.009
20	0.020	0.009	0.024						0.018	0.004
30	0.028	0.009	0.023						0.020	0.006
40	0.032	0.003	0.023						0.019	0.009
50	0.030	0.018	0.007						0.018	0.007

Table A.17. The initial rate of conversion of HMG-CoA to mevalonate by HMG-CoA reductase in the presence of different concentrations of IB/66/1.

Substrates HMG-CoA and NADPH both have a final concentration in the reaction of 200 µM and the HMG-CoA reductase concentration was 10 nM in all assays. All assays were biological repeats and errors are standard error of the mean. Initial rate of reaction is shown in procedure defined units as it is calculated from absorption measurements which have no units.

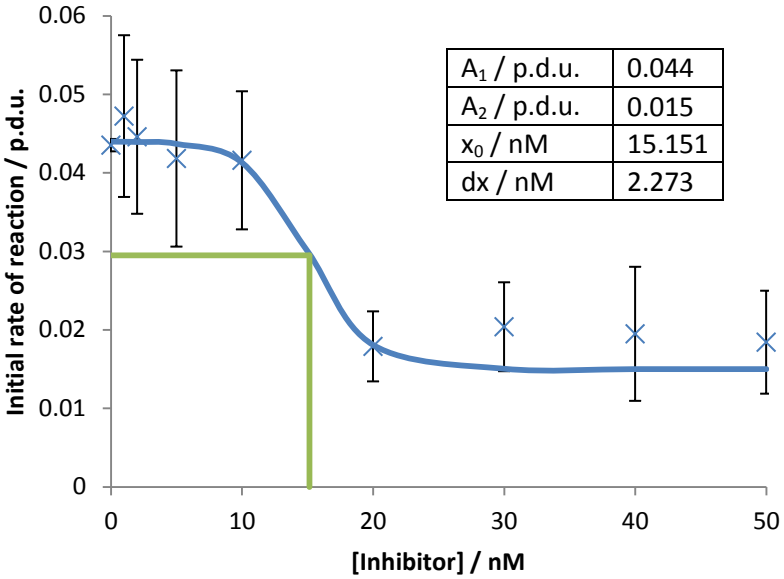

Figure A.17. The initial rate of conversion of HMG-CoA to mevalonate by HMG-CoA reductase in the presence of different concentrations of IB/66/1.

Data plotted are those shown in table A.17. The curve fitted is a Boltzmann function with the parameters shown, where A_1 is the initial rate of reaction at minimal inhibition, A_2 is the initial rate of reaction at maximal inhibition, x_0 is the IC50 and dx is the concentration range over which inhibition changes from minimal to maximal.

	Initial Rate of Reaction / p.d.u.									
[Inhibitor] / nM	Assay 1	Assay 2	Assay 3	Assay 4	Assay 5	Assay 6	Assay 7	Assay 8	Mean	Error
0	0.047	0.046	0.041	0.043	0.043	0.042	0.042	0.045	0.044	0.001
1	0.046	0.054	0.032						0.044	0.006
2	0.064	0.045	0.033						0.047	0.009
5	0.023	0.009	0.010						0.014	0.005
10	0.004	0.013	0.004						0.007	0.003
20	0.001	0.015	0.019						0.012	0.005
30	0.020	0.006	0.006						0.010	0.005
40	0.007	0.014	0.006						0.009	0.003
50	0.016	0.012	0.011						0.006	0.003

Table A.18. The initial rate of conversion of HMG-CoA to mevalonate by HMG-CoA reductase in the presence of different concentrations of IB/67/1.

Substrates HMG-CoA and NADPH both have a final concentration in the reaction of 200 µM and the HMG-CoA reductase concentration was 10 nM in all assays. All assays were biological repeats and errors are standard error of the mean. Initial rate of reaction is shown in procedure defined units as it is calculated from absorption measurements which have no units.

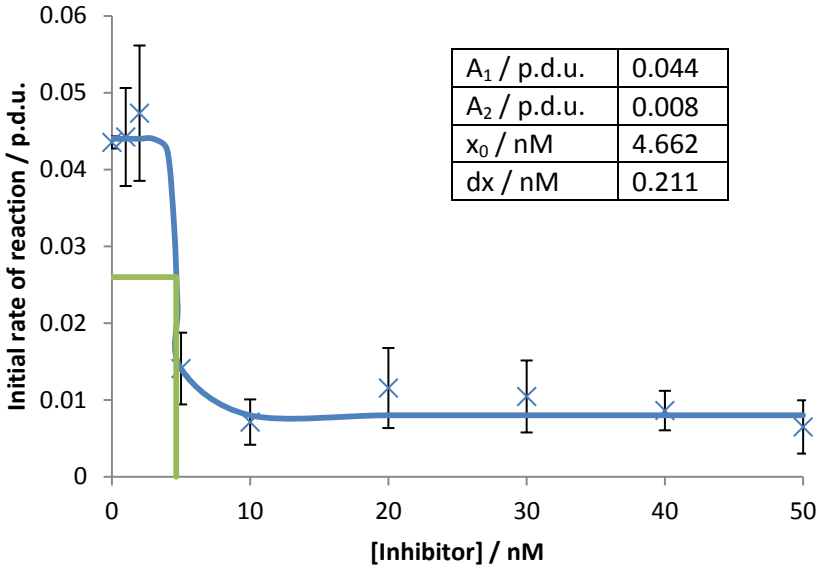

Figure A.18. The initial rate of conversion of HMG-CoA to mevalonate by HMG-CoA reductase in the presence of different concentrations of IB/67/1.

Data plotted are those shown in table A.18. The curve fitted is a Boltzmann function with the parameters shown, where A_1 is the initial rate of reaction at minimal inhibition, A_2 is the initial rate of reaction at maximal inhibition, x_0 is the IC50 and dx is the concentration range over which inhibition changes from minimal to maximal.

	Initial Rate of Reaction / p.d.u.									
[Inhibitor] / nM	Assay 1	Assay 2	Assay 3	Assay 4	Assay 5	Assay 6	Assay 7	Assay 8	Mean	Error
0	0.047	0.046	0.041	0.043	0.043	0.042	0.042	0.045	0.044	0.001
1	0.039	0.043	0.044						0.042	0.002
2	0.037	0.021	0.056	0.038					0.038	0.007
5	0.016	0.029	0.020	0.033					0.024	0.004
10	0.018	0.015	0.016						0.016	0.001
20	0.019	0.010	0.026						0.018	0.005
30	0.022	0.018	0.007						0.015	0.005
40	0.008	0.014	0.022						0.015	0.004
50	0.024	0.027	0.025						0.025	0.001

Table A.19. The initial rate of conversion of HMG-CoA to mevalonate by HMG-CoA reductase in the presence of different concentrations of IB/83/1/4.

Substrates HMG-CoA and NADPH both have a final concentration in the reaction of 200 µM and the HMG-CoA reductase concentration was 10 nM in all assays. All assays were biological repeats and errors are standard error of the mean. Initial rate of reaction is shown in procedure defined units as it is calculated from absorption measurements which have no units.

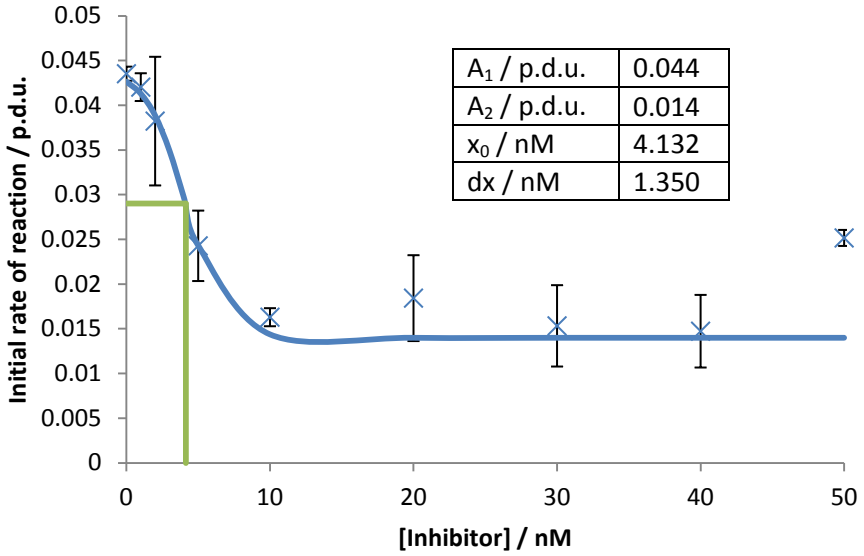

Figure A.19. The initial rate of conversion of HMG-CoA to mevalonate by HMG-CoA reductase in the presence of different concentrations of IB/83/1/4.

Data plotted are those shown in table A.19. The curve fitted is a Boltzmann function with the parameters shown, where A_1 is the initial rate of reaction at minimal inhibition, A_2 is the initial rate of reaction at maximal inhibition, x_0 is the IC50 and dx is the concentration range over which inhibition changes from minimal to maximal.

	Initial Rate of Reaction / p.d.u.									
[Inhibitor] / nM	Assay 1	Assay 2	Assay 3	Assay 4	Assay 5	Assay 6	Assay 7	Assay 8	Mean	Error
0	0.047	0.046	0.041	0.043	0.043	0.042	0.042	0.045	0.044	0.001
1	0.032	0.040	0.037						0.036	0.002
2	0.029	0.035	0.024						0.030	0.003
5	0.020	0.023	0.026						0.023	0.002
10	0.002	0.015	0.013						0.010	0.004
20	0.004	0.008	0.018						0.010	0.004
30	0.016	0.002	0.009						0.009	0.004
40	0.020	0.029	0.018						0.022	0.003
50	0.003	0.021	0.015						0.013	0.005

Table A.20. The initial rate of conversion of HMG-CoA to mevalonate by HMG-CoA reductase in the presence of different concentrations of IB/87/1/2.

Substrates HMG-CoA and NADPH both have a final concentration in the reaction of 200 µM and the HMG-CoA reductase concentration was 10 nM in all assays. All assays were biological repeats and errors are standard error of the mean. Initial rate of reaction is shown in procedure defined units as it is calculated from absorption measurements which have no units.

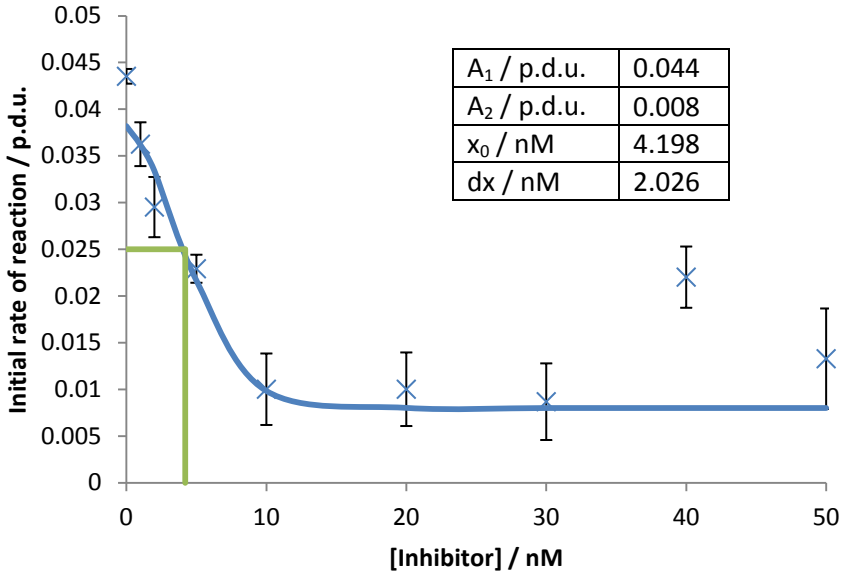

Figure A.20. The initial rate of conversion of HMG-CoA to mevalonate by HMG-CoA reductase in the presence of different concentrations of IB/87/1/2.

Data plotted are those shown in table A.20. The curve fitted is a Boltzmann function with the parameters shown, where A_1 is the initial rate of reaction at minimal inhibition, A_2 is the initial rate of reaction at maximal inhibition, x_0 is the IC50 and dx is the concentration range over which inhibition changes from minimal to maximal.

	Initial Rate of Reaction / p.d.u.									
[Inhibitor] / nM	Assay 1	Assay 2	Assay 3	Assay 4	Assay 5	Assay 6	Assay 7	Assay 8	Mean	Error
0	0.047	0.046	0.041	0.043	0.043	0.042	0.042	0.045	0.044	0.001
1	0.032	0.043	0.040						0.038	0.003
2	0.017	0.045	0.012	0.050					0.031	0.010
5	0.019	0.027	0.018	0.012					0.019	0.003
10	0.011	0.014	0.016						0.014	0.001
15	0.006	0.016	0.023						0.015	0.005
20	0.012	0.009	0.011						0.011	0.001
30	0.006	0.016	0.023						0.015	0.005
40	0.010	0.013	0.009						0.011	0.001
50	0.023	0.002	0.012						0.012	0.006

Table A.21. The initial rate of conversion of HMG-CoA to mevalonate by HMG-CoA reductase in the presence of different concentrations of IB/87/1/3.

Substrates HMG-CoA and NADPH both have a final concentration in the reaction of 200 µM and the HMG-CoA reductase concentration was 10 nM in all assays. All assays were biological repeats and errors are standard error of the mean. Initial rate of reaction is shown in procedure defined units as it is calculated from absorption measurements which have no units.

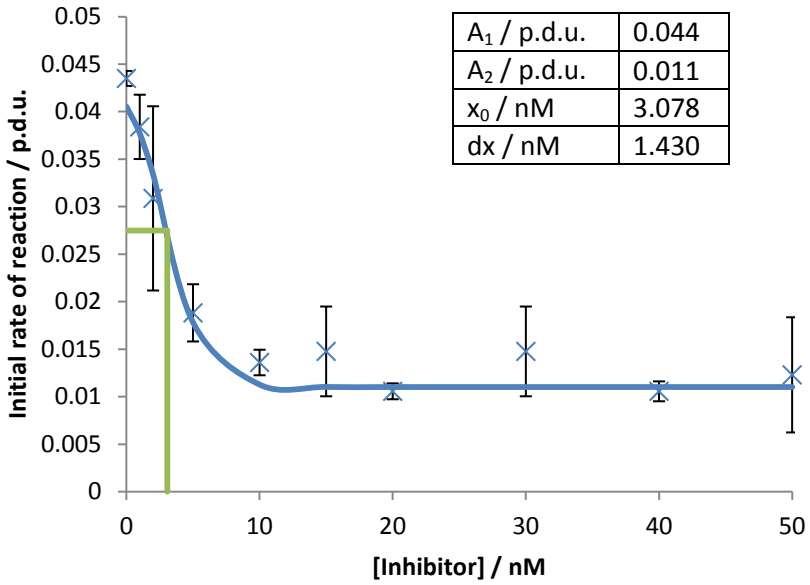

Figure A.21. The initial rate of conversion of HMG-CoA to mevalonate by HMG-CoA reductase in the presence of different concentrations of IB/87/1/3.

Data plotted are those shown in table A.21. The curve fitted is a Boltzmann function with the parameters shown, where A_1 is the initial rate of reaction at minimal inhibition, A_2 is the initial rate of reaction at maximal inhibition, x_0 is the IC50 and dx is the concentration range over which inhibition changes from minimal to maximal.

	Initial Rate of Reaction / p.d.u.									
[Inhibitor] / nM	Assay 1	Assay 2	Assay 3	Assay 4	Assay 5	Assay 6	Assay 7	Assay 8	Mean	Error
0	0.047	0.046	0.041	0.043	0.043	0.042	0.042	0.045	0.044	0.001
1	0.042	0.046	0.038						0.042	0.002
2	0.038	0.039	0.044						0.040	0.002
5	0.033	0.034	0.041						0.036	0.003
10	0.031	0.031	0.034						0.032	0.001
15	0.021	0.025	0.026						0.024	0.002
20	0.038	0.030	0.031						0.033	0.003
30	0.022	0.023	0.027						0.024	0.002
40	0.010	0.036	0.030						0.025	0.008
50	0.021	0.025	0.024						0.023	0.001

Table A.22. The initial rate of conversion of HMG-CoA to mevalonate by HMG-CoA reductase in the presence of different concentrations of IB/89/1T.

Substrates HMG-CoA and NADPH both have a final concentration in the reaction of 200 µM and the HMG-CoA reductase concentration was 10 nM in all assays. All assays were biological repeats and errors are standard error of the mean. Initial rate of reaction is shown in procedure defined units as it is calculated from absorption measurements which have no units.

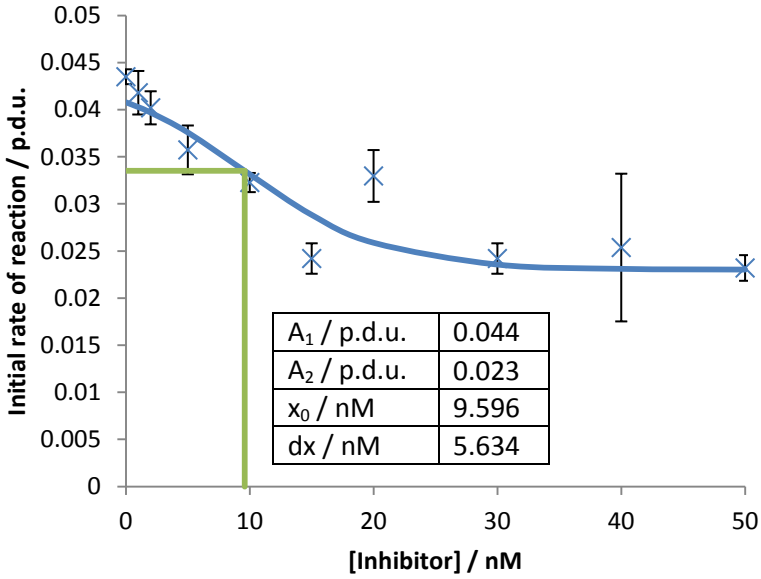

Figure A.22. The initial rate of conversion of HMG-CoA to mevalonate by HMG-CoA reductase in the presence of different concentrations of IB/89/1T.

Data plotted are those shown in table A.22. The curve fitted is a Boltzmann function with the parameters shown, where A_1 is the initial rate of reaction at minimal inhibition, A_2 is the initial rate of reaction at maximal inhibition, x_0 is the IC50 and dx is the concentration range over which inhibition changes from minimal to maximal.

	Initial Rate of Reaction / p.d.u.									
[Inhibitor] / nM	Assay 1	Assay 2	Assay 3	Assay 4	Assay 5	Assay 6	Assay 7	Assay 8	Mean	Error
0	0.047	0.046	0.041	0.043	0.043	0.042	0.042	0.045	0.044	0.001
1	0.042	0.047	0.046						0.045	0.002
2	0.023	0.037	0.057						0.039	0.010
5	0.035	0.043	0.037	0.027	0.032	0.040			0.036	0.002
10	0.024	0.023	0.024						0.023	0.000
15	0.013	0.032	0.023						0.023	0.005
20	0.021	0.013	0.020						0.018	0.002
30	0.005	0.013	0.010						0.009	0.003
40	0.022	0.017	0.015						0.018	0.002
50	0.005	0.009	0.010						0.008	0.002

Table A.23. The initial rate of conversion of HMG-CoA to mevalonate by HMG-CoA reductase in the presence of different concentrations of ED/05/01B.

Substrates HMG-CoA and NADPH both have a final concentration in the reaction of 200 µM and the HMG-CoA reductase concentration was 10 nM in all assays. All assays were biological repeats and errors are standard error of the mean. Initial rate of reaction is shown in procedure defined units as it is calculated from absorption measurements which have no units.

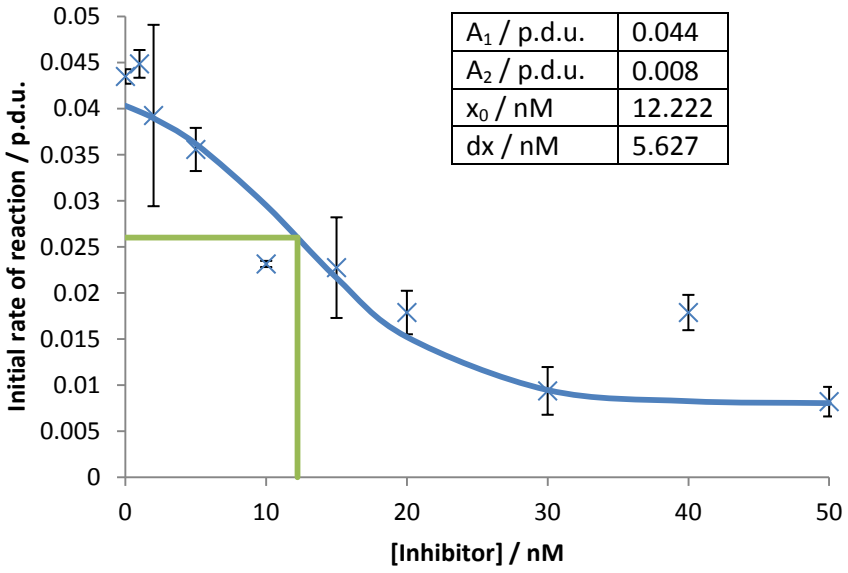

Figure A.23. The initial rate of conversion of HMG-CoA to mevalonate by HMG-CoA reductase in the presence of different concentrations of ED/05/01B.

Data plotted are those shown in table A.23. The curve fitted is a Boltzmann function with the parameters shown, where A_1 is the initial rate of reaction at minimal inhibition, A_2 is the initial rate of reaction at maximal inhibition, x_0 is the IC50 and dx is the concentration range over which inhibition changes from minimal to maximal.

	Initial Rate of Reaction / p.d.u.									
[Inhibitor] / nM	Assay 1	Assay 2	Assay 3	Assay 4	Assay 5	Assay 6	Assay 7	Assay 8	Mean	Error
0	0.047	0.046	0.041	0.043	0.043	0.042	0.042	0.045	0.044	0.001
1	0.053	0.037	0.027						0.039	0.008
2	0.045	0.049	0.025	0.022	0.025				0.033	0.006
5	0.016	0.012	0.016	0.019	0.028				0.018	0.003
10	0.021	0.006	0.003						0.010	0.005
15	0.018	0.013	0.013						0.015	0.002
20	0.008	0.014	0.009						0.010	0.002
30	0.016	0.012	0.016						0.015	0.001
40	0.018	0.008	0.014						0.013	0.003
50	0.017	0.000	0.017						0.012	0.006

Table A.24. The initial rate of conversion of HMG-CoA to mevalonate by HMG-CoA reductase in the presence of different concentrations of ED/05/01T.

Substrates HMG-CoA and NADPH both have a final concentration in the reaction of 200 µM and the HMG-CoA reductase concentration was 10 nM in all assays. All assays were biological repeats and errors are standard error of the mean. Initial rate of reaction is shown in procedure defined units as it is calculated from absorption measurements which have no units.

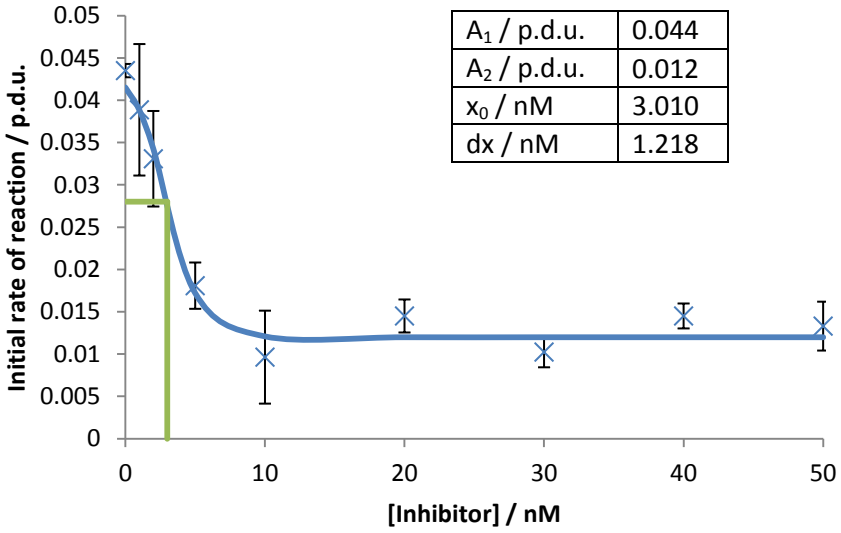

Figure A.24. The initial rate of conversion of HMG-CoA to mevalonate by HMG-CoA reductase in the presence of different concentrations of ED/05/01T.

Data plotted are those shown in table A.24. The curve fitted is a Boltzmann function with the parameters shown, where A_1 is the initial rate of reaction at minimal inhibition, A_2 is the initial rate of reaction at maximal inhibition, x_0 is the IC50 and dx is the concentration range over which inhibition changes from minimal to maximal.

	Initial Rate of Reaction / p.d.u.									
[Inhibitor] / nM	Assay 1	Assay 2	Assay 3	Assay 4	Assay 5	Assay 6	Assay 7	Assay 8	Mean	Error
0	0.047	0.046	0.041	0.043	0.043	0.042	0.042	0.045	0.044	0.001
1	0.041	0.044	0.048	0.034	0.037	0.043	0.037	0.035	0.040	0.002
2	0.026	0.024	0.025	0.025	0.026	0.023	0.030	0.029	0.026	0.001
5	0.019	0.021	0.025	0.013	0.025	0.025	0.021	0.021	0.021	0.001
10	0.016	0.020	0.014	0.016	0.021	0.018	0.016	0.020	0.018	0.001
15	0.021	0.014	0.013						0.016	0.003
20	0.014	0.005	0.015	0.005	0.015	0.012	0.014	0.010	0.011	0.002
30	0.014	0.010	0.005	0.007	0.007	0.013	0.009	0.011	0.010	0.001
40	0.010	0.010	0.008	0.006	0.012	0.010	0.013	0.011	0.010	0.001
50	0.003	0.020	0.027	0.026	0.004	0.002	0.003	0.006	0.011	0.004

Table A.25. The initial rate of conversion of HMG-CoA to mevalonate by HMG-CoA reductase in the presence of different concentrations of ED/05/02T.

Substrates HMG-CoA and NADPH both have a final concentration in the reaction of 200 µM and the HMG-CoA reductase concentration was 10 nM in all assays. All assays were biological repeats and errors are standard error of the mean. Initial rate of reaction is shown in procedure defined units as it is calculated from absorption measurements which have no units.

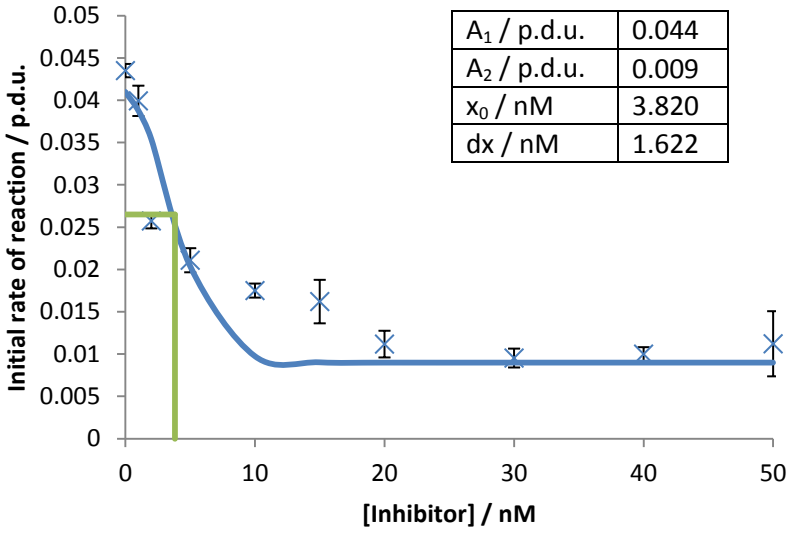

Figure A.25. The initial rate of conversion of HMG-CoA to mevalonate by HMG-CoA reductase in the presence of different concentrations of ED/05/02T.

Data plotted are those shown in table A.25. The curve fitted is a Boltzmann function with the parameters shown, where A_1 is the initial rate of reaction at minimal inhibition, A_2 is the initial rate of reaction at maximal inhibition, x_0 is the IC50 and dx is the concentration range over which inhibition changes from minimal to maximal.

	Initial Rate of Reaction / p.d.u.									
[Inhibitor] / nM	Assay 1	Assay 2	Assay 3	Assay 4	Assay 5	Assay 6	Assay 7	Assay 8	Mean	Error
0	0.047	0.046	0.041	0.043	0.043	0.042	0.042	0.045	0.044	0.001
1	0.046	0.045	0.031	0.043	0.037	0.044	0.042	0.042	0.041	0.002
2	0.037	0.033	0.034	0.022	0.038	0.034	0.022	0.047	0.033	0.003
5	0.022		0.030	0.022		0.028	0.030	0.020	0.025	0.002
10	0.015	0.030	0.033	0.015	0.011	0.017	0.014	0.021	0.020	0.003
15	0.020	0.012	0.014						0.015	0.002
20	0.015	0.016	0.017	0.009	0.017	0.011	0.009	0.025	0.015	0.002
30	0.012	0.013	0.016	0.006	0.010	0.016	0.010	0.016	0.012	0.001
40	0.009	0.012	0.016	0.014	0.007	0.003	0.012	0.009	0.010	0.001
50	0.009	0.012	0.008	0.007	0.014	0.015	0.007	0.013	0.011	0.001

Table A.26. The initial rate of conversion of HMG-CoA to mevalonate by HMG-CoA reductase in the presence of different concentrations of ED/06/02.

Substrates HMG-CoA and NADPH both have a final concentration in the reaction of 200 µM and the HMG-CoA reductase concentration was 10 nM in all assays. All assays were biological repeats and errors are standard error of the mean. Initial rate of reaction is shown in procedure defined units as it is calculated from absorption measurements which have no units.

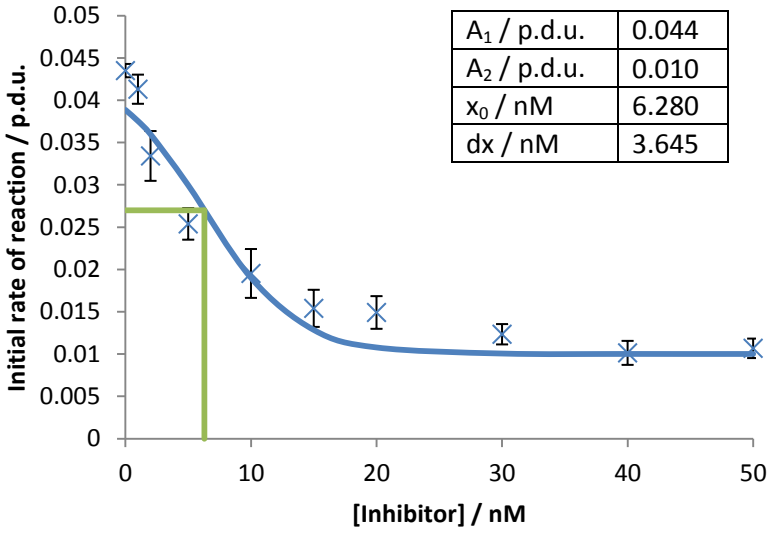

Figure A.26. The initial rate of conversion of HMG-CoA to mevalonate by HMG-CoA reductase in the presence of different concentrations of ED/06/02.

Data plotted are those shown in table A.26. The curve fitted is a Boltzmann function with the parameters shown, where A_1 is the initial rate of reaction at minimal inhibition, A_2 is the initial rate of reaction at maximal inhibition, x_0 is the IC50 and dx is the concentration range over which inhibition changes from minimal to maximal.

	Initial Rate of Reaction / p.d.u.									
[Inhibitor] / nM	Assay 1	Assay 2	Assay 3	Assay 4	Assay 5	Assay 6	Assay 7	Assay 8	Mean	Error
0	0.047	0.046	0.041	0.043	0.043	0.042	0.042	0.045	0.044	0.001
1	0.051	0.034	0.057						0.047	0.007
2	0.042	0.030	0.039						0.037	0.004
5	0.029	0.016	0.040	0.029	0.038	0.013			0.028	0.004
10	0.029	0.019	0.025						0.024	0.003
15	0.020	0.035	0.035						0.030	0.005
20	0.020	0.031	0.030						0.027	0.003
30	0.025	0.025	0.040						0.030	0.005
40	0.022	0.028	0.031						0.027	0.002
50	0.016	0.023	0.024						0.021	0.003

Table A.27. The initial rate of conversion of HMG-CoA to mevalonate by HMG-CoA reductase in the presence of different concentrations of ED/07/02.

Substrates HMG-CoA and NADPH both have a final concentration in the reaction of 200 µM and the HMG-CoA reductase concentration was 10 nM in all assays. All assays were biological repeats and errors are standard error of the mean. Initial rate of reaction is shown in procedure defined units as it is calculated from absorption measurements which have no units.

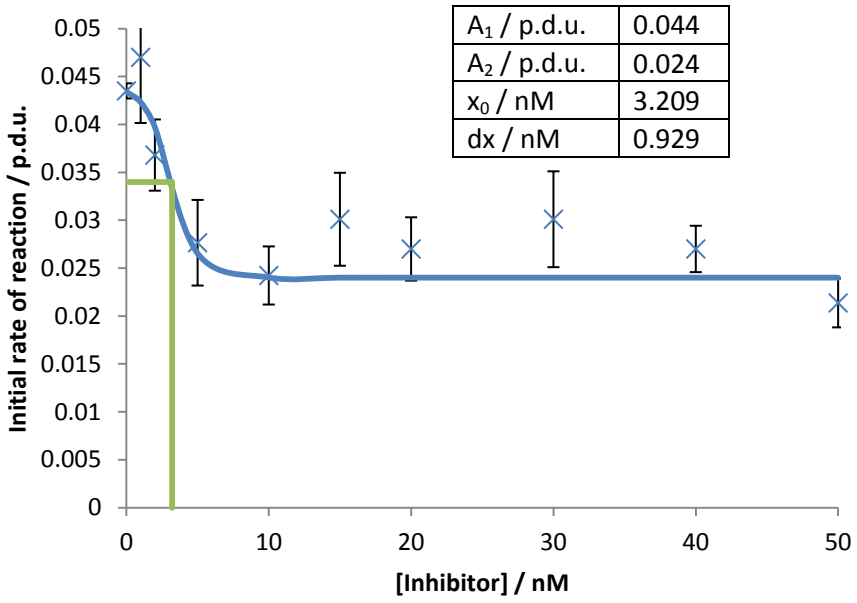

Figure A.27. The initial rate of conversion of HMG-CoA to mevalonate by HMG-CoA reductase in the presence of different concentrations of ED/07/02.

Data plotted are those shown in table A.27. The curve fitted is a Boltzmann function with the parameters shown, where A_1 is the initial rate of reaction at minimal inhibition, A_2 is the initial rate of reaction at maximal inhibition, x_0 is the IC50 and dx is the concentration range over which inhibition changes from minimal to maximal.

	Initial Rate of Reaction / p.d.u.									
[Inhibitor] / nM	Assay 1	Assay 2	Assay 3	Assay 4	Assay 5	Assay 6	Assay 7	Assay 8	Mean	Error
0	0.047	0.046	0.041	0.043	0.043	0.042	0.042	0.045	0.044	0.001
1	0.044	0.043	0.041						0.043	0.001
2	0.029	0.036	0.032						0.032	0.002
5	0.024	0.035	0.031						0.030	0.003
10	0.028	0.028	0.032						0.029	0.001
20	0.027	0.016	0.027						0.023	0.004
30	0.020	0.016	0.021						0.019	0.002
40	0.015	0.012	0.018						0.015	0.002
50	0.015	0.011	0.012						0.013	0.001

Table A.28. The initial rate of conversion of HMG-CoA to mevalonate by HMG-CoA reductase in the presence of different concentrations of ED/09/02.

Substrates HMG-CoA and NADPH both have a final concentration in the reaction of 200 µM and the HMG-CoA reductase concentration was 10 nM in all assays. All assays were biological repeats and errors are standard error of the mean. Initial rate of reaction is shown in procedure defined units as it is calculated from absorption measurements which have no units.

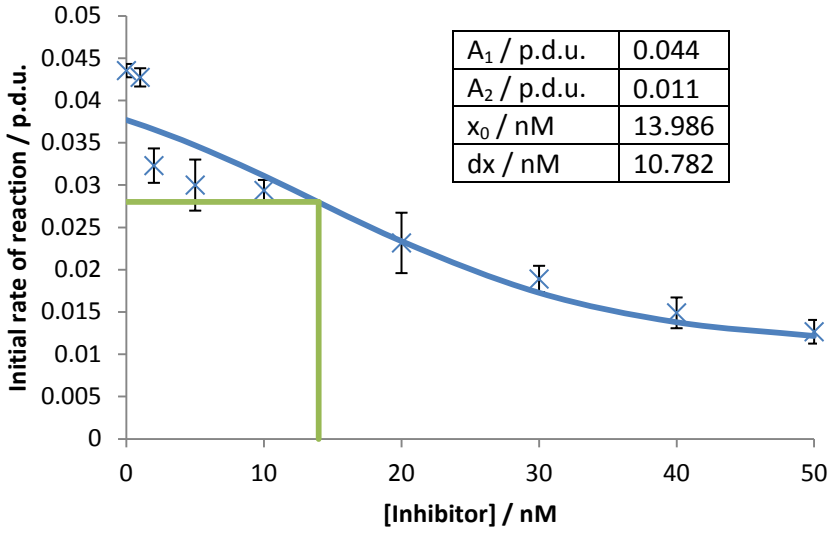

Figure A.28. The initial rate of conversion of HMG-CoA to mevalonate by HMG-CoA reductase in the presence of different concentrations of ED/09/02.

Data plotted are those shown in table A.28. The curve fitted is a Boltzmann function with the parameters shown, where A_1 is the initial rate of reaction at minimal inhibition, A_2 is the initial rate of reaction at maximal inhibition, x_0 is the IC50 and dx is the concentration range over which inhibition changes from minimal to maximal.

	Initial Rate of Reaction / p.d.u.									
[Inhibitor] / nM	Assay 1	Assay 2	Assay 3	Assay 4	Assay 5	Assay 6	Assay 7	Assay 8	Mean	Error
0	0.047	0.046	0.041	0.043	0.043	0.042	0.042	0.045	0.044	0.001
1	0.023	0.022	0.027						0.024	0.002
2	0.019	0.022	0.024						0.022	0.001
5	0.027	0.022	0.022						0.024	0.002
10	0.021	0.023	0.022						0.022	0.001
20	0.022	0.022	0.017						0.020	0.002
30	0.016	0.027	0.020						0.021	0.003
40	0.014	0.012	0.013						0.013	0.000
50	0.018	0.016	0.026						0.020	0.003

Table A.29. The initial rate of conversion of HMG-CoA to mevalonate by HMG-CoA reductase in the presence of different concentrations of ED/11/02.

Substrates HMG-CoA and NADPH both have a final concentration in the reaction of 200 µM and the HMG-CoA reductase concentration was 10 nM in all assays. All assays were biological repeats and errors are standard error of the mean. Initial rate of reaction is shown in procedure defined units as it is calculated from absorption measurements which have no units.

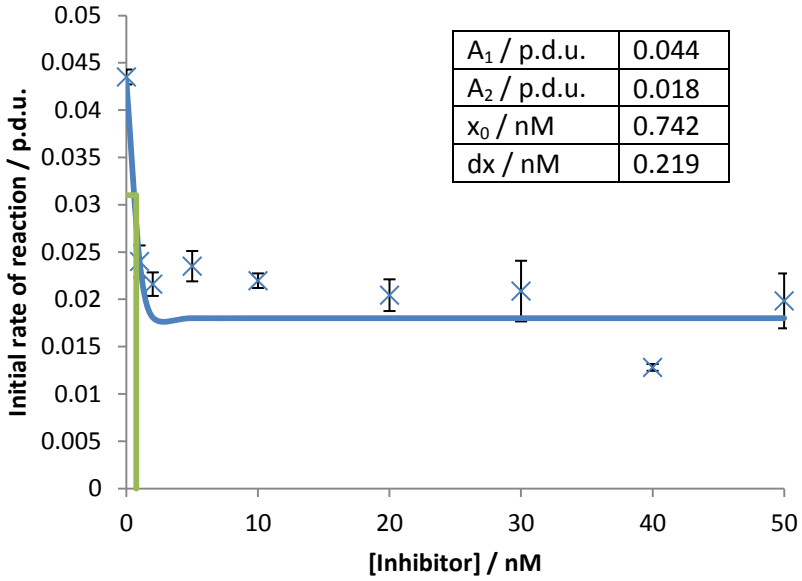

Figure A.29. The initial rate of conversion of HMG-CoA to mevalonate by HMG-CoA reductase in the presence of different concentrations of ED/11/02.

Data plotted are those shown in table A.29. The curve fitted is a Boltzmann function with the parameters shown, where A_1 is the initial rate of reaction at minimal inhibition, A_2 is the initial rate of reaction at maximal inhibition, x_0 is the IC50 and dx is the concentration range over which inhibition changes from minimal to maximal.

	Initial Rate of Reaction / p.d.u.									
[Inhibitor] / nM	Assay 1	Assay 2	Assay 3	Assay 4	Assay 5	Assay 6	Assay 7	Assay 8	Mean	Error
0	0.047	0.046	0.041	0.043	0.043	0.042	0.042	0.045	0.044	0.001
1	0.033	0.034	0.033						0.033	0.000
2	0.027	0.021	0.041						0.030	0.006
5	0.023	0.038	0.038						0.033	0.005
10	0.026	0.035	0.033						0.031	0.003
20	0.026	0.029	0.025						0.027	0.001
30	0.025	0.025	0.034						0.028	0.003
40	0.013	0.016	0.015						0.015	0.001
50	0.025	0.025	0.025						0.025	0.000

Table A.30. The initial rate of conversion of HMG-CoA to mevalonate by HMG-CoA reductase in the presence of different concentrations of SH-II-87A.

Substrates HMG-CoA and NADPH both have a final concentration in the reaction of 200 µM and the HMG-CoA reductase concentration was 10 nM in all assays. All assays were biological repeats and errors are standard error of the mean. Initial rate of reaction is shown in procedure defined units as it is calculated from absorption measurements which have no units.

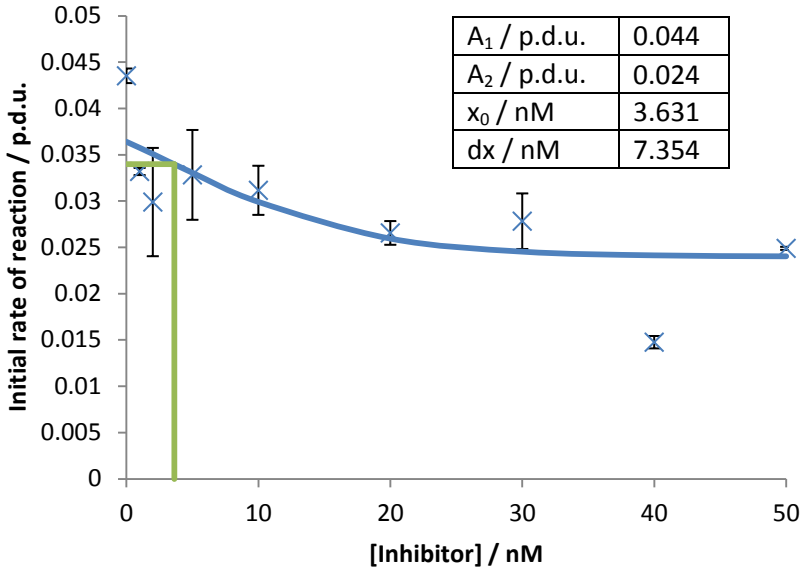

Figure A.30. The initial rate of conversion of HMG-CoA to mevalonate by HMG-CoA reductase in the presence of different concentrations of SH-II-87A.

Data plotted are those shown in table A.30. The curve fitted is a Boltzmann function with the parameters shown, where A_1 is the initial rate of reaction at minimal inhibition, A_2 is the initial rate of reaction at maximal inhibition, x_0 is the IC50 and dx is the concentration range over which inhibition changes from minimal to maximal.

	Initial Rate of Reaction / p.d.u.									
[Inhibitor] / nM	Assay 1	Assay 2	Assay 3	Assay 4	Assay 5	Assay 6	Assay 7	Assay 8	Mean	Error
0	0.047	0.046	0.041	0.043	0.043	0.042	0.042	0.045	0.044	0.001
1	0.031	0.027	0.030						0.029	0.001
2	0.022	0.032	0.022						0.025	0.003
5	0.025	0.029	0.031						0.028	0.002
10	0.021	0.019	0.021						0.020	0.001
20	0.026	0.023	0.024						0.024	0.001
30	0.017	0.024	0.027						0.022	0.003
40	0.015	0.016	0.026						0.019	0.003
50	0.021	0.023	0.018						0.021	0.002

Table A.31. The initial rate of conversion of HMG-CoA to mevalonate by HMG-CoA reductase in the presence of different concentrations of TD-I-31A.

Substrates HMG-CoA and NADPH both have a final concentration in the reaction of 200 µM and the HMG-CoA reductase concentration was 10 nM in all assays. All assays were biological repeats and errors are standard error of the mean. Initial rate of reaction is shown in procedure defined units as it is calculated from absorption measurements which have no units.

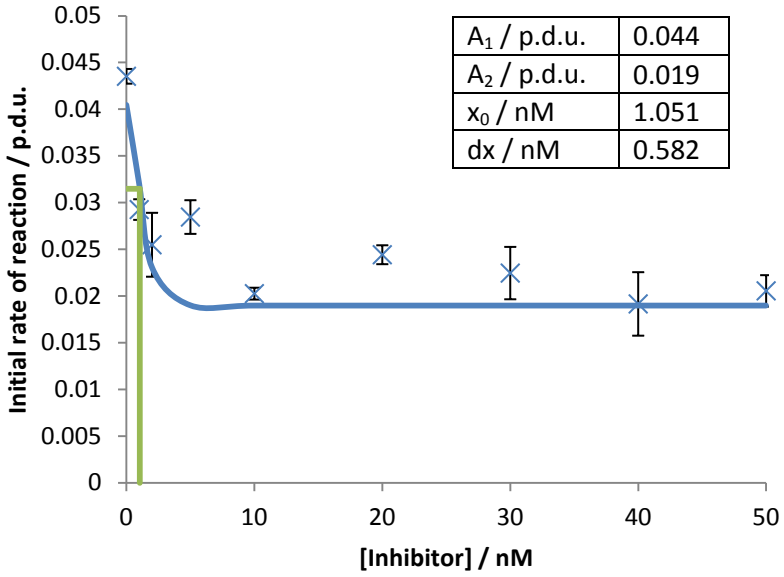

Figure A.31. The initial rate of conversion of HMG-CoA to mevalonate by HMG-CoA reductase in the presence of different concentrations of TD-I-31A.

Data plotted are those shown in table A.31. The curve fitted is a Boltzmann function with the parameters shown, where A_1 is the initial rate of reaction at minimal inhibition, A_2 is the initial rate of reaction at maximal inhibition, x_0 is the IC50 and dx is the concentration range over which inhibition changes from minimal to maximal.

Appendix B

B. Antibacterial Plates

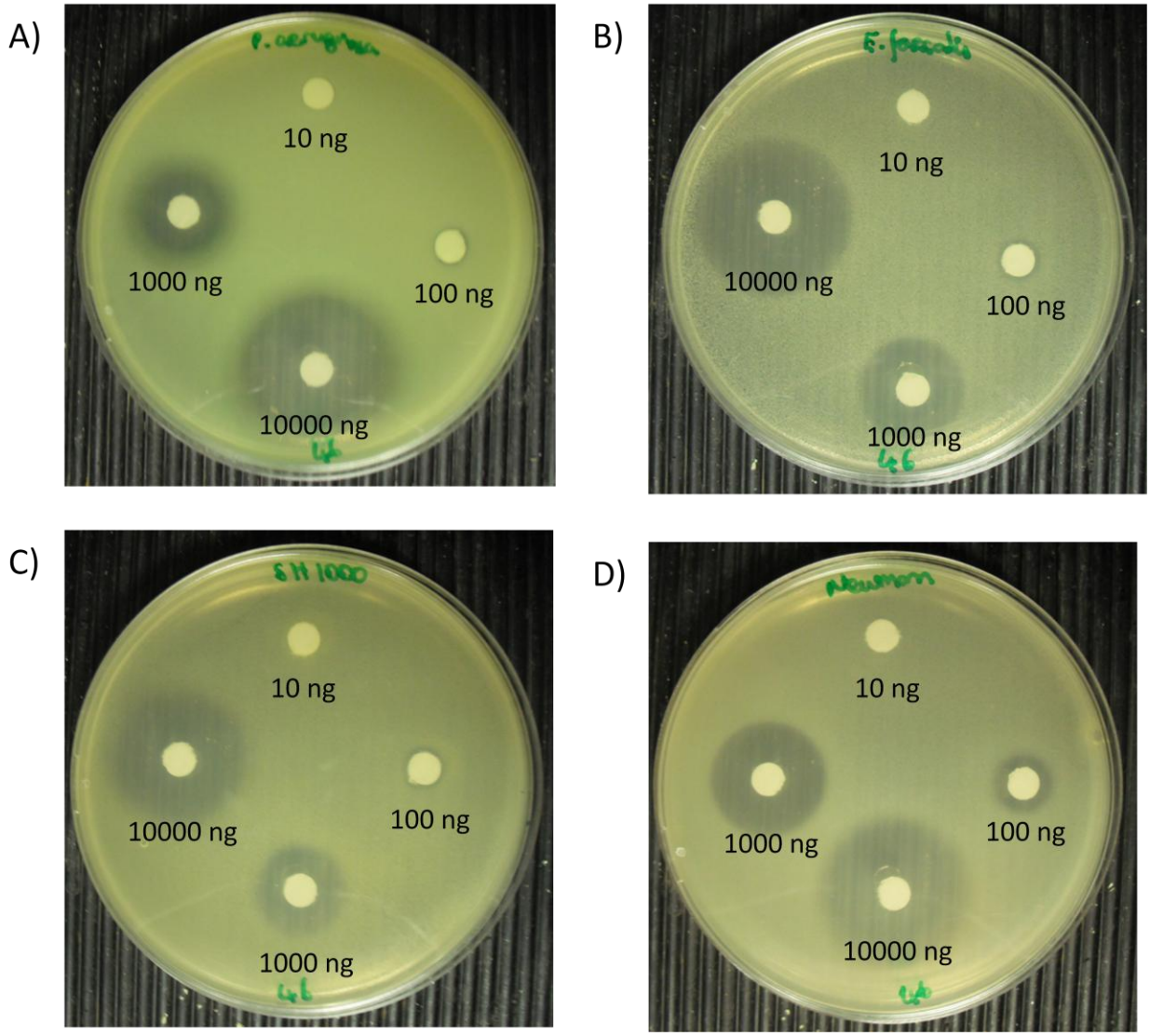

Figure B.1. Activity of levofloxacin against A) P. aeruginosa B) E. faecalis C) S. aureus SH1000 D) S. aureus Newman

Discs of filter paper soaked with different masses of levofloxacin dissolved in 5 µl of DMSO are placed onto Mueller-Hinton agar (21 g l^{-1} Mueller-Hinton broth, 1.5 % (w/v) agar) plates inoculated with Mueller-Hinton top agar (21 g l^{-1} Mueller-Hinton broth, 0.7 % (w/v) agar) different strains of bacteria which are incubated at 37 °C for 18 hours. The control used is 100 ng of levofloxacin.

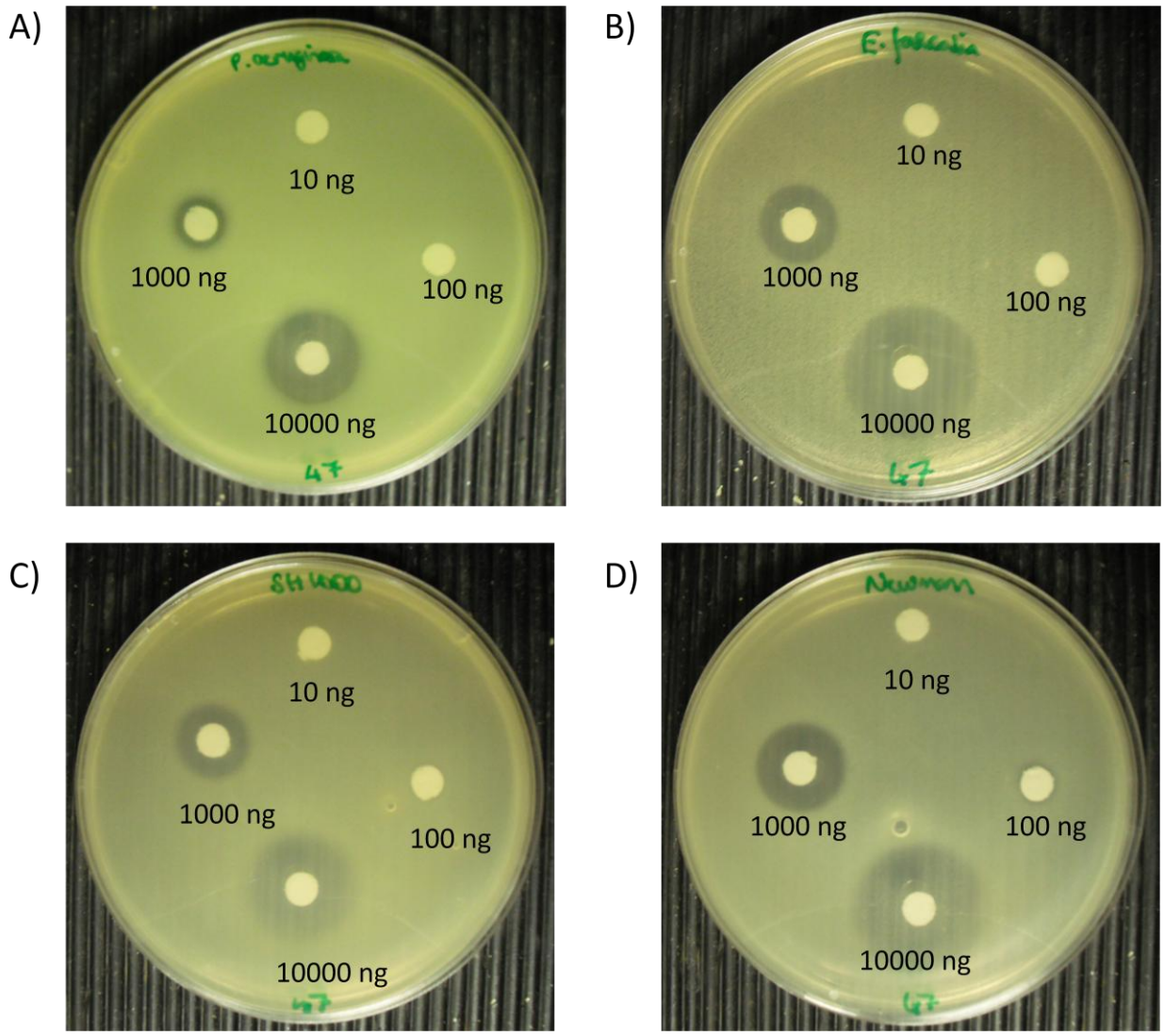

Figure B.2. Activity of pefloxacin mesylate against A) P. aeruginosa B) E. faecalis C) S. aureus SH1000 D) S. aureus Newman

Discs of filter paper soaked with different masses of pefloxacin mesylate dissolved in 5 µl of DMSO are placed onto Mueller-Hinton agar (21 g l^{-1} Mueller-Hinton broth, 1.5 % (w/v) agar) plates inoculated with Mueller-Hinton top agar (21 g l^{-1} Mueller-Hinton broth, 0.7 % (w/v) agar) different strains of bacteria which are incubated at 37 °C for 18 hours. The control used is 100 ng of levofloxacin.

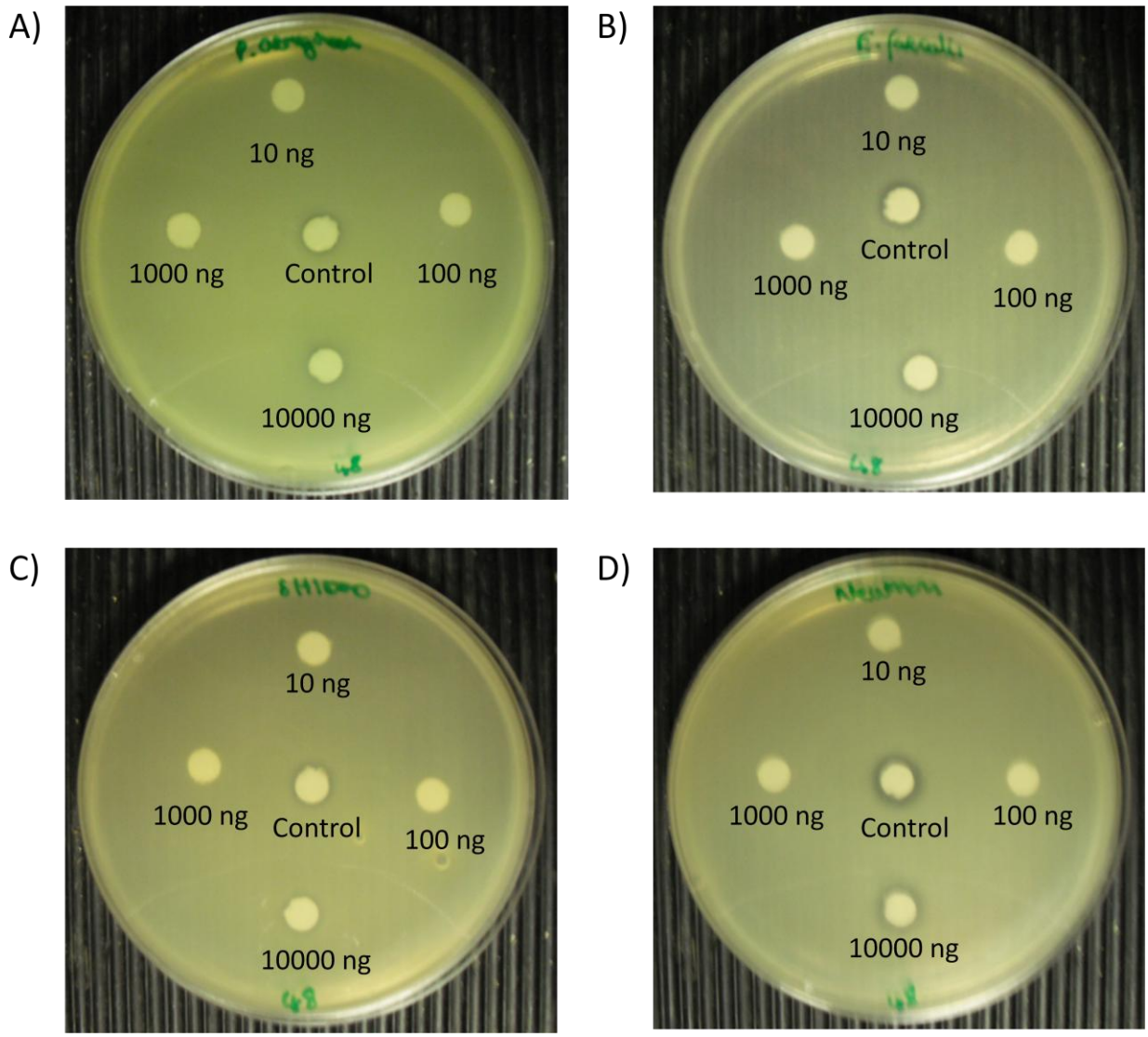

Figure B.3. Activity of a 3-formyl levofloxacin derivative against A) P. aeruginosa B) E. faecalis C) S. aureus SH1000 D) S. aureus Newman

Discs of filter paper soaked with different masses of a 3-formyl levofloxacin derivative dissolved in 5 µl of DMSO are placed onto Mueller-Hinton agar (21 g l^{-1} Mueller-Hinton broth, 1.5 % (w/v) agar) plates inoculated with Mueller-Hinton top agar (21 g l^{-1} Mueller-Hinton broth, 0.7 % (w/v) agar) different strains of bacteria which are incubated at 37 °C for 18 hours. The control used is 100 ng of levofloxacin.

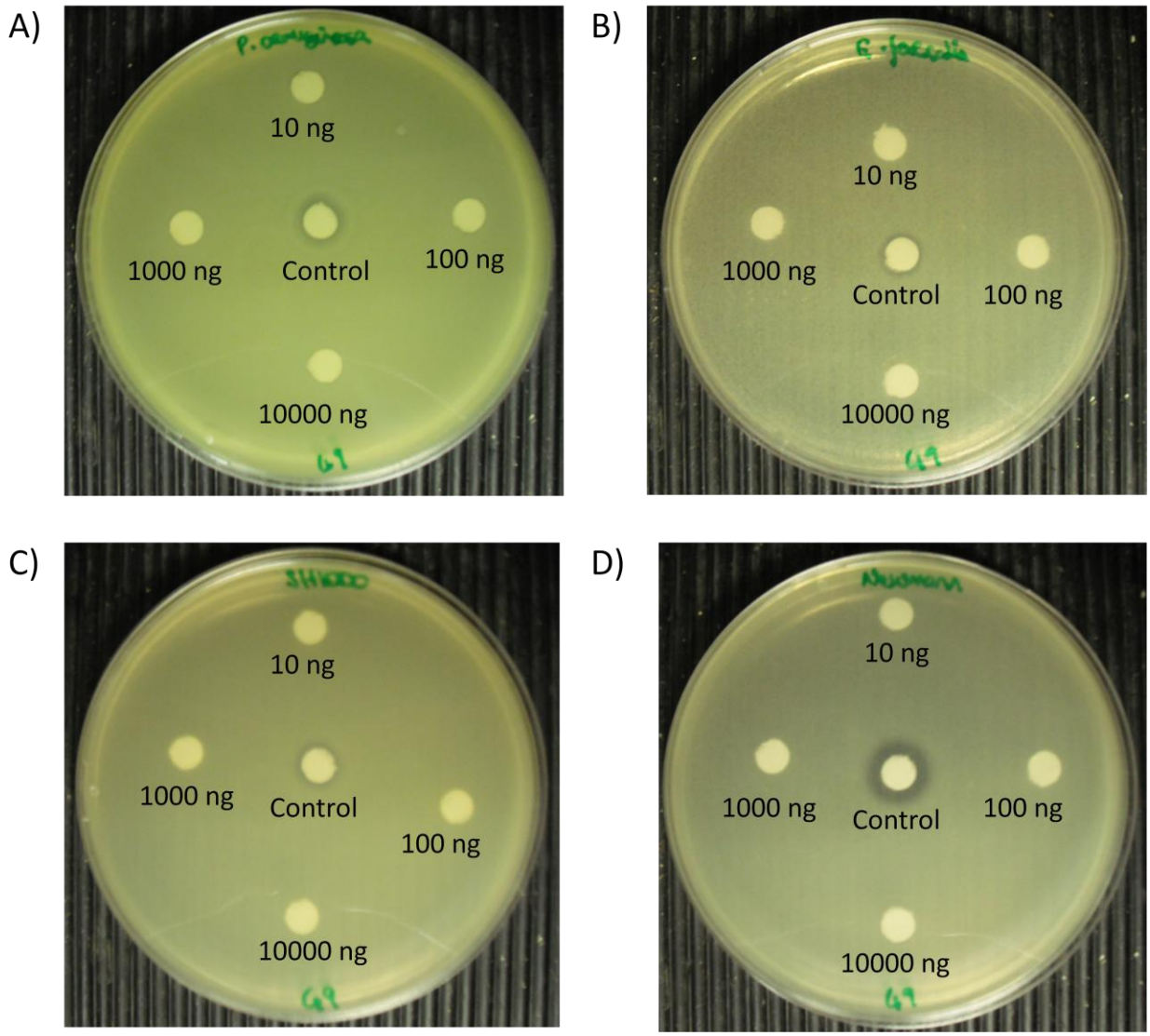

Figure B.4. Activity of fluoroquinolone derivative number one against A) P. aeruginosa B) E. faecalis C) S. aureus SH1000 D) S. aureus Newman

Discs of filter paper soaked with different masses of fluoroquinolone derivative number one dissolved in 5 µl of DMSO are placed onto Mueller-Hinton agar (21 g l^{-1} Mueller-Hinton broth, 1.5 % (w/v) agar) plates inoculated with Mueller-Hinton top agar (21 g l^{-1} Mueller-Hinton broth, 0.7 % (w/v) agar) different strains of bacteria which are incubated at 37 °C for 18 hours. The control used is 100 ng of levofloxacin.

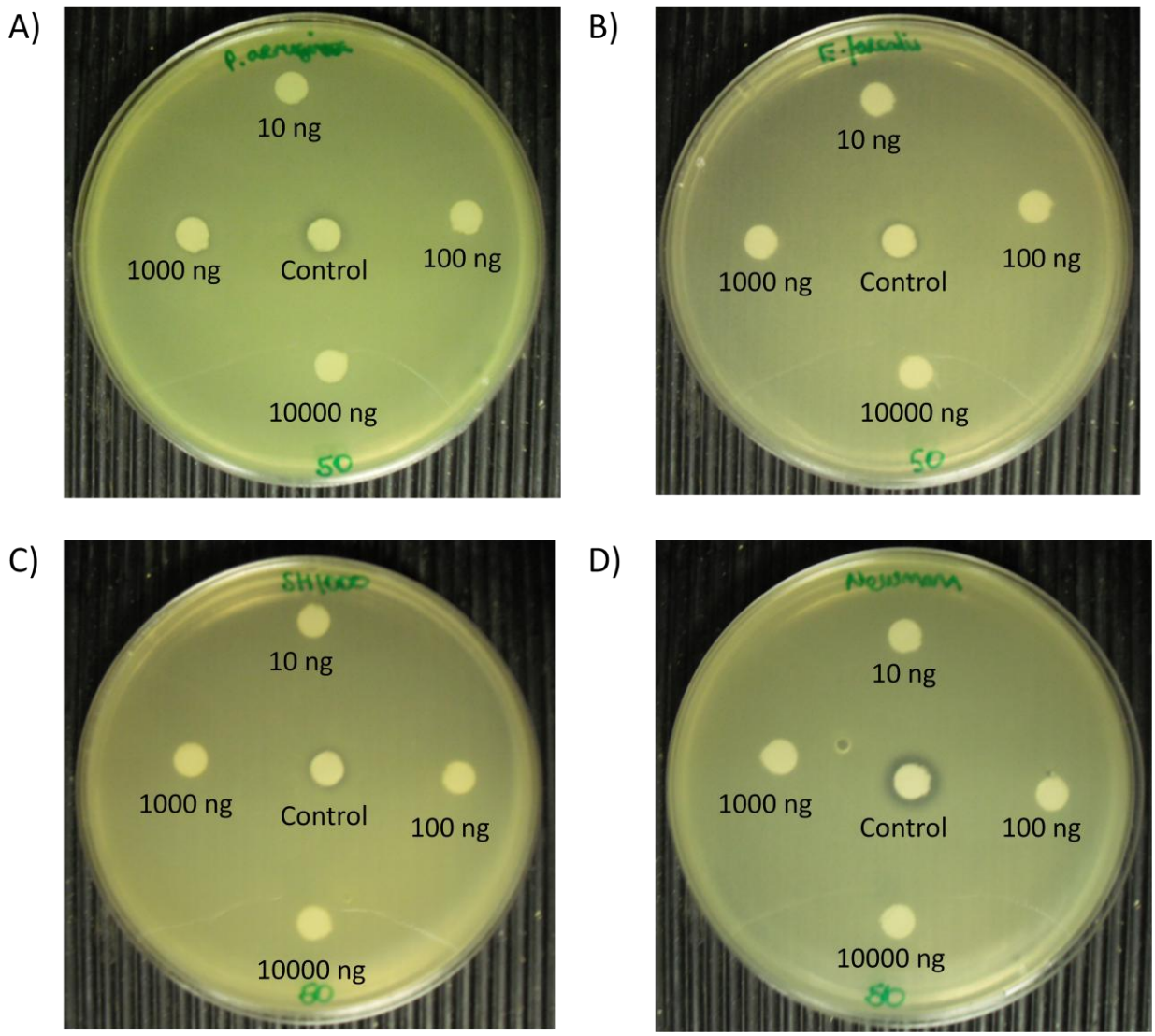

Figure B.5. Activity of fluoroquinolone derivative number two against A) P. aeruginosa B) E. faecalis C) S. aureus SH1000 D) S. aureus Newman

Discs of filter paper soaked with different masses of fluoroquinolone derivative number two dissolved in 5 µl of DMSO are placed onto Mueller-Hinton agar (21 g l^{-1} Mueller-Hinton broth, 1.5 % (w/v) agar) plates inoculated with Mueller-Hinton top agar (21 g l^{-1} Mueller-Hinton broth, 0.7 % (w/v) agar) different strains of bacteria which are incubated at 37 °C for 18 hours. The control used is 100 ng of levofloxacin.

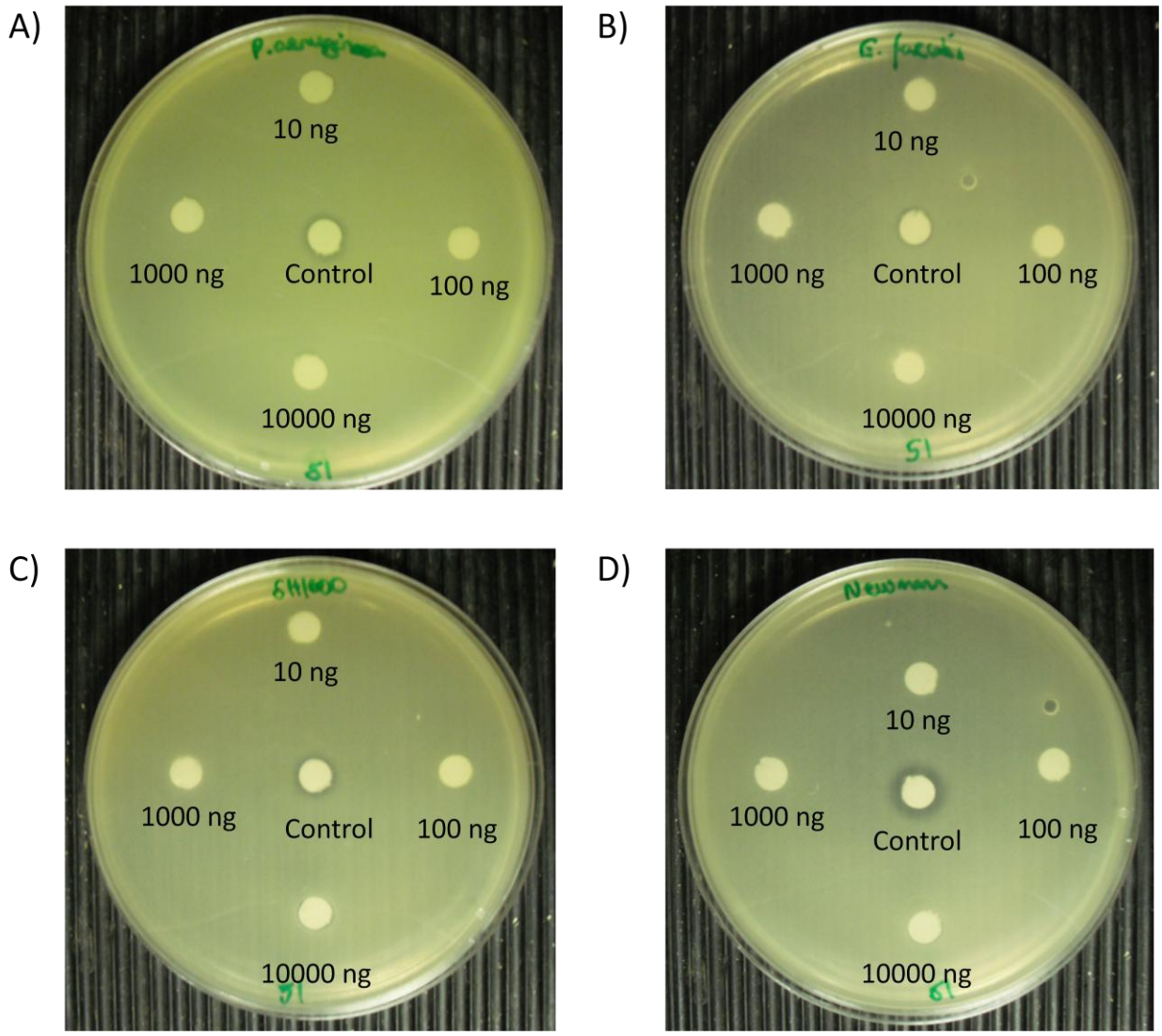

Figure B.6. Activity of fluoroquinolone derivative number three against A) P. aeruginosa B) E. faecalis C) S. aureus SH1000 D) S. aureus Newman

Discs of filter paper soaked with different masses of fluoroquinolone derivative number three dissolved in 5 µl of DMSO are placed onto Mueller-Hinton agar (21 g l^{-1} Mueller-Hinton broth, 1.5 % (w/v) agar) plates inoculated with Mueller-Hinton top agar (21 g l^{-1} Mueller-Hinton broth, 0.7 % (w/v) agar) different strains of bacteria which are incubated at 37 °C for 18 hours. The control used is 100 ng of levofloxacin.

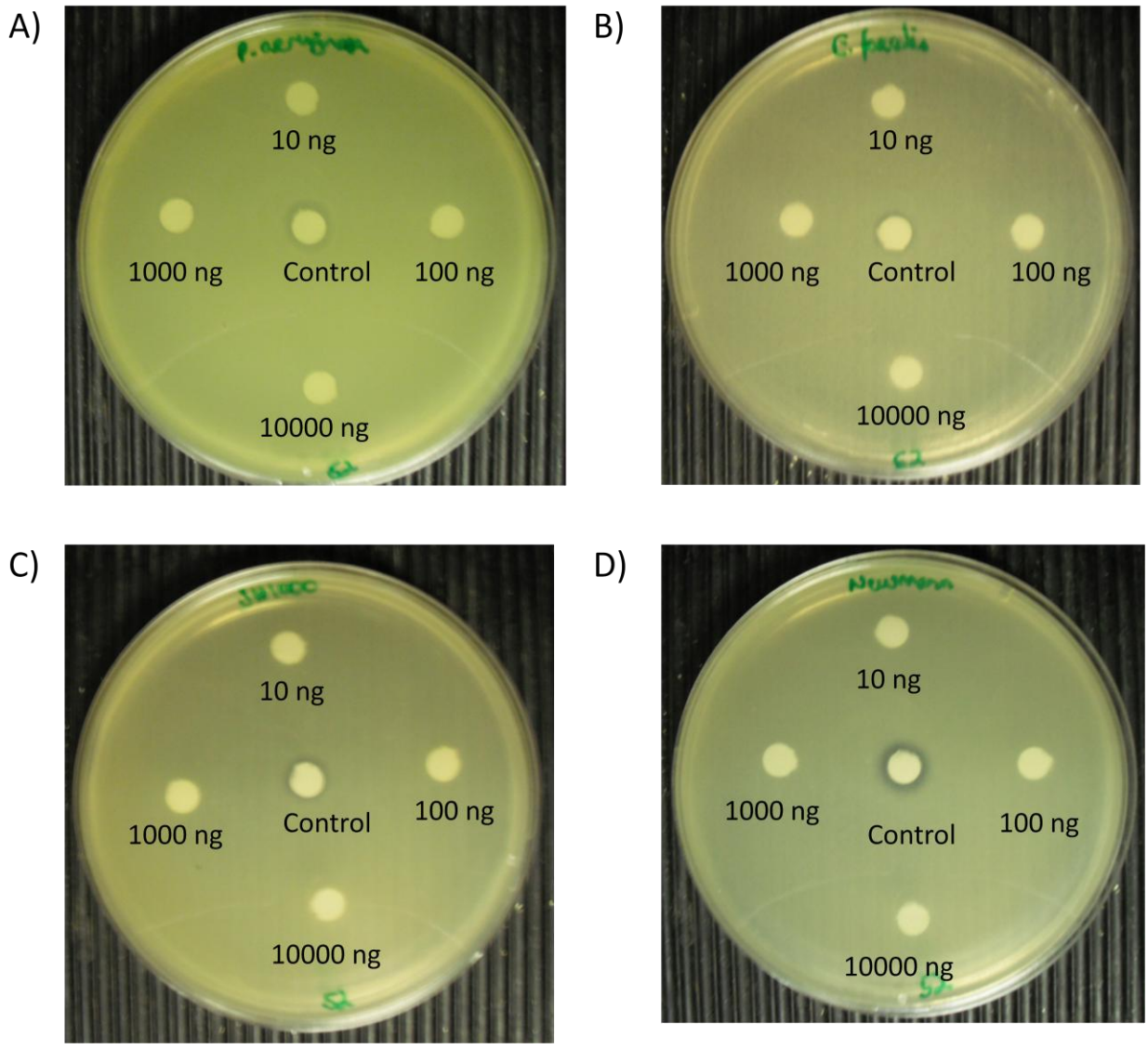

Figure B.7. Activity of fluoroquinolone derivative number four against A) P. aeruginosa B) E. faecalis C) S. aureus SH1000 D) S. aureus Newman

Discs of filter paper soaked with different masses of fluoroquinolone derivative number four dissolved in 5 µl of DMSO are placed onto Mueller-Hinton agar (21 g l^{-1} Mueller-Hinton broth, 1.5 % (w/v) agar) plates inoculated with Mueller-Hinton top agar (21 g l^{-1} Mueller-Hinton broth, 0.7 % (w/v) agar) different strains of bacteria which are incubated at 37 °C for 18 hours. The control used is 100 ng of levofloxacin.

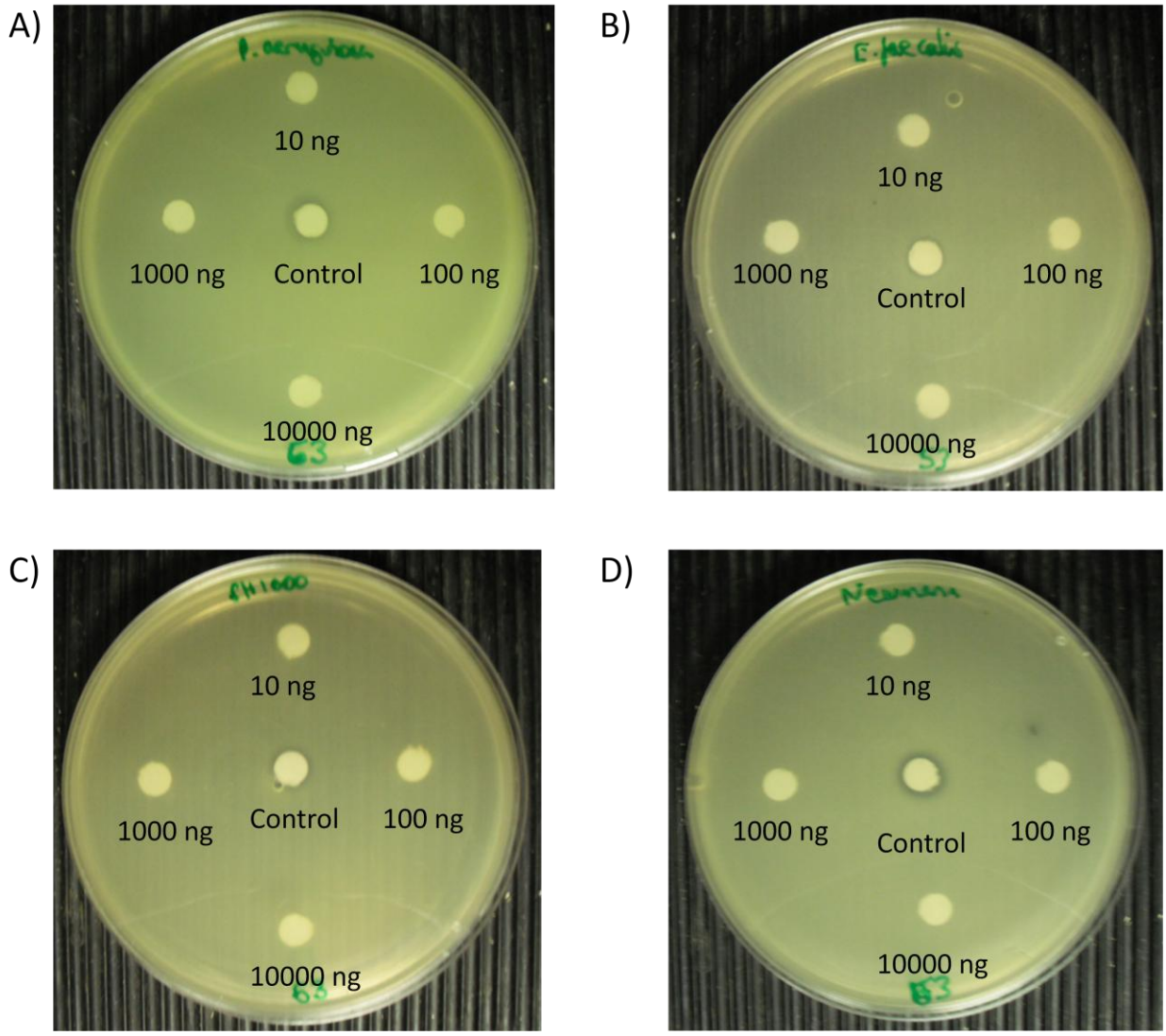

Figure B.8. Activity of fluoroquinolone derivative number five against A) P. aeruginosa B) E. faecalis C) S. aureus SH1000 D) S. aureus Newman

Discs of filter paper soaked with different masses of fluoroquinolone derivative number five dissolved in 5 µl of DMSO are placed onto Mueller-Hinton agar (21 g l^{-1} Mueller-Hinton broth, 1.5 % (w/v) agar) plates inoculated with Mueller-Hinton top agar (21 g l^{-1} Mueller-Hinton broth, 0.7 % (w/v) agar) different strains of bacteria which are incubated at 37 °C for 18 hours. The control used is 100 ng of levofloxacin.

Appendix C

C. Raw Data For Cellulose Breakdown Assays

C.1 Determination of Optimum Cellulolytic Enzymes

	Δ Absorbance / no units						
	Assay 1	Assay 2	Assay 3	Assay 4	Assay 5	Mean	Error
Reaction		0.066	0.064	0.062	0.069	0.066	0.001
Control 1	0.026	0.017	0.021	0.034	0.036	0.027	0.004
Control 2	0.002	0.000	0.006		0.001	0.003	0.001

Table C.1. Initial absorbance data for enzyme mixture A.

Composition of enzyme mixture is described in table 4.1. Control 1 contains no cellulose substrate, control 2 contains no enzyme. Reactions were diluted 40-fold to ensure absorbance is within a suitable range to calculate the mass of glucose produced. Substrate was digested by cellulolytic enzymes for 20-hours before being placed on ice to terminate the reaction. The change in absorption of the supernatant in a hexokinase/glucose-6-phosphate dehydrogenase assay was monitored by UV-spectrophotometry.

	Δ Absorbance / no units						
	Assay 1	Assay 2	Assay 3	Assay 4	Assay 5	Mean	Error
Reaction	0.003		0.001		0.004	0.003	0.001
Control 1	-0.006	-0.003	-0.005	0.004	0.004	-0.001	0.002
Control 2	0.002	0.000	0.006		0.001	0.003	0.001

Table C.2. Initial absorbance data for enzyme mixture B.

Composition of enzyme mixture is described in table 4.1. Control 1 contains no cellulose substrate, control 2 contains no enzyme. Reactions were diluted 40-fold to ensure absorbance is within a suitable range to calculate the mass of glucose produced. Substrate was digested by cellulolytic enzymes for 20-hours before being placed on ice to terminate the reaction. The change in absorption of the supernatant in a hexokinase/glucose-6-phosphate dehydrogenase assay was monitored by UV-spectrophotometry.

	Δ Absorbance / no units						
	Assay 1	Assay 2	Assay 3	Assay 4	Assay 5	Mean	Error
Reaction	0.019	0.015	0.018		0.010	0.016	0.002
Control 1	0.113	0.125	0.120			0.120	0.003
Control 2	0.002	0.000	0.006		0.001	0.003	0.001

Table C.3. Initial absorbance data for enzyme mixture C.

Composition of enzyme mixture is described in table 4.1.Control 1 contains no cellulose substrate, control 2 contains no enzyme. Reactions were diluted 10-fold to ensure absorbance is within a suitable range to calculate the mass of glucose produced. Substrate was digested by cellulolytic enzymes for 20-hours before being placed on ice to terminate the reaction. The change in absorption of the supernatant in a hexokinase/glucose-6-phosphate dehydrogenase assay was monitored by UV-spectrophotometry.

	Δ Absorbance / no units						
	Assay 1	Assay 2	Assay 3	Assay 4	Assay 5	Mean	Error
Reaction	0.035		0.042	0.033	0.038	0.025	0.002
Control 1	0.012	0.008	0.011	0.014	0.008	0.011	0.001
Control 2	0.002	0.000	0.006		0.001	0.003	0.001

Table C.4. Initial absorbance data for enzyme mixture D.

Composition of enzyme mixture is described in table 4.1. Control 1 contains no cellulose substrate, control 2 contains no enzyme. Reactions were diluted 60-fold to ensure absorbance is within a suitable range to calculate the mass of glucose produced. Substrate was digested by cellulolytic enzymes for 20-hours before being placed on ice to terminate the reaction. The change in absorption of the supernatant in a hexokinase/glucose-6-phosphate dehydrogenase assay was monitored by UV-spectrophotometry.

	Δ Absorbance / no units						
	Assay 1	Assay 2	Assay 3	Assay 4	Assay 5	Mean	Error
Reaction	0.230			0.219	0.237	0.229	0.005
Control 1	0.056	0.067	0.068	0.057	0.059	0.062	0.003
Control 2	0.002	0.000	0.006		0.001	0.003	0.001

Table C.5. Initial absorbance data for enzyme mixture E.

Composition of enzyme mixture is described in table 4.1. Control 1 contains no cellulose substrate, control 2 contains no enzyme. Reactions were diluted 40-fold to ensure absorbance is within a suitable range to calculate the mass of glucose produced. Substrate was digested by cellulolytic enzymes for 20-hours before being placed on ice to terminate the reaction. The change in absorption of the supernatant in a hexokinase/glucose-6-phosphate dehydrogenase assay was monitored by UV-spectrophotometry.

	Δ Absorbance / no units						
	Assay 1	Assay 2	Assay 3	Assay 4	Assay 5	Mean	Error
Reaction	0.008	0.003			0.004	0.005	0.002
Control 1	0.006	0.005	0.011	0.001	0.000	0.005	0.002
Control 2	0.002	0.000	0.006		0.001	0.003	0.001

Table C.6. Initial absorbance data for enzyme mixture F.

Composition of enzyme mixture is described in table 4.1. Control 1 contains no cellulose substrate, control 2 contains no enzyme. Reactions were diluted 40-fold to ensure absorbance is within a suitable range to calculate the mass of glucose produced. Substrate was digested by cellulolytic enzymes for 20-hours before being placed on ice to terminate the reaction. The change in absorption of the supernatant in a hexokinase/glucose-6-phosphate dehydrogenase assay was monitored by UV-spectrophotometry.

	Δ Absorbance / no units						
	Assay 1	Assay 2	Assay 3	Assay 4	Assay 5	Mean	Error
Reaction	0.157	0.139	0.134	0.132		0.141	0.006
Control 1	0.038	0.026	0.033	0.040	0.036	0.035	0.002
Control 2	0.002	0.000	0.006		0.001	0.003	0.001

Table C.7. Initial absorbance data for enzyme mixture G.

Composition of enzyme mixture is described in table 4.1. Control 1 contains no cellulose substrate, control 2 contains no enzyme. Reactions were diluted 40-fold to ensure absorbance is within a suitable range to calculate the mass of glucose produced. Substrate was digested by cellulolytic enzymes for 20-hours before being placed on ice to terminate the reaction. The change in absorption of the supernatant in a hexokinase/glucose-6-phosphate dehydrogenase assay was monitored by UV-spectrophotometry.

	Δ Absorbance / no units						
	Assay 1	Assay 2	Assay 3	Assay 4	Assay 5	Mean	Error
Reaction	0.159		0.142	0.159	0.155	0.154	0.004
Control 1	0.036	0.037	0.034	0.036	0.041	0.037	0.001
Control 2	0.002	0.000	0.006		0.001	0.003	0.001

Table C.8. Initial absorbance data for enzyme mixture H.

Composition of enzyme mixture is described in table 4.1. Control 1 contains no cellulose substrate, control 2 contains no enzyme. Reactions were diluted 40-fold to ensure absorbance is within a suitable range to calculate the mass of glucose produced. Substrate was digested by cellulolytic enzymes for 20-hours before being placed on ice to terminate the reaction. The change in absorption of the supernatant in a hexokinase/glucose-6-phosphate dehydrogenase assay was monitored by UV-spectrophotometry.

	Δ Absorbance / no units						
	Assay 1	Assay 2	Assay 3	Assay 4	Assay 5	Mean	Error
Reaction	0.086	0.088	0.090	0.086	0.102	0.091	0.003
Control 1	0.007	0.010	0.014		0.012	0.011	0.001
Control 2	0.002	0.000	0.006		0.001	0.003	0.001

Table C.9. Initial absorbance data for enzyme mixture I.

Composition of enzyme mixture is described in table 4.1. Control 1 contains no cellulose substrate, control 2 contains no enzyme. Reactions were diluted 10-fold to ensure absorbance is within a suitable range to calculate the mass of glucose produced. Substrate was digested by cellulolytic enzymes for 20-hours before being placed on ice to terminate the reaction. The change in absorption of the supernatant in a hexokinase/glucose-6-phosphate dehydrogenase assay was monitored by UV-spectrophotometry.

	Δ Absorbance / no units						
	Assay 1	Assay 2	Assay 3	Assay 4	Assay 5	Mean	Error
Reaction	0.001			0.004	0.002	0.003	0.001
Control 1	0.000	0.007	0.009	-0.005	-0.005	0.001	0.003
Control 2	0.002	0.000	0.006		0.001	0.003	0.001

Table C.10. Initial absorbance data for enzyme mixture J.

Composition of enzyme mixture is described in table 4.1. Control 1 contains no cellulose substrate, control 2 contains no enzyme. Reactions were diluted 40-fold to ensure absorbance is within a suitable range to calculate the mass of glucose produced. Substrate was digested by cellulolytic enzymes for 20-hours before being placed on ice to terminate the reaction. The change in absorption of the supernatant in a hexokinase/glucose-6-phosphate dehydrogenase assay was monitored by UV-spectrophotometry.

C.2 Breakdown of Different Substrates

	Δ Absorbance / no units						
	Assay 1	Assay 2	Assay 3	Assay 4	Assay 5	Mean	Error
Reaction	0.346		0.310	0.298	0.341	0.216	0.012
Control 1	0.061	0.072	0.073	0.062	0.064	0.066	0.003
Control 2	0.000	0.002	0.002			0.002	0.001

Table C.11. Initial absorbance data for the breakdown of simple cellulose film.

The enzyme mixture used is mixture E described in table 4.1. Control 1 contains no cellulose substrate, control 2 contains no enzyme. Reactions were diluted 60-fold to ensure absorbance is within a suitable range to calculate the mass of glucose produced. Substrate was digested by cellulolytic enzymes for 20-hours before being placed on ice to terminate the reaction. The change in absorption of the supernatant in a hexokinase/glucose-6-phosphate dehydrogenase assay was monitored by UV-spectrophotometry.

	Δ Absorbance / no units						
	Assay 1	Assay 2	Assay 3	Assay 4	Assay 5	Mean	Error
Reaction	0.243	0.244	0.232			0.240	0.004
Control 1	0.061	0.072	0.073	0.062	0.064	0.066	0.003
Control 2	-0.004	0.010	-0.001	-0.001	0.000	0.001	0.002

Table C.12. Initial absorbance data for the breakdown of coated cellulose film.

The enzyme mixture used is mixture E described in table 4.1. Control 1 contains no cellulose substrate, control 2 contains no enzyme. Reactions were diluted 40-fold to ensure absorbance is within a suitable range to calculate the mass of glucose produced. Substrate was digested by cellulolytic enzymes for 20-hours before being placed on ice to terminate the reaction. The change in absorption of the supernatant in a hexokinase/glucose-6-phosphate dehydrogenase assay was monitored by UV-spectrophotometry.

	Δ Absorbance / no units						
	Assay 1	Assay 2	Assay 3	Assay 4	Assay 5	Mean	Error
Reaction	0.196	0.207	0.208	0.215	0.240	0.214	0.007
Control 1	0.061	0.072	0.073	0.062	0.064	0.066	0.003
Control 2	0.008	-0.008	0.009	-0.002	-0.002	0.001	0.003

Table C.13. Initial absorbance data for the breakdown of microcrystalline cellulose.

The enzyme mixture used is mixture E described in table 4.1. Control 1 contains no cellulose substrate, control 2 contains no enzyme. Reactions were diluted 40-fold to ensure absorbance is within a suitable range to calculate the mass of glucose produced. Substrate was digested by cellulolytic enzymes for 20-hours before being placed on ice to terminate the reaction. The change in absorption of the supernatant in a hexokinase/glucose-6-phosphate dehydrogenase assay was monitored by UV-spectrophotometry.

	Δ Absorbance / no units						
	Assay 1	Assay 2	Assay 3	Assay 4	Assay 5	Mean	Error
Reaction	0.230			0.219	0.237	0.229	0.005
Control 1	0.056	0.067	0.068	0.057	0.059	0.062	0.003
Control 2	0.002	0.000	0.006		0.001	0.003	0.001

Table C.14. Initial absorbance data for the breakdown of Whatman filter paper.

The enzyme mixture used is mixture E described in table 4.1. Control 1 contains no cellulose substrate, control 2 contains no enzyme. Reactions were diluted 40-fold to ensure absorbance is within a suitable range to calculate the mass of glucose produced. Substrate was digested by cellulolytic enzymes for 20-hours before being placed on ice to terminate the reaction. The change in absorption of the supernatant in a hexokinase/glucose-6-phosphate dehydrogenase assay was monitored by UV-spectrophotometry.

C.3 Breakdown of Composite Films

	Δ Absorbance / no units						
	Assay 1	Assay 2	Assay 3	Assay 4	Assay 5	Mean	Error
Reaction	0.218	0.258	0.197	0.220	0.221	0.223	0.010
Control 1	0.030	0.034	0.034	0.033	0.032	0.033	0.001
Control 2	0.001		0.004	0.004	0.005	0.003	0.001

Table C.15. Initial absorbance data for the breakdown of a composite film containing PVOH type 4-88.

The enzyme mixture used is mixture E described in table 4.1 with a load of 0.7 units per mg of cellulose film. Control 1 contains a PVOH film with cellulolytic enzymes incorporated, control 2 contains no enzyme. Reactions were diluted 40-fold to ensure absorbance is within a suitable range to calculate the mass of glucose produced. Substrate was digested by cellulolytic enzymes for 20-hours before being placed on ice to terminate the reaction. The change in absorption of the supernatant in a hexokinase/glucose-6-phosphate dehydrogenase assay was monitored by UV-spectrophotometry.

	Δ Absorbance / no units						
	Assay 1	Assay 2	Assay 3	Assay 4	Assay 5	Mean	Error
Reaction	0.219	0.231	0.249	0.239	0.228	0.234	0.005
Control 1	0.045	0.046	0.051	0.053	0.055	0.050	0.002
Control 2	0.001		0.004	0.004	0.005	0.003	0.001

Table C.16. Initial absorbance data for the breakdown of a composite film containing PVOH type 8-88.

The enzyme mixture used is mixture E described in table 4.1 with a load of 0.7 units per mg of cellulose film. Control 1 contains a PVOH film with cellulolytic enzymes incorporated, control 2 contains no enzyme. Reactions were diluted 40-fold to ensure absorbance is within a suitable range to calculate the mass of glucose produced. Substrate was digested by cellulolytic enzymes for 20-hours before being placed on ice to terminate the reaction. The change in absorption of the supernatant in a hexokinase/glucose-6-phosphate dehydrogenase assay was monitored by UV-spectrophotometry.

	Δ Absorbance / no units						
	Assay 1	Assay 2	Assay 3	Assay 4	Assay 5	Mean	Error
Reaction	0.209	0.247		0.190	0.198	0.211	0.013
Control 1	0.034	0.041	0.035	0.051	0.048	0.042	0.003
Control 2	0.001		0.004	0.004	0.005	0.003	0.001

Table C.17. Initial absorbance data for the breakdown of a composite film containing PVOH type 40-88.

The enzyme mixture used is mixture E described in table 4.1 with a load of 0.7 units per mg of cellulose film. Control 1 contains a PVOH film with cellulolytic enzymes incorporated, control 2 contains no enzyme. Reactions were diluted 40-fold to ensure absorbance is within a suitable range to calculate the mass of glucose produced. Substrate was digested by cellulolytic enzymes for 20-hours before being placed on ice to terminate the reaction. The change in absorption of the supernatant in a hexokinase/glucose-6-phosphate dehydrogenase assay was monitored by UV-spectrophotometry.

	Δ Absorbance / no units						
	Assay 1	Assay 2	Assay 3	Assay 4	Assay 5	Mean	Error
Reaction	0.240	0.207	0.211	0.244	0.228	0.226	0.007
Control 1	0.087	0.053	0.063	0.057	0.055	0.063	0.006
Control 2	0.001		0.004	0.004	0.005	0.003	0.001

Table C.18. Initial absorbance data for the breakdown of a composite film containing PVOH type 4-98.

The enzyme mixture used is mixture E described in table 4.1 with a load of 0.7 units per mg of cellulose film. Control 1 contains a PVOH film with cellulolytic enzymes incorporated, control 2 contains no enzyme. Reactions were diluted 40-fold to ensure absorbance is within a suitable range to calculate the mass of glucose produced. Substrate was digested by cellulolytic enzymes for 20-hours before being placed on ice to terminate the reaction. The change in absorption of the supernatant in a hexokinase/glucose-6-phosphate dehydrogenase assay was monitored by UV-spectrophotometry.

	Δ Absorbance / no units						
	Assay 1	Assay 2	Assay 3	Assay 4	Assay 5	Mean	Error
Reaction	0.242	0.217	0.263	0.211		0.234	0.012
Control 1	0.051	0.074	0.079	0.078	0.083	0.073	0.006
Control 2	0.001		0.004	0.004	0.005	0.003	0.001

Table C.19. Initial absorbance data for the breakdown of a composite film containing a mixture of PVOH types 6-98 and 40-88.

The enzyme mixture used is mixture E described in table 4.1 with a load of 0.7 units per mg of cellulose film. Control 1 contains a PVOH film with cellulolytic enzymes incorporated, control 2 contains no enzyme. Reactions were diluted 40-fold to ensure absorbance is within a suitable range to calculate the mass of glucose produced. Substrate was digested by cellulolytic enzymes for 20-hours before being placed on ice to terminate the reaction. The change in absorption of the supernatant in a hexokinase/glucose-6-phosphate dehydrogenase assay was monitored by UV-spectrophotometry.

	Δ Absorbance / no units						
	Assay 1	Assay 2	Assay 3	Assay 4	Assay 5	Mean	Error
Reaction	0.249	0.209	0.224	0.223	0.226	0.227	0.006
Control 1	0.068	0.070	0.074	0.056	0.063	0.067	0.003
Control 2	0.001		0.004	0.004	0.005	0.003	0.001

Table C.20. Initial absorbance data for the breakdown of a composite film containing PVOH type 6-98.

The enzyme mixture used is mixture E described in table 4.1 with a load of 0.7 units per mg of cellulose film. Control 1 contains a PVOH film with cellulolytic enzymes incorporated, control 2 contains no enzyme. Reactions were diluted 40-fold to ensure absorbance is within a suitable range to calculate the mass of glucose produced. Substrate was digested by cellulolytic enzymes for 20-hours before being placed on ice to terminate the reaction. The change in absorption of the supernatant in a hexokinase/glucose-6-phosphate dehydrogenase assay was monitored by UV-spectrophotometry.

	Δ Absorbance / no units						
	Assay 1	Assay 2	Assay 3	Assay 4	Assay 5	Mean	Error
Reaction			0.254	0.250	0.268	0.172	0.005
Control 1	0.078	0.069	0.070	0.075	0.073	0.073	0.002
Control 2	0.001		0.004	0.004	0.005	0.003	0.001

Table C.21. Initial absorbance data for the breakdown of a composite film containing a mixture of PVOH types 10-98 and 4-88.

The enzyme mixture used is mixture E described in table 4.1 with a load of 0.7 units per mg of cellulose film. Control 1 contains a PVOH film with cellulolytic enzymes incorporated, control 2 contains no enzyme. Reactions were diluted 60-fold to ensure absorbance is within a suitable range to calculate the mass of glucose produced. Substrate was digested by cellulolytic enzymes for 20-hours before being placed on ice to terminate the reaction. The change in absorption of the supernatant in a hexokinase/glucose-6-phosphate dehydrogenase assay was monitored by UV-spectrophotometry.

	Δ Absorbance / no units						
	Assay 1	Assay 2	Assay 3	Assay 4	Assay 5	Mean	Error
Reaction	0.225	0.226			0.235	0.229	0.003
Control 1	0.054	0.066	0.060	0.059	0.054	0.059	0.002
Control 2	0.001		0.004	0.004	0.005	0.003	0.001

Table C.22. Initial absorbance data for the breakdown of a composite film containing PVOH type 10-98.

The enzyme mixture used is mixture E described in table 4.1 with a load of 0.7 units per mg of cellulose film. Control 1 contains a PVOH film with cellulolytic enzymes incorporated, control 2 contains no enzyme. Reactions were diluted 40-fold to ensure absorbance is within a suitable range to calculate the mass of glucose produced. Substrate was digested by cellulolytic enzymes for 20-hours before being placed on ice to terminate the reaction. The change in absorption of the supernatant in a hexokinase/glucose-6-phosphate dehydrogenase assay was monitored by UV-spectrophotometry.

	Δ Absorbance / no units						
	Assay 1	Assay 2	Assay 3	Assay 4	Assay 5	Mean	Error
Reaction	0.262	0.268	0.249		0.241	0.170	0.006
Control 1	0.073	0.044	0.073	0.050	0.090	0.066	0.008
Control 2	0.001		0.004	0.004	0.005	0.003	0.001

Table C.23. Initial absorbance data for the breakdown of a composite film containing a mixture of PVOH types 20-98 and 8-88.

The enzyme mixture used is mixture E described in table 4.1 with a load of 0.7 units per mg of cellulose film. Control 1 contains a PVOH film with cellulolytic enzymes incorporated, control 2 contains no enzyme. Reactions were diluted 60-fold to ensure absorbance is within a suitable range to calculate the mass of glucose produced. Substrate was digested by cellulolytic enzymes for 20-hours before being placed on ice to terminate the reaction. The change in absorption of the supernatant in a hexokinase/glucose-6-phosphate dehydrogenase assay was monitored by UV-spectrophotometry.

	Δ Absorbance / no units						
	Assay 1	Assay 2	Assay 3	Assay 4	Assay 5	Mean	Error
Reaction	0.272	0.228	0.194	0.211	0.245	0.230	0.014
Control 1	0.076	0.061	0.009	0.081	0.079	0.062	0.014
Control 2	0.001		0.004	0.004	0.005	0.003	0.001

Table C.24. Initial absorbance data for the breakdown of a composite film containing PVOH type 20-98.

The enzyme mixture used is mixture E described in table 4.1 with a load of 0.7 units per mg of cellulose film. Control 1 contains a PVOH film with cellulolytic enzymes incorporated, control 2 contains no enzyme. Reactions were diluted 40-fold to ensure absorbance is within a suitable range to calculate the mass of glucose produced. Substrate was digested by cellulolytic enzymes for 20-hours before being placed on ice to terminate the reaction. The change in absorption of the supernatant in a hexokinase/glucose-6-phosphate dehydrogenase assay was monitored by UV-spectrophotometry.

	Δ Absorbance / no units						
	Assay 1	Assay 2	Assay 3	Assay 4	Assay 5	Mean	Error
Reaction			0.241	0.289	0.211	0.247	0.023
Control 1	0.063	0.059	0.064	0.063	0.061	0.062	0.001
Control 2	0.001		0.004	0.004	0.005	0.003	0.001

Table C.25. Initial absorbance data for the breakdown of a composite film containing PVOH type 28-99.

The enzyme mixture used is mixture E described in table 4.1 with a load of 0.7 units per mg of cellulose film. Control 1 contains a PVOH film with cellulolytic enzymes incorporated, control 2 contains no enzyme. Reactions were diluted 40-fold to ensure absorbance is within a suitable range to calculate the mass of glucose produced. Substrate was digested by cellulolytic enzymes for 20-hours before being placed on ice to terminate the reaction. The change in absorption of the supernatant in a hexokinase/glucose-6-phosphate dehydrogenase assay was monitored by UV-spectrophotometry.

	Δ Absorbance / no units						
	Assay 1	Assay 2	Assay 3	Assay 4	Assay 5	Mean	Error
Reaction	0.013		0.013		0.011	0.013	0.001
Control 1	0.006	0.014	0.010	0.016	0.017	0.013	0.002
Control 2	0.001		0.004	0.004	0.005	0.003	0.001

Table C.26. Initial absorbance data for the breakdown of a composite film containing PVOH type 28-99 with a low enzyme loading.

The enzyme mixture used is mixture E described in table 4.1 with a load of 0.04 units per mg of cellulose film. Control 1 contains a PVOH film with cellulolytic enzymes incorporated, control 2 contains no enzyme. Reactions were diluted 40-fold to ensure absorbance is within a suitable range to calculate the mass of glucose produced. Substrate was digested by cellulolytic enzymes for 20-hours before being placed on ice to terminate the reaction. The change in absorption of the supernatant in a hexokinase/glucose-6-phosphate dehydrogenase assay was monitored by UV-spectrophotometry.

C.4 Glucose Standard Curve

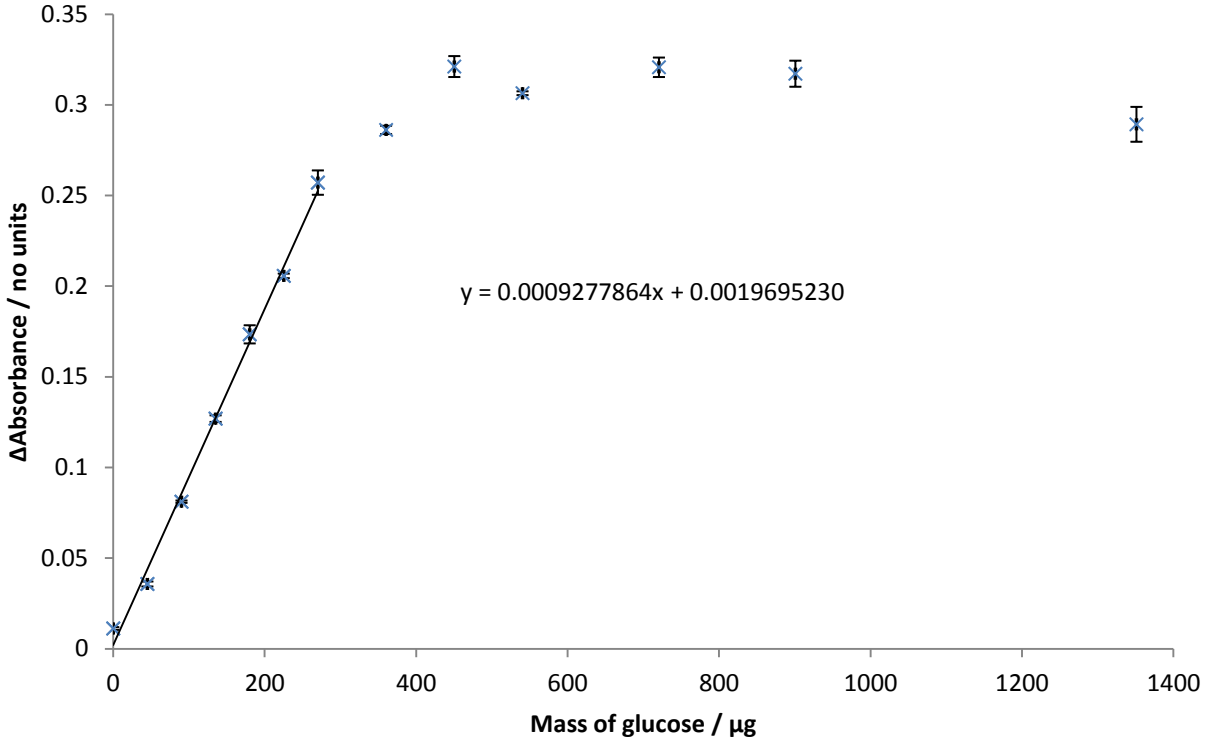

C.1. Glucose standard curve for hexokinase/glucose-6-phosphate dehydrogenase assay.

The change in absorbance at 340 nm of solutions of different concentrations of glucose was measured. Each measurement was repeated at least three times. The error bars shown are standard error. The equation of the linear part of the curve was calculated by a least-squares regression method and is show.